Targeting therapeutic vulnerabilities associated with EWS fusion proteins in Ewing sarcoma

Antonio Romo Morales

This thesis is submitted to the University of London for the degree of Doctor of Philosophy

September 2020

Sarcoma Molecular Pathology Team

Divisions of Molecular Pathology and Cancer Therapeutics

The Institute of Cancer Research

15 Cotswold Road

Sutton

Surrey

UK

SM2 5NG

Declaration

I confirm that the work presented in this thesis is my own, unless otherwise stated.

Signed

Antonio Romo Morales

Date 28 September 2020

Poster/Oral Presentations

Poster Presentation: Therapeutic combination strategies targeting EWSR1 fusion gene positive sarcomas – ICR annual conference, 25/06/19

Abstract

Ewing sarcoma (ES) is a rare and aggressive bone tumour affecting children and young adults and that requires better therapeutic options to improve patient outcomes. ES is characterised by chromosomal rearrangements producing a fusion gene, the most predominant occurring between *EWSR1* and *FLI1* (~85%). Recent evidence shows that the chimeric oncoprotein EWS-FLI recruits chromatin remodellers that epigenetically rewire transcription to establish its oncogenic programme. Additionally, transcriptional dysregulation is known to induce replication stress (RS) and genomic instability. To mitigate potential genotoxic damage, ES cells are particularly dependent on the replication stress response (RSR). Based on these EWS-FLI1-specific molecular effects, this thesis investigates two separate therapeutic strategies: (i) inhibition of the epigenetic modifier KDM1A, and (ii) exploiting the dependency on the RSR.

Catalytic inhibition of histone demethylase KDM1A is demonstrated to be insufficient as a therapeutic strategy for ES, although roles beyond its demethylase function remain a possibility. To identify therapeutic combinations targeting the dependency on the RSR, clinically available drugs inhibiting the ATR-CHK1-WEE1 axis were tested in 3D spheroids of ES cell lines. Each drug candidate was combined at clinically relevant doses with SN-38, the active metabolite of topoisomerase I inhibitor irinotecan, currently used to treat relapsed ES. Combinations revealed cytotoxicity and decreased growth in ES spheroids following WEE1 and ATR inhibition, both concurrent with SN-38. Based on the strength of responses, further investigations prioritised the effects of the WEE1 inhibitor AZD1775 combined with SN-38 in additional ES cell lines and a model ectopically expressing EWS-FLI1. DNA damage, apoptosis, and cell cycle analysis uncovered two responses in ES cell lines, one characterised by cell death, the other resembling growth arrest. These may be dependent on the cell lines' mutational background and could act as a predictive biomarker. Taken together these findings identify a promising novel therapeutic strategy for ES.

Acknowledgements

This project would not have been possible without the encouragement and guidance of my supervisor Prof Janet Shipley. Working in her team has been a deeply rewarding experience and I am very thankful to have had this opportunity. I would also like to thank my associate supervisor, Dr Susanne Gatz, for her continued insight and enthusiasm that have spurred me on throughout my PhD. Special thanks to Dr Ewa Aladowicz, my other associate supervisor, for her invaluable practical advice and going above and beyond to support me to complete this project. Both have been fantastic mentors throughout this time. I would also like to thank Dr Joanna Selfe for always offering useful advice and her help with statistical analysis. Thank you to Carolina, Stella, Sami, Anastasia, Olivia, Lucile, Sarah and all other past members of the Sarcoma Molecular Pathology Team. Their kind and supportive words created a friendly atmosphere in the lab and made me feel very fortunate to have been part of this group. Also, special thanks to Louise Howell for always being ready to help with any image analysis problem. I am also very grateful to the Elin Rose Appeal, particularly Martin and Sian Waite and their family for funding this project. Their close interest in our work kept me motivated throughout these years.

This thesis is dedicated to the memory of my grandfather and other family members that have been affected by cancer. I am very thankful to my parents and my brother; without their efforts and encouragement it would not have been possible for me to be where I am. I would also like to extend thanks to Maurice, Will, Jacob, Dan, and Jasmine for their supportive friendship. I am very grateful to the Wilkinson family for their kindness and welcoming me into their home. Lastly, I would like to thank Kate, her love and enthusiasm have been my strength and inspiration.

Table of Contents

List of figures

List of tables

Abbreviations

2D	Two-dimensional
3D	Three-dimensional
53BP1	p53-binding protein 1
ADP	Adenosine diphosphate
AID	Activation-induced cytidine deaminase
AML	Acute myeloid leukaemia
ANOVA	Analysis of variance
APOBEC	Apolipoprotein B mRNA editing enzyme, catalytic polypeptide-like
ATM	Ataxia Telangiectasia Mutated
ATP	Adenosine triphosphate
ATR	Ataxia Telangiectasia and Rad3-Related Protein
AUC	Area under the curve
BAF	Brg/Brahma-associated factors
BCA	Bicinchoninic acid
BD	Bis in die (Twice a day)
BER	Base excision repair
BFB	Breakage-fusion-bridge
BLM	Bloom RecQ Like Helicase
BRCA1	BRCA1 DNA repair associated
BRCA2	BRCA2 DNA repair associated
BSA	Bovine Serum Albumin
C	Cytosine (base)
CDC	Cell division cycle
CDK	Cyclin-dependent kinase
cDNA	Complementary DNA
CDT1	Chromatin licensing and DNA replication factor 1
CDX	Cell line-derived xenograft
CFS	Common fragile site
CHD4	Chromodomain 4
ChIP-seq	Chromatin immunoprecipitation sequencing
CHK1	Checkpoint kinase 1
CHK2	Checkpoint kinase 2
CML	Chronic myeloid leukaemia
CMV	Cytomegalovirus
CST	Cell signaling technology
CTD	C terminal domain
DAPI	4′,6-diamidino-2-phenylindole
DDR	DNA damage response
DHX9	DExH-Box Helicase 9
DLBCL	Diffuse large B-cell lymphoma
DM	Double minute
DMEM	Dulbecco's modified eagle medium
DMSO	Dimethylsulphoxide
DNA	Deoxyribonucleic acid
dNTP	Deoxyribonucleotide
DOX	Doxycycline
DPX	Dibutylphthalate Polystyrene Xylene
DRIP-seq	DNA:RNA hybrid IP-sequencing
DSB	DNA double strand break
DSRCT	Desmoplastic small round cell tumour
DTT	Dithiothreitol
E. coli	*Escherichia coli*
ECL	Enhanced chemiluminescence
EDTA	Ethylenediaminetetraacetic acid
EGFR	Epidermal growth factor receptor
EMA	European Medicines Agency
EMT	Epithelial-to-mesenchymal transition
ES	Ewing sarcoma

ETAA1	Ewing's tumour associated antigen 1	IC50	Half maximal inhibitory concentration
ETS	E-twenty-six-specific sequence, or E26 transforming sequence	IGF-1	Insulin-like growth factor 1
EV	Empty vector	IP	Immunoprecipitation
EWSR1	EWS RNA binding protein 1	iPSC	Induced pluripotent stem cell
EZH2	Enhancer of zeste homolog 2	IR	Ionising radiation
		kb	Kilobases
FA	Fanconi anaemia	kDa	Kilodaltons
FAD	Flavin adenine dinucleotide	KDM1A	Lysine specific demethylase 1A
FANCD2	FA complementation group D2	KMT2A	Histone-lysine N-methyltransferase 2A
FBS	Foetal bovine serum	LB	Lysogeny broth
FDA	Food Drug Administration	LDS	Lithium dodecyl sulphate
FEN1	Flap-endonuclease 1	LOH	Loss of heterozygosity
FLI1	Friend leukaemia integrated 1	LSD1	Lysine specific demethylase 1
G	Guanosine (base)	mA	Milliamperes
GFI1	Growth factor independence 1	Mb	Megabases
GI50	Half maximal concentration for growth inhibition	MCM2–7	Minichromosome maintenance complex 2–7
GSK3β	Glycogen synthase kinase 3β	MDC1	Mediator of DNA checkpoint 1
Gy	Gray	MDM2	MDM2 Proto-oncogene
h	Hours	MDM4	MDM4 regulator of p53
H&E	Haematoxylin and eosin	MEF	Mouse embryonic fibroblast
H2A	Histone 2A		
H2AX	H2A histone family member X	mg	Milligrams
		ml	Millilitres
H3K	Histone 3 lysine residue	MLL	Mixed lineage leukaemia 1
HDAC	Histone deacetylase	mM	Millimolar
HEK	Human embryonic kidney	MOPS	3-(N-morpholino) propanesulfonic acid
hESC	Human embryonic stem cell	MRN	MRE11-Rad50-Nibrin
HIF-1α	Hypoxia-inducible factor 1α	mRNA	Messenger RNA
		MSC	Mesenchymal stem cell
HPLC	High-performance liquid chromatography	MTA1	Metastasis-associated protein 1
HPV	Human papillomavirus	mTOR	Mammalian target of Rapamycin
HR	Homologous recombination		

MTS	3-(4,5-dimethylthiazol-2-yl)-5-(3-carboxymethoxyphenyl)-2-(4-sulfophenyl)-2H-tetrazolium		RIPA	Radio immunoprecipitation assay
NBN	Nibrin		RMS	Rhabdomyosarcoma
NEB	New England Biolabs		RNA	Ribonucleic acid
ng	Nanograms		RNAPII	RNA polymerase II
NHEJ	Non-homologous end joining		RNR	Ribonucleotide reductase
nM	Nanomolar		ROI	Region of interest
nm	Nanometres		RPA	Replication protein A
NTD	N terminal domain		RPM	Revolutions per minute
NuRD	Nucleosome Remodelling Deacetylase Complex		RPMI	Roswell Park Memorial Institute medium
P53RM2	Ribonucleotide Reductase Regulatory TP53 Inducible Subunit M2B		RRM2	Ribonucleotide reductase regulatory subunit M2
PAR	Poly ADP-ribosylation		RS	Replication stress
PARP	Poly ADP-ribose polymerase		RSR	Replication stress response
PBS	Phosphate buffered saline		RT	Room temperature
PCR	Polymerase chain reaction		RT	Reverse transcription
PD	Pharmacodynamic		RTEL1	Regulator of telomerase elongation helicase 1
PDO	Patient-derived organoid		SBRCT	Small blue round cell tumours
PDX	Patient-derived xenograft		SCLC	Small cell lung cancer
pH	Potential of hydrogen		SDS	Sodium dodecyl sulphate
PI	Propidium iodide		SDS-PAGE	SDS-polyacrylamide gel electrophoresis
PIF1	ATP-dependent DNA helicase PIF1		SEAP	Secreted embryonic alkaline phophatase
PK	Pharmacokinetic		Ser (S)	Serine
pmol	Picomoles		shRNA	Short hairpin RNA
PRC2	Polycomb repressive complex 2		siRNA	Short interfering RNA
PVDF	Polyvinylidene difluoride		SSB	Single strand break
qRT-PCR	Quantitative real-time		ssDNA	Single-stranded DNA
Rb	Retinoblastoma		STAG2	Stromal antigen 2
RCF	Relative centrifugal force		STR	Short tandem repeat
			SWI/SNF	Switch/Sucrose Non-Fermentable
			T	Thymine (base)
			TAE	Tris-acetate-EDTA
			TBS	Tris buffered saline
			TBST	TBS tween20
			TE	Tris-EDTA
			Tet	Tetracycline

Thr (T)	Threonine	VIDE	Vincristine, Ifosfamide, Doxorubicin, Etoposide
TLR2	Toll-like receptor 2		
TOBP1	Topoisomerase binding protein 1		
TSS	Transcription start site	WRN	Werner RecQ Like Helicase
ULA	Ultra-low attachment		
UR-DNA	Under-replicated DNA	WT	Wild-type
UV	Ultraviolet	γH2AX	Phosphorylated H2AX
V	Volts	μg	Micrograms
VAC	Vincristine, Actinomycin D, Cyclophosphamide	μl	Microlitres
		μm	Micrometres
		μM	Micromolar
VAI	Vincristine, Actinomycin D, Ifosfamide		

Chapter 1 Introduction

1.1 Cancer

1.1.1 Cancer and tumourigenesis

Cancer is an umbrella term for a large group of diseases characterised by abnormal, unregulated cell growth. Tumours can develop locally, but most cancers have the potential to metastasise to distant tissues away from the primary site. Cancer can be regarded as a genetic disease with models of tumour development proposing a series of acquired 'hits' as disease drivers (1). These "hits" can take the form of mutations in genes broadly categorised as oncogenic or tumour suppressive (see 1.1.3). Collectively, the resulting changes in phenotype lead to dysregulation of cellular processes that not only permit, but actively promote tumour growth and survival. This process involves an initiating 'driver mutation' which provides an advantageous trait for tumour development. During the expansion of this clonal population, in a background of genomic instability, mutation rates increase together with the acquisition of genetic alterations that aid tumour development and enable distinct molecular mechanisms (1, 2). However, not all mutations are beneficial resulting in clonal selection against them. The occurrence of driver mutations depends on the status of the specific pathway affected. This is because, if it is already compromised, a second would not add any further selective advantage (2, 3). This exclusivity principle has been validated through integrated analysis of canonical pathways mutated in a wide range of tumour samples, and has also identified the co-occurrence of certain alterations (2). Additionally, there are genes known to be common drivers in many cancers playing key roles in pathways, traditionally linked with tumour development. Most notably, *TP53* is the most commonly mutated gene, shown to be associated with more than 27 different malignancies (2).

Whilst the somatic mutation theory highlights an important process contributing to tumour development, genetic alterations exist in dynamic microenvironments that contribute phenotypic heterogeneity (4-6). This intra-tumoural heterogeneity is also underpinned by subclonal populations with differing growth rates, metastatic potential, immunogenicity, and drug response (6, 7). This diversity is partially explained by these clones being genetically heterogeneous, with alternative gene defects but a common driver mutation (2, 6). Although originally put forward to describe the process of metastasis, the 'seed and soil hypothesis' offers another explanation supporting the view

that microenvironmental cues strongly dictate tumour behaviour (8). In this way, fluctuations in the tumour microenvironment, together with accessibility to nutrients such as growth factors and oxygen, have been suggested to play a role in the variation in cancer cells (5, 6). In the context of metastasis, a pre-metastatic niche describes an environment possessing the suitable nutrients for migrating cells to invade and establish a secondary site (8). This can also be applied to the origin of cancer, in which the need for a suitable fertile niche where a tumour can develop is as important as the accumulation of genetic mutations. Similarly, certain genetic changes are only tumorigenic in specific permissive tissues due to different tumour suppressive signalling mechanisms in place. For example, in mouse models, expression of *KRAS* mutations in lung cells are highly oncogenic, whilst in muscle cells p19 upregulation acts as a tumour suppressive barrier that need to be overcome, for tumourigenesis (9). Overall, the interplay between the genetic diversity, the microenvironment, and the tumour background of cancer cells, creates a dynamic ecosystem driving tumour evolution.

1.1.2 Hallmarks of cancer

Cancer can arise in any organ or tissue giving it distinct histological and pathophysiological features associated with the loss of function in that respective tissue. These phenotypic characteristics together with a diverse genetic background including a wide range of driver mutations, make cancer a set of vastly different diseases. As noted previously, even within the same tumour type, there are genetic subtypes and heterogeneous populations that affect drug response and clinical outcomes. In contrast to this variability, there are shared mechanisms commonly hijacked by cancer cells to promote tumour development (5, 10). These biological processes, originally defined as the "hallmarks of cancer", include the ability to independently sustain growth signalling, evading growth-suppressing factors, escaping cell death mechanisms, enabling limitless replicative potential, induction of angiogenesis, and metastatic and invasive potential (10). Acquisition of these hallmarks requires genetic alterations enabling the dysregulation of these biological processes. This is made possible by an underlying state of genomic instability, with increased propensity for these mutations to arise and to remain unchecked. Since this model was established, twenty years of cancer research have led to a revision of this list and inclusion of additional processes such as metabolic reprogramming, immune system evasion, and replication stress (5, 11, 12) (Replication stress as a hallmark of cancer is discussed further in section 1.2). Caveats to this model

are that not all cancer cells necessarily display all hallmarks, and importantly, these processes are affected by the tumour microenvironment making them context-dependent. As part of this context, the supporting tissue or tumour stroma is also capable of conferring tumourigenic properties and facilitating modulation of these processes that characterise cancer cells (5). In some instances, such as metastasis, cancer cells are known to undergo phenotype switching, which promotes invasion whilst suppressing growth signalling and proliferation (13). In this way, cancer cell behaviour constantly has to respond to microenvironmental cues in order to adapt and ensure tumour survival. One clinical implication of these adaptations is acquired drug-resistance driven by heterogenous cancer cell populations arising from different genetic subtypes and their tumour microenvironment (5, 6). Altogether, the hallmarks of cancer remain a useful way to categorise and understand tumourigenesis, as well as offering hints of the functional consequences of oncogenes and tumour suppressor genes.

1.1.3   Oncogenes and tumour suppressor genes

Oncogenes are the result of alterations in the activity or control of genes associated with promoting tumour development, often referred to as proto-oncogenes. In contrast to tumour suppressor genes, the nature of oncogenes is usually dominant, meaning that only one alteration on one allele is required for their transformation (14). This 'initiating event' can take the form of a gain-of-function mutation, amplification, translocation, or dysregulation of epigenetic control, leading to increased oncogene expression and activity (14). The functional properties of oncogenes fall under the previously described hallmarks of cancer, providing tumours with a survival advantage favouring tumour progression (5).

Activating mutations in proto-oncogenes commonly affect the structure of the encoded protein. This is the case in point mutations where a change in a single nucleotide base results in an amino acid substitution with the potential of increasing its activity (14). One example of this is the V600E missense mutation in *BRAF*, which is commonly found in a range of tumour types, such as melanoma, colorectal cancer, and hepatocellular carcinomas (14). This mutation modifies the regulatory site of this kinase causing it to be constitutively active. Similarly, mutations in the RAS proto-oncogenes *HRAS*, *KRAS*, and *NRAS* result in permanent activation of these effectors, which transduce growth stimulating signals (15). Constitutive activation can also result from other genetic

alterations such as through deletions of regulatory gene regions. Notably, both point mutations and deletions can occur in the promoter region of a proto-oncogene and result in increased transcription.

Gene amplification is another mechanism of oncogene activation that refers to the gain in copy number of a particular gene (14, 16). This can arise from chromosomal abnormalities where a whole portion of the chromosome is amplified, increasing the copies of more than one gene. The appearance of extrachromosomal circular DNA structures named double-minute (DM) chromosomes and homogeneously staining regions (HSRs) are the result of amplification events. One of the proposed mechanisms behind these alterations is breakage–fusion–bridge (BFB) cycles (reviewed in (17)). The most commonly amplified genes in cancer include *MYC*, *CCND1*, *RAS,* and *EGFR* (2). Other notable examples include *MDM2* and *MDM4*, which destabilise p53 to decrease its tumour suppressive role (18). Amplification of these regulators of p53 occur in sarcomas, neuroblastoma, and glioma (2, 17).

Chromosomal translocations leading to the creation of a fusion gene, and their resulting fusion proteins, are another form of oncogene activation driving cancer progression (19). The most well-known, and first to be described, example is the Philadelphia chromosome present in chronic myeloid leukaemia (CML), which arises from the t(9;22)(q34;q11) joining the *BRC* and *ABL1* genes (20). The resulting chimeric product has novel oncogenic properties in the form of abnormal activation of the ABL tyrosine kinase activation and increased proliferation (20). Alternatively, a second type of chromosomal rearrangements can also place the promoter region of a gene next to a proto-oncogene, leading to increased expression. This occurs in another haematological malignancy, acute T-cell leukaemia, where the T-cell receptor alpha gene is placed adjacently to *MYC* (21). Ewing sarcoma (ES), rhabdomyosarcoma (RMS) and desmoplastic small round cell tumour (DSRCT), amongst other sarcomas, are characterised by examples of the first type of translocations, however, with important differences to fusion proteins like BCR-ABL1. Specifically, these chromosomal rearrangements give rise to chimeric proteins that act as abnormal transcription factors with different downstream target genes and unique novel oncogenic properties (19) (detailed 1.4 for ES).

Lastly, another mechanism leading to oncogene activation is epigenetic regulation, which is a form of gene expression control, either through direct DNA methylation or histone modifications. DNA methylation status is more commonly associated with hypermethylation of promoters of tumour suppressor genes, silencing their expression (22, 23). However, oncogene activation and overexpression is possible through promoter hypomethylation, primarily through the absence of methylcytosine residues (24). Importantly, dysregulation of chromatin remodellers can also affect the organisation of DNA, having the potential to activate oncogenes and causing vast changes to gene expression profiles (detailed in 1.5.1) (22, 23).

Tumour suppressor genes are often regarded as counterparts to oncogenes, also contributing to tumour development when aberrant, resulting in loss of function. Rather than through gain-of-function mutations, their inactivation is what results in their tumorigenic phenotype. As their name indicates, these group of genes are generally involved in processes protecting genome integrity or acting as checkpoints and performing other control mechanisms, such as ensuring orderly cell division. In this way, tumour suppressor genes may not always directly affect specific processes contributing to tumour growth, but rather, their absence increases genomic instability and mutation rates. Inactivation of these genes involves similar processes to oncogene activation, including mutations, deletions, chromosomal rearrangements, or an altered form of epigenetic control. One key difference is that tumour suppressor genes can, but do not exclusively, operate in a recessive manner. This behaviour means that one copy of the gene can be sufficient to carry out its function, and therefore, both alleles need to be inactivated to suppress its function (25). One method describing this relationship is the traditional 'two-hit hypothesis' presented by Knudson in 1971 to explain the genetic mechanism underlying the tumour suppressor retinoblastoma (Rb) transcriptional corepressor 1 gene *RB1* (25). Briefly, without an inherited mutation on one allele, developing retinoblastoma was suggested to require two mutations, one in each allele of *RB1*. In contrast, cases with a germline mutation would pass on this susceptibility, only needing one additional hit to develop this malignancy (25). Loss of heterozygosity (LOH) is often used to describe how the second copy of a mutated gene can be lost for this one to become homozygous. This is usually through a deletion encompassing a large region of DNA or even an entire portion of a chromosome through chromosomal missegregation (26).

Notably, not all tumour suppressor genes behave in a recessive manner. There are cases in which a single mutated allele can disrupt the activity of the encoded protein or can lead to insufficient protein levels (27). The first case is usually described as a dominant-negative effect where the mutated protein antagonises the function of the wild-type (WT) copy. This type of mutations affecting tumour suppressor genes are common in proteins forming complexes or polymeric structures, such as the tetrameric transcription factor p53. This protein is crucial in regulating gene expression of targets in apoptosis, DNA repair, cell growth and differentiation (18). Mutations in the tumour suppressor gene *TP53* are the most frequent alterations in cancer. Point mutations R270H and P275S have been shown to limit p53 function decreasing its tumour suppressive role in a dominant-negative fashion (28). As in oncogene activation, translocations can create fusion products in which the tumour suppressive function of a gene is lost in the novel oncoprotein. Alternatively, the fusion protein can also compete with the wild-type copy in a dominant-negative manner (detailed in 1.5).

The other exception to the two-hit hypothesis is haploinsufficiency, which describes sensitive genes that cannot tolerate a reduction in gene dosage and therefore only require one mutated allele (26, 27). There are different models of haploinsufficiency, the first describes gene dosage and the resulting stoichiometric protein levels as being under a fine balance. Over or under-expression can create an imbalance in the protein levels, which in turn affects cellular processes. Similarly, another hypothesis suggests haploinsufficiency simply reduces the amount of protein, thus limiting its function (27). Whilst both models may apply to different genes, these mechanisms paint a more diverse and complex picture of the process of acquiring genetic lesions to promote tumour development.

1.2   Replication stress as a hallmark of cancer

DNA replication stress (RS) has been proposed to be a prevalent feature, driving genomic instability in human cancers, and so contributing to tumour development (29). The sources of RS detailed in this section are directly relevant to the biological processes studied in this project and the scope of this thesis. These can be broadly divided into endogenous and exogenous causes, however, the focus here is on endogenously generated DNA damage arising from DNA replication and how this process is further dysregulated in cancer in what is known as oncogene-induced RS.

1.2.1 Endogenous sources of replication stress

DNA replication is susceptible to a vast range of exogenous and endogenous stresses, creating obstacles for the accurate copying of genetic information (Fig. 1.1). In turn, disruption of the replication fork brings replication to a stop generating DNA lesions, which can result in chromosome rearrangement, missegregation, and breakage (12, 30). These events fall under the umbrella term of RS, however, this phenomenon specifically defines the transient slowing down or stalling of the replication fork machinery (31-33). Overall, RS results in genomic instability, and can therefore contribute to malignant transformation (11, 12).
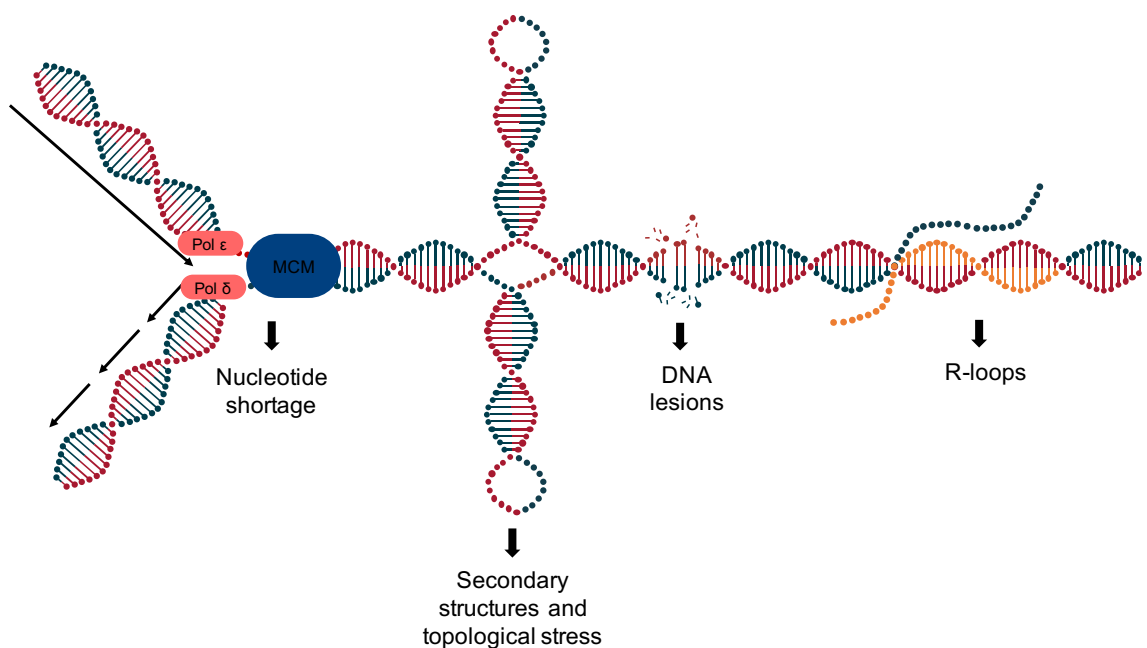
Figure 1.1 Endogenous sources of RS

Diagram showing a summary of some common sources of endogenous RS, such as nucleotide shortage, directly affecting polymerases ε and δ, secondary structures and topological stress, DNA lesions, from nicks to DSBs, and R-loops (three-stranded structures where a nascent strand of mRNA in orange binds to DNA, displacing the non-template DNA strand). Adapted from Petropoulos et al. (2019) (34).

Examples of endogenous sources of RS include unusual DNA structures that are inherently difficult to replicate. These sequences usually involve secondary DNA structures, such as hairpins and triplexes, which slow down the replication machinery and

are prone to induce DNA double strand breaks (DSBs) (30, 31, 35). Another example are G-quadruplexes, consisting of four-stranded structures rich in GC content that are commonly present near the transcription start site of highly transcribed genes (30). Some of these genes include powerful oncogenes such as *MYC* and *KRAS*, and tumour suppressor gene *PTEN* (2, 36). Other causes of endogenous RS are torsional stress ahead and behind the replication fork, taking the form of negative or positive supercoiling. Topoisomerase I and II minimise RS by creating single nicks or cutting both strands on DNA, respectively, in order to alleviate and relax positive supercoiling (35). In addition, a range of helicases are known to contribute to the resolution of these secondary structures and G-quadruplexes, for example DExH-Box Helicase 9 (DHX9), ATP-dependent DNA helicase PIF1, and regulator of telomerase elongation helicase 1 (RTEL1) (30, 35).

1.2.1.1 *Transcription and replication conflicts*

Interference between replication and transcription is another source of RS and DNA damage. One example is inappropriate hybridisation of the RNA nascent strand with a DNA template behind the transcriptional machinery, and displacement of the non-template strand (32, 33). The formation of these RNA-DNA hybrids, also named R-loops, is believed to arise when the replication fork collides with the transcriptional machinery, either co-directionally or via a head-on collision (31, 32). R-loops are naturally occurring and can have regulatory roles in gene expression (33). Their accumulation induces further RS and can lead to genomic instability; however, the mechanisms are not fully understood (33, 37). One proposition is that the loose single stranded DNA (ssDNA) in R-loops is vulnerable to cytosine deamination by activation-induced cytidine deaminase (AID) or other members of the apolipoprotein B mRNA editing enzyme, catalytic polypeptide-like (APOBEC) family of cytidine deaminases (33, 38). In this way, mutational changes in the genome are created by these conversions. As with DNA secondary structures, R-loops can be resolved by helicases (senataxin, aquarius, DHX9, PIF1) and topoisomerases (32, 33). Other important factors, mitigating RS and R-loops, are proteins in the Fanconi Anaemia (FA) pathway such as FA complementation group D2 (FANCD2), FA complementation group I (FANCI), FA complementation group A (FANCA), and flap endonuclease 1 (FEN1) (39, 40). Lastly, defects in RNA processing have been suggested to contribute to R-loop formation as in normal circumstances, these factors limit interaction between the RNA transcript and DNA undergoing replication (33).

1.2.1.2 Nucleotide metabolism and origin firing

Nucleotide metabolism and DNA synthesis are tightly linked with replication and therefore are prone to affect replication fork progression. Thus, any decrease in nucleotide supply has the potential to stall replication and produce RS (31, 41). Limited availability of deoxyribonucleotide triphosphates (dNTPs) and histone shortage results in uncoupling of the minichromosome maintenance complex 2–7 (MCM2–7) helicase and DNA polymerases (31). This creates stretches of exposed ssDNA and replication fork stalling (31). For this reason, timely and regulated activity of ribonucleotide reductase (RNR) and its catalytic subunit RRM2 is crucial. This enzyme catalyses the conversion of ribonucleotides to deoxyribonucleotides (41, 42). Expression of RRM2 rises in S-phase and is increased upon DNA damage ensuring substrate availability for replication and DNA repair (42).

Closely interlinked with nucleotide metabolism, origin firing is another key determinant of replication dynamics, and therefore, of pressures on the replication fork. In order to ensure accurate duplication of the genome in one cell cycle, careful control of origin licensing and firing in S-phase is necessary. Main regulators involve protein Ataxia Telangiectasia Mutated (ATM), Ataxia Telangiectasia and Rad3-related (ATR) kinases, and their interaction with cell division cycle 7-related (CDC7) protein kinase and cyclin-dependent kinases (CDKs), particularly CDK2 (43-45). Origin firing and replication fork rate have been found to have an inverse relationship (45). That is, a reduction in licensing factors and decrease in origin firing, will increase fork rate speed. In this way, MCM2-7 availability at replication origins and disrupting CDK2 activity in G1 can limit or prevent loading of the replisome onto DNA, respectively (12). Interestingly, having a low number of licensed origins can in turn promote increase of their own fork rate (45). One proposed explanation is through a substrate- and competition-dependent mechanism, ordinarily restraining fork rate (45). Unscheduled CDK activity through direct dysregulation, or abnormal activity upstream of CDK2 and CDC7, triggers increased origin firing. This has the potential to exhaust nucleotides and histones, as well as to maximise the possibility for collisions with the transcriptional machinery, leading to extensive RS. Regardless of how origin firing is altered, alterations to fork progression can lead to DNA being under- or over-replicated, causing genomic instability (46, 47).

1.2.2 Oncogene-induced replication stress

By definition, oncogenes result in tumorigenic properties that enable uncontrolled proliferation and cell cycle progression. These phenotypes are often achieved through direct dysregulation of DNA replication, in what is known as oncogene-induced RS (12, 31, 36, 48, 49). Of note, oncogene-induced RS also encompasses tumour suppressor genes such as deletions in *RB1*, leading to cell cycle changes and a secondary effect on replication regulation. Aberrant modifications in genes involved in replication initiation, licensing, and origin firing are all common sources of oncogene-induced RS. Additionally, these changes are the underlying mechanisms that have the capacity to increase nucleotide consumption and promote fork collisions, contributing further to RS (49).

Mutations or amplifications affecting CDK activity, Rb, and the E2F family of transcription factors can all alter licensing initiation causing unscheduled firing (31). The viral oncogene and major cause of cervical cancer, human papillomavirus (HPV) E6/7, specifically degrades Rb, dysregulating E2F transcription factor 1 activation to promote cell proliferation. Other oncogene-driven sources of RS include decrease in licensing factors, such as CDC6 and Chromatin licensing and DNA replication factor 1 (CDT1). Under normal circumstances, origins of replication are licensed in G1. If cells enter S-phase without sufficient licensed origins, it is likely that the copying of the genome will be incomplete, in what is known as under-replicated DNA (UR-DNA) (47, 50). Disruptions such as these, become problematic for equal chromosome segregation, creating genomic instability. In this context of loss of licensing factors, p53 activity can promote arrest in G1, delaying S-phase entry until origin licensing is restored (50). However, through mutations in *TP53*, this checkpoint-like mechanism is commonly lost, allowing unchecked S-phase progression and the potential accumulation of RS (50). Other key oncogenes include *CCNE1*, commonly amplified in multiple malignancies causing overexpression of cyclin E1. The increased levels of this protein bring together a number of other factors that ultimately disrupt replication and cell cycle dynamics. These include elevated CDK2 activity, disruption of the Rb/E2F pathway, shortening the length of G1 and promoting early entry into S-phase – all giving rise to nucleotide depletion and slowing replication fork progression (42, 49). A well-studied example is the proto-oncogene *MYC*, coding for a powerful transcription factor involved in proliferation, differentiation, and apoptosis (51). In two distinct models of ectopic expression of *MYC*

in cancer cell lines, induction of this gene modulated cell cycle progression, particularly increasing proliferation and the percentage of the S-phase population (52, 53). These changes can be attributed to MYC-driven transcriptional control of proteins cyclin D2, cyclin E1, CDK4, CDC25A, and members of the E2F family amongst others (51). Together, MYC's wide ranging role in the G1-S transition, replication initiation, nucleotide and protein synthesis, make its deregulation an important source of oncogene-induced RS (reviewed in (36, 51)).

Overall, this is not an exhaustive review of all causes of RS and examples of oncogene-induced RS. Other sources include reactive oxygen species and common fragile sites (CFSs), which also add pressures to the replication machinery (reviewed in (31). In addition, within oncogene-induced RS, fusions proteins that behave as aberrant transcription factors can be potent causes of RS, as it is the case in ES (described in 1.5).

1.2.3   The replication stress response

1.2.3.1   The ATR and CHK1 signalling pathway

The consequences of RS trigger a complex signalling response to enable replication fork protection, DNA damage repair, and replication fork restart. Failing to stabilise the replication machinery results in fork collapse, primarily described in the literature as dissociation of the replisome and/or formation of DSBs at these sites (30, 54, 55). ATR is the main orchestrator of the replication stress response (RSR) (reviewed in (30, 56, 57)) (Fig. 1.2). Briefly, this signalling cascade begins when stretches of ssDNA are exposed, including the displaced DNA strand in R-loops. These are sensed and protected by the heterotrimeric replication protein A (RPA), which also has wider roles in DNA repair signalling (58). As described before, exposed ssDNA results from the uncoupling of DNA polymerases ε and δ and MCM2-7 due to reduced replication fork speed. In turn, ssDNA coated with RPA causes recruitment of ATR through its obligate partner ATRIP, along with RAD9, RAD1, and HUS1, which form the 9-1-1 complex. Interaction of this complex with topoisomerase binding protein 1 (TOPBP1) and RAD17 then promotes activation of ATR. ATR signalling also involves other regulators such as Ewing's Tumour Associated Antigen 1 (ETAA1), TIMELESS/TIPIN, and CLASPIN. These events result in activation of checkpoint kinase 1 (CHK1) through phosphorylation of serine 317 (S317) and 345 (S345) (31, 59). In turn, CHK1 contributes to the RSR by incorporating cell cycle control signalling and checkpoint activation, through CDK1/2

regulation (60, 61). Also involved in this process is the kinase WEE1, reported to be phosphorylated on serine 642 (S642) by AKT (62). Arrest of cell cycle progression incorporates the DDR into these mechanisms and facilitates repair of accumulated DNA lesions arising from RS. Together with ATR, these two kinases – CHK1 and WEE1 – coordinate a concerted response to RS promoting fork stabilisation, activating dormant origin firing to ensure complete replication, inhibiting late origin firing, and arresting cell cycle progression to allow sufficient time for DNA repair (31, 56).
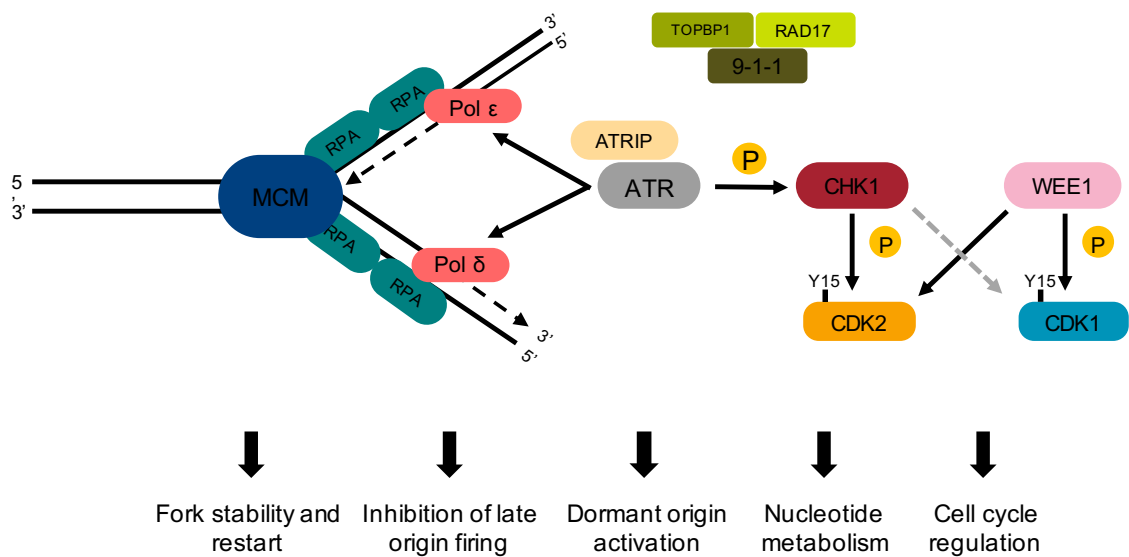
Figure 1.2 Activation and outcomes of the RSR.

Diagram summarising the RSR along with the outcomes of activation of this pathway contributing to regulate DNA replication and promote replication fork stability and protection. Uncoupling of MCM helicase and DNA polymerases ε and δ creates stretches of ssDNA, exposed to RPA binding. RPA coating protects ssDNA promoting a series of events recruiting and activating ATR. In turn, this kinase phosphorylates CHK1, which together with WEE1, incorporate checkpoint control in the cell cycle through direct phosphorylation of CDK1 and CDK2. Indirect regulation of CDK1 by CHK1 (grey arrow) occurs through phosphorylation of phosphatase CDC25C.

1.2.3.2 Further roles for ATR and CHK1

Alongside the previously described roles, there are additional ATR-specific mechanisms that contribute to minimising RS. One example involves ATR antagonising downregulation of E2F transcription factor 1 (E2F1), which increases expression of RRM2 to ensure sufficient nucleotide synthesis (61). This kinase also inhibits origin firing through phosphorylation and stabilisation of protein mixed-lineage leukaemia

(MLL), also known as acute lymphoblastic leukaemia-1 (ALL-1), or histone-lysine N-methyltransferase 2A (KMT2A) (63). Stable MLL can then methylate H3K4 to prevent loading of CDC45 at replication origins (63). CDC45 is a replication factor and critical component in activated MCM2-7. Whilst there are mechanisms that are ATR-dependent alone, there is also an overlap with CHK1 activity. For example, CDC45 loading can also be inhibited by CHK1 through interaction with TRESLIN (64).

Through independent and combined processes, ATR and CHK1 mount a response to alleviate pressures on the replication fork, avoiding collapse of the replisome (61, 65). Their concerted activity is also crucial for restarting stalled replication forks (30). This process requires the supply of dNTPs to have resumed and the obstructing DNA lesions to have been repaired. A characteristic step during stabilisation and restart is fork reversal and the formation of a 'chicken foot' structure (66). This process sees the re-annealing of the parental DNA strands and binding of the newly synthesised ones, which are then forced out into this distinctive shape (66). Checkpoint activation and ATR signalling are important to limit how frequently reversed fork structures form and to protect them from nucleolytic cleavage, respectively (66, 67). The benefits of these structures towards stabilisation and restart have been debated continuously, with evidence suggesting fork reversal can also lead to fork collapse if not controlled (67, 68). Often, fork restart will need remodelling of these structures through DNA helicases. Several of these proteins have been linked to contribute to processing replication forks *in vitro*. Examples include helicases INO80, SMARCAL1, and others in the RECQ family such as Bloom RecQ Like Helicase (BLM), WRN RecQ Like Helicase (WRN), and RECQ1, and in the FA family such as FANCM, FANCJ, (35, 66, 69, 70). Testing whether their roles are maintained *in vivo* remains technically challenging.

1.2.4   WEE1 checkpoint kinase and cell cycle regulation

Traditionally, ATR and CHK1 kinases have been regarded as the main actors in the RSR preserving genomic instability. This is partially due to WEE1, the terminal kinase in this axis, being primarily thought of as the regulator of the G2/M transition, with little bearing on DNA replication. In recent years, however, WEE1 has been found to play an important role in relaying the response alleviating RS and ensuring orderly cell cycle progression in S-phase (Fig 1.3). These emerging roles, together with its function controlling mitotic entry, make this tyrosine kinase relevant in the discussion of the RSR.
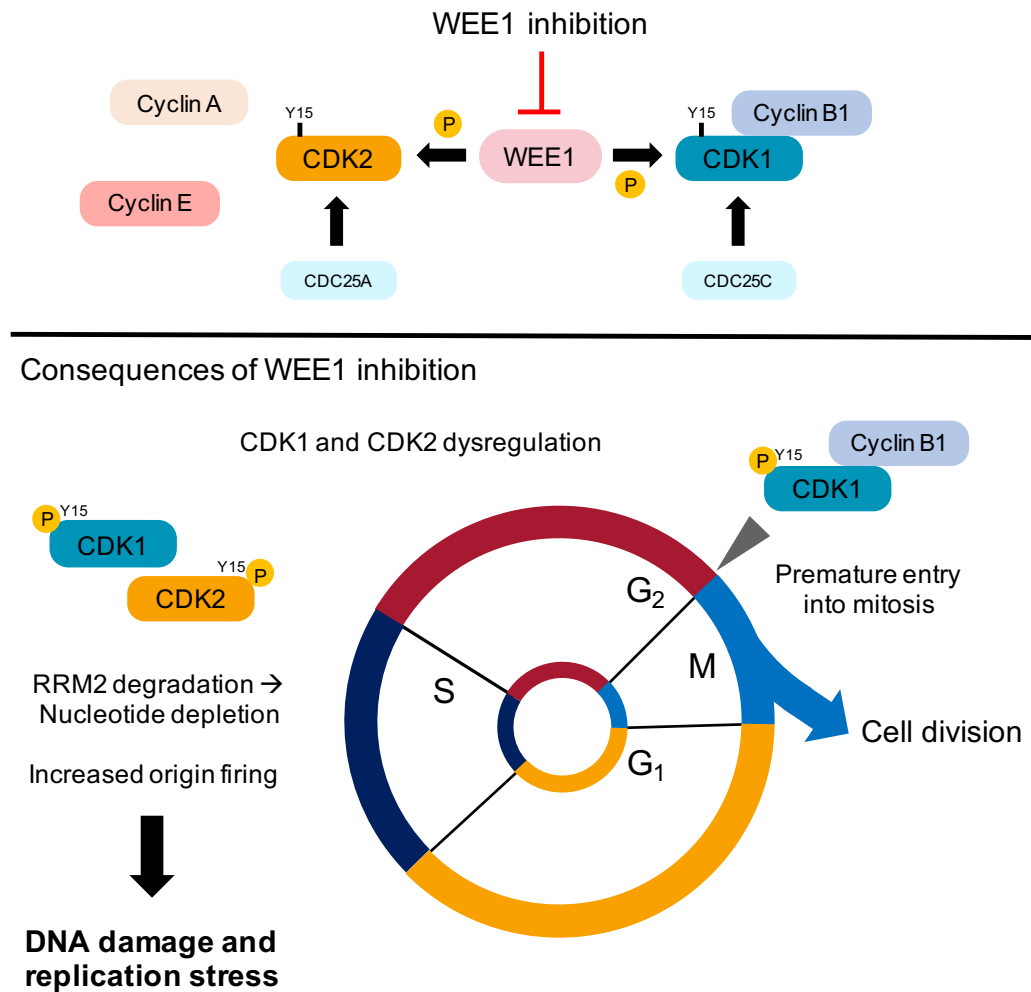
Figure 1.3 Consequences of WEE1 inhibition and CDK1/2 dysregulation

WEE1's role in the G2/M transition through control of CDK1 activity by phosphorylation of tyrosine 15 (Y15) stopping entry into mitosis promoted by the CDK1-Cyclin B1 complex. CDK1's homolog, CDK2, is also phosphorylated by WEE1 leading to unscheduled activation during S-phase and complex formation with cyclin A and cyclin E throughout S-phase. Dysregulated activity of CDK1 and CDK2 contributes to DNA damage and RS through degradation of RRM2 and increased origin firing.

WEE1's activity relates to the regulation of the G2/M transition and controlled entry into mitosis (55). Briefly, upon activation by CHK1, WEE1 phosphorylates tyrosine 15 (Y15) on CDK1, preventing complex formation with cyclin B1. Inactivation of the CDK1-Cyclin B1 complex stops cell cycle progression, enabling sufficient time to repair DNA damage prior to cell division (55). The role of WEE1 on CDK1 is in balance with CDC25C phosphatase, where the determining factor is the phosphorylation status of Y15 on CDK1 (71). Removing this inhibitory mechanism alone, activates the CDK1-Cyclin

B1 complex and promotes entry into mitosis (71). Overall, coordination of the activity and expression of WEE1 and CDC25C determines cell cycle progression and timely cell division (71, 72). Similarly, this regulatory mechanism applies to CDK1's closest homolog, CDK2, albeit the main phosphatase dephosphorylating CDK2 is CDC25A (43, 73). As mentioned before, CDK2 is primarily responsible for replication initiation through MCM2-7 activation and replisome loading onto DNA, early in G1 and S-phase (43, 44). Functional studies of WEE1 in cancer cells have identified that in its absence, CDK2 dysregulation causes increased origin firing and degradation of RRM2 (41, 42, 55). These effects have the potential of rapidly depleting nucleotide pools and other rate-limiting factors of replication, thus contributing to RS and DNA damage (42, 55). In the same context of loss of WEE1 activity, uncontrolled CDK1 activation overrides the G2/M checkpoint resulting in premature entry into mitosis (55, 74). The consequence of these two effects converging is that DNA damage arising from RS in S-phase would remain unrepaired, as cells advance through the cell cycle. Altogether, this results in severe problems for chromosome segregation, cell division, and genome stability.

With the catastrophic events arising from loss of WEE1 activity, it is not surprising that this gene is regarded as a common essential gene, showing high pan-cancer dependency in the Broad Institute's Cancer Dependency Map database (75, 76). WEE1's role in safeguarding the genome through fine-tuning of both CDK1 and CDK2 activity, expands on its function beyond G2/M control. Similarly, the ingrained view of CDK2 acting in S-phase and CDK1 in G2/M alone has been put in question. Research in the last decades has provided increasing evidence of compensatory roles for these two kinases (43). An important example is the viability of *CDK2-/-* mice, potentially due to functional substitution by CDK1, with CDK1 being also activated by cyclin E (44). Despite overlapping functions, there are unique effects to CDK1 activity. One relevant example is CDK1-mediated processing of replication intermediates through endonuclease activation (77, 78). Consistent with the rise in CDK1 expression prior to mitotic entry, SLX4 along with its binding partner MUS81, catalyse processing of stalled replication forks (78). This serves as a protective mechanism to ensure these intermediates do not interfere with chromosome segregation and cell division (55, 78). However, dysregulation of CDK1 through abnormal WEE1 signalling, has the potential to induce cleavage of active replication forks during S-phase, inducing chromosome breakage (78).

In summary, WEE1's involvement in the RSR is underpinned by its control of CDK1 and CDK2. Regardless of potential redundancy between these kinases, dysregulation of both induces RS, highlighting the importance of WEE1 in the ATR-CHK1 axis in protecting the genome.

1.3 Targeting double strand break repair and replication stress in cancer

1.3.1 DNA Double strand break repair

The concerted work of ATR, CHK1, and WEE1 triggers a series of processes that alleviate RS and promote fork progression. Amongst these mechanisms, checkpoint activation creates a pause in the cell cycle enabling repair of lesions caused by endogenous and exogenous stresses, such as replication fork collapse and DNA-damaging agents, respectively (30, 31). The DNA damage response (DDR) is complex and multifaceted process, incorporating a range of parallel mechanisms, such as regulation of transcription and chromatin remodelling in order to facilitate access to the damaged site (11). In terms of the actual process of repairing DNA damage, this encompasses a number of different pathways, which depend on the type and context of the DNA lesions (11). The cell cycle phase, for example, can determine the repair pathway of choice due to the availability of DNA templates for faithful copying of the damaged region (11). Whilst there are several forms of DNA damage including base mismatches, base adducts and cross-links, this section is primarily focused on DSB signalling and repair, as these are the most common lesions occurring at stalled replication forks (12, 30). Notably, DSBs are a major driver of cancer development contributing to genomic rearrangements, whilst also being highly toxic and can ultimately inducing cell death (12, 30, 48, 59).

The two major and widely studied pathways in DSB repair are non-homologous end joining (NHEJ) and homologous recombination (HR). In addition to ATR in the RSR, the main proteins conducting the activation of these repair pathways are ATM and DNA protein kinase catalytic subunit (DNA-PKcs). Together, these three phosphoinositide 3-kinase (PI3K)-related proteins have a degree of overlapping functions and substrates, and are crucial factors preserving genome stability (57). The majority of DSBs are largely repaired through NHEJ, which primarily involves heterotrimer DNA-PK, consisting of

Ku (70 and 80 kDa subunits) and DNA-PKcs. As its name indicates, this repair mechanism consists of ligating two DNA ends without the need of a homologous template (79). In contrast to HR, which commonly uses a sister chromatid as a template and therefore is limited to S and G2 phases, NHEJ can operate throughout interphase. Additionally, some NHEJ factors are functionally flexible meaning they can operate in the absence of others (79) . NHEJ is initiated by DNA-PK recruitment to DSBs through heterodimer Ku70 and Ku80. Its activity promotes DNA-end tethering and further recruitment and stabilisation of key additional NHEJ factors, such as XRCC4, XLF, and DNA ligase IV. Assembly of these factors contributes to alignment and ligation of the broken DNA-ends, completing their repair (79). If necessary, DNA-PK can coordinate additional processing of DNA-ends through recruitment of factors like endonuclease Artemis (79). Regarding the fidelity of this DSB repair mechanism, NHEJ is often broadly described as error-prone due to the lack of a homologous template as HR repair. However, this an oversimplified view with growing evidence of the conservative nature of the canonical NHEJ pathway (80). Still, when canonical NHEJ fails, the activity of alternative NHEJ can be highly mutagenic, generating lesions at the repair site (80). Ultimately, NHEJ is an important and flexible pathway, and when its core factors are mutated, this leads to radiosensitisation and genomic instability.

DSBs created by collapsed replication forks in S-phase are one-ended, and thus are primarily repaired through HR, as the attempt of repairing one-sided DSBs by NHEJ would result in chromosomal rearrangements and translocations (81). For these reasons, successful activity of the RSR relies on effective DSB repair to follow up on the lesions resulting from replication fork stalling and collapse (59). Exploiting this partnership has been the focus of many anticancer therapies due to the presence of oncogene-induced RS and genetic alterations in 'caretaker' genes, specifically in the HR pathway (59, 74, 82, 83). This form of DNA repair involves DNA-end resection to produce ssDNA tracts for strand invasion of the sister chromatid template for faithful copying and repair of DSBs (84, 85). Initially, upon DNA damage, histone H2A histone family member X (H2AX) is phosphorylated on serine 139 (S139) by ATM, forming the characteristic marker of DNA damage γH2AX (86, 87). H2AX can also be phosphorylated by DNA-PK and ATR (86). DSBs decorated with γH2AX are then sensed by the protein mediator of DNA checkpoint 1 (MDC1), which is further phosphorylated and stabilised by ATM (88). At this point, MDC1 interacts with the MRN complex containing MRE11-Rad50-Nibrin (NBN,

previously NBS1), and through a positive-feedback loop, it can further recruit ATM through its activator NBN (89). Following DSB recognition, exonuclease activity of MRE11 in MRN together with CtIP coordinate DNA resection to produce ssDNA (90, 91). BRCA1 is then involved downstream of resection and also has an antagonising relationship with p53-binding protein 1 (53BP1) in which it promotes its removal from DSBs during S-phase to promote HR in favour of NHEJ (92). Stretches of ssDNA are bound by RPA and serve as probes for finding a homologous template (93). At the core of this step is the activity of Rad51, which together with mediator proteins (XRCC2, XRCC3, RAD51B, RAD51C, and RAD51D and Rad57), BRCA1, and BRCA2 overcome the inhibitory effect which RPA has on RAD51 to successfully load this recombinase and form RAD51-ssDNA filaments (84, 85, 93). In a step termed synapsis, binding and invasion of a homologous duplex DNA is catalysed by Rad51 leading to the formation of a heteroduplex DNA, commonly known as a D-loop (85, 93). Lastly, DNA synthesis takes place using the homologous invaded strand as a template. In summary, coordination of HR and NHEJ by ATM and DNA-PK, together with ATR sitting at the top of the RSR, oversee mechanisms of DNA repair preserving genome integrity.

1.3.2   Synthetic lethality and targeted DNA repair therapy

Increased understanding of the impact of DNA repair factors in cancer cells through functional experiments investigating the deficiencies created by their absence, has led to the identification of targetable synthetically lethal relationships (83). Synthetic lethality describes a relationship between two genes, that only when simultaneously altered, results in cell death (83). A well-studied example of this is the use of inhibitors of poly(ADP-ribose) polymerase (PARP) in the context of *BRCA1/2* deficiencies (82, 94). After over a decade of work, this approach has now been successfully integrated as a targeted treatment in the clinic with approval of the European Medicines Agency (EMA) and the Food and Drug Administration (FDA) (83). These enzymes operate as sensors of DNA damage, binding to DNA breaks and mediating single strand break (SSB) repair, particularly through base excision repair (BER) (95). Additionally, PARP1 and PARP2 have roles in DSB signalling, and extend this cascade through PARylation and recruitment of other effectors in the DDR (82, 96, 97). More recently, however, the mechanism of action behind their cytotoxicity has been linked to their 'trapping' on DNA (83, 95). Specifically, PARP inhibition blocks autoPARylation which is necessary for its release from DNA. In turn, trapped PARP impairs replication fork progression and can

potentially cause further DSBs (83, 95). The inability to repair these lesions at the replication fork through HR, results in alternative repair pathways (NHEJ) being used. These other non-conservative forms of repair are more prone to causing genetic deletions and rearrangements leading to cell death and/or genomic instability (79). Since the discovery of this vulnerability, several other factors contributing to an HR-deficient setting have been identified and demonstrated to confer sensitivity to PARP inhibition when disrupted *in vitro* (83). The success of this synthetic lethal interaction has served as a proof-of-concept of the therapeutic potential these relationships can have as anticancer treatment (83). These interactions can be extrapolated beyond HR-deficiencies to other molecular mechanisms that preserve genomic stability. As cancer cells develop dependencies on these transformed molecular states, they become vulnerable to chemical inhibition. Through empirical and predictive methods, such as genetic screens and computational tools, further synthetic lethal interactions can pave the way for identifying novel treatments.

1.3.3 Targeting the replication stress response in cancer

Recently, targeting oncogene-induced RS has become an attractive area to develop new therapeutic strategies (56, 59). As described before, the presence of genetic alterations causing RS, triggers a series of changes enabling cells to deal with the newly acquired pressures on replication and increased DNA damage (98). In this way, cancer cells can become addicted to expression of factors protecting replication fork progression and genomic stability (59). Amongst these proteins, ATR, CHK1, and WEE1 have been the focus of drug discovery projects developing drug candidates for clinical testing (Fig. 1.4). Currently, these compounds are undergoing trials for several malignancies as monotherapies and in combination with DNA-damaging agents (99-102). The main rationale behind these combinations is to inhibit the response mitigating oncogene-induced RS and exacerbate the already present genotoxic damage, pushing cells towards cell death. Based on the increased dependency on these mechanisms, it is believed that, clinically, there is a therapeutic window that can be exploited. Additionally, it has been suggested that the partnership between the RSR and other pathways of DSB repair, particularly HR, make tumours defective in HR vulnerable to inhibition of the ATR-CHK1-WEE1 axis (56, 67). One example illustrating this, is the observation that cyclin E1 amplification, causing RS, is mutually exclusive with mutations on *BRCA1/2* and in breast cancer (103). This means that to repair DSBs arising from RS due to cyclin E1

overexpression, functional BRCA1/2 and proficient HR are needed (103). This suggests that the use of inhibitors of the RSR could have a wider impact beyond malignancies with traditional oncogenes causing RS. Regarding the potential for combining these agents with existing chemotherapies, RS-inducing agents such as topoisomerase I inhibitors have shown strong synergistic effects (104). Given their mechanism of action, agents inducing interstrand crosslinks, PARP inhibitors, and nucleoside analogues have the potential to increase cytotoxicity in combination with ATR inhibitors (56, 105-107). Synergistic effects between CHK1 inhibition and gemcitabine has also been tested in different malignancies in pre-clinical models and in patients (100, 108-110). WEE1 inhibition has also been proposed and tested as a single-agent and in combination (39, 54, 99, 111-114). These compounds and drug targets have important mechanistic differences that will need to be understood to harness their potential in the clinic. Altogether, the increasing evidence of an altered DNA replication state in cancer, and the genomic instability stemming from it, make targeting the RSR an attractive therapeutic option.
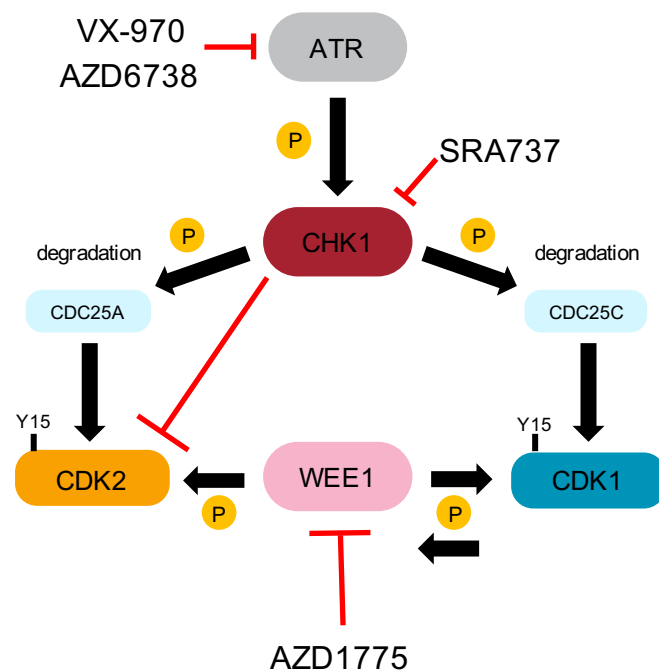
Figure 1.4 Targeting the ATR-CHK1-WEE1 axis in the RSR.

Clinical drug candidates against the ATR-CHK1-WEE1 axis in the RSR. ATR activity links replication fork protection and stability with cell cycle checkpoint activation by phosphorylating CHK1, and in turn WEE1 is phosphorylated by CHK1. Activity of these kinases can be chemically inhibited disrupting their protective function on DNA replication and genome integrity.

1.4 Ewing sarcoma

Having introduced biological mechanisms relating RS and therapeutic targeting the RSR as an anti-cancer therapy, these relationships will now be explored in in the context of ES.

1.4.1 Overview

ES belongs to the family of small blue round cell tumours (SBRCTs), a group of neoplasms characterised by their histology of small undifferentiated cells and a blue staining with haematoxylin and eosin (H&E). This highly aggressive malignant tumour is found in bone and soft-tissue. It is the second most common bone malignancy in children, adolescents, and young adults with around 100 patients diagnosed every year in the UK, with an average age of 15 (115, 116). Treatment of localised disease has proven to be effective with an approximate 5-year survival rate of 70%, however, outcomes in patients with metastatic and relapsed disease are significantly worse, dropping to a 5-year survival rate of <30%. At the time of diagnosis, around 20-25% of patients present disseminated disease, highlighting the need for novel therapies tackling this form of the disease. Importantly, over the past decades, treatments for this sarcoma have remained largely unchanged, with multi-agent chemotherapy together with resection and/or radiotherapy still being the standard of care. Nevertheless, there have been adjustments to the regimens, with modifications to the chemotherapeutics agents and schedules used.

1.4.2 Genetic alterations and translocations in Ewing sarcoma

ES is characterised by chromosomal rearrangements between the gene *EWSR1* (EWS RNA binding protein 1), encoding for RNA-binding protein EWS (hereafter EWS), and members of the E-twenty-six-specific sequence, or E26 transforming sequence (ETS)-domain family of transcription factors (117, 118). The most common translocation is t(11;22)(q12;q24), in which gene Friend Leukaemia Integration 1 (*FLI1*) on chromosome 11 fuses with *EWSR1* on chromosome 22 (118) (Fig. 1.5). This occurs in approximately 85%-90% of cases. Within this fusion type, different breakpoint regions in the *EWS-FLI1* transcript give rise to four different subtypes of the EWS-FLI1 fusion protein. Fusion subtype I between exons 1-7 of *EWSR1* and 6-9 of *FLI1* is the most predominant (Table 1.1) (118). The distinct fusion transcripts for *EWS-FLI1* are not considered to be prognostic factors (119). Similarly, the multiple variants of EWS-ETS fusions produce

comparable phenotypes, without modifying clinical presentation and outcome (120) (Table 1.1). Overall, these observations suggest that there is genetic redundancy in the drivers of this sarcoma. This can be partially explained by the shared canonical binding motif of ETS transcription factors, which reduces the potential variation in the fusions' DNA-binding ability, and therefore downstream targets (16, 121). Additionally, EWS remains constant as a binding partner across ES fusion variants, maintaining its contribution and functional roles in the chimeric oncoprotein. This functional interchangeability is also seen with proteins FUS and TAF15, that together with EWS, make up the FET family of RNA-binding proteins. These three FET proteins have important roles in transcription, RNA processing and transport, and DNA repair (122). Fusions involving these proteins are also seen in other sarcomas, usually occurring between their N-terminal domain (NTD) and the DNA-binding domains of different transcription factors. One example is DSRCT, where *EWSR1* is fused with the Wilms tumour transcription factor (*WT1*) gene to create EWS-WT1, found in 95% of cases of DSRCT (118, 123). Fusions containing the paralogues of EWS are seen in myxoid liposarcoma (EWS-CHOP and FUS-CHOP) and extra skeletal myxoid chondrosarcoma (EWS-NR4A3 and TAF15-NR4A3) (124, 125).
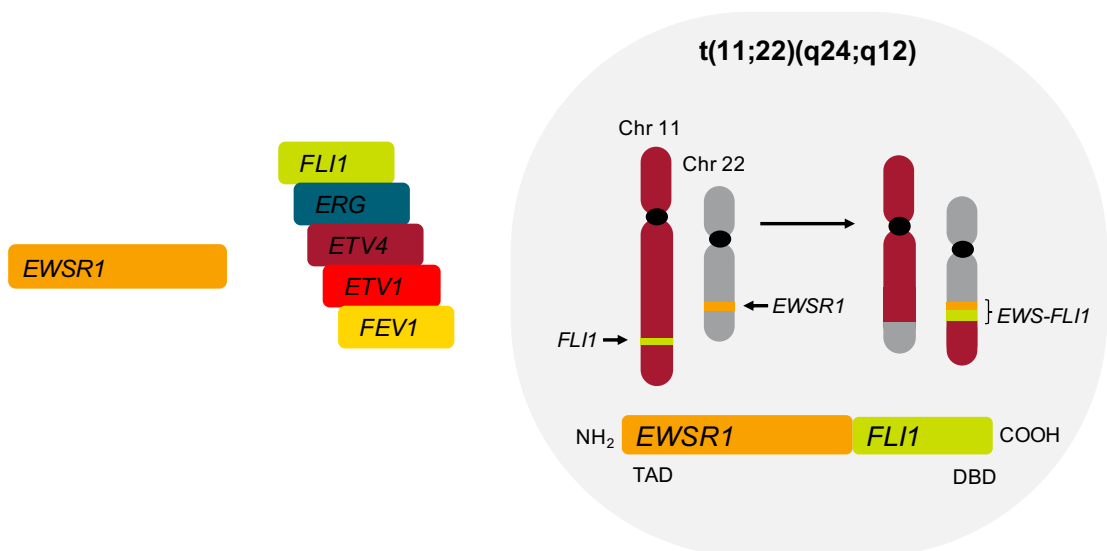
Figure 1.5 *EWS-FLI1* fusion gene formation

Characteristic chromosomal rearrangements leading to fusion genes between *EWSR1* and ETS family members in ES. The *EWS-FLI1* fusion gene is the most common product of these translocation, coding for an oncoprotein containing *EWSR1*'s transactivation domain and *FLI1*'s DNA-binding domain.

Table 1.1 EWS-ETS fusion genes in Ewing sarcoma

Fusion protein	Type of sarcoma	Translocation	Frequency (%)	Fusion type	Reference
EWS-FL1	ES	t(11;22)(q24;q12)	~85%	I (exon 7/exon 6)	(117)
				II (exon 7/exon 5)	
				III (exon 10/exon 6)	
				IV (exon 7/exon 7)	
EWS-ERG		t(21;22)(q22;q12)	5-10%	exon 7/exon 6, 7 or 9	(126)
EWS-ETV1		t(7;22)(p22;q12)	<1	exon 7/exon 11	(127)
EWS-ETV4		t(17;22)(q12;q12)	<1	exon 7/exon 9	(128)
EWS-FEV		t(2;22)(q33;q12)	<1	exon 7/exon 2	(129)

1.4.3 Somatic mutations and their phenotypic relevance

There have been three main large-scale genomic studies of ES tumours and cell lines, describing their genome as silent, with a low somatic mutation rate at diagnosis (130-132). The most common inactivating mutations are found in *STAG2* (15-22%). This gene encodes for protein stromal antigen 2 (STAG2), a key subunit of the cohesin complex, also consisting of STAG1, SMC1A, SMC3, and RAD21 (133). This ring-like complex holds sister chromatids together and is cleaved during cell division to allow chromosome separation. Loss of *STAG2* has been associated with defective cell division and aneuploidy (134). Additionally, STAG2 depletion has been found to be synthetically lethal with subunit STAG1 (133, 135). Other frequent mutations in ES are found in *TP53*, present in approximately 5-7% of tumours. In terms of their prognostic value, mutations in *STAG2,* alone or together with *TP53,* have been linked to poorer outcome (130-132). The relationship between these two mutations was explored in a recent study by Mondal *et al.* (2019). This work showed that in non-transformed cell lines, depletion of *STAG2* induced cellular senescence seen as intra-S-phase arrest and disruption of replication fork progression, leading to replication fork collapse and DNA damage (133). However, the intra-S-phase arrest was overridden in the context of a *TP53* mutation, establishing a functional link between the co-occurrence of these mutations. It can be hypothesised that inactivation of p53 enables the genomic instability, induced by *STAG2* loss, to become tumorigenic and account for poorer outcomes in these tumours. It remains to be addressed whether *STAG2*-deficient but *TP53* WT ES tumours have additional mechanisms to resolve replication fork instability and maintain cell cycle progression. The genomic instability of *STAG2*-deficient has been exploited with PARP1 inhibitors in a

synthetically lethal relationship in glioblastoma and acute myeloid leukaemia (AML) (136).

Homozygous deletion of the tumour suppressor *CDKN2A* is the other major mutation reported in 10-22% of cases of ES (130-132). The *CDKN2A* locus encodes for cyclin-dependent kinase inhibitors (CDKi) p14 and p16, involved in activation of p53 and regulation of G1 checkpoint control. Briefly, p14 binds to mouse double minute 2 (MDM2), triggering its degradation, which in turn prevents degradation of p53 (137). The other CDKi, p16, antagonises the activity of CDK4/6, which ordinarily phosphorylates Rb. Inhibition of the cyclin D-CDK4/6 complex maintains Rb hypophosphorylated and bound to the E2F1, resulting in G1 arrest (137). Inversely, lack of p16 causes hyperphosphorylation of Rb, through dysregulated CDK4/6, leading to dissociation of E2F1. E2F1 transcription then promotes S-phase entry and cell cycle progression (137). Together, *CDK2NA* loss results in degradation of p53 and abrogation of the G1 checkpoint. Interestingly, *CDKN2A* deletions and *STAG2* mutations were found to be mutually exclusive in tumour samples and cell lines (130). Whilst this mainly holds true, cell lines TC32 and WE68 possess both types of mutations (see Materials and Methods, table 2.2). Importantly, genetic alterations in ES cell lines occur at a higher frequency than in patients' tumours (130, 131). Regarding the genetic landscape at relapse, one study by Crompton *et al*. (2011) identified an increase in the mutation rate post-treatment, suggesting important acquired differences between diagnosis and relapse (131). This has raised the interest in ES tumour heterogeneity and how chemotherapeutic treatments can potentially influence tumour evolution.

1.4.4 Copy-number variation

Gain of whole chromosomes 8 and 12, and the 1q portion of chromosome 1 are the most common copy-number gains in this tumour type (130). In particular, 1q gain has been linked to poorer outcome and is seen in approximately 25% of cases. 1q gain is also associated with 16q loss. This is the most common copy-number loss, together with deletion of the portion of chromosome 9, where the *CDNK2A* locus is (131). Interestingly, 1q gain was found to be more common in treated samples than diagnostic samples, suggesting a role for therapeutic interventions in driving this form of genetic alterations. Furthermore, investigations into candidate genes contributing to worse prognosis with 1q gain have proposed gene *DLT* (also *CDT2*), with functions in cell cycle control (138).

1.5 Novel oncogenic properties of EWS-FLI1

Functional work in ES has primarily focused on studying the most frequent fusion protein of this malignant tumour, EWS-FLI1. As the main oncogenic driver, the fusion harnesses different molecular mechanisms shaping its transcriptional programme and overall promoting oncogenic transformation. Here, three key areas of ES pathophysiology: (i) epigenetic dysregulation, (ii) EWS-FLI1-driven heterogeneity, and (iii) transcriptional dysregulation are introduced, highlighting some of the relevant mechanisms to this sarcoma driving the development of novel therapeutic opportunities.

1.5.1 EWS-FLI1-mediated epigenetic dysregulation

Chromatin exists in a dynamic state, constantly exposed to modifications that alter its conformation, which in turn affect DNA availability and access of the transcriptional machinery (22). Broadly, these modifications involve direct changes on DNA or on histone tails, creating docking sites that enable new interactions and recruitment of additional proteins. In this way, specific gene loci are repressed or activated, depending on the chromatin state (22). One example of these modifications is acetylation of lysine residues on the histone tail, which neutralises the positively charged histones, loosening the binding of the negatively charged DNA (22, 139). Acetylation of lysine 27 in histone 3 (H3K27Ac) is a major epigenetic mark, characteristic of open chromatin and enhancer activity (140). Together with histone tail modifications, chemical changes on DNA bases such as cytosine methylation, are known to contribute to establishing the chromatin environment. Tumour suppressor gene silencing through aberrant hypermethylation of CpG islands on gene promoters is a common alteration in cancer (22, 23). In fact, genome-wide profiling studies have found this mechanism to affect a greater number of genes compared to inactivating mutations in protein-coding genes (141). In addition, one attractive aspect of cancer epigenetics is the reversible nature of these modifications, opening up the possibility of chemically reversing malignant transcriptional programmes.

The EWS-FLI1 oncoprotein acts as an aberrant transcription factor capable of binding DNA, and regulating various transcriptional targets, through two alternative binding mechanisms. The first one involves recognising the canonical ETS binding motif containing a GGAA/T core sequence (16, 121, 142). The second mechanism, a novel oncogenic property of the fusion, requires interaction with a series of tandem GGAA

repeats (121, 142, 143). It is through these microsatellite repeats that EWS-FLI1 can epigenetically regulate further activation and repression of its target genes. In this way, EWS-FLI1 has been described as a pioneer transcription factor inducing *de novo* enhancers to establish its oncogenic programme (121, 143, 144). Like traditional enhancers, these interact with the promoter region of the fusion's target genes to coordinate and promote transcriptional activation (140, 145). Characteristically, these regions are rich in GGAA microsatellite repeats where the fusion can bind to (121, 142). Originally, it was demonstrated that upon insertion and expression of EWS-FLI1 in mesenchymal stem cells (MSCs), chromatin conformation switched into a more 'open' state at the site of these GGAA repeats. This was marked by global methylation of lysine 4 in histone 3 (H3K4me1), typical in active transcription, together with a high signal of enhancer activity in the form of H3K27Ac, the most strongly affected mark (143, 146). These findings have led to a model of epigenetic rewiring at GGAA tandem repeats that increases chromatin accessibility, driving transcription of EWS-FLI1 target genes (Fig. 1.6) (143, 144, 147).

Within this model, one of the key complexes associated with ES tumourigenesis is the ATP-dependent chromatin remodelling complex Brg/Brahma-associated factors (BAF), also known as Switch/Sucrose Non-Fermentable (SWI/SNF) (144). This large multi-subunit complex is combinatorially assembled resulting in different configurations with diverse and tissue-specific functions (148). Through immunodepletion using an antibody for transcriptional activator BRG1 (one of the two mutually exclusive catalytic ATPase subunits in the BAF complex), EWS-FLI1 was significantly depleted, indicating association between the fusion protein and this chromatin remodelling complex (144). The reciprocal experiment using EWS as the probe only caused partial depletion of BAF complexes, suggesting EWS-FLI1 binding is limited to a small percentage of these complexes. Functionally, fusion protein-bound complexes were found to overlap GGAA tandem repeats (Fig.1.6); this interaction was dependent on EWS-FLI1, as shRNA depletion of the fusion removed the presence of BAF on these sites (144). Ectopic expression of EWS-FLI1 in MSCs recapitulated association with BAF and occupancy at GGAA regions, further confirming these as novel oncogenic properties of the fusion protein in ES. Knockdown of BAF155, one of the highly conserved core subunits, in ES cell lines also decreased expression of EWS-FLI1 target genes. Overall, hijacking of chromatin remodelling complexes allows EWS-FLI1 to carry out its pioneer activity in

gene expression regulation. Importantly, the work by Boulay *et al*. (2017) narrowed down the key functional regions in the fusion to a set of tyrosine residues found in the prion-like domain of EWS (144).
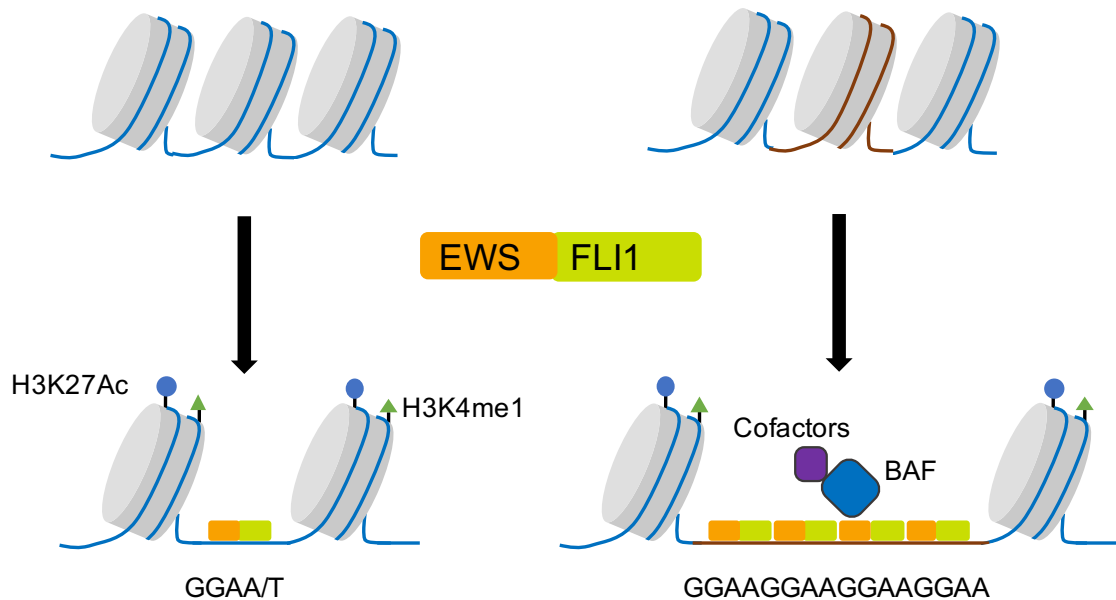
Figure 1.6 EWS-FLI1-mediated epigenetic dysregulation and transcriptional reprogramming.

Diagram showing EWS-FLI1 mechanisms of DNA binding and transcriptional regulation through the canonical ETS core motif GGAA/T and GGAA microsatellite repeats in the fusion protein's target genes. At these regions, recruitment of chromatin remodelling complexes, such as BAF and additional cofactors, enables changes in chromatin conformation marked by H3K27Ac and H3K4me1 marks, which are characteristic of open chromatin and enhancer activity. This contributes to creating *de novo* enhancers to reprogramme transcription in ES cells. Model adapted from Boulay *et al.,* (2017) and Grünewald *et al*., (2018) (144, 147).

Furthermore, large chromatin-remodelling complexes often have individual methyltransferases and demethylases directly changing the epigenetic status through the addition and removal of methyl groups on histone tails. A relevant mediator of EWS-FLI1 activity is the Nucleosome Remodelling Deacetylase Complex (NuRD; also known as Mi-2), a multi-subunit chromatin-remodelling complex commonly associated with repression of transcriptional activity (149, 150). Similar to the BAF complex, different combinations of the subunits in the NuRD complex suggest possible functional specificity and context dependent roles in regulating chromatin conformation (151, 152). Lysine-specific demethylase 1 (KDM1A; also known as LSD1, AOF2, and BHC110) provides

part of the catalytic activity in this complex, contributing to regulation of gene expression in ES. Targeting this demethylase has been shown to reverse the ES transcriptional target, making it an attractive therapeutic target (149, 150). Other known histone modifying enzymes altering the epigenetic landscape in ES include the methyltransferase enhancer of Zeste Homolog 2 (EZH2), whose expression is upregulated through promoter activation by the fusion (153). EZH2 belongs to the polycomb repressor complex 2 (PRC2), which methylates lysine 27 on histone 3 (H3K27) to silence gene expression in ES and promote tumourigenesis (153). Together, these proteins provide therapeutic targets to inhibit EWS-FLI1-driven transformation and novel biomarkers of its activity.

1.5.2 Cell-of-origin and tumour heterogeneity

Identifying the developmental origin of ES remains an open question in the study of this sarcoma. Given the vast transcriptional changes through epigenetic dysregulation, identifying the identity of the ES cell-of-origin has been very difficult. Its varied and heterogeneous histopathology, encompassing undifferentiated, mesenchymal and neuroectodermal features, has led to different potential cell-of-origin candidates being proposed (146, 154, 155). These include early bone progenitors, such as neural-crest-derived stem cells and bone-marrow-derived MSCs, which have also been shown to be able to survive expression of EWS-FLI1 (146, 154). These findings propose that ES arises from an oncogenic event during the development of this lineage, although the timing of this event can result in slight variations in their histological and molecular profile (147, 156). Consistent with this, studies examining the DNA methylation status of ES tumour samples have not identified clear subtypes, but rather a spectrum of epigenetic signatures. This continuum was described to range from a pluripotent stem cell-like profile to a more mesenchymal one at the other end, contributing to the clinical heterogeneity in ES (157). A recent report also verified this proposition by using transcriptomic analysis to identify ES-like tissues and permissible environments for EWS-FLI1 (40). The tissues found included induced-pluripotent stem cells (iPSCs) and human embryonic stem cells (hESCs), in addition to other previously known permissible contexts such as neural crest cells, neural progenitors, and MSCs (40, 154). In this study, an algorithm grouping samples based on transcriptomic signatures and highlighting subtle transitions amongst them, placed ES tumours along a normal developmental transition between pluripotent/neuroectodermal to mesodermal tissues (40). This is consistent with the role of EZH2 in maintaining stemness and blocking neuroectodermal differentiation (153).

Overall, there is greater understanding of the context in which EWS-FLI1 arises and how it modifies these developmental transitions to give rise to the observed tumour heterogeneity in ES. Uncertainty regarding the cell-of-origin has affected understanding the process behind generation of the fusion gene in ES. However, recent analysis have suggested this to involve chromoplexy, a series of concerted chromosome rearrangements that ultimately form the *EWS-FLI1* fusion gene, rather than only a standard translocation between two chromosomes (156). However, the underlying causes driving the formation of the EWS-ETS fusions remain unknown.

In addition to EWS-FLI1-driven epigenetic and transcriptomic changes determining tumour heterogeneity, expression levels of the fusion have been suggested to modify ES intra-tumoural populations and cell behaviour (158). This was originally studied in the context of metastasis, where a rare slow-proliferating cell population that expresses low levels of EWS-FLI1 was found to exhibit a more mesenchymal phenotype (158). This is in agreement with other reports in which knockdown of the fusion pushes ES cells towards a mesodermal gene expression signature and increases mesenchymal markers (40, 159). Functionally, 'EWS-FLI1 low' cells favour cell-matrix interactions correlating with greater migration and invasion (158). In contrast, the more predominant cell population with high expression of the fusion was broadly associated with a highly proliferative state, but a poor invasive phenotype. Following from these findings, a recent single-cell sequencing study in ES cells added a new layer of complexity to EWS-FLI1 heterogeneity (159). Through a more robust score system measuring the fusion's transcriptional signature, this novel work clarified that the population with the highest and lowest EWS-FLI1 signature are in fact both not proliferative (159). Unlike the cycling cells with an intermediate score of EWS-FLI1 activity, cells in the extreme ends of this spectrum were associated with hypoxia-inducible factor 1α (HIF-1α) activation (159). The existence of this heterogeneity, underpinned by varying transcript and protein levels of EWS-FLI1, suggests ES cells may be able to adapt to different contexts by switching between these states. The understanding of the mechanisms regulating ES cell plasticity is, however, limited. Whilst EWS-FLI1 heterogeneity could be a random process, internal and external pathways have been suggested to play a role. Hypoxia has already been demonstrated to upregulate EWS-FLI1 expression and modulate expression of downstream targets (160). This could represent the identified population with the highest fusion protein signature (159). Additionally, it is likely other microenvironmental cues

and pressures shape tumour heterogeneity and influence the transition between these phenotypes. Importantly, changes in EWS-FLI1 levels have the potential to affect clinical outcome through direct promotion of metastasis and by limiting the cytotoxic effects of therapeutic agents (147). This is because chemotherapy is aimed at fast-proliferating cell populations, leaving the slow cycling and low-expressing EWS-FLI1 cells unaffected. It remains to be addressed whether treatments can act as pressures encouraging ES cells to lower EWS-FLI1 expression as a resistance mechanism. In addition, the increased metastatic potential of this population, may lead to reconsidering therapies directly aimed at reducing EWS-FLI1 expression.

A final source of heterogeneity has been recently found to be linked to heritable germline variants determining the number of consecutive GGAA repeats present in the enhancer region of EWS-FLI1 target genes (161, 162). As described before, these DNA elements are used by the fusion to modulate target gene expression, with the level of enhancer activity depending on the number of GGAA microsatellite repeats (121, 143, 161-163). In this way, these germline variants create inter-tumour heterogeneity affecting drug response and clinical outcomes (161-163).

1.5.3   Transcriptional dysregulation in Ewing sarcoma

Transcriptional dysregulation driven by EWS-FLI was recently described as an example of the dominant-negative effect EWS-FLI1 has on the EWS protein (37, 164). One consequence of this phenotypic difference was found to be formation and accumulation of R-loops, RNA-DNA hybrids with an additional single stranded DNA. Consistent with this, DNA-RNA hybrids immunoprecipitation sequencing (DRIP-seq) to map genomic regions rich in R-loops found accumulation at EWS-FLI1 binding sites (37). Mechanistically, accumulation of these three-stranded nucleic acid structures was attributed to dysregulated transcription through sustained phosphorylation of the C-terminal domain (CTD) of RNA polymerase II (RNAPII). RNAPII is present in its hyperphosphorylated form during elongation, when both EWS and EWS-FLI1 are known to interact with this polymerase (165, 166). Importantly, EWS' ability to regulate RNAPII by inhibiting CDK9 phosphorylation of the CTD was suggested to be lost in EWS-FLI1 (37) (Fig. 1.7). Overall, presence of the fusion interferes with EWS activity, increasing basal levels of transcription and leading to conflicts with the replication machinery (37). In addition, a DNA-binding mutant EWS-FLI1 was able to induce R-loop accumulation,

highlighting the role of the N-terminal of the fusion (EWS) in this process (37). It is not known whether other *EWSR1* gene fusion positive malignancies show this form of loss of function, and consequently have aberrant transcription and develop R-loops and RS.
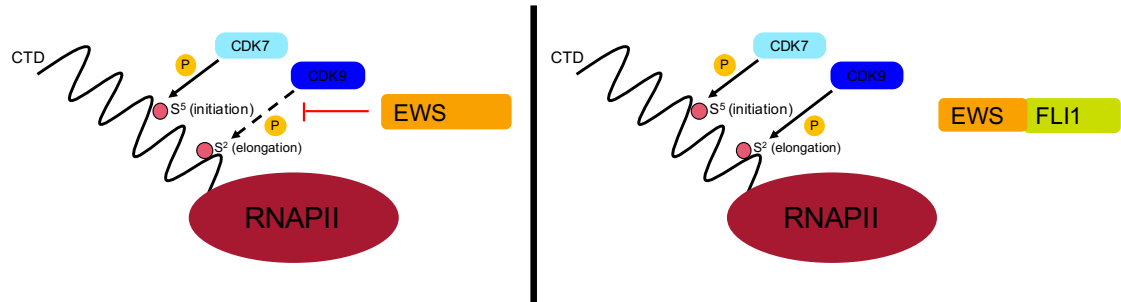
Figure 1.7 Transcriptional dysregulation in Ewing sarcoma

EWS-FLI1 has a dominant-negative effect on protein EWS, resulting in hyperphosphorylated RNAPII and dysregulated transcription. EWS blocks CDK9 phosphorylation of RNAPII's C-terminal domain on serine 2, associated with transcription elongation. EWS-FLI1 does not recapitulate this function and antagonises EWS leading to increased basal levels of transcription.

R-loops are sources of RS and their accumulation can lead to further genotoxic damage (33). Given the innate levels produced by EWS-FLI1 activity, ES tumours have an activated RSR (37, 98, 108, 167, 168). Importantly, this creates a dependency on this branch of the DDR and can therefore be used as the basis of therapeutic options (see 1.6.2.). A recent study looking for permissible contexts for the fusion EWS-FLI1, postulated that these cell types would also have to express factors that resolve R-loops and RS, arising from the presence of EWS-FLI1 (40). Indeed, high levels of expression of proteins FANCI, FANCD2, FANCA, and FEN1 are observed in ES cells and are also found in iPSCs, hESCs, and neural stem cells (40). In contrast to other normal tissues in which EWS-FLI1 expression is lethal, these cell types allow expression of this oncogene (40). Additionally, whilst knockdown of FEN1 is embryonically lethal, depletion of the other factors in ES cells induced growth inhibition (40). It remains to be addressed whether this response is a direct consequence of EWS-FLI1 activity, characterised by dysregulated transcription, instead of an independent correlation of the altered proliferative state in tissues that are pluripotent/multipotent (40).

Alongside transcription and gene expression, there is also evidence of mRNA processing dysregulation in this sarcoma (164, 169). This has been proposed to be due to compromised EWS activity in alternative splicing, specifically through the loss of important RNA-binding domains in the EWS-FLI1 fusion protein (164, 170). The best example in ES relates to splicing dysregulation of *CCND1,* encoding for cyclin D1 (166). This protein is the key binding partner of CDK4/6 in promoting the G1-S transition, and therefore highly relevant to EWS-FLI1 increased levels of proliferation. The *CCND1* gene is commonly upregulated in cancer and has two isoforms, cyclin D1a and D1b, which are regulated through splicing at the pre-mRNA level by EWS (166, 171). Transcription and alternative splicing are closely interlinked since the elongation rates of RNAPII can affect the splice sites (172). Also, transcriptional regulators such as EWS can recruit additional RNA processing factors to influence the splicing of transcripts (164). In this way, EWS and EWS-FLI1 have both been shown to affect overall cyclin D1 expression, particularly through RNAPII elongation dynamics (166, 171). On one hand, EWS increases the speed of elongating RNAPII over *CCND1,* splicing out intron 4 and favouring the cyclin D1a transcript terminating with polyadenylated exon 5. EWS-FLI1, on the other hand, decreases the elongating rate, resulting in more transcripts of the cyclin D1b isoform (171). In summary, the difference in the increase of cyclin D1b through EWS-FLI1 regulation, is relevant since this splicing variant has been linked with greater oncogenic potential than D1a (173, 174). Interestingly, the cyclin D1b variant lacks a regulatory threonine 286 residue found in the absent exon 5. Phosphorylation of this site by glycogen synthase kinase 3β (GSK3β) determines its export into the nucleus from the cytosol (173, 174). In this way, cyclin D1b is constitutively localised in the nucleus, where it can promote Rb phosphorylation and transition from G1 into S-phase. Together with enhanced transforming capacity, greater expression of cyclin D1b in ES cells has the potential to shorten G1 and promote early entry into S-phase and cell proliferation. Cyclin D1 is one amongst other proteins regulated by EWS which are potentially affected by EWS-FLI1 (164). Importantly, EWS-mediated alternative splicing affects proteins involved in DNA damage signalling and repair, such as CHK2, c-ABL, and MAP4K2 (164). This could have wider implications to tumour progression in the ES setting through disruption of EWS activity by the fusion protein.

Taken together, expression of EWS-FLI1 dysregulates gene expression epigenetically and by directly disrupting EWS activity in transcription and mRNA processing.

Modulation of levels of the fusion protein is another important factor determining ES biology and tumourigenesis. Whilst these three areas provide the basis for disease progression, there are other EWS-FLI1 driven mechanisms enabling further oncogenic changes (reviewed in (147)). The increased understanding of molecular mechanisms in this tumour offer hope for novel targeted therapies to improve clinical outcomes.

1.6 Ewing sarcoma treatment and development of novel therapies

1.6.1 Disease management and treatment

1.6.1.1 Chemotherapy regimens in ES

Standard treatment for ES patients consists of local control measures in the form of tumour resection, when possible, and/or radiotherapy treatment. Usually, patients receive multi-agent chemotherapy prior to local treatment as an effort to reduce tumour size and also target micrometastatic disease (147). Treatment starts with VIDE, a combination of vincristine, ifosfamide, doxorubicin, and etoposide. Following local control, patients continue with VAI or VAC in a randomised setting, these regimens consist of vincristine, actinomycin D (also known as dactinomycin), and ifosfamide or cyclophosphamide. Overall, these agents have differing mechanisms of DNA damage induction, but overlapping cytotoxic effects, providing a broad range of anti-cancer effects in combination. Vincristine is a microtubule inhibitor blocking polymerisation, ultimately preventing chromosome separation in metaphase and cell division (175). Actinomycin D intercalates DNA and stabilises cleavable complexes between topoisomerases I and II with DNA. Ifosfamide and cyclophosphamide are alkylating agents, forming intra- and inter-strand crosslinks with DNA. Recently, ifosfamide has replaced the older structural analogue cyclophosphamide in some protocols (176), although they still possess different metabolic and toxicity profiles and are not entirely interchangeable (177). Doxorubicin belongs to the anthracycline class of antibiotic drugs and forms complexes with DNA through intercalation between base pairs. Etoposide's overall effect results in DNA synthesis inhibition and it can inhibit topoisomerase II-catalysed religation in the same way as doxorubicin. The number of different chemotherapeutic agents used demonstrates the lack of targeted therapy for ES and justifies the need for better alternatives to improve outcomes in patients.

1.6.1.2   Irinotecan and temozolomide for relapsed ES patients

Overall, relapsed ES patients have worse outcomes and a 5-year survival rate as low as <10%, when relapse occurs two years after diagnosis (178). Other factors that contribute to determine prognosis in these cases, are age and whether the tumour relapse is localised or metastatic (179). One of the treatment options for these patients consists of a protocol of irinotecan and temozolomide, amongst other regimens such as cyclophosphamide and topotecan, and gemcitabine and docetaxel (180-183). Irinotecan (CPT-11) is a water-soluble camptothecin analogue, which acts as the prodrug of the more potent topoisomerase I inhibitor, SN-38 (184). Temozolomide is an oral DNA alkylating agent, which also causes DNA methylation and in turn recruitment of topoisomerase I. This mechanism has been proposed to be relevant to their combined treatment, which has been found to provide greater synergistic effect, particularly when irinotecan is administered 1 hour after temozolomide (185). The use of irinotecan has been tested clinically for a range of childhood cancers and it used and approved for many cancers (184, 186). One existing regimen for ES paediatric patients involves a protracted schedule with daily administration of irinotecan for five consecutive days for two weeks (d 5 2) in a 21-day cycle (181). This has been tested and compared to a shorter schedule with administration only occurring for five consecutive days throughout the entire 21-day cycle (187).

Maximising exposure *in vivo* faces a number of pharmacological challenges crucial to achieving optimal responses. Obtaining the active metabolite of irinotecan, SN-38, requires the activity of endogenous carboxylesterases, whose conversion rate is very low (184). Similarly, inactivation of SN-38 by glucuronidation is another mechanism determining its bioavailability (188). This process is affected by polymorphisms in the gene *UGT1A1*, encoding for one of these glucuronosyltransferases catalysing this reaction. To minimise toxicity for patients that have the particular *UGT1A1**28 genotype resulting in reduced conversion of SN-38 to its inactive form, a lower dose of irinotecan has been recommended (188). However, this pharmacogenomic factor has been found to have less of an impact in paediatric trials (180, 181, 187). The most common dose-limiting toxicities for irinotecan are diarrhoea and myelosuppression (180-182). For these reasons it is often administered with a gastrointestinal prophylactic (181, 182). Antibiotics are sometimes given too, in order to reduce gram-negative aerobic bacteria that produce a glucuronidase enzyme converting inactive SN-38 glucuronide into its active form, thus damaging the colon (188).

Recently, a randomised comparison of relapse regimens in ES found that the irinotecan and temozolomide combination was inferior to two other relapse regimens consisting of topotecan with cyclophosphamide and high-dose ifosfamide (183). Whilst the development of an optimal combination treatment for relapsed ES patients continues, it is likely that the future use of these agents will involve the addition of targeted therapy. In this way, chemotherapy will serve as a backbone with which to combine novel agents of interest. Already, there are a range of drugs undergoing pre-clinical testing such as bevacizumab, antibodies against the insulin-like growth factor 1 (IGF-1) receptor, mammalian target of rapamycin (mTOR) inhibitor temsirolimus, and PARP inhibitors (96, 182, 189-191) . However, the inclusion of new agents will require further *in vitro* mechanistic-driven research occurring in parallel to ongoing clinical testing to address the challenges of combining and maximising response to these targeted drugs (113).

1.6.2   New therapeutic opportunities in Ewing sarcoma

In recent years, the increased understanding of the oncogenic processes driven by EWS-FLI1 has paved the way for research into blocking these mechanisms as therapeutic options. As outlined before, two of the main novel properties of the oncoprotein EWS-FLI1 enable dysregulation of epigenetic and transcriptional mechanisms to alter gene expression and promote tumour growth. This has led to raised interest in investigating epigenetic targets known to interact with EWS-FLI1-mediated reprogramming. Most efforts have focused on inhibiting the catalytic function of key histone modifying enzymes in larger chromatin remodelling complexes. This has been the case with EZH2, histone deacetylase 1-3 (HDAC), and lysine-specific demethylase 1 (LSD1, also known as KDM1A), and also DNA methyltransferases. Importantly, these proteins are all druggable targets with a range of available tool compounds and clinical drug candidates at various stages of development (149, 150, 153, 192-195). These studies have the potential to tease out more details of their direct contribution to reprogramming and identify further epigenetic targets interacting with the fusion protein. Whilst the reversible nature of epigenetic modifications is an attractive form of therapy, treatment with this type of inhibitors may also lead to unintended modifications contributing to disease progression and/or toxicity (22, 23). This remains an ongoing challenge that needs to be addressed, as epigenetic therapies are translated into the clinic to improve ES management.

In recent years there has been great interest regarding the targeting of the RSR as a form of cancer therapy. This is due to its potential for combination with DNA damaging agents, which is already being exploited in chemotherapy regimens for several cancer types (56, 59). In ES, an additional rationale for this form of therapy is the observation that EWS-FLI1 increases replication fork rate through dysregulation of transcription, and thus develops a dependency on mechanisms that mitigate the resulting genomic instability (37, 98). High innate levels of RS mean that activation of the RSR, together with factors that resolve replication fork collapse, are vital for the survival of ES cells (37, 40, 98). One example of this acquired dependency is high expression of CHK1 in ES tumours (98, 167). This has also been tested therapeutically in *in vitro* and *in vivo* pre-clinical models of ES, where ATR inhibition as a single agent caused a reduction of cell viability and tumour xenografts growth (98). In addition, sensitivity to tool compounds against ATR was shown to be induced upon insertion of EWS-FLI1 in mouse embryonic fibroblasts (MEFs) (98). Targeting of other key kinases in the RSR, such as CHK1 and WEE1, has also been more recently explored and with differing degrees of success (167, 168). Of note, combination strategies with chemotherapeutic agents used in ES had so far only been tested with prexasertib, a discontinued CHK1 inhibitor (196). These studies are thoroughly addressed in the results chapters and discussion of this thesis.

The sensitivity to inhibition of the RSR, also makes the status of other DNA repair mechanisms particularly important and therapeutically relevant. This has been an ongoing area of research in this sarcoma, originating from the observation that ES cells are sensitive to PARP inhibition *in vitro* and that PARP1 is a downstream target of the fusion (197, 198). The presence of R-loops as a form of RS has been recently suggested as an additional reason for the reported sensitivity of ES cells to inhibitors of PARP (37, 147). Strikingly, however, single agent PARP inhibitor sensitivity *in vivo* is limited and single agent PARP inhibitor treatment in patients is ineffective (189, 199). Whilst different studies have searched for genetic vulnerabilities in DNA repair pathways in ES (189, 200, 201), this has not been conclusively addressed. Rather than through a genetically HR-deficient context, BRCA1 activity has been proposed to be defective due to being chromatin-bound (37). Increased understanding of these functional differences and the phenotype created by EWS-FLI1, particularly in terms of DNA replication and genomic instability, will be an important step to develop novel therapies harnessing these vulnerabilities in this sarcoma.

1.6.3 Identification and validation of novel targets

Before pre-clinical testing of new therapies, the process of drug discovery involves identifying relevant and druggable targets that promote tumour growth; this process has been broadly characterised by target- or phenotypic-based approaches (reviewed in (202)). More recently, however, mechanistic and clinically-driven considerations are being incorporated into the identification and validation of novel targets in oncology (202). One example is the adaptation of cell-based assays to test more complex phenotypes beyond a simple cytotoxic assay, in order to provide a more clinically-relevant assessment of novel therapies. Other developments have taken place in the platforms and pre-clinical models used for drug-based screening, improving on the long-standing reliance on immortalised cancer cell lines as tumours surrogates (202, 203). Whilst vital to the discovery of many anticancer therapies and highly amenable for molecular analysis and high-throughput testing, cancer cell lines remain limited models of tumour physiology. This is partially due to cell lines being homogenous populations lacking microenvironmental components that can influence tumour progression (203). In addition, cell monolayers have very specific growth and metabolic rates, with uniform cell morphology and cell-cell interactions, restraining the possibility of more complex tissue architecture and self-organisation (204). For these reasons, a number of three-dimensional (3D) cell culture platforms have been developed, offering improvements through the incorporation of microenvironmental cues such as perfusion flow, oxygen gradients, and increased number in cell-cell interactions enabled by three-dimensionality (203, 205). Models such as spheroids and organoids enable testing compounds in 'mini-tumours', where gradients of nutrients and oxygen supply more closely resemble tumour physiology. However, despite the range of 3D cell culture platforms, there is no single technology that mimics all aspects of tumour physiology. Rather, these are tools that should be carefully considered to address specific questions, because changing the cell culture environment can also affect reproducibility and amenability for high-throughput applications.

Other shortcomings of conventional 2D cancer cell line models are intrinsically linked to cancer cell lines having been isolated from single individuals and being continuously passaged and maintained in culture for long periods of time (203). This process of adaptation to an artificial environment can have an impact on gene expression and cell behaviour, as well as encouraging clonal selection for populations favouring growth in

culture (203). In turn, this can lead to a loss of tumour heterogeneity, which is an important factor known to contribute to drug resistance and impacting on therapeutic efficacy (6). Although not perfect, patient-derived organoids (PDOs), patient-derived xenografts (PDXs) and the cell lines obtained from these tumours, have been shown to better preserve the mutational background of parental tumours and even some components of the tumour stroma (7, 203). Together with the use of co-cultures of heterogenous cell populations, these tools have been welcomed additions for *in vitro* drug testing.

Improving cell-based assays with more representative pre-clinical models is as important as careful experimental design. Traditionally, cytotoxicity assays used in drug development test efficacy based on continuous exposure to drug agents in a short period of time (72 h – 96 h). This is a useful method for calculating standard measurements of drug response, such as 50% of growth inhibition (GI50s), which facilitate comparisons across many different compounds and tumour types. However, these assays have some limitations, for example, continuous drug exposure is not always achieved in the clinical setting. A short window to assess cell killing does not allow for investigating cell recovery, and often, producing observable cytotoxic effects requires higher doses than what is achievable in patients (206). In the context of inhibition of epigenetic targets and cell cycle checkpoint activators, timing is key. The effect of these treatments may take longer to achieve maximal efficacy, given that it requires reversing the epigenetic status of DNA and the changes in transcription and gene expression that follow. Similarly, different outcomes outside cytotoxicity could also be relevant, especially in the context of ES and epigenetic targets. EZH2 in particular is known to cooperate with EWS-FLI1 to maintain stemness, therefore inhibition of this methyltransferase has seen induction of differentiation (153). In terms of chemotherapeutic agents, the majority of DNA-damaging drugs operate by binding DNA and eventually causing breaks, which activate cell cycle checkpoints and repair mechanisms. Cell death is only achieved when these safeguards fail or a threshold of damage is exceeded (65, 206). Mechanistically, enhancing this effect may require acting during a specific cell cycle phase as well as building up DNA damage through a number of cell divisions (184, 206, 207). In this way, mechanism of action determines the type and length of the assay to evaluate such therapies.

Overall, these are key considerations that can improve pre-clinical validation of targets improving the translational impact of oncological research. These ideas shaped and informed the methodology used in the experiments throughout this thesis.

1.7 Thesis aims

The EWS-FLI1 fusion protein is the main oncogenic driver in ES, dysregulating epigenetic and transcriptional processes to promote malignant transformation (detailed in 1.5). Tumour heterogeneity in this sarcoma has also been found to be underpinned by a spectrum of transcriptional programmes driven by EWS-FLI1 activity. Despite increased understanding of how these processes are hijacked, targeted therapies have not yet reached the clinical setting. For these reasons, the overarching aim of this project was to investigate novel therapies targeting vulnerabilities associated with the activity of EWS-FLI1 (Fig. 1.8):

(1) EWS-FLI1 orchestrates vast epigenetic rewiring through recruitment of chromatin remodellers and histone modifying enzymes. Amongst these, KDM1A is a highly expressed demethylase, known to have a functional role contributing to gene expression changes in ES. The first aim of this project was to evaluate catalytic inhibition of this epigenetic modifier as a therapeutic strategy.

(2) In addition to altering gene expression epigenetically, EWS-FLI1 directly disrupts transcriptional processes leading to conflicts with the replication machinery in the form of RS. To mitigate the resulting DNA damage, this sarcoma relies on the RSR, a branch of DNA repair alleviating RS and protecting replication fork progression. In this way, the presence of EWS-FLI1 creates a targetable vulnerability, opening up the use of inhibitors targeting the RSR as a therapeutic strategy. Based on this rationale, the second aim was to explore combination strategies using spheroid models of ES and advance the development of these targeted therapies for this tumour.
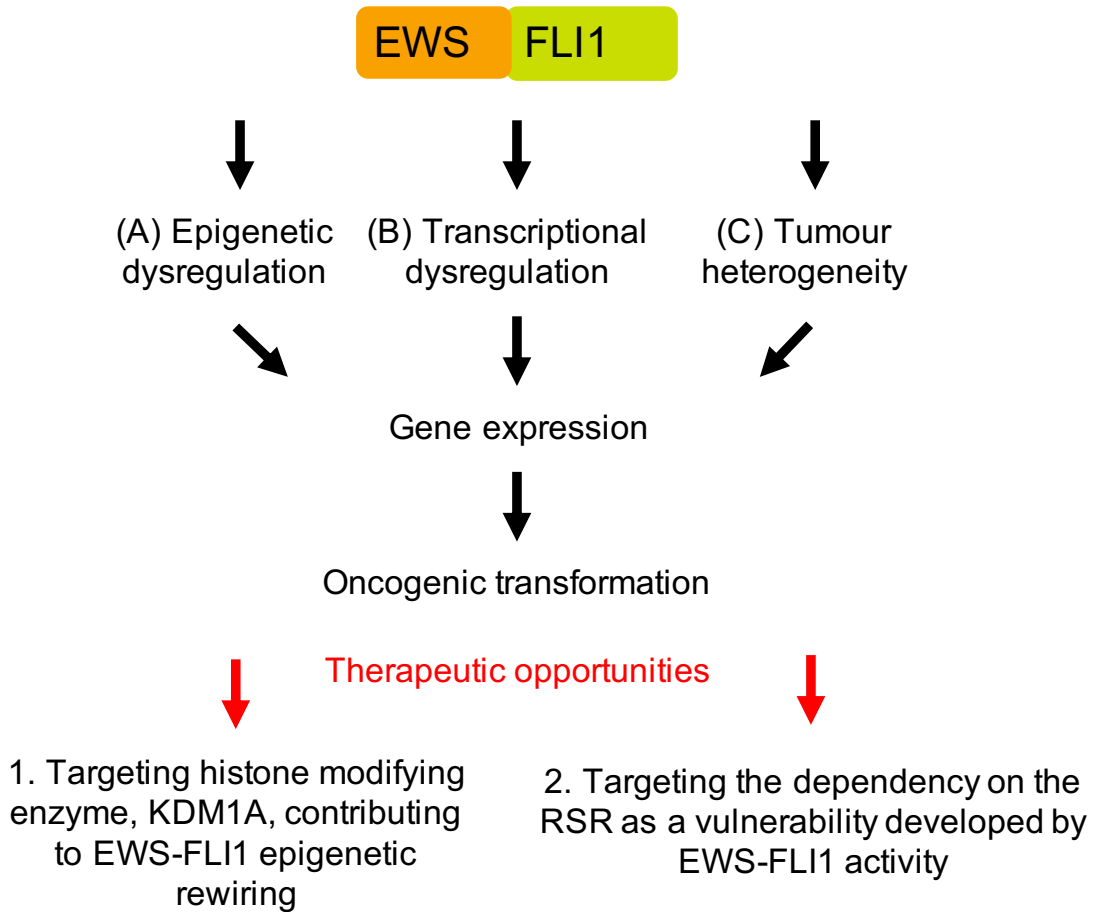
Figure 1.8 EWS-FLI1 mediated processes for oncogenic transformation.

The EWS-FLI1 oncoprotein is at the heart of the development of this tumour through (A) epigenetic and (B) transcriptional dysregulation, and as an important mediator of (C) intra-tumoural heterogeneity. The relevance of these EWS-FLI1 mediated processes in modifying gene expression to promote oncogenic transformation opened up the possibility of therapeutically targeting these through two independent approaches: (1) Inhibition of histone modifying enzyme, KDM1A, and (2) by targeting the reliance on the RSR developed by the presence of the fusion protein in ES.

Chapter 2 Materials and Methods

In this chapter, the methods used to address the key aims of this thesis are detailed. These include methods to culture cells using traditional techniques as well as 3D spheroids and the subsequent processing and further molecular and biochemical analysis. In addition, the development of a model of ectopic inducible expression of the EWS-FLI1 fusion expression is detailed.

2.1 Cell culture

Human ES cell lines were used for the majority of experiments unless otherwise stated. Cells were cultured in the appropriate media supplemented with 10% foetal bovine serum (FBS) (Gibco, Thermo Fisher Scientific, UK), 1% Penicillin-Streptomycin (Gibco) and 1% GlutaMAX (Gibco) in a humidified incubator at 37°C and 5% CO_2. Specific culture conditions are detailed in Table 2.1. Cell lines were authenticated with short tandem repeat (STR) testing using the GenePrint 10 system according to manufacturer's instructions (Promega, UK). Mutational status of ES cell lines used in this study (Table 5.1) was confirmed with the publicly available Broad Institute's Cancer Cell Line Encyclopedia and Cancer Dependency Map database (75, 208).

Cryovials with frozen cells were thawed rapidly, mixed with 9 ml of media and centrifuged at 1250 rpm for 5 min. After discarding the supernatant, the cell pellet was resuspended in the appropriate volume of media depending on the size of the flask and the pellet. Cells were checked for mycoplasma 72 hours after being thawed using the PlasmoTest™ Mycoplasma Detection Kit (InvivoGen, UK). This is a colorimetric assay involving HEK-Blue™-2 cells that recognise mycoplasma through Toll-like Receptor 2 (TLR2), which in turn triggers activation of transcription factors inducing secretion of secreted embryonic alkaline phosphatase (SEAP). This, then causes a change in the colour of the HEK-Blue™ Detection medium, indicating the presence of mycoplasma.

Cells were maintained to approximately no more than 80% confluence and passaged using standard procedures. Cells were washed in 1.5 ml of 1X phosphate buffered saline (PBS) or Versene (Gibco), prior to incubation for 3 min at 37°C with 1 ml or 1.5 ml of 0.05% Trypsin-EDTA (Gibco) in a T25 or T75, respectively. Cell lines were passaged for a maximum of 2-3 months, before using a new batch. In order to freeze cells for long-

term storage, these were harvested, centrifuged at 1250 rpm for 5 min, and resuspended in freezing medium, containing FBS supplemented with 10% dimethylsulphoxide (DMSO) (Sigma-Aldrich, UK). 1 ml of cell suspension was transferred to each cryovial and frozen at -80°C in a cryo 1°C freezing container (Thermo Fisher Scientific) with isopropanol (VWR Chemicals, UK), followed by transferal to liquid nitrogen storage 48 hours later.

Experiments were set up by harvesting cells and resuspending in 3-10 ml of media. 30 µl of cell suspension were mixed with 270 µl of PBS and counted with a sceptre handheld automated cell counter (Merck Millipore, MA, USA), determining the number of cells per millilitre. Using this measurement, a dilution of 1×10^6 cells/ml was made to facilitate seeding specific cell densities, indicated for each method and experiment.

Table 2.1 Cell lines

Cell line	Cell type and disease	Culture condition	Source
A4573	ES	RPMI-1640 10% FBS	Prof Enrique de Álava, Biomedicine Institute of Sevilla, Spain
A673	ES	DMEM 10% FBS	Prof Enrique de Álava, Biomedicine Institute of Sevilla, Spain
CADO-ES1	ES	RPMI-1640 10% FBS	Prof Enrique de Álava, Biomedicine Institute of Sevilla, Spain
SK-ES-1	ES	RPMI-1640 10% FBS	Prof Enrique de Álava, Biomedicine Institute of Sevilla, Spain
RM82	ES	RPMI-1640 10% FBS	Prof Enrique de Álava, Biomedicine Institute of Sevilla, Spain
SKNMC	ES	RPMI-1640 10% FBS	Prof Enrique de Álava, Biomedicine Institute of Sevilla, Spain
RD-ES	ES	RPMI-1640 10% FBS	Prof Enrique de Álava, Biomedicine Institute of Sevilla, Spain
TC32	ES	RPMI-1640 10% FBS	Prof Enrique de Álava, Biomedicine Institute of Sevilla, Spain
TC71	ES	RPMI-1640 10% FBS	Prof Enrique de Álava, Biomedicine Institute of Sevilla, Spain
HFF-1	Human foreskin fibroblasts	DMEM, 15% FBS	ATCC

MV(4;11)	Biphenotypic B myelomonocytic leukemia	RPMI-1640 20% FBS	DSMZ
MOLT-4 (ACC 362)	Acute Lymphoblastic Leukemia	RPMI-1640 20% FBS	DSMZ
JN-DSRCT	DSRCT	DMEM/F12 10% FBS	Sean B. Lee
U-2 OS	Osteosarcoma	McCoy's 10% FBS	ATCC
WiDr	Colorectal adenocarcinoma	EMEM 10% FBS	Prof Andrew Beggs, University of Birmingham, UK

2.1.1 Spheroids culture

3D spheroids were generated and cultured using 96-well Ultra-Low Attachment (ULA) plates (Corning, UK) and GravityTRAP™ ULA Plate 96-well (PerkinElmer, UK). For the latter, prior to seeding, wells were pre-wet with 40 µl of pre-warmed medium. Then, 1000 cells in 70 µl were slowly seeded into each well. Then, plates were spun for 2 min at 250 RCF to remove trapped air bubbles. Routine medium changes were performed every 48 hours by carefully aspirating the medium from the ledge at the inside wall of the well and replenishing it with fresh medium. In the case of ULA plates, 1000 cells were seeded in 100 µl, with a further 100 µl added 48-72 hours later. Medium changes were performed by removing half of the volume and adding half of fresh medium.

2.1.2 Image analysis of spheroids

Digital images of spheroids were captured throughout the duration of the experiments using an IN Cell Analyzer 2200 imaging system (GE Healthcare Life Sciences, UK) and the Celigo Imaging Cytometer (Nexcelom Bioscience, MA, USA). The spheroid area was assessed at the focal plane with maximum diameter. The area of cross-sections of spheroids was then measured using ImageJ (NIH), In Cell Investigator Software (GE Healthcare Life Sciences), and the Celigo Imaging Cytometer software (Nexcelom Bioscience). Spheroid area measurements were taken from 6-10 replicates at the indicated timepoints to then calculate the spheroid mean area.

2.2 Drug treatments

A673 cells were seeded at 2000 cells/well and TC71 cells at 4000 cells/well in a 96-well plate (Nunclon delta surface, Thermo Fisher Scientific) for cell viability assays to calculate GI50s. For investigations on inhibition of KDM1A, the inhibitors used were: SP-2509 (SelleckChem, UK), ORY-1001 (SelleckChem), and GSK2879552 (SelleckChem). For drug treatments on spheroids, 1000 cells were seeded and cultured for 5 days prior to treatment in order to allow for spheroid formation. In GravityTRAP™ ULA Plate 96-well, drugs were diluted to the desired concentration and 70 µl were added per well. Alternatively, ULA plates required removing 100 µl of a total of 200 µl of media before adding 100 µl with double the desired concentration. In this way, the added drug was diluted 1:1 with the remaining volume to reach the desired concentration.

The clinical drug candidates inhibiting DNA repair proteins used in this study were: PARP1/2 inhibitor Olaparib (SelleckChem), ATR inhibitors VX-970 (SelleckChem) and AZD6738 (SelleckChem), CHK1 inhibitor SRA737 (SelleckChem), and WEE1 inhibitor AZD1775 (SelleckChem). All compounds were reconstituted with neat DMSO at 10mM stocks except for ORY-1001 and GSK2879552 reconstituted in ultra-filtered water. Aliquots were stored at -80°C.

2.3 Ionising radiation treatment

Cells and spheroids were irradiated with X-ray cabinet AGO HS 320/260. The generator was run at 250 kV and 10 mA.

2.4 Cell viability assay

Cell viability was analysed indirectly through the metabolic MTS (3-(4,5-dimethyl-2-yl)-5-(3- carboxymethoxyphenyl)-2-(4-sulfophenyl)-2H-tetrazolium, inner salt) assay using the CellTiter 96® Aqueous One Solution Cell Proliferation Assay (Promega). This assay measures the reduction of tetrazolium salt to a blue formazan product by the activity of mitochondrial dehydrogenases. Media was replaced with 100 µl of opti-MEM (Gibco) and 20 µl of CellTiter 96® Aqueous One Solution Cell Proliferation Assay, including 6 blank wells for background correction. Plates were incubated for 2 hours in normal culturing conditions prior to measuring the absorbance of each well at 492 nm.

2.5 Spheroid invasion assays

A673, TC71 and JN-DSRCT-1 cells were cultured in ULA plates for 5-15 days, depending on whether drug-treatment was performed.

2.5.1 Spheroid invasion assay in collagen I

Flat-bottom 96-well plates were coated with 50 µl of a collagen mix containing DMEM, +/– 10% FBS, HEPES pH 7.5 (Final concentration: 20 mM), at a final concentration of 2 mg/ml and 1.2 mg/ml. Collagen mix was prepared on ice to prevent it from solidifying. Mix was allowed to set for 1 h in an incubator at 37°C and 5% CO_2. Spheroids were collected into eppendorf tubes using a 200 µl cut pipette tip to avoid breaking the spheroids (1 spheroid/eppendorf). The same collagen mix as below was prepared on ice again, prior to carefully removing medium from spheroids in eppendorf tubes. Each spheroid was mixed with 100 µl of collagen mix and added to each well of the precoated plate. Plate was incubated for 1 hour at 37°C and 5% CO_2 and left to solidify before covering collagen gel with 50 µl of the corresponding medium. Images of spheroids were taken on a Leica DFC3000 G microscope camera system and the Leica Suite software at 10x magnification.

2.5.2 Spheroid invasion assay in Matrigel

Matrigel (Corning) was thawed overnight and kept at 4°C prior to usage. Pipette tips and reservoirs were cooled at -20°C to facilitate handling of Matrigel. 100 µl of medium were carefully removed from ULA plates without aspirating spheroids. 100 µl of Matrigel were slowly added to each well in order avoid bubble formation. The mix was allowed to set for 20-30 min at 37°C and wells were topped up with 30 µl of medium to prevent Matrigel from drying out. Plates were incubated and invasion monitored in an IncuCyte ZOOM (Sartorius, UK) at 37°C and 5% CO_2. Invasion area was quantified with IncuCyte® Analysis Software (Sartorius).

2.6 siRNA Transfections

A set of four ON-TARGET plus Human *KDM1A* siRNAs (GE Dharmacon, CO, USA) (Table 2.2) were utilised for transfections in A673 cells. All transfections were forward transfections (transfected 24 hours after seeding), carried out in 6-well plates (Nunclon delta surface, Thermo Fisher Scientific). A673 cells were seeded at 312,500 cells/well in

antibiotic-free medium 24 hours prior to transfection. Oligonucleotides were reconstituted with siRNA buffer (GE Dharmacon) to make up a 20 μM stock solution. ON-TARGET plus control non-targeting pool siRNA (GE Dharmacon) was used as a negative control, whilst TOX transfection control (GE Dharmacon) as a positive cell death control. 24 hours after transfection cells were plated in 96-well plates (Nunclon delta surface, Thermo Fisher Scientific) for viability assays, in 12-well plates (Nunclon delta surface, Thermo Fisher Scientific) for RNA extraction, and in 6-well plates for protein extraction or whole cell lysates.

Table 2.2 Oligonucleotides for siRNA transfection.

Name	Sequence (5'-3')	Concentration in experiments (pmol)	Supplier
J-009223-05, KDM1A	GGAAGUUGUCAUUCAGUUA	75	GE Dharmacon
J-009223-06, KDM1A	CCACCGAGUUCACAGUUAU	75	GE Dharmacon
J-009223-07, KDM1A	CAUAAGUGACGAUGUGAUU	75	GE Dharmacon
J-009223-08, KDM1A	CUAUAAAGCUCCAAUACUG	75	GE Dharmacon

2.7 RNA extraction

RNA was extracted with TRIzol™ using the standard protocol for this reagent. RNA concentration was then measured using a Nanodrop 2000 spectrophotometer (Thermo Fisher Scientific) using 260 nm wavelength and RNase-free water as a blank.

2.8 Quantitative Real-Time Polymerase Chain Reaction (qRT-PCR)

2.8.1 Complementary DNA (cDNA) synthesis

cDNA was synthesised from RNA with the high-capacity cDNA kit (Applied Biosystems, CA, USA) following the manufacturer's instructions. Samples were loaded onto the thermocycler with the following programme:

Table 2.3 Thermocycler conditions for cDNA synthesis

Step	Temperature (°C)	Time (min)
1	25	10
2	37	120
3	85	5
4	4	∞

2.8.2   TaqMan qRT-PCR

The TaqMan™ method was used for qRT-PCR. Multiplex PCR reactions were set up in 384-well optical-reaction PRC plates (Applied Biosystesms) with optical adhesive covers (Applied Biosystems). Three technical repeats of the specified reaction volumes were carried out (Table 2.4). Plates were analysed with the Applied Biosystems ViiA™ 7 Real-Time PCR System. Quantification of gene expression was done with the standard curve method using *RPLP0* as the TaqMan control gene assay for normalisation.

Table 2.4 Reaction volumes for TaqMan qRT-PCR

Component in final reaction	Volume (μl)
TaqMan master mix	5
cDNA (5 ng/μl)	1
20X TaqMan gene assay (Table 2.5)	0.5
20X TaqMan control gene assay	0.5
RNase-free water	3
Total	10

Table 2.5 List of TaqMan probes used in this report

Gene of interest	TaqMan Probe	Label or Dye
KDM1A	Hs01002741_m1	FAM/MGB
LOX	Hs00942480_m1	FAM/MGB
TGFBR2	Hs00234253_m1	FAM/MGB
HMOX1	Hs01110250_m1	FAM/MGB
E2F1	Hs00153451_m1	FAM/MGB

CAV1	Hs00971716_m1	FAM/MGB
RPLP0	4310879E	VIC/TAMRA

2.9 Whole cell lysates

Cells were seeded in 6-well plates or T25 flasks for making whole cell lysates. After treatment or transfection, cells were washed in 1X PBS, trypsinised and counted. Cells were then frozen as cell pellets prior to addition of 3X Laemmli buffer; 50 µl were added to 2.5×10^5 cells. Stock of 3X Laemmli buffer was made up with 2 ml of 1M Tris Base pH 6.8, 3 ml of 100% Glycerol, 8 ml of 10% SDS, 300 µl of 1% Bromophenol blue, and 400 µl of β-mercaptoethanol (freshly added at the time of whole cell lysate preparation).

2.10 Protein extraction

Cells were seeded in 6-well plates for protein harvesting. After treatment or transfection, cells were washed in ice-cold 1X PBS. For cell lysis, 60 µl of cell lysis buffer (Cell Signalling Technology (CST), MA, USA) were added to each well before scraping the cells with a sterile cell scraper. Samples were collected in cool eppendorf tubes and left on ice for 50 min. Lysates were then centrifuged at 14000 x g for 10 min at 4°C and the supernatant was collected and stored at −20°C. Regarding protein extraction from spheroids, 30 spheroids per condition were pooled, washed in ice-cold 1X PBS, and resuspended in 60 µl of Radio immunoprecipitation assay (RIPA) buffer (1X) (CST). Samples were incubated for 5 min on ice before sonication, followed by spinning at 12000 x g for 10 min at 4°C and collecting the supernatant. Regarding immunoblotting for phospho-proteins, 10 ml of RIPA buffer (1X) were supplemented with a tablet of protease inhibitor cocktail cOmplete™ ULTRA (Roche, UK), and one of PhosSTOP™ phosphatase inhibitor tablets (Roche). Protein concentration was determined following the standard protocol for a bicinchonicic acid (BCA) assay (Pierce, Thermo Fisher Scientific) (209, 210).

2.11 Western blotting

2.11.1 SDS-PAGE

The equivalent volume to 5-30 µg of protein extract was mixed with 8.75 µl 4X NuPAGE LDS buffer (Invitrogen, CA, USA), and 1 µl DTT (Invitrogen) in order to make a total volume of 35 µl to be loaded in 10-well NuPAGE 4-12% Bis-Tris protein gels (Invitrogen). When using whole cell lysates, 5 µl in 3X Laemmli buffer were loaded. An additional well was reserved for 5 µl of Spectra Multicolor Broad Range protein ladder (Thermo Fisher Scientific) as a molecular weight ladder. Samples were incubated at 90°C for 10 min prior to separation by sodium dodecyl sulfate-polyacrylamide gel electrophoresis (SDS-PAGE). Gels were run with the XCell SureLock™ at 175 V and 200 mA for 1 hour in 1X NuPAGE MES SDS running buffer (Invitrogen) or 1X NuPAGE MOPS SDS running buffer (Invitrogen).

2.11.2 Transfer

Protein gels were transferred onto PVDF membranes with iBlot2 transfer stacks on the iBlot2 transfer system (Invitrogen) following manufacturer's instructions. The iBlot2 transfer system was run at 20V for 7 min. Alternatively, protein gels were transferred onto nitrocellulose membranes using the XCell II™ Blot Module. Gels were rinsed in distilled water and carefully placed in the blot sandwich between the filter paper and the nitrocellulose membrane. Trapped air bubbles were removed with a blotting roller before finishing assembly of the blot module. Gels were run at 25 V and 200 mA for 1.25 hour in 1X NuPAGE™ Transfer Buffer buffer with 10-20% methanol with cold tap water on either side of the module.

2.11.3 Antibody incubation and membrane development

Membranes were blocked in 5% milk (Marvel) in TBST (1X Tris buffered saline with 0.1% Tween-20 (Sigma-Aldrich), pH 8.0) for 1 hour at room temperature (RT) on a rocker. Membranes were incubated with primary antibody overnight at 4°C on a rocker using the dilutions in Table 2.6. After three 10-min washes in TBST at RT on a rocker, membranes were incubated at RT with their respective secondary antibody. Membranes were washed once again three times for 10 min before detection. Blots were developed with the ECL™ Prime Western Blotting System (GE Healthcare) and Pierce™ ECL

Western Blotting Substrate (Thermo Fisher Scientific) according to the manufacturer's instructions and detected on a Chemidoc Touch Imaging System (Bio-Rad, CA, USA).

Table 2.6 Antibodies used in this report

Name	Species	Dilution	Molecular weight (kDa)	Supplier	Product Code
Anti-Mouse HRP-conjugated	Rabbit	1:4000	-	Sigma-Aldrich	A9044
Anti-Rabbit HRP-conjugated	Donkey	1:4000	-	Santa Cruz	SC-2313
CDK1	Mouse	1:1000	34	CST	9116
CHK1	Rabbit	1:4000	56	Abcam	40866
EWS	Rabbit	1:10000	68	Novus Biologicals	NB200-182
FLI1	Mouse	1:500	51	BD Pharmingen	554266
GAPDH	Mouse	1:10000	37	Merck Millipore	MAB374
H3K4me1	Rabbit	1:3000	17	Abcam	ab8895
H3K4me2	Rabbit	1:10000	17	Merck Millipore	07-030
Histone H3	Rabbit	1:1000	15	Abcam	1791
Histone H3	Mouse	1:1000	15	Abcam	10799
KDM1A	Rabbit	1:1000	93	CST	C69G12
PARP1	Rabbit	1:1000	89, 116	CST	9542
Phospho-CDK1/2	Rabbit	1:4000	34	CST	9111
Phospho-CHK1 (S345)	Rabbit	1:1000	56	CST	2348
PUMA	Rabbit	1:1000	22	CST	12450T
RRM2		1:2000	45	Merck Millipore	
TetR	Mouse	1:5000		MoBiTec	TET02
Immunofluorescence					
53BP1	Rabbit	1:500	214	Bethyl	A300-272A
Cleaved-caspase 3 (Asp175)	Rabbit	1:50	17/19	CST	9661

γH2AX	Mouse	1:100	14	Millipore	05-636-I
Phospho-Histone H3 (Ser10)	Rabbit	1:1000	17	Millipore	06-570
AlexaFluor 555 goat anti-mouse	Goat	1:800	-	Life Technologies	A-21422
AlexaFluor 488 goat anti-rabbit	Goat	1:800	-	Life Technologies	A-11034

2.12 Tissue processing of spheroids

2.12.1 Fixing and embedding in agarose

Medium was aspirated off in GravityTRAP™ ULA Plate 96-well plates followed by two washes with 1X PBS. Spheroids were fixed in 4% PFA overnight at 4°C or for 2 hours at RT. Following fixation, spheroids were washed twice in the plates with 1X PBS and then collected in eppendorf tubes and allowed to set at the bottom for embedding in 2% agarose (Invitrogen). Carefully, 1X PBS was aspirated off and replaced with 2% agarose (~65°C). Eppendorf tubes were placed in a heating block at 65°C to ensure the spheroids sank to the bottom. Some samples required being spun at 2000 rpm for 1 min. Agarose was allowed to cool down and solidify and PBS was added to the top of each tube.

2.12.2 Tissue processing and embedding in paraffin wax for sectioning

Agarose blocks with embedded spheroids were removed from eppendorf tubes and covered in tissue processing paper (CellPath, UK). Samples were placed in tissue processing cassettes and run through the programme detailed in table 2.7 involving dehydration, clearing with xylene, and paraffin wax infiltration in a tissue processor (Tissue-Tek VIP, Sakura, Netherlands) (Table 2.7).

Table 2.7 Tissue processing programme schedule

Step	Time	Solution
1	10 min	70% Alcohol
2	1 h	80% Alcohol
3	1 h	90% Alcohol
4	1 h	100% Alcohol
5	1 h	100% Alcohol
6	1 h	100% Alcohol
7	2 h	100% Alcohol
8	1 h	Xylene
9	1 h	Xylene

10	1.5 h	Xylene
11	1 h	Paraffin wax
12	1 h	Paraffin wax
13	2 h	Paraffin wax

Subsequently, samples were carefully embedded in moulds with molten paraffin wax, trying to maintain all blocks of agarose on the same plane to facilitate sectioning. Paraffin wax blocks were left to solidify before removing the metal moulds and were placed at −20°C for a few minutes prior to cutting 5 μm-thick sections with microtome LeicaRM2135. Sections were moved to a histology water bath (Leica HI1220) at 40°C prior to being placed on microscope slides and left to dry on a hot plate (Leica HI1220) at 60°C. Slides were stored at −20°C until use.

2.13 Haematoxylin and eosin staining

Histological staining of sections of paraffin-embedded samples with H&E followed a standard protocol. Slides with sections of paraffin-embedded spheroids were incubated at 60°C for 10 min, prior to two deparaffinisation steps in xylene for 5 min each. Slides were rehydrated in two changes of absolute alcohol for 3 min each followed by carefully rinsing in running tap water for 30 seconds without aiming directly at the samples. Slides were stained in haematoxylin for 7 min and the excess was removed before rinsing again for 30 seconds. Samples were differentiated in 1% acid alcohol by dipping slides in and out three times and then rinsed in running tap water for 30 seconds. Slides were then 'blued' in Scott's Tap Water for 1 min and rinsed in running tap water for 30 seconds. Tissue sections were stained with eosin for 3 min, followed by dipping in running tap water three times. Rack with slides was drained from the excess of water and dehydrated in three changes of absolute alcohol for 1 min each. Slides were then cleared in two changes of xylene for 2 min each before mounting in DPX, without allowing the slides to dry out.

2.14 Immunohistochemistry with immunofluorescence detection

Slides with sections of paraffin-embedded spheroids were incubated at 60°C for 15 min, prior to two deparaffinisation steps in xylene for 10 min each. Slides were then hydrated through a series of decreasing concentrations of alcohol (100%, 95% and 70%) for 5 min

each. Slides were washed in H_2O for 5 min before performing antigen retrieval in sodium citrate buffer (10 mM, pH 6) for 50 min at 95°C. Slides were cooled down for 20 min at RT, washed once in H_2O, and twice in Tris-buffered saline (1X TBS) for 3 min. Using a Dako pen (Agilent Pathology Solutions, UK), a region around tissue sections was drawn to confine the liquid. Samples were incubated in blocking buffer (1X TBS, 10% Goat serum, 1% bovine serum albumin (BSA), 0.02% Tween20) for 1 hour at RT. Primary antibodies were diluted in 1X TBS, 1% BSA, and 0.02% Tween20 at the concentrations in table 2.7 and incubated for 1 hour or overnight at 4°C. Slides were washed three times for 5 min in 1X TBS, prior to a 30 min incubation with respective secondary antibodies, also diluted in 1X TBS, 1% BSA, and 0.02% Tween20. Slides were washed three times for 5 min in 1X TBS and excess buffer drained. Vector® TrueVIEW™ Reagent (Vector Laboratories, UK) was prepared at a ratio of 1:1:1 of reagents A, B and C, adding equal volumes of reagent A and reagent B first, mixing for 10 seconds, before adding reagent C and mixing again. Samples were incubated with Vector® TrueVIEW™ Reagent for 2 min and washed in 1X TBS for 5 min. Tissue sections were incubated with DAPI (1:5000 in 1X TBS) for 5 min and washed three times for 5 min in 1X TBS. Excess buffer was removed and samples were mounted in VECTASHIELD® Vibrance™ Antifade Mounting Medium (Vector Laboratories).

2.15 Flow cytometry of spheroids

2.15.1 Hanging drop technique for spheroid formation

To maximise spheroid and cell numbers, spheroids were cultured using T75 ULA flasks, rather than 96-well ULA plates. Spheroids were initially formed using the hanging drop technique to ensure homogenous spheroid size. Using the lid of 25 cm culture dishes, cells were seeded at a density of 2000 cells per 40 µl drop, with approximately 60 drops per cover. The lid was carefully flipped and placed on top of the culture dish filled with 1X PBS to keep hanging drops humidified. Around 300 spheroids were needed for DNA content analysis by flow cytometry. Spheroids were cultured as such for 2 days prior two transferal into a T75 ULA flask where they were cultured for a further 24 hours prior to treatment. 48 hours was the maximum length of treatment to prevent spheroid aggregation and a heterogeneous population.

2.15.2 Dissociation spheroids and cell fixation

Treated spheroids were collected from T75 ULA flasks into 50 ml falcon tubes and spun at 1250 rpm for 5 min. Medium was aspirated off and replaced with 500 µl of 0.05% Trypsin-EDTA, used to transfer samples into 1.5 ml eppendorf tubes and dissociate spheroids. Samples were incubated at 37°C and 5% CO_2 for 2 min, before pipetting up and down to ensure complete disaggregation. Trypsin-EDTA was inactivated with 600 µl of the cell line's respective medium. Cells were centrifuged at 1250 rpm for 5 min and supernatant removed. The remaining cell pellet was washed once in 1 ml of 1X PBS and cells were centrifuged again at 1250 rpm for 5 min before. After removing the supernatant, cells were fixed in ice-cold 70% ethanol. Eppendorf tubes were vortexed to ensure samples were fixed as a cell suspension, rather than as a pellet. Samples were initially stored at 4°C overnight and then transferred to −20°C.

2.15.3 Propidium iodide staining for DNA content analysis

Eppendorf tubes were spun at 1250 rpm for 4 min and washed in 0.5 ml of 1X PBS, twice. Propidium iodide (PI) (Thermo Fisher Scientific) and RNAse A (Thermo Fisher Scientific) solution was prepared to a final concentration of 50 mg/ml and 0.5 µg/ml, respectively. Stock concentrations for PI and RNAse A were 1 mg/ml and 10 mg/ml. 250 µl of PI/RNase A solution were added to each sample and stored at 4°C until analysis.

2.15.4 DNA content analysis by flow cytometry

Samples were analysed on a BD™ LSRII Flow Cytometer (BD Biosciences, CA, USA). PI was detected in the 575/26 nm channel on the BD™ LSRII cytometer. Initial cell population was gated on a forward scatter height (FSC-H) vs. forward scatter area (FSC-A) to exclude cell aggregates and debris. The single cell gate was then displayed as a histogram and adjusted so that the P4, P5 and P6 gate were respectively gating on G1, S, and G2/M phases. Cell cycle analysis of histograms from treated samples was performed with BD FACSDiva™ Software and FlowJo™ Software v10. Univariate modelling was used to create a fit to the cell cycle data obtained. All data was analysed using the Watson Pragmatic algorithm (211).

2.16 Molecular cloning

2.16.1 Vectors

The EWS-FLI1 fusion gene was cloned out of plasmid pCDH-puro-EWS-FLI1 (212) (Fig. 2.1A) and sub-cloned into pcDNA™5/TO by Dr. Ewa Aladowicz. The pcDNA™5/TO plasmid vector is part of the T-REx™ Expression System (Thermo Fisher Scientific) enabling tetracycline (Tet)-controlled expression a gene of interest in mammalian cells. This plasmid has Tet operator 2 (TetO2) sites upstream the human cytomegalovirus (CMV) promoter, which serve as binding sites for two Tet repressor (TetR) homodimers. Additionally, this plasmid vector includes hygromycin and ampicillin resistance genes for selection in mammalian cell culture and in transformed *E. coli*, respectively (Fig. 2.1B). To express the TetR protein, plasmid pCAGTetRnls was used; this vector also contains a puromycin resistance gene (Fig. 2.1C) and was obtained from Gaetano Zafarana, Erasmus MC-University Medical Center Rotterdam. The pCDH-puro-EWS-FLI1 plasmid vector was a gift from Jialiang Wang (Addgene plasmid #102813; http://n2t.net/addgene:102813; RRID:Addgene_102813).
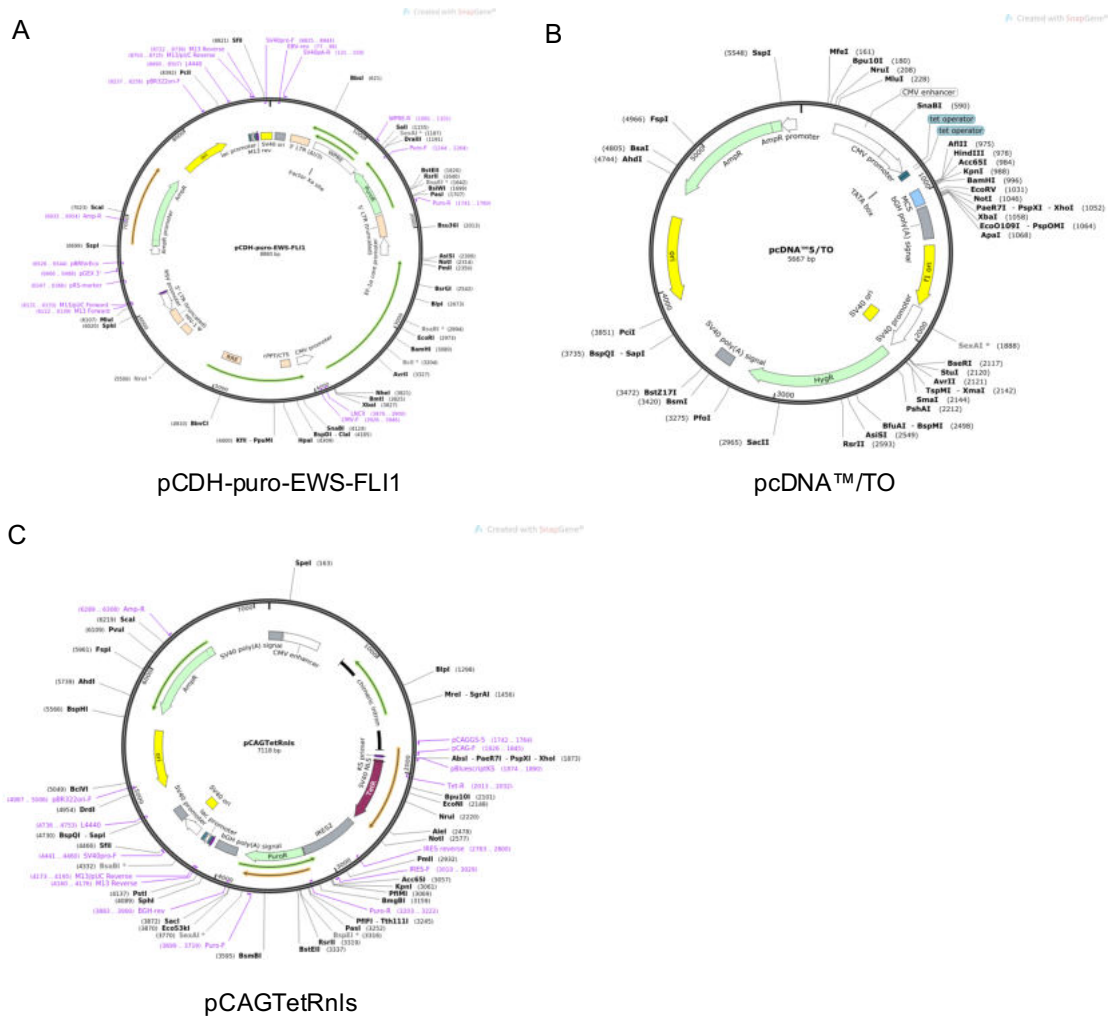
Figure 2.1 Vector maps for plasmids for inducible EWS-FLI1 overexpression.

Vector maps for (A) pCDH-puro-EWS-FLI1, (B) pcDNA™5/TO, and (C) pCAGTetRnls including cloning sites.

2.16.2 Cloning of *EWS-FLI1* to pcDNA5™/TO

Fusion gene *EWS-FLI1* was cloned from pCDH-puro-EWS-FLI1 by nested PCR. First, DNA fragment with *EWS-FLI1* was amplified using outer primers EF1outF and EF1outR (sequences in table 2.8) using Phusion High-Fidelity PCR Master Mix (New England BioLabs (NEB)). Next, amplified fragment was used as template for fusion gene amplification using inner primers EF1inF and EF1inR. The PCR product was purified using PCR Purification Kit (Qiagen, Hilden, Germany).

Table 2.8 Primer sequences to amplify *EWS-FLI1*

EF1outF	5' CACGGCGACTACTGCACTTA 3'
EF1outR	5' AGCTCGTTTAGTGAACCGTCAGATC 3'
EF1inF	5' ATAAGAATGCGGCCGCCTAGTAGTAGCTGCCTAAGTGTGAAGGCACGTGGG 3'
EF1inR	5' GAGATATCACCATGTACCCATACGACGTCCCAGACTACGCTGCGTCCACGGATTACAGTACCTATAGCCAAGCTGC 3'

2.16.3 Restriction digestion

The *EWS-FLI1* insert and pcDNA5™/TO plasmid were digested using first EcoRV-HF restriction enzyme (NEB) and sequentially with NotI-HF (NEB). Digests were set up with 5 µg of 10X CutSmart Buffer (NEB), 2 µl (40 units) of EcoRV-HF (NEB), 5 µg of DNA (either plasmid or insert) with reactions made up to 50 µl with nuclease-free water. The reaction was incubated at 37°C for 15 min and inactivated at 65°C for 20 minutes. Next, 1 µl (40 units) of NotI-HF (NEB) was added to the reaction. Samples were further incubated at 37°C for 15 min and inactivated at 65°C for 20 min. Reactions were purified with PCR Purification Kit (Qiagen).

2.16.4 Ligation

The purified and digested *EWS-FLI1* insert was ligated into the pcDNA5™/TO plasmid using Quick Ligation Kit (NEB). Molar concentrations were calculated by dividing the weight of plasmid DNA equated to using 188 ng of the insert DNA. 20 µl of ligation reaction was set up using 10 µl of 2x Reaction Buffer, 1 µl of Quick Ligase, 100 ng of plasmid DNA, 188 ng insert DNA and made up to 20 µl with nuclease-free water. Negative control ligations were set up containing plasmid DNA only that indicates background levels of self-ligation. Reactions were incubated at 25°C for 5 min.

2.16.5 Bacterial transformation

Plasmids were transformed using competent *E. coli* cells OneShot Top10 (Invitrogen). Bacteria were thawed on ice, adding 5 µl of ligation reaction followed by incubation on ice for 30 min. Eppendorf tubes were then heat-shocked on a heating block at 42°C for 30 seconds and returned immediately to ice for 2 min. 200 µl of pre-warmed Lysogeny broth (LB) were added to each bacterial transformation and incubated at 37°C shaking at

250 rpm for 1 h. Meanwhile, LB agar plates were prepared with a final concentration of 100 µg/ml of ampicillin (Sigma-Aldrich) maintaining aseptic conditions. Once set, the plates were pre-warmed at 37°C and 200 µl of bacteria were spread for overnight culture at 37°C.

2.16.6 Miniprep

Single colonies were picked from agar plates and cultured in 3 ml of LB with 100 µg/ml of ampicillin for selection for 16 h at 37°C shaking at 225 x g. The QIAprep Miniprep kit (Qiagen) was used to extract and purify the plasmids following manufacturer's instructions. Bacterial cells were centrifuged at 13000 x g for 5 min and pellets were resuspended in Buffer P1 containing RNase A. Next, Buffer P2 containing SDS was added and mixed thoroughly by inverting the tubes to ensure cell lysis. The reaction was not allowed to proceed for longer than 5 min. Neutralising buffer N3 was then added and mixed by inverting the tubes, precipitating any remaining bacterial debris. Samples were centrifuged at 13000 x g for 10 min. The supernatant was then passed through a QIAprep spin column, centrifuging the sample at 13000 x g for 30 seconds and discarding the flow-through. The spin column was washed again in PE buffer containing ethanol, then centrifuged again at 13000 x g for 30 seconds, and spun for an additional min at 13 000 x g in order to remove any residual wash buffer. Plasmid DNA was then eluted using the miniprep kit elution buffer and the concentration was measured on a Nanodrop 2000 spectrophotometer at 260 nm wavelength.

2.16.7 Diagnostic digests

Diagnostic restriction digests of pcDNA ™5/TO-*EWS-FLI1* were also used to ensure the plasmid contained the expected size of the insert and if it was cloned in the correct orientation. Digests were set up with 5 µl of 10X CutSmart Buffer (NEB), 1 µl (20 units) of EcoRV-HF (NEB), 1 µl (20 units) of XbaI (NEB), 1 µg of DNA plasmid with reactions made up to 50 µl with nuclease-free water. The reaction was incubated at 37°C for 15 min and inactivated at 65°C for 20 min.

2.16.8 Gel electrophoresis

Agarose gel electrophoresis was used to confirm successful restriction digestion of DNA fragments. 1% agarose gels were prepared by dissolving 1 g of agarose in 100 ml of 1X Tris-acetate-EDTA (TAE) buffer, using a microwave to heat up the mixture and facilitate

the process. After dissolving the agarose, this was let to cool down and 4 µl of Midori Green Direct (NipponGenetics) were added before pouring the mix into a gel tray. Gels were submerged into a tank with 1X TAE buffer and samples were prepared in a volume of 10 µl for loading. This mix included 2 µl of loading buffer, containing bromophenol blue marking the samples as the gel was run. One well containing MassRuler DNA ladder mix (Thermo Fisher Scientific) was run alongside in order to analyse the size of the DNA fragments. Gels were run at 75 V for 45 min to an hour separating DNA and bands were visualised under UV light using a Chemidoc Touch Imaging System (BioRad).

2.16.9 Gel extraction

In order to extract a reaction product from a gel, a Dark Reader® Non-UV transilluminator (Clare Chemical Research, CO, USA) was used to visualise but preserve the integrity of DNA fragments. The desired band was excised with a clean scalpel and purified using a QIAEX II gel extraction kit (Qiagen) according to manufacturer's instructions. The excised gel was weighed and 3 volumes of buffer QX1 were added to solubilise the sample, vortexing for 30 seconds (3 volumes of buffer QX1 are recommended for 100 bp – 4 kb). Then, QIAEX II was added to the sample, 30 µl for 2–10 µg DNA. Samples incubated at 50°C for 10 min, vortexing every 2 min to facilitate DNA adsorption to QIAEX II silica particles. Samples were centrifuged at 14000 x g for 30 seconds. After removing the supernatant, the pellet was washed three times, once in wash buffer QX1 followed by PE buffer, always centrifuging for 30 seconds and removing the supernatant. The remaining pellet was air dried for 15 min and dissolved in HPLC grade water to elute DNA through the membrane. The sample was centrifuged for 30 seconds. The supernatant containing the extracted DNA was passed through the membrane again in order to increase the DNA yield from the elution. The final DNA was then measured with a Nanodrop 2000 spectrophotometer at 260 nm wavelength.

2.16.10 DNA sequencing

In addition to the diagnostic digests, the cloned samples were analysed by DNA sequencing to ensure the *EWS-FLI1* insert was intact and correctly introduced and had not acquired mutations in the process. These substitutions can be introduced when exposed to UV light used to visualise and extract the desired gel band. Sanger sequencing was performed by Eurofins Genomics using the following primers.

Table 2.9 Primers for Sanger sequencing

CMV-F	5' CGCAAATGGGCGGTAGGCGTG 3'
EWSFLI_1	5' CAGACCGCCTATGCAACTTC 3'
EWSFLI_2	5' AGCTATGGTCAACAAAGCAG 3'
EWSFLI_3	5' AAAGCAAGCCCAACATGAATTACG 3'

2.16.11 Maxiprep

Following manufacturer's instructions, the Maxiprep kit (Qiagen) was used to prepare large concentrations of plasmid DNA (up to 500 µg). Clones harbouring pcDNA ™5/TO-EWS-FLI1 were propagated as outlined in 2.16.7 to obtain bacterial cell pellets. Pellets were resuspended in buffer containing RNase A, followed by the addition of lysis buffer, inverting the tubes to mix and lyse the samples thoroughly. Samples were incubated at RT for 5 min prior to adding neutralising buffer to precipitate bacterial debris and genomic DNA. Samples were then incubated on ice for 30 min and centrifuged at 3000 x g for 30 min at 4°C. QIAGEN-tips 500 were equilibrated with buffer QBT before adding the supernatant. The supernatant containing the plasmid DNA was then applied to the QIAGEN-tip and gravity flow making it enter the resin in the tip. The QIAGEN-tip was washed twice with buffer QC followed by elution with buffer QF. The eluted DNA was then precipitated with isopropanol, mixing and centrifuging immediately at 3000 x g for 30 min at 4°C. The supernatant was carefully removed and the pellet resuspended in 70% ethanol, centrifuging further at 3000 x g for 10 min at 4°C. Lastly, after discarding the supernatant, the remaining pellet was airdried and resuspended in Tris-EDTA (TE) buffer. The plasmid DNA concentration was measured on a Nanodrop 2000 spectrophotometer at 260 nm wavelength.

2.17 Inducible overexpression of *EWS-FLI1*

2.17.1 Tet-on inducible system

Inducible overexpression of *EWS-FLI1* in osteosarcoma cell line U-2 OS was achieved using a tetracycline-inducible expression system (tet-on). Initially, plasmid pCAGTetRnls containing a tet repressor (tetR) was transfected in U-2 OS cells. Following puromycin selection and stable expression of tetR, a range of clones were tested for tetR expression levels. Clones possessing the highest expression were then

carried forward. The fusion gene *EWS-FLI1* was cloned into pcDNA ™5/TO and placed under the control of a tetracycline-responsive promoter (described in 2.16.1). pcDNA™5/TO-*EWS-FLI1* and empty vector control pcDNA™5/TO-EV were then transfected into tetR-expressing U-2 OS clones selected in the previous step. U-2 OS clones were cultured in media containing 0.5 µg/ml of puromycin and 50 µg/ml of hygromycin B.

In the absence of tetracycline, expression of the fusion gene *EWS-FLI1* is repressed by binding of tetR homodimers. Conversely, addition of doxycycline, an antibiotic derived from tetracycline, modifies and sequesters the tetR, derepressing expression of the fusion gene. In this way, this Tet-on system enabled doxycycline inducible expression of *EWS-FLI1* in the U-2 OS cell line.

2.17.2 Monoclonal expansion

In order to achieve homogeneous expression of the gene of interest, expansion of single clones was performed. Cells were seeded in 90 mm culture dishes (Thermo Fisher Scientific) at a density of 1 cell per plate in the appropriate selection medium. Whilst it was difficult to seed exclusively one cell per plate, cells were spread out facilitating monitoring the growth of single colonies. These were then marked under the culture dish, and using cloning cylinders (Sigma-Aldrich), single colonies were harvested and plated in a 24-well plate (Nunclon delta surface, Thermo Fisher Scientific). Cells were passaged into 6-well plates and t25s once they reached confluence in the original plate. Selected single clones were then tested for expression of the gene of interest.

2.17.3 Transfection of pcDNA™5/TO-EWS-FLI1

Following transfection of plasmid pCAGTetRnls in U-2 OS cells with to produce stable clones, three high-expressing TetR clones U-2 OS A1, B3, and B4 were seeded for further transfection. 200,000 cells/well in 2 ml of medium without antibiotics were plated in 6-well plates. U-2 OS clones were transfected with purified pcDNA™5/TO-*EWS-FLI1*. Transfection mixes were made with 4 µg of the plasmid DNA in 250 µl of opti-MEM per well, and 7.5 µl of Lipofectamine 2000 (Invitrogen) in opti-MEM 250 µl/well. Each individual mix was incubated for 5 min at RT prior to being combined together and incubated for a further 20 min at RT. 500 µl of the mixed transfection reagents were then added to each well and incubated for 6 hours. Medium was then removed and replaced

with fresh medium containing antibiotics. Selection antibiotics hygromycin B or puromycin were added 24 hours post-transfection.

2.18 In silico methods

2.18.1 Graphpad Prism 7.0

Growth curves and bar charts showing cell viability were plotted using the absorbance values from MTS assays on Graphpad Prism 7.0 software. GI50 values were calculated using the same software.

2.18.2 Definiens Tissue Studio®

Image analysis of immunofluorescence staining for quantification of CC3, γH2AX, 53BP1 and pHH3 was carried out with Definiens Tissue Studio®. Regions of interest (ROI) were selected manually by drawing polygons around the spheroids to be analysed, with at least three spheroids per condition. Nuclear segmentation was done by intensity of the nuclear layer stain and size, excluding fragments of nuclei. Positive nuclei for each dye were identified using the algorithms for marker or spot detection, adjusted by staining intensity and area within the nucleus. In terms of foci analysis, nuclei were classified based on the number of spots per nuclei with the threshold for a true positive nucleus set to greater than 5 foci.

2.19 Statistical Analysis

Graphs representing means ± standard deviation from various independent experiments, or representative graphs showing means ± standard deviation from multiple internal repeats are shown as stated in figure legends. Statistical significance was established with one-way or two-way analysis of variance (ANOVA), where applicable. Post-hoc testing with Dunnett's, Sidak's, or Tukey's multiple comparisons tests were performed to compare every mean to a control group mean. Actual p-values are shown in graphs. Only meaningful statistically significant comparisons were reported and shown on graphs, unless otherwise stated.

Chapter 3 Catalytic inhibition of KDM1A in Ewing sarcoma
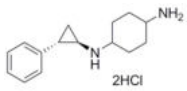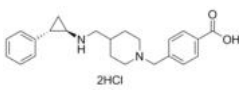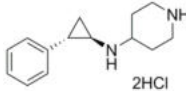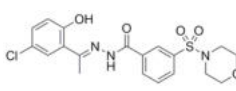
3.1 Introduction

EWS-FLI1 has been identified as an oncogenic 'pioneer' factor, creating *de novo* enhancer elements and altering the epigenetic status of genomic regions through chromatin-remodelling complexes (144). In particular, the NuRD complex, previously introduced as a multi-subunit chromatin-remodelling complex modulating transcriptional activity and EWS-FLI1 target genes (22, 149, 151, 213). A working model proposed by Sankar *et al*., (2014) suggests EWS-FLI1 binds to promoters of repressed target genes and recruits the NuRD complex through interaction between subunits chromodomain 4 (CHD4), metastasis associated protein 1 (MTA1), and the EWS portion of the fusion protein (149, 150). In turn, the catalytic part of the NuRD complex consisting of histone deacetylase 2 and 3 (HDAC2/3), and KDM1A, triggers histone modifications that contribute to the ES transcriptional signature (149, 214, 215). In support of this model, treatment with SP2509, a tool compound targeting KDM1A, reversed the EWS-FLI transcriptional programme. Inhibition of KDM1A with SP2509 also resulted in apoptosis and disruption of the ES oncogenic phenotype suggesting therapeutic potential through the targeting of this demethylase (149, 150).

KDM1A is a well-characterised histone lysine demethylase that belongs to the family of flavin-dependent amine oxidases with important roles in regulating stem cell maintenance and gene expression (214, 216, 217). Besides this, KDM1A is involved in cell migration and invasion by controlling epithelial-to-mesenchymal transition (EMT), a process implicated but not limited to tumour development (215, 218). This demethylase is overexpressed in ES and other sarcomas including DSRCT and RMS (219). In addition, the interaction with chromatin remodelling complexes, enabled by the EWS portion of the fusion, made inclusion of DSRCT (EWS-WT1 fusion-positive) relevant to this study. Based on the rationale presented, the primary aim of this first chapter was to test the potential for repurposing available clinical drug candidates against KDM1A as a novel treatment for these sarcomas. Prior to this work, the use of inhibitors of KDM1A as a therapeutic strategy for ES had not been comprehensively assessed. At the start of this study, available inhibitors of KDM1A included ORY-1001 (also known as Iadademstat, RG6016 or RO7051790) and GSK2879552 (Table 3.1). These clinical drug candidates are potent irreversible inhibitors of KDM1A, which covalently modify the flavin adenine

dinucleotide (FAD) cofactor of this demethylase to inhibit catalytic activity (216, 220-222)(216, 220-222)(215, 219-221)(214, 218-220)(214, 218-220)(214, 218-220)(213, 217-219). Additional tool compounds targeting KDM1A discussed in this study are listed in Table 3.1.

Table 3.1 KDM1A inhibitors.

Compound	Clinical drug candidates		Tool compounds	
	ORY-1001	GSK2879552	GSK-LSD1	SP2509
Structure				
	IC50: 18 nM	Kiapp of 1.7 µM	IC50: 16 nM	IC50: 13 nM
Mechanism of action	Irreversible inhibitor covalently modifying the FAD cofactor	Irreversible inhibitor covalently modifying the FAD cofactor	Irreversible inhibitor covalently modifying the FAD cofactor	Reversible non-competitive inhibitor
Clinical status	Completed phase I/IIa study in AML (EudraCT Number: 2013-002447-29) and completed phase I study in SCLC (NCT02913443). Phase I combination studies with azacytidine for AML (EudraCT Number: 2018-000482-36) and platinum-etoposide chemotheraphy for SCLC (EudraCT Number: 2018-000469-35)	Phase I or I/II studies in SCLC (NCT02034123), AML (NCT02177812), and myelodysplastic syndrome (MDS) (NCT02929498) have been terminated because the risk benefit does not favour continuation.	NA	NA

3.2 Results

3.2.1 Effect of catalytic inhibition of KDM1A on ES cell growth

No evidence was available demonstrating whether the clinical drug candidates for KDM1A are active against preclinical models of ES. To begin to address this issue, ES cell lines A673 and TC71 were treated with compounds for 96 h to investigate the effect of KDM1A inhibition on cell viability. The cell lines tested showed no sensitivity to treatment with the irreversible inhibitors of KDM1A demethylase function: ORY-1001 and GSK2879552 (Fig. 3.1A-B). Conversely, treatment with tool compound SP2509 revealed a rapid decrease in viability with GI50s in the sub-micromolar range (A673: 123 nM and TC71: 355 nM). Morphological assessment of cells following treatment with clinical drug candidates showed no differences between treated and untreated groups. Cell morphology in the SP2509-treated cells was consistent with apoptosis (Fig. 3.1C). These effects were replicated in the DSRCT cell line, which only showed sensitivity to SP2509 but not to the clinical drug candidates (Fig. 3.1D). To address the discrepancy between the KDM1A inhibitors, a chemical probe validated as a potent and selective inhibitor of KDM1A catalytic demethylase activity (GSK-LSD1) was also tested in these sarcoma cell lines (http://www.thesgc.org/chemical-probes/LSD1) (223). Again, treatment had no meaningful effect on growth, with only a 50% reduction at 10 µM in cell line TC71 (Fig. 3.1E-F). As a positive control of compound activity, drug response was assessed in leukaemia cell lines, a context in which catalytic inhibition of KDM1A with ORY-1001 had previously been shown to inhibit growth (220). In agreement with published findings, ORY-1001 and chemical probe GSK-LSD1 treatment at 10 nM reduced cell counts in two leukaemia cell lines (Fig. 3.2). Importantly, the clinical candidate GSK2879552 also decreased growth in this context (Fig. 3.2). These results suggest the biological role of KDM1A in leukaemia and ES cells may be different.
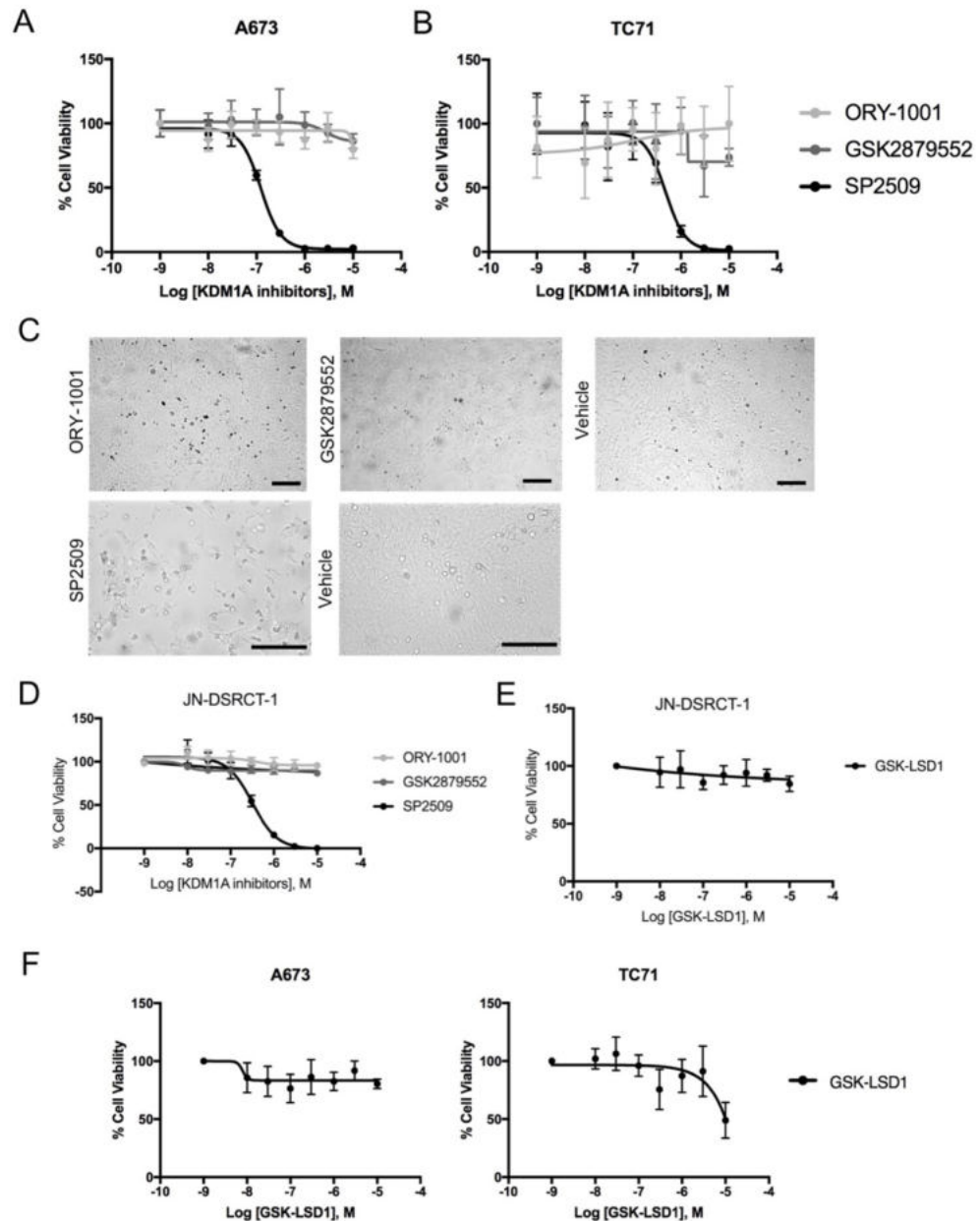
Figure 3.1 Effects of KDM1A inhibition on ES cell lines viability.

(A-B) Dose-response to KDM1A inhibitors in ES cell lines A673 and TC71 after 96 h. (C) Brightfield images of ES cell line A673 treated with SP2509 and vehicle control, ORY-1001, GSK2879552 and vehicle control [2 µM]. Scale bars for SP2509 and vehicle: 200 µm and ORY-1001, GSK2879552, vehicle: 100 µm. (D-E) Dose-response to ORY-1001, GSK2879552, SP2509, and GSK-LSD1 in JN-DSRCT-1 cell line after 96 h. (F-G). Dose-response to GSK-LSD1 in A673 and TC71 cell lines. Cell viability was assessed by MTS assay. Means ± SD of 6 replicates, graphs are representative of three independent repeats.
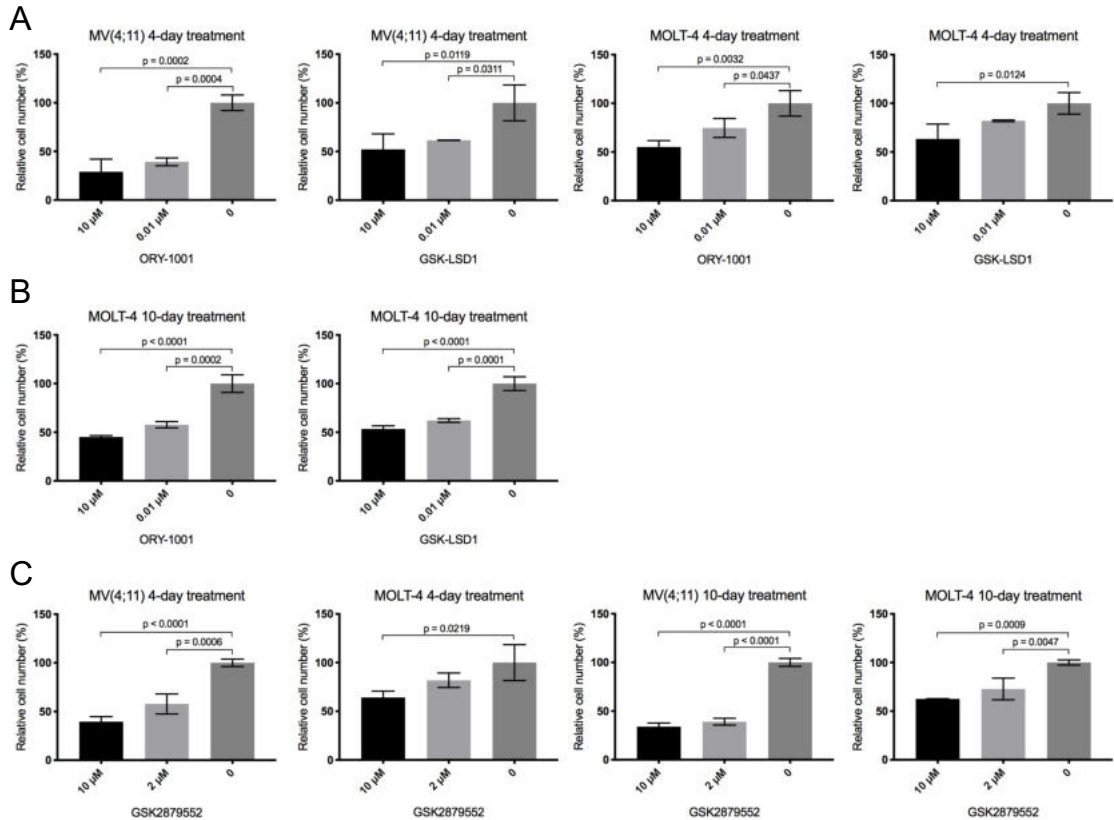
Figure 3.2 Effect of KDM1A inhibition on leukaemia cell lines viability.

(A-B) Viable cell counts of leukaemia cell lines MV(4;11) and MOLT-4 treated with ORY-1001 and GSK-LSD1 (10 µM and 0.01 µM) relative to vehicle control at indicated time-points. Cell counts were determined by Trypan blue assay. Means ± SD of 3 replicates, graphs are representative of two independent repeats. (C) MV(4:11) and MOLT-4 cells treated with GSK2879552 (10 and 2 µM) for 4 days and 10 days. Means ± SD of 3 replicates, single experiment was performed. All p-values were calculated with a one-way ANOVA with Sidak's multiple comparisons test, only significant comparisons are shown.

3.2.2 Catalytic inhibition of KDM1A does not affect EWS-FLI1 transcriptional activity

In order to confirm the drug agents' capacity to inhibit KDM1A's catalytic activity, the H3K4 methyl mark, a well-characterized KDM1A substrate was assessed by Western blotting. Importantly, consistent with their *in vitro* inhibition of KDM1A demethylase activity, all four compounds were able to modulate KDM1A-mediated demethylation of H3K4me2. Figure 3.3 indicates that following 72 h of treatment with 2 µM for all drugs, including the tool compound GSK-LSD1, there was an increase in the global levels of H3K4me2 in both ES cell lines tested (Fig. 3.3). Furthermore, to investigate the impact of catalytic inhibition of KDM1A on EWS-FLI1-driven transcription, validated

downstream target genes of the fusion protein were selected from publicly available datasets and assessed by qRT-PCR following treatment with ORY-1001 and GSK2879552 (150, 224). Extended exposure of up to two weeks (336 h) was conducted to ensure prolonged catalytic inhibition, which is recognised to be important to achieve maximal efficacy with inhibitors targeting epigenetic enzymes (221, 225). Changes in the selected five downstream target genes were observed following treatment with ORY-1001 and GSK2879552 at 2 and 10 µM (Fig. 3.3C-G). Despite statistical significance, these changes did not appear to be dose-dependent and were not consistent across all time-points, casting doubt over their biological significance. As a positive control in this experiment, treatment with tool compound SP2509 (250 nM), reversed expression of repressed genes *LOX* and *HMOX1* in agreement with a previous report, but not *TGFBR2* or EWS-FLI1 activated genes *E2F1* and *CAV1* (Fig. 3.3E-G). One explanation for the difference between these results and the previous study is that the concentration in these qRT-PCR experiments for SP2509 was lower than the 2 µM used in Sankar et al., (2014). Importantly, the GI50 in A673 cell line at 96 h was 123 nM (lower than in Sankar et al., (2014)), and therefore due to SP2509's potent cytotoxic effect, higher concentrations would result in cell death, interfering with gene expression after treatment and limiting the window to assess such changes.
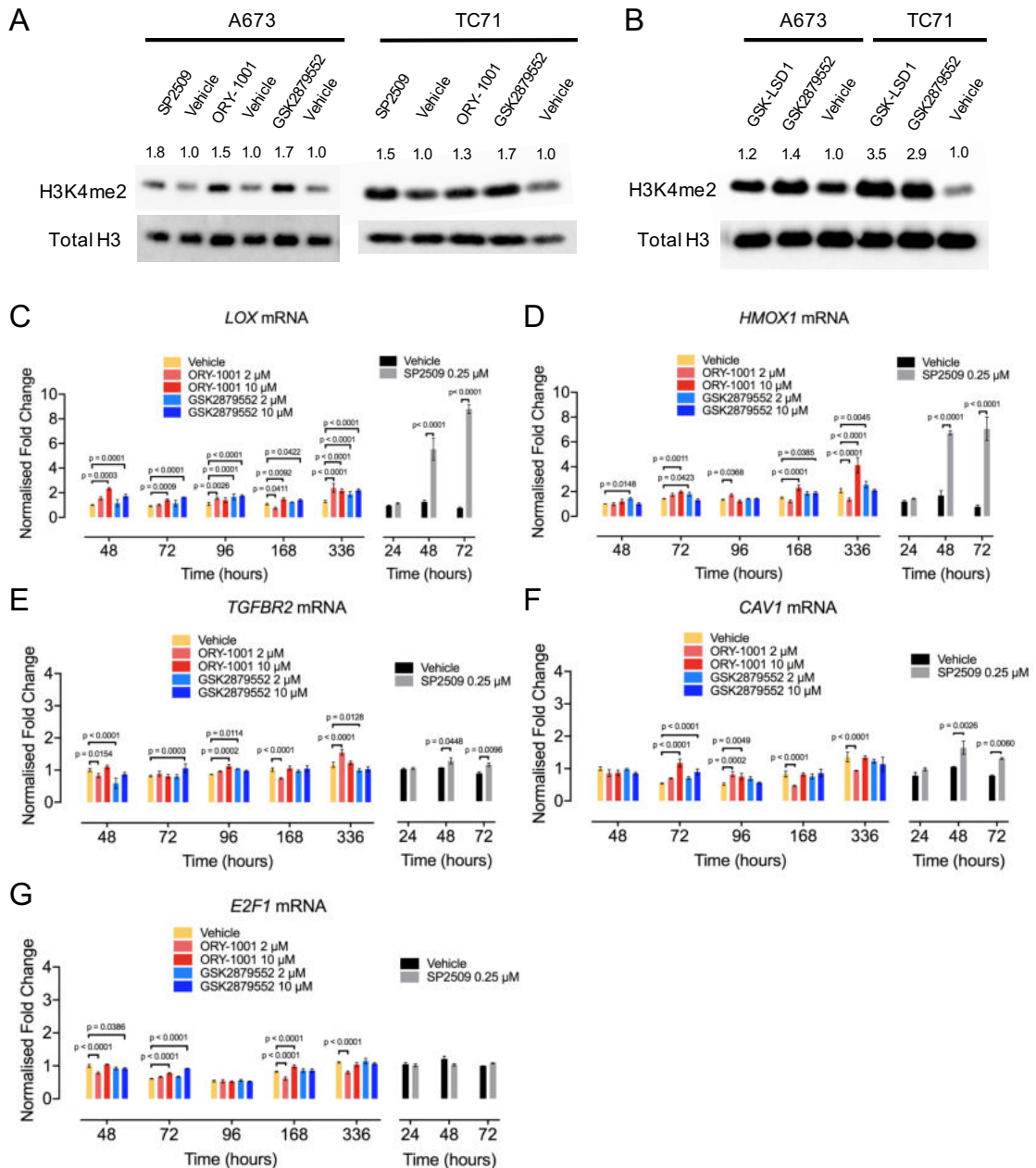
Figure 3.3 Downstream effects of catalytic inhibition of KDM1A on ES cell lines.

(A-B) Western blot of H3K4me2 of A673 and TC71 cell lines treated with KDM1A inhibitors (SP2509, ORY-1001, GSK2879552 and GSK-LSD1) [2 μM] and their respective vehicle controls. Densitometry values shown above each blot were normalised to total H3 and relative to each vehicle control. Western blots are representative of at least two independent repeats. (C-G) Effect of KDM1A inhibitors on EWS-FLI1 target genes expression. qRT-PCR analysis of *LOX, HMOX1, TGFBR2, CAV1, E2F1* in A673 cells treated with vehicle or KDM1A inhibitors ORY-1001 (2 μM, 10 μM), GSK2879552 (2 μM, 10 μM), and SP2509 (250 nM). Normalised fold change was adjusted to human *RPLPO* endogenous control. Means ± SD of three replicates. Data is representative of two independent repeats. All p-values were calculated with a two-way ANOVA with Dunnet's multiple comparisons test, only significant comparisons are shown.

3.2.3 Effect of catalytic inhibition of KDM1A on 3D spheroid models of ES

To perform a more comprehensive evaluation of the effect of KDM1A inhibition, phenotypic assessment, including viability and invasion, was expanded to 3D models of ES. 3D cell culture systems have become more prominent in preclinical studies due to their ability to more closely represent tissue architecture and enable longer experimental time-frames. Tumour spheroids, for example, can recapitulate gradients of nutrients and greater cell-cell interactions that ultimately influence drug response (4, 204). A673 spheroid cultures were treated with ORY-1001 and SP2509 for 10 days with a dose range between 0.3-10 μM (Fig. 3.4). Again, no effect on growth was observed with the irreversible inhibitor of KDM1A catalytic function ORY-1001, whereas SP2509 was active, albeit at higher concentrations compared to its effect in 2D cultures (Fig. 3.4). Drugs targeting epigenetic modifying enzymes often require prolonged inhibition for maximal drug potency and response to treatment. Therefore, spheroids were additionally treated for up to 21 days with a maximum concentration of 100 μM of both clinical candidates (ORY-1001 and GSK2879552). Neither had an effect upon spheroid growth in the extended assay (Fig. 3.4D-E).
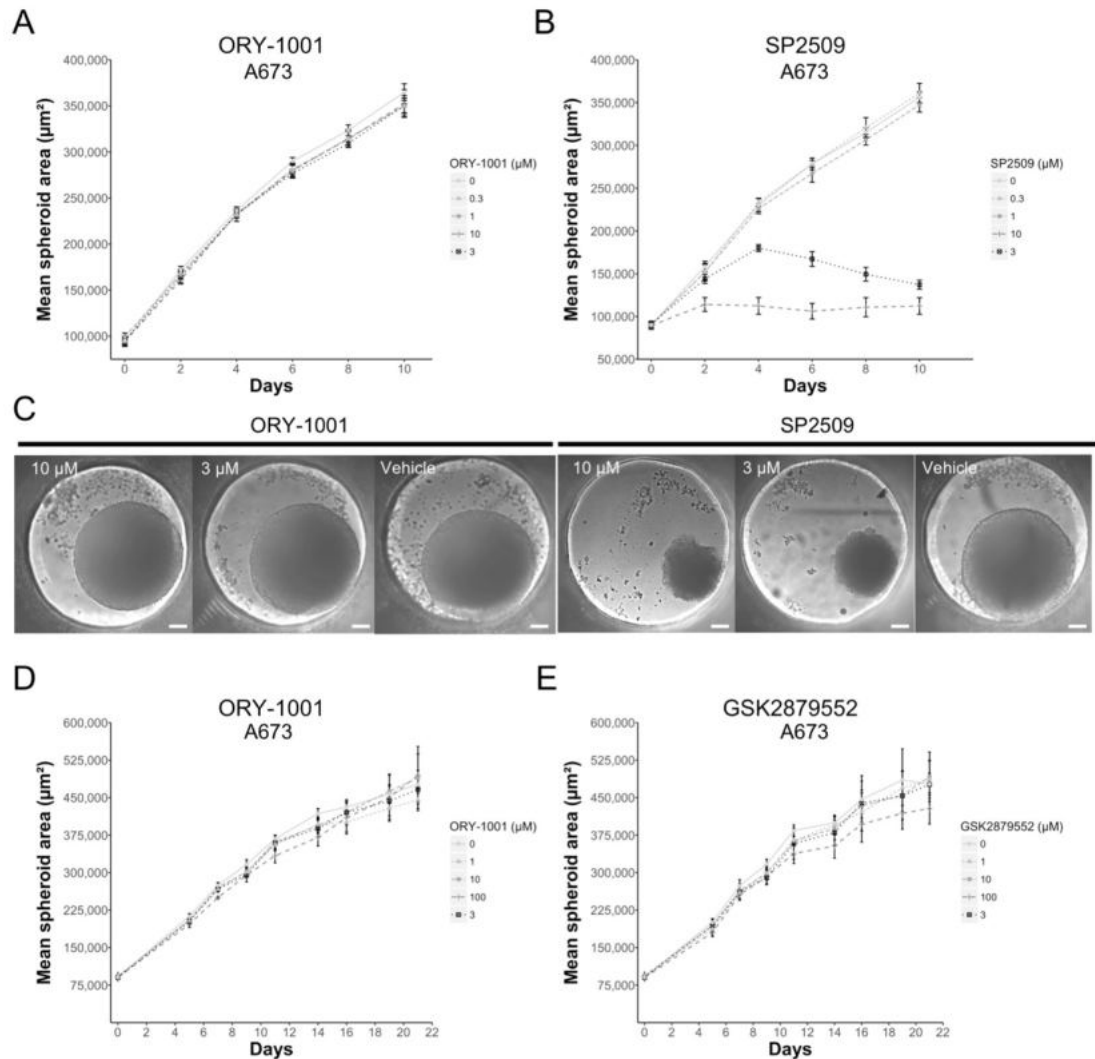
Figure 3.4 Effect of KDM1A inhibition on viability of ES spheroids.

Growth curve of A673 spheroids treated with a range of concentrations of KDM1A inhibitors ORY-1001 (A) and SP2509 (B) for 10 days. (C) Wells containing representative spheroids at day 10 of treatment with ORY-1001 and SP2509 at 10 μM, 3 μM, and vehicle, respectively. Scale bars: 100 μm. Long-term treatment of A673 spheroids with clinical candidates ORY-1001 (D) and GSK2879552 (E) for 21 days. Maximum area at greater width of a sphere was measured in images taken over the different time courses. Means ± SD of 6-10 replicates.

As introduced before, KDM1A has been reported to have a role in migration and invasion (214, 215). To complete phenotypic assessment of KDM1A inhibition, we evaluated if ES cells showed a change in their invasive phenotype upon inhibition of KDM1A catalytic activity. Prior to testing, ES spheroids were embedded in a collagen I matrix (1.3 mg/ml and 2 mg/ml) in serum-free and 10% serum to investigate the suitability of this

substrate to measure cell invasion. Collagen I was initially selected as a matrix for a single pilot study, as this substrate had been used in previous reports of a spheroid-based invasion assay with ES cells (158). However, invasion from A673 spheroids into the collagen matrix was not observed over a period of 24 h and serum starvation was not sufficient to encourage it (Fig. 3.5). This is in agreement with findings in Franzetti *et al.*, (2017) in which unstimulated A673 spheroids did not invade into a collagen matrix (158). On the other hand, JN-DSRCT-1 spheroids successfully invaded in all conditions tested (Fig. 3.6), with serum starvation and a collagen I concentration of 2 mg/ml having the most invasion after 12 and 24 h. Interestingly, morphology between JN-DSCRT-1 invasive cells dissociating from spheroids appeared to be different depending on serum status (Fig. 3.6). Matrigel was then tested as an alternative substrate for invasion in A673 and JN-DSRCT-1 spheroids. This basement membrane extract proved to promote greater invasion of A673 spheroids than collagen I, and was therefore selected for further testing (Fig. 3.7)
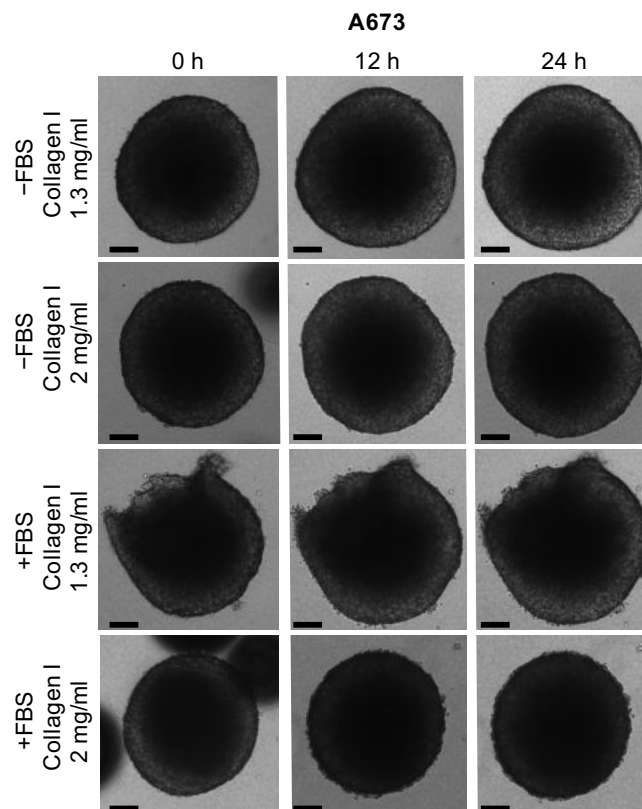
Figure 3.5 3D spheroid invasion assay in A673 spheroids.

A673 spheroids embedded in a collagen I matrix (1.3 mg/ml or 2 mg/ml) in serum-free conditions or 10% FBS. Invasion was monitored over time and pictures taken every 12 h. Scale bars: 100 μm
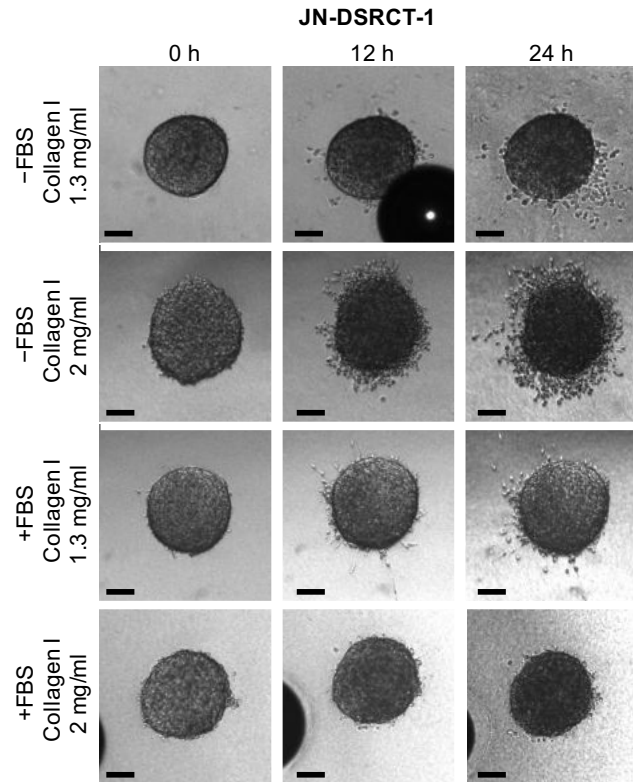
Figure 3.6 3D spheroid invasion assay in JN-DSRCT-1 spheroids.

JN-DSRCT1 spheroids embedded in a collagen I matrix (1.3 mg/ml or 2 mg/ml) in serum-free conditions or 10% FBS. Invasion was monitored over time and pictures taken every 12 h. Scale bars: 100 μm.
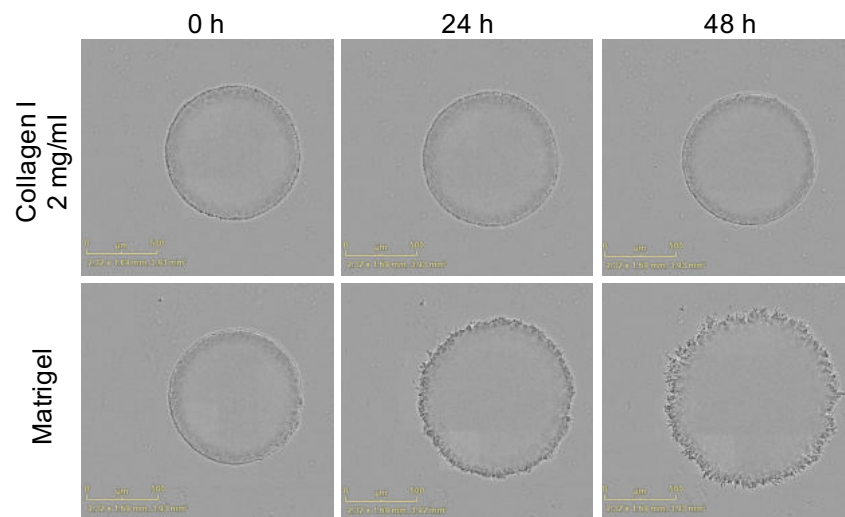
Figure 3.7 Matrix type comparison for spheroid invasion assay

A673 spheroids embedded in a collagen I matrix (2 mg/ml) and Matrigel matrix in 10% FBS. Invasion was monitored over time with observable morphological changes around the edge of the spheroids in the Matrigel matrix. Scale bars: 500 μm.

To continue assessment of this phenotype, A673 and TC71 spheroids were pre-treated for 10 days with the KDM1A inhibitors ORY-1001 and GSK2879552, and subsequently cultured in a Matrigel matrix, in which invasion was monitored for a further 48 h. Morphological changes were noted at the edge of A673 and TC71 spheroids, indicative of invasion of the Matrigel matrix (Fig. 3.8A, Fig. 3.9A). Comparison of the total spheroid area indicated that treatment with catalytic inhibitors of KDM1A had no significant impact on the invaded area in A673 or TC71 spheroids over time (Fig. 3.8B, Fig. 3.9B). Again, chemical probe GSK-LSD1 was included in the assay with no effect on invasion (Fig. 3.8B, Fig. 3.9B).

To ensure this was not a concentration-dependent effect, the 10-day pre-treatment with KDM1A inhibitors was increased to 10 µM in a repeat experiment. Spheroid area was not significantly different indicating invasion was not affected (Fig. 3.8B, Fig. 3.9B). Consistent with our previous results regarding viability, spheroid area was not affected in the 10-day pre-treatment with either 2 µM or 10 µM concentrations of compound (area at 0 h) (Fig. 3.8B, Fig. 3.9B).
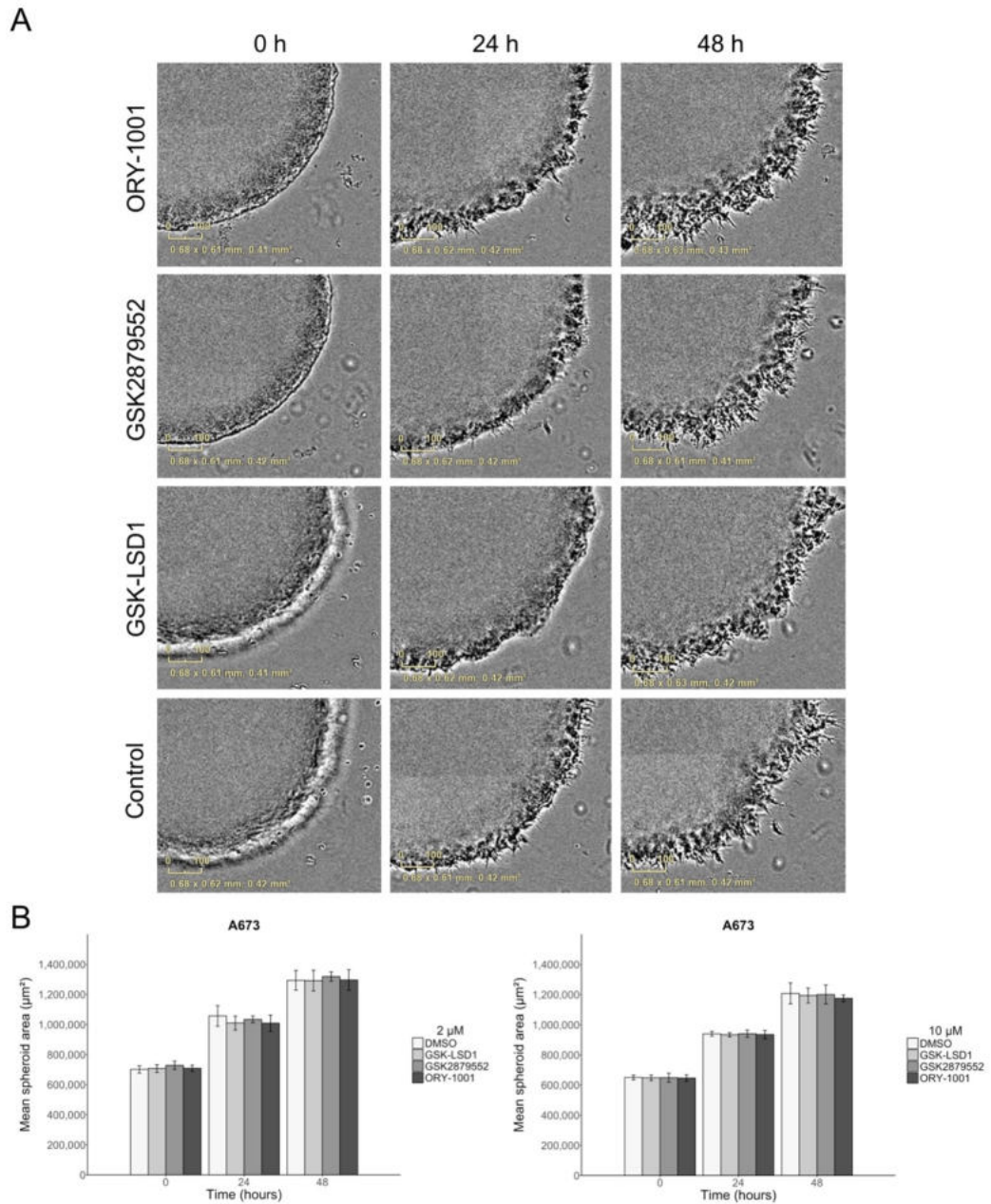
Figure 3.8 3D spheroid invasion assay in A673 spheroids.

(A) A673 spheroids pre-treated with KDM1A inhibitors ORY-1001, GSK2879552, and GSK-LSD1 (2 μM) for 10 days and embedded in a Matrigel matrix. Invasion was monitored over time and pictures taken every 24 h. (B) A673 spheroids area measured with IncuCyte ZOOM software over 48 h with a 10-day pre-treatment of either 2 or 10 μM of KDM1A inhibitors. Means ± SD of 3-5 replicates; graphs are representative of two repeats.
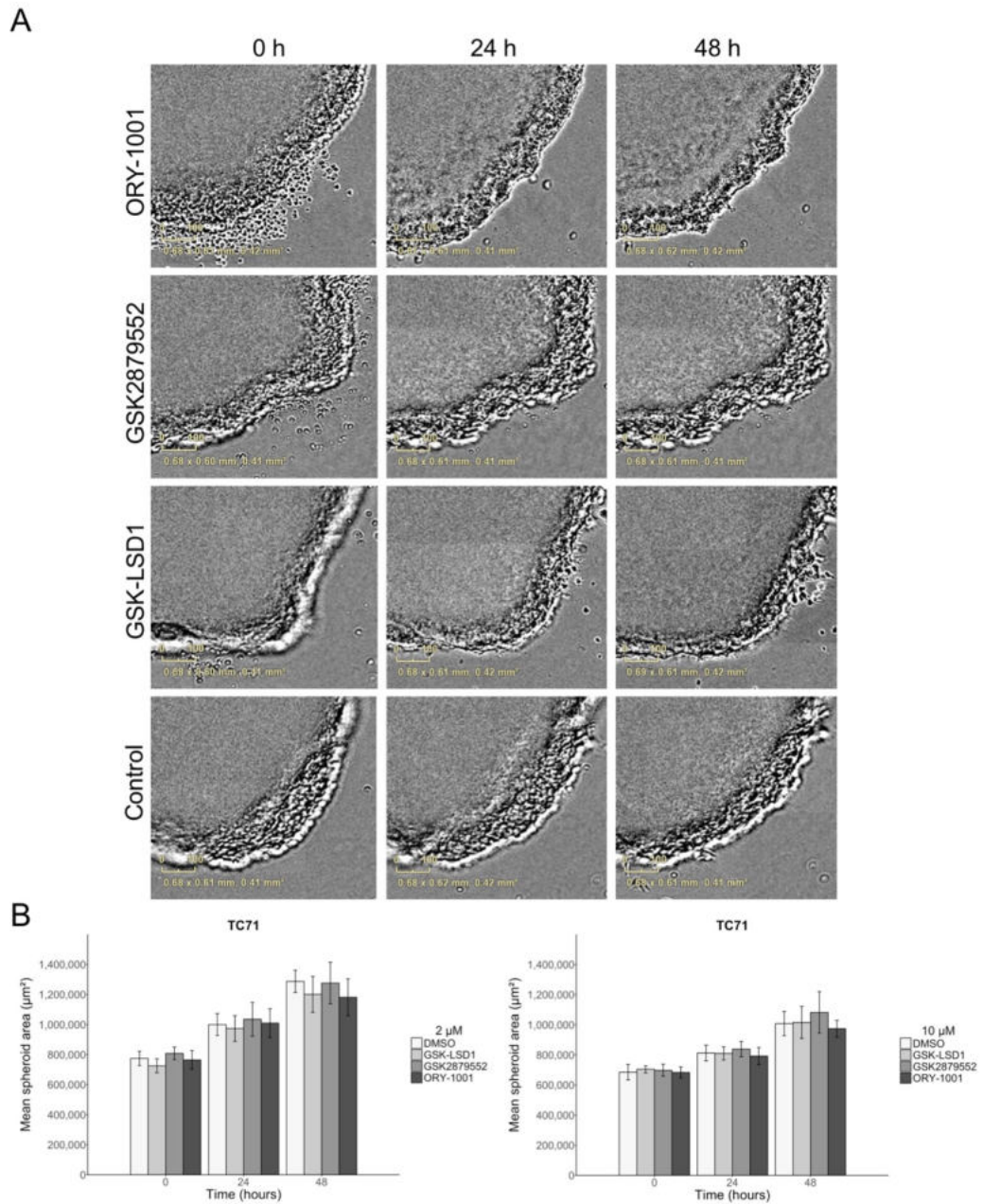
Figure 3.9 3D spheroid invasion assay in TC71 spheroids.

(A) TC71 spheroids pre-treated with KDM1A inhibitors ORY-1001, GSK2879552, and GSK-LSD1 (2 µM) for 10 days and embedded in a Matrigel matrix. Invasion was monitored over time and pictures taken every 24 h. (B) TC71 spheroids area measured with IncuCyte ZOOM software over 48 h with a 10-day pre-treatment of either 2 or 10 µM of KDM1A inhibitors. Means ± SD of 3-5 replicates; graphs are representative of two repeats.

3.2.4 Validation of KDM1A as a therapeutic target in ES and DSRCT

Given the discrepancy in the phenotype observed between the KDM1A inhibitors, knockdown experiments were performed to further verify the role KDM1A has in ES cells. Figure 3.10A shows the panel of siRNAs against KDM1A used in Sankar *et al.,* (2014) and where they are directed on the transcripts of the two isoforms of KDM1A (Fig. 3.10A) (150). siRNAs were transfected separately in A673 cells and protein level was assessed 120 h post-transfection to confirm knockdown of this demethylase. From the four siRNAs tested, siKDM1A 6 and siKDM1A 8 induced 60% and 70% knockdown of KDM1A, respectively, detected by Western blot (Fig. 3.10B). Cell viability was assessed at 96 h and 120 h post-transfection to test whether depletion of KDM1A affected the growth of ES cells (Fig. 3.10C-D). Compared to the non-targeting (NT) control, there was an overall statistically significant difference at 96 h (Fig. 3.10C-D). One caveat to these results is the variation introduced by cell counts and seeding density during replating post-transfection. Importantly, when assessing the effect on cell viability in the context of the level of knockdown of each siRNA, there was no association between protein knockdown (densitometry analysis) and cell viability (r^2=0.05672, p=0.6495, Pearson's correlation) (Figure 3.10E). This suggests siRNA knockdown of KDM1A is not consistent with an effect on cell viability in ES cells in short-term cultures. The same experiment was repeated in JN-DSRCT-1 cells, with the most effective siRNAs also silencing KDM1A in this cell line (Fig. 3.10F). The effect on cell viability was only significant at 96 h (Fig. 3.10F-H), but not at 120 h. Again, it was not dependent on presence of KDM1A overall suggesting siRNA depletion of KDM1A does not affect short-term survival of ES and DSRCT cells.
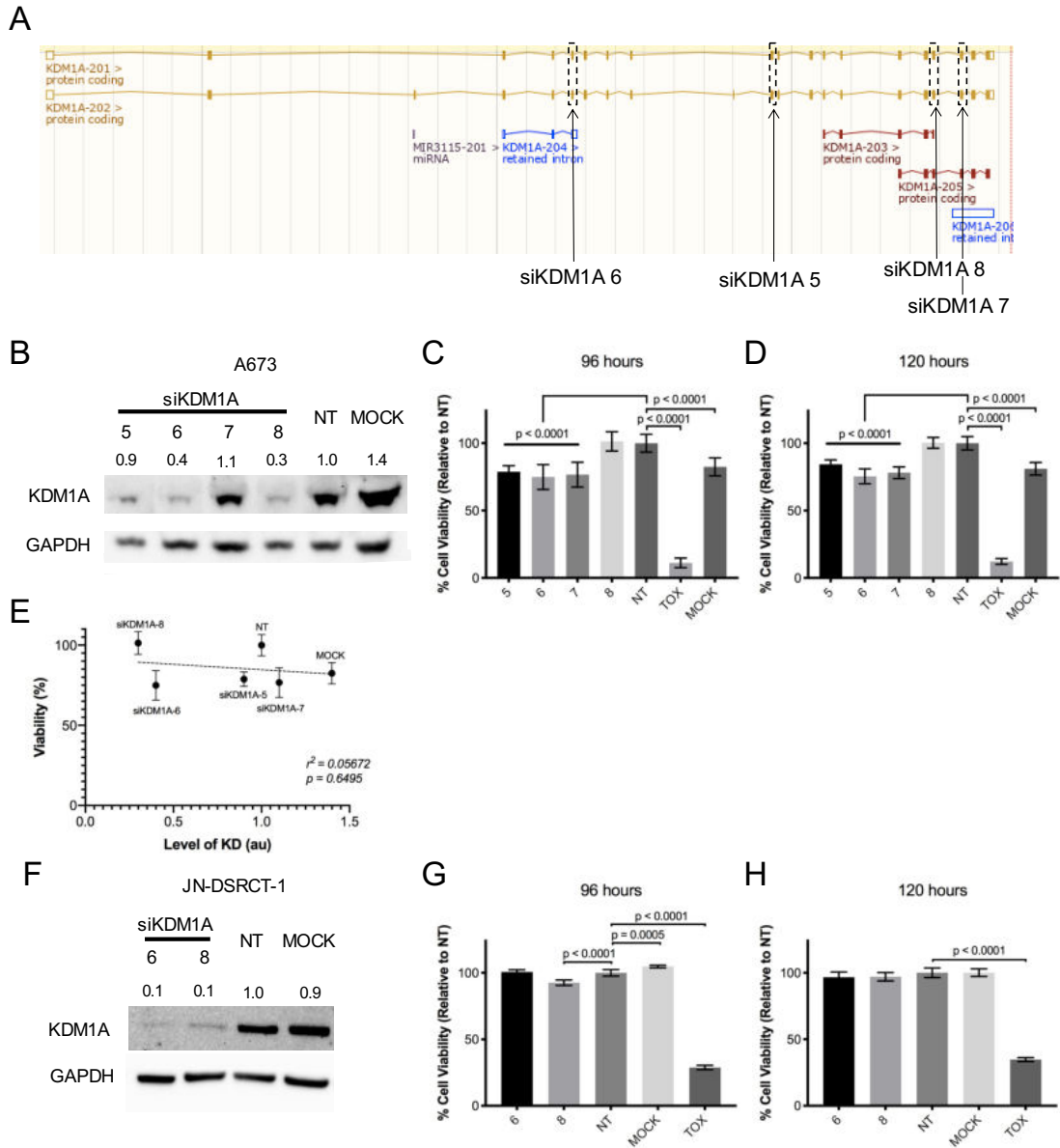
Figure 3.10 Effect of siRNA knockdown of KDM1A on ES and DSRCT cell viability.

(A) siRNAs used by Sankar *et al*., (2013) and mapped on the two KDM1A transcripts variants KDM1A-202 and KDM1A-201, coding for the two KDM1A isoforms A and B, respectively. (B, F) Western blot of KDM1A after siRNA knockdown in A673 and JN-DSRCT-1 cells. Densitometry values shown above each blot were normalised to GAPDH and relative to each vehicle control. MTS assays indicating cell viability of A673 and JN-DSRCT-1 cells at 96 h (C, G) and 120 h (D, H) after transfection with siRNAs against KDM1A. (E) Correlation between cell viability (%) and level of KDM1A knockdown measured by densitometry analysis in transfected A673 cells (r^2=0.05672, p=0.6495, Pearson's correlation). TOX = Positive cell death control. MOCK = Transfection reagent only. NT = Non-targeting siRNA control. Error bars represent standard deviation. Graphs are representative of two independent repeats. All p-values were calculated with a one-way ANOVA with Dunnet's multiple comparisons test, only significant comparisons are shown.

3.2.5 Effects of catalytic inhibition of KDMIA or protein knockdown in combination with ionising radiation

In order to continue exploring the therapeutic potential of targeting this demethylase, the next step was to investigate whether KDM1A depletion or inhibition could sensitise ES cells to DNA damage. A previous study identified KDM1A's recruitment to DSBs following DNA damage, suggesting involvement in the DDR and the potential benefit of a combination with DNA damaging agents (226). A673 cells were pre-treated with 2 μM of KDM1A inhibitors ORY-1001 and GSK2879552 for 72 h and 3 h prior to exposure to doses of ionising radiation (IR) doses of 2 or 6 Gray (Gy) (Fig. 3.11A). The 72-hour pre-treatment with KDM1A inhibitors was selected to test the potential downstream transcriptional effect of inhibiting KDM1A, in addition to suppression of its suggested catalytic-dependent roles in the DDR. Previously in this study, levels of H3K4me2, repressive epigenetic mark and substrate of KDM1A, had been confirmed to change 72 h after treatment with catalytic inhibitors by Western blot, with significant changes in selected downstream targets of KDM1A (Fig. 3.2). On the other hand, the limited 3-hour pre-treatment only encompassed the impact of catalytic inhibition of KDM1A on the proposed role in the DDR (Fig. 3.11). To allow for a 72-hour pre-treatment, these groups were replated prior to IR treatment. Viability was assessed 96 and 144 h after radiation treatment. As expected, there was an overall decrease in cell viability due to the radiation treatment across all three conditions (ORY-1001, GSK2879552, and untreated control) for both pre-treatment schedules (Fig. 3.11). In the 72-h pre-treated groups, there was a statistically significant interaction between the two variables of IR and catalytic inhibition of KDM1A, measured at 96 h and 144 h post-IR (Fig. 3.11B-C). This suggests the effect of IR on viability was linked to catalytic inhibition of KDM1A, but interpretation of these should be done with care. Post-hoc Dunnett's multiple comparisons test revealed significant differences in the mock-IR group between KDM1A-inhibited and vehicle-treated samples (Vehicle vs. ORY-1001, p =<0.01, Vehicle vs. GSK2879552, p =<0.0001, Dunnett's test), which do not relate to a potential radiosensitisation effect. In addition, reduction in viability after ORY-1001 or GSK2879552 treatment alone was not a consistent effect in previous experiments (Figure 3.1). Combination of 2 Gy with 72 h pre-treatment with GSK2879552 appeared to be statistically significant (Vehicle vs. GSK2879552, p =<0.0001, Dunnett's test), but not consistent across the 144 h timepoint. Rather, replating before IR treatment in this KDM1A-inhibited group, could have accounted for variation in cell density, and therefore an overall effect on viability.

Regarding the 3-hour pre-treated groups, there was no significant relation between the mock-IR group and KDM1A-inhibited samples at 96 h post-IR and at 144 h post-IR (Fig. 3.11D-E). Overall, these experiments do not provide strong evidence of radiosensitisation through catalytic inhibition of KDM1A in ES cell line A673.
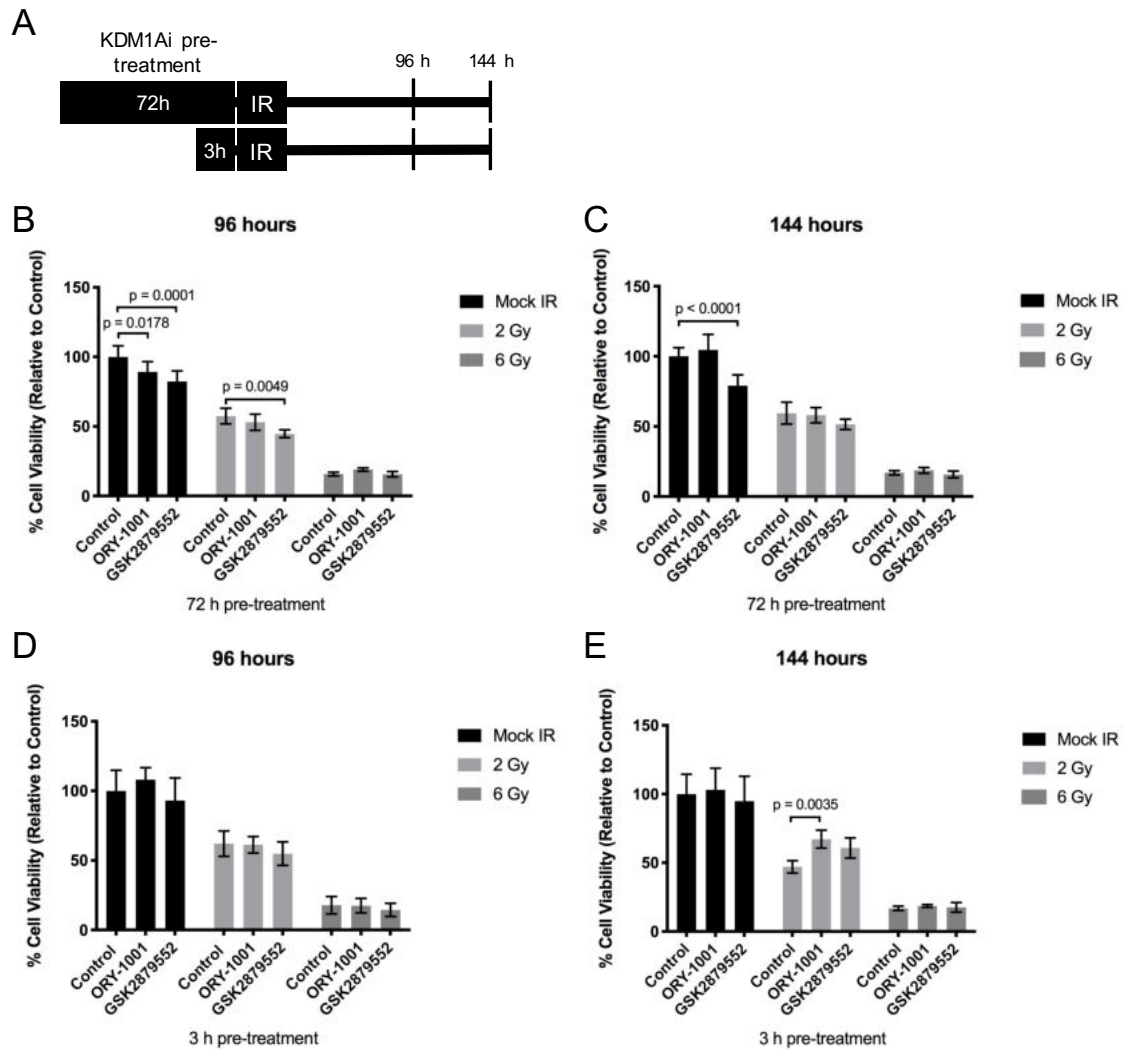
Figure 3.11 Effect of catalytic inhibitors of KDM1A in combination with ionising radiation on cell viability.

(A) Pre-treatment schedules for KDM1A inhibition (KDM1Ai) with ORY-1001 and GSK2879552 in combination with ionising radiation (IR). (B-E) MTS assay indicating cell viability 96 h and 144 h post-treatment with IR (2 Gy, 6 Gy). B and C received a 72-hour pre-treatment with KDM1A inhibitors ORY-1001 and GSK2879552 [2 μM], and D and E were treated for 3 h before irradiation. Error bars represent SD. All p-values were calculated with a one-way ANOVA with Tukey's multiple comparisons test, only significant comparisons are shown.

To test whether radiation had an effect in combination with depletion of KDM1A, transfected cells were exposed to IR 48 h post-transfection and viability assessed 96 h later (120 h post-transfection) (Fig 3.12A). Protein knockdown was verified at the time of IR treatment by Western blot (Fig. 3.11B). Assessment of cell viability at 96 h indicated statistical significance between knockdown of this demethylase and IR treatment (Fig. 3.12C). However, as shown before, the effects of KDM1A depletion on viability, were not consistent with the level of knockdown achieved (Fig. 3.10), and therefore cannot be associated with depletion of this demethylase.
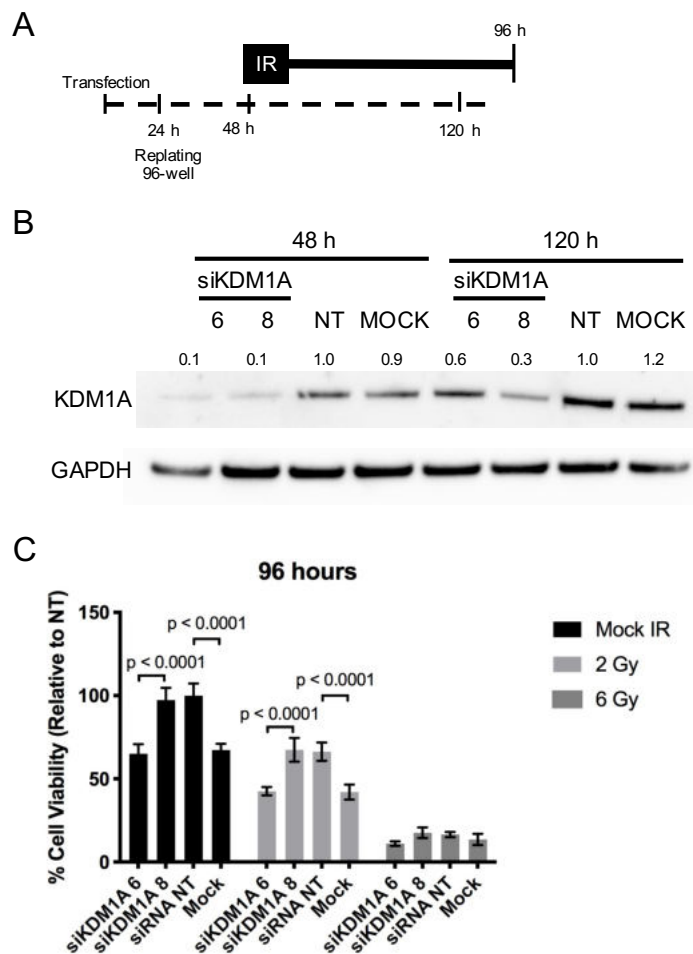
Figure 3.12 Effect of KDM1A depletion in combination with ionising radiation on cell viability.

(A) Schedule of transfection, radiation treatment, and viability assessment in A673 cells. (B) Western blot of KDM1A after knockdown with siRNA oligonucleotides in A673. Densitometry values shown above each blot were normalised to GAPDH and relative to each vehicle control. (C) MTS assay indicating cell viability 96 h and 144 h post-treatment with IR (2 Gy, 6 Gy). All p-values were calculated with a one-way ANOVA with Tukey's multiple comparisons test, only significant comparisons are shown.

3.3 Discussion

3.3.1 Evaluating the potential of catalytic inhibition of KDM1A on ES cells tumourigenesis

KDM1A's proposed functional role in ES oncogenesis, alongside high expression in this and other sarcomas such as DSRCT, has made it a promising therapeutic target (195, 227). To examine this, a comprehensive evaluation of phenotypes following treatment with clinically available inhibitors of KDM1A was carried out. Overall, findings in this results chapter do not support repurposing clinical compounds ORY-1001 and GSK2879552 as a therapeutic strategy targeting EWS-FLI1 activity in ES.

Firstly, inhibitors of catalytic activity of KDM1A did not exhibit significant cytotoxic effects in 2D and 3D viability assays, with only a mild effect at 10 µM in TC71 cells in 2D. Compound GSK-LSD1 was then tested in parallel as a selective chemical probe for inhibition of KDM1A catalytic function (http://www.thesgc.org/chemical-probes/LSD1) (221, 223). This validated tool compound has the same chemical scaffold as the clinical drug candidates and shares its mechanism of action through irreversible covalent modification of the FAD cofactor. Treatment with GSK-LSD1 however, had no effect on ES cell viability in 2D and 3D assays. Alternatively, prolonged inhibition (10 and 21 days of treatment) was explored in order to achieve maximal efficacy, as suggested in reports with inhibitors of EZH2 in lymphoma (220, 221, 225). Length of treatment did not affect the response to inhibition of KDM1A catalytic function with clinical drug candidates. Lastly, clinical drug candidates had been demonstrated to have growth inhibitory effects in leukaemia and small cell lung cancer (SCLC) cell lines (220, 221). Hence two leukaemia cell lines were used as a positive control, in which these results were reproduced with both clinical drug candidates and tool compound GSK-LSD1. Together, this suggests that whilst catalytic inhibition of KDM1A has anticancer effects in leukaemia, it does not affect survival of ES in *in vitro* models.

The original model in Sankar *et al.* (2014) (150) proposed KDM1A as a mediator of EWS-FLI1 transcription activity that can be targeted through small molecule inhibition. This model, however, does not address the extent to which catalytic function of KDM1A is key to establishing the EWS-FLI1 transcriptional programme. Given the absence of an effect on viability, it was important to assess whether catalytic inhibition blocks

KDM1A's proposed role in the transcriptional programme of this sarcoma. Firstly, levels of H3K4me2 were assessed and seen to increase following treatment with all KDM1A inhibitors, demonstrating effective reduction of catalytic activity of this demethylase. The literature reports that global or promoter-specific accumulation of methylation of H3K4 is not always seen after KDM1A inhibition, regardless of decreased KDM1A activity (221, 228). Thus, to continue to address this issue, expression of downstream genes was measured after treatment. Genes were selected from publicly available data sets of modified genes following EWS-FLI1 knockdown and KDM1A knockdown, and therefore expected to be affected if indeed they are regulated through this demethylase (150, 224). Expression of downstream targets of EWS-FLI1 after ORY-1001 and GSK2879552 treatment was not reversed by catalytic inhibition of KDM1A, regardless of the length of treatment. This suggests that blocking catalytic activity alone is insufficient to reverse its transcriptional targets. Assessment of differentially expressed genes after KDM1A knockdown in ES cell lines, followed by chromatin immunoprecipitation-sequencing (ChIP-seq) of KDM1A, could be a way of determining which of the 'putative KDM1A-regulated genes' are actually bound by KDM1A and their activation or repression depends on their methylation status (229).

The disease context and the nature of the role that KDM1A plays in various malignancies are key determinants of how effective KDM1A inhibition is as a therapeutic strategy. In leukaemia, KDM1A activity involves silencing regulators of haematopoiesis, essential in maintaining leukaemia stem cells undifferentiated (230). This differentiation arrest has been shown to be abrogated through targeting KDM1A activity or protein knockdown (220, 228, 230). Initially this was thought to be through catalytic activity of this demethylase, however, it has now been shown that catalytic KDM1A inhibitors block interaction with transcription factor growth factor independence 1 (GFI1) to elicit their cytotoxic effect in AML cell lines (228, 231). In the context of ES, blocking this interaction between KDM1A and this myeloid transcription factor is likely not relevant to disease mechanisms of this sarcoma. In addition, inhibition of its canonical demethylase activity was also insufficient to modify expression of a selection of known target genes of EWS-FLI and impair ES cells survival.

Comprehensive evaluation of the clinical potential of targeting KDM1A's catalytic function, required investigating additional phenotypes related to the activity of this

demethylase and relevant to ES tumourigenesis. For example, additional roles for KDM1A in modulating self-renewal and differentiation in ESCs also encompass regulation of migration during normal mammalian development and promoting EMT in breast cancer tumour development (218, 232). Importantly, in solid tumours, high levels of KDM1A have been associated with metastasis and inhibition of this demethylase has been shown to attenuate migration and invasion in breast cancer cell lines (215). ES patients with metastatic disease have dismal survival rates below 30%, making invasion part of the phenotypic assessment of KDM1A inhibition as therapy highly relevant (233). However, in a spheroid invasion assay, KDM1A inhibition did not alter cell morphology associated with an invasive phenotype and failed to suppress invasion in a Matrigel matrix.

3.3.2 Investigating the potential of catalytic inhibition of KDM1A in combination with DNA damaging agents

KDM1A has been shown to be recruited to sites of double strand breaks in DNA, after which H3K4me2 levels decreased, potentially to repress transcription at these sites following damage (226). Other chromatin-modifying factors have been shown to play a role in the DDR, including members of the NuRD complex of which KDM1A is associated to (213). Given this link to the DDR, inhibition of this demethylase together with a DNA damaging agent was hypothesised to work as a combination therapy. Ionising radiation, which is part of the standard of care for ES patients, was chosen as a general inducer of DNA damage. However, combination studies with catalytic inhibitors or depletion of KDM1A failed to produce a radiosensitising effect. To verify any potential radiosensitising effect, a known radiosensitising agent such as a DNA-PK inhibitor, could have been used as a positive control for this experiment. Future work could also investigate KDM1A's contribution in the DDR by modulating the repair pathway of choice, for example promoting activation of NHEJ. This is because loss of the catalytic function of this demethylase, was shown to particularly affect 53BP1 foci formation possibly due to not being able to interact with RNF168. Overall, this resulted in increased activation of HR (226).

3.3.3 Model for KDM1A's role in EWS-FLI1-mediated transcriptional activity

The effects of catalytic inhibition of KDM1A in ES in these results strongly contrasts the effects seen with compound SP2509 in this work and in previous findings (150, 224).

One explanation for the difference could be attributed to the mechanism of action of these inhibitors. Clinical drug candidates against KDM1A bind and trigger irreversible covalent modification of the FAD cofactor (220, 221), whilst the tool compound is thought to reversibly bind to the H3 pocket region of KDM1A (229). It is possible that inhibitor class, specifically the mechanism of inactivating KDM1A is a determining factor to elicit anticancer effects in ES. Importantly, SP2509 has been shown to cause cell death in a KDM1A-knockout leukaemia cell line and its isogenic control, suggesting it also has additional cytotoxic effects independent from KDM1A binding (234). Consistent with this, the 2-hydroxyphenyl-hydrazone structural motif within SP2509, has previously been identified as a pan-assay interference flag with the potential of causing promiscuous biological activity (222, 235, 236). Determining the mechanism of action and binding partners of this compound still remains an important area of investigation. Particularly so, since SP2577, the clinical formulation and analogue of this compound, is currently in a phase I trial for refractory Ewing sarcoma (237, 238).

Regarding validation of KDM1A as a target for this malignancy, siRNA depletion of this demethylase did not result in a strong effect on cell viability. This is challenged by recent findings showing shRNA-mediated knockdown of KDM1A causes severe growth impairment and cell death in ES cells, thus confirming their dependency on this demethylase (224). The difference between the effect caused by the knockdown techniques could be explained by the transient and partial nature of siRNA technology, achieving 60-70% knockdown of the protein in this work. It is plausible that the stability and long-term depletion achieved by shRNA is necessary to fully eliminate KDM1A's function. Overall, the discrepancy between the results regarding inhibition of KDM1A catalytic function, reversible inhibitor SP2509, and knockdown of the multidomain protein strongly suggests a non-canonical role for KDM1A, independent from its demethylase function. These characteristics coincide with other epigenetic regulators such as EZH2. Its emerging methyltransferase- and polycomb-independent roles provide novel therapeutic potential for inhibitors disrupting its docking capacity (239). In line with this model, recent reports in prostate cancer cell lines described a scaffolding role for KDM1A, whereby a catalytically inactive KDM1A mutant was still able to establish the prostate cancer gene network and ensure survival of castration-resistant prostate cancer cell lines (229). This was further confirmed with tool compound SP2509, proposed as an allosteric inhibitor, capable of inducing cell death in prostate cancer cell lines.

Similarly, future work could express this 'catalytically dead' K661A KDM1A mutant in an ES KDM1A-knockout cell line to investigate how much of EWS-FLI1 transcriptional activity, and importantly, cell viability can be rescued. Recently, novel non-enzymatic functions for KDM1A have been found in cancer cell lines and non-malignant contexts (231, 240). It is foreseeable that KDM1A's role as a docking element for additional proteins may play a more prominent part in helping EWS-FLI1 drive tumourigenesis (217). Already, fusion protein EWS-FLI1 has been demonstrated to require cooperation of chromatin remodelling complexes such as PRC2 and BAF in order to modify gene expression (143, 144, 153). Identifying additional binding partners of KDM1A and their relevance in the context of ES remains an unexplored area. Different KDM1A constructs with mutated residues could be an approach to continue to elucidate key binding sites on this demethylase, particularly those contributing to EWS-FLI1 activity (149). Importantly, knowing whether these sites are already targeted by allosteric inhibitors of KDM1A, or can be druggable, will be key to future therapies.

In conclusion, assessment of tumorigenic phenotypes following catalytic inhibition of KDM1A in ES did not provide strong evidence to pursue this as a therapeutic strategy. These findings were particularly relevant at the time when a Phase I trial in ES patients with INCB059872 started (NCT03514407) (241), given that this drug was of the same mechanistic class of KDM1A inhibitors ORY-1001 and GSK2879552. This trial, however, has now been terminated citing strategic business decisions. Phase I trials with ORY-1001 in adult patients with AML and SCLC have been completed and are continuing in combination with front-line chemotherapeutic agents. However, previous clinical trials with GSK2879552 have been stopped citing that the benefits do not outweigh the risk (242-245). Whilst KDM1A remains a potential target in this sarcoma and other malignancies, non-canonical functions rather than inhibiting catalytic activity should be explored as a therapeutic prospect.

Chapter 4 A novel assay to identify combination strategies targeting the replication stress response

4.1 Introduction

The previous chapter presented an approach to targeting the fusion protein EWS-FLI1 through catalytic inhibition of KDM1A, a histone modifying enzyme which contributes to the ES transcriptional programme. In light of this not being successful as a therapeutic prospect, the aim of this study was to continue identifying alternative novel combination strategies for this sarcoma. To achieve this, the strategy encompassed mechanism-informed selection of drug targets, together with a focus on clinical relevance and translational potential. Therefore, instead of basing decisions on immediate drug response and target inhibition alone, cell-based assays were designed to study the long-term impact of combination treatments and cell recovery. A set of criteria served as a prioritisation plan to select and rank the combination strategies tested. The results from these combination studies are presented and discussed here, together with an evaluation of the methodology.

As detailed in the introduction of this thesis, one consequence of EWS-FLI1-activated malignant transformation is interference with EWSR1 activity, which results in sustained phosphorylation of RNAPII and higher basal levels of transcription (37). Dysregulated transcription leads to conflicts with the replication machinery, apparent in the form of R-loops and replication stress (32, 33). To deal with the innate levels of RS generated by the presence of EWS-FLI1, ES cells depend on the activity of the DDR mitigating accumulation of DNA damage and maintaining genome integrity (31). Some evidence of this dependency are high levels of CHK1 expression and sensitivity to single-agent inhibition of ATR (98, 167), the apical kinase in the ATR-CHK1-WEE1 axis in the RSR. Based on this rationale, it was hypothesised that treating ES cells with inhibitors targeting the RSR, involving cell cycle checkpoint activation, and/or DNA repair could exploit their dependency on this pathway due to increased innate levels of RS. In addition, combination with DNA damaging agents inducing replication stress could further exploit this vulnerability. For these reasons, drug targets selected were ATR, CHK1, WEE1, and PARP1. Of note, PARP1 inhibition as a single agent has been clinically tested as therapeutic strategy obtaining no significant response (199) (discussed below in 4.3).

However, other studies investigating PARP inhibition in combination with irinotecan are currently ongoing (190, 191, 246). Some of these trials include combination arms with temozolomide as well (NCT02392793) (246).

4.2 Results

4.2.1 Clinical drug candidate selection and methodology for combination studies

Regarding the process of identifying novel targets, there were three key points making up the mechanism-informed phenotypic approach in this study.

(i) Spheroid cultures of ES cell lines were established and used for drug testing. These models have greater potential of developing heterogeneity driven by microenvironmental gradients affecting tumour physiology, and also allow for medium-term culturing (three-week assays) (Fig. 4.1B) (204, 247). Initially, two ES cell lines A673 and RM82 were selected to test all drug combinations with further validation to be carried out in additional cell lines.

(ii) Only drug targets relevant to the hypothesis with a clinical drug candidate undergoing trials were selected (Table 4.1). This was to facilitate their introduction into the clinic given the lack of targeted therapies for this sarcoma. Additionally, having chosen compounds that have undergone phase I trials, data on pharmacokinetic (PK) and pharmacodynamic (PD) parameters, informed the concentrations used in *in vitro* experiments where possible (Table 4.1).

 (iii) Irinotecan was chosen as the combination partner for the chemotherapy backbone for two reasons. Firstly, this chemotherapeutic agent forms part of the regime administered to Ewing sarcoma patients during relapse alongside temozolomide (181, 248). Importantly, any novel therapeutic approach or combination partner would be trialled in the relapse setting and could be directly compared to irinotecan and temozolomide in a randomised setting. In this way, potential successful combinations could act as preclinical evidence for translation into the clinic. Secondly, irinotecan is an inhibitor of topoisomerase I, which creates a single nick on DNA to relieve the torsional stress existing behind and ahead of the replication fork (182, 184). Mechanistically, irinotecan treatment results in enhanced replication fork stalling and DSB accumulation, making it suitable for combination with inhibitors of the RSR. Examples of similar combination strategies with irinotecan have been successful in colorectal cancer and are being considered for other malignancies (184, 186). Importantly, during the course of this study, a recent randomised comparison of relapse regimens in ES found the

irinotecan/temozolomide combination to be inferior to two other arms consisting of topotecan in combination with cyclophosphamide, and high-dose ifosfamide (183). Whilst topotecan and irinotecan have clinical differences, mechanistically this other topoisomerase I inhibitor would still be a suitable combination partner (182, 184).
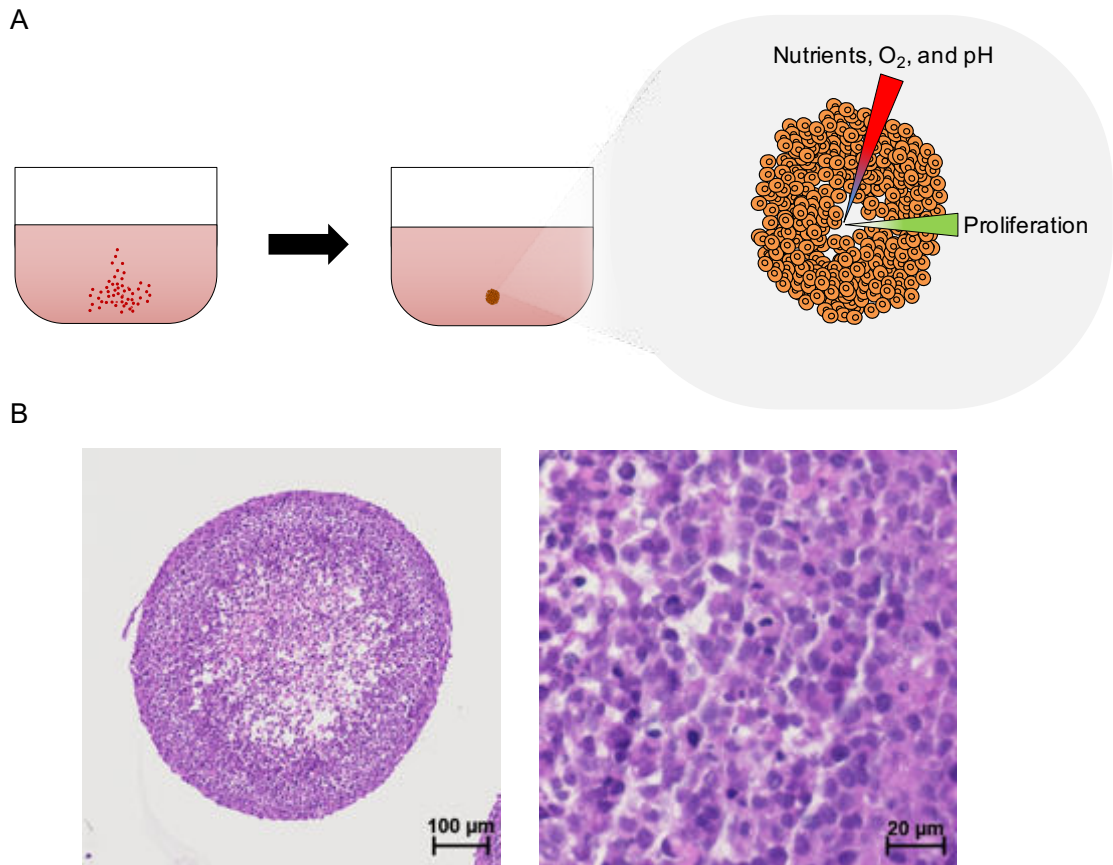
Figure 4.1 3D spheroids as tumour models of ES.

(A) Diagram illustrating the process of spheroid formation in an ultra-low attachment plate, from seeding single cells to a spheroid. These models naturally develop microenvironmental gradients of nutrients, oxygen, and pH, amongst other factors. These cues help to shape a layered structure of zones with different proliferation levels away from a necrotic core, overall contributing to creating a heterogeneous model. (B-C) Haematoxylin and eosin staining of a paraffin-embedded section of ES cell line A673 cultured as a spheroid. This spheroid shows less cellularity in the centre, with distinct regions throughout the spheroid. The higher magnification image shows the characteristic small blue round cells arrangement of this type of tumour.

Table 4.1 Drug targets and clinical drug candidates

Drug target	Clinical drug candidate	Pharmacokinetic data					Biomarker	Reference
		Clinical Dose	AUC	C_{max}	C_{trough}	$t_{1/2}$ (h)		
WEE1	AZD1775 (MK1775, Adavosertib)	225 mg BD	8590 nM·min	1.38 μM	776 nM	-	Tyr15 on CDK1	(99, 101)
ATR	AZD6738 (Ceralasertib)	160 mg BD	-	5000 ng/ml	1000 ng/ml	6.1-12.1 h	pS317 and pS345 on CHK1	(102)
				12.12 μM	2.4 μM			
	VX-970 (M6620, Berzosertib)	1 h infusion of 60 mg/m2	-	343 ng/mL	-	-		(249)
			-	739.93 nM	-			
CHK1	SRA737	150 mg tablet per day	3550 ng·h/ml	548 ng/ml	52 ng/ml	-	Auto-phosphorylation (pS296)	(100)
			9.35 μM·h	1.44 μM	137 nM			
PARP1/2	Olaparib (Lynparza)	300 mg tablet BD	49.0 μg·h/ml	7.7 μg/ml	-	14.9 h ± 8.2 h (after a single 300 mg tablet)	PARylation detected with anti-PAR, seen smear by Western blot	(97)
			112.60 μM·h	17.69 μM	-			

4.2.2 A novel *in vitro* spheroid-based assay to test drug combinations

In terms of the experimental set up for testing drug combinations, irinotecan's schedule used in paediatric trials was translated into an *in vitro* spheroid-based assay. A standard cycle consists of a daily schedule of intravenously-administered 50 mg/m^2/day of irinotecan for 5 consecutive days every 21 days (248) (Fig. 4.2A). As irinotecan gets metabolised and activated in the liver of the patient, in the experimental setting, SN-38, the active metabolite of irinotecan was used instead, and was tested alone and in combination with selected clinical drug candidates for 5 consecutive days, at the beginning of this 21-day cycle (Fig. 4.2B). Spheroid area was monitored throughout the experiment as a proxy for spheroid growth, respectively. The optimal result for

combination treatments was complete cell killing with no surviving population or an overall cytotoxic effect, determined to be any decrease in spheroid size from the original at day 0 (Fig. 4.3A-B). Alternatively, any slowing down in spheroid growth compared to the untreated control would be classified as an inhibitory effect, with no overall cell killing. Importantly, spheroids in this category would still be viable and could represent a 'disease progression' outcome in the clinic (Fig. 4.3C). Having a long-term window to assess cell recovery after a 5-day treatment was important to observe more phenotypes that may take more time to develop such as a sustained cytostatic effect (Fig. 4.3D). Overall, this model allowed study of the effects of the clinical drug candidates more thoroughly because of the nature of the drug targets, requiring continuous cell cycling to observe the full effect of their inhibition. Once DNA damage is generated, its accumulation triggers signalling mechanisms opening up multiple fates for affected cells. Continuous drug incubation on the other hand, limits the potential for recovery and does not capture the context of how drugs are administered to patients, failing to fully assess their therapeutic effects.
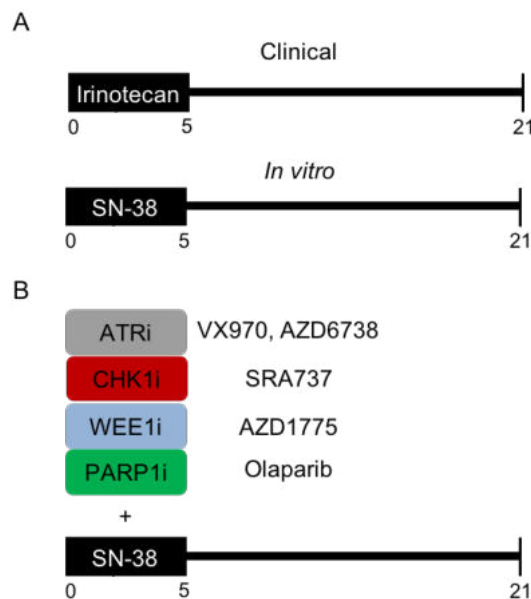
Figure 4.2 Treatment schedule for drug combination studies.

(A) 21-day chemotherapy schedules with 5 consecutive days of irinotecan (clinical) or SN-38 (*in vitro*) treatment. (B) Outline for schedule with combination treatments with selected drug targets and their respective clinical drug candidates.
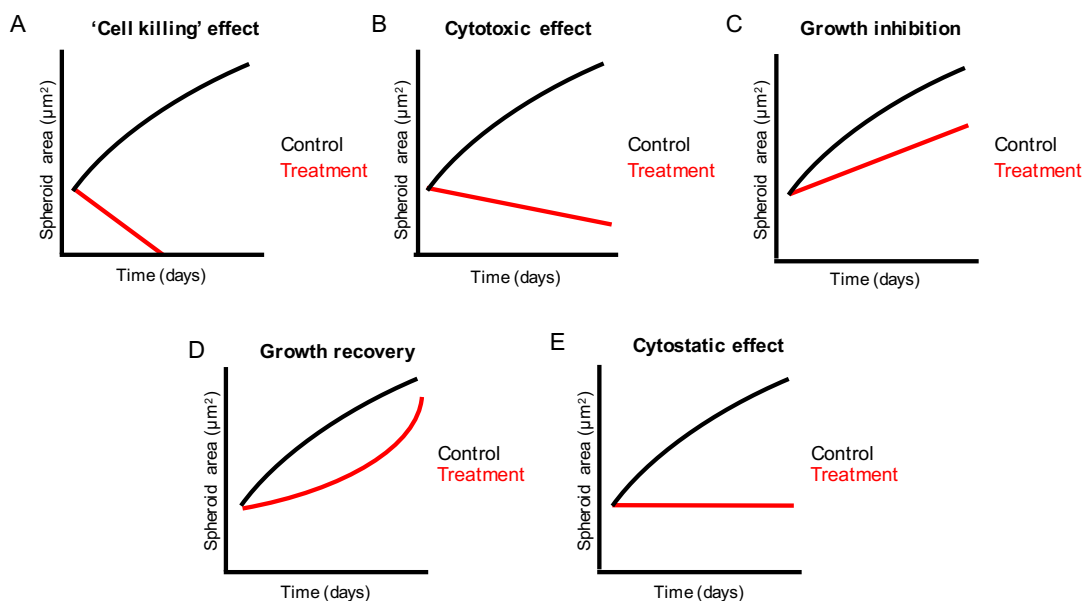
Figure 4.3 Theoretical responses to treatment in the spheroid-based assay.

Spheroid growth curves showing theoretical responses to treatments. (A) An outcome of complete 'cell killing' is determined by a sharp decrease in spheroid area representing a spheroid breaking up, and so limiting any possible assessment of size. (B) A cytotoxic effect is characterised by an overall decrease in spheroid area, without complete cell killing. (C) Growth inhibition is when the spheroid growth rate is only reduced upon treatment, but the net effect is not an overall cytotoxic effect. (D) A growth recovery effect shows an initial response, followed by recovery, similar to relapse. (E) A cytostatic effect occurs when growth is halted and spheroid area remains unchanged.

4.2.3   Establishing a SN-38 backbone

Before assessing the clinical drug candidates in combination, a clinically achievable concentration range for SN-38 was determined from published PK data from a phase II trial in children with refractory solid tumours (180). From a daily dose of irinotecan of 50 mg/m^2 intravenously administered, this study calculated the parameters in table 4.2, adapted from Bomgaars *et al.* 2007 (180). Following conversion to nanomolar concentrations, these parameters served as guidelines to establish a threshold for achievable concentrations of SN-38 in ES spheroids. The *in vivo* half-life of SN-38 at the specific dose of irinotecan was determined to be 7.6 hours, based on an average C_{max} of 13 ng/ml (33 nM) (Table 4.2). Although this will be dependent on the drug metabolism in the liver, varying from patient to patient, the high C_{max} achieved together with this drug clearance rate provide a favourable window of exposure to the active compound.

Sensitivity to SN-38 differed in dose-responses in ES spheroids (Fig. 4.4). Concentrations that resulted in a growth inhibitory effect, with viable spheroids at the end of the 21-day cycle, were taken forward for testing in combination with clinical drug candidates. These concentrations were 2 nM in spheroid models of cell lines A673 and RM82 and 1 nM in TC32, SKNMC, and WE68 spheroids (tested later in the validation experiments in 5.2.1). These concentrations were selected as they caused a growth inhibitory response, seen as a decrease in spheroid area. Importantly, at these concentrations there was a window to observe an additional effect in combination with clinical drug candidates on top of single-agent treatment with SN-38.
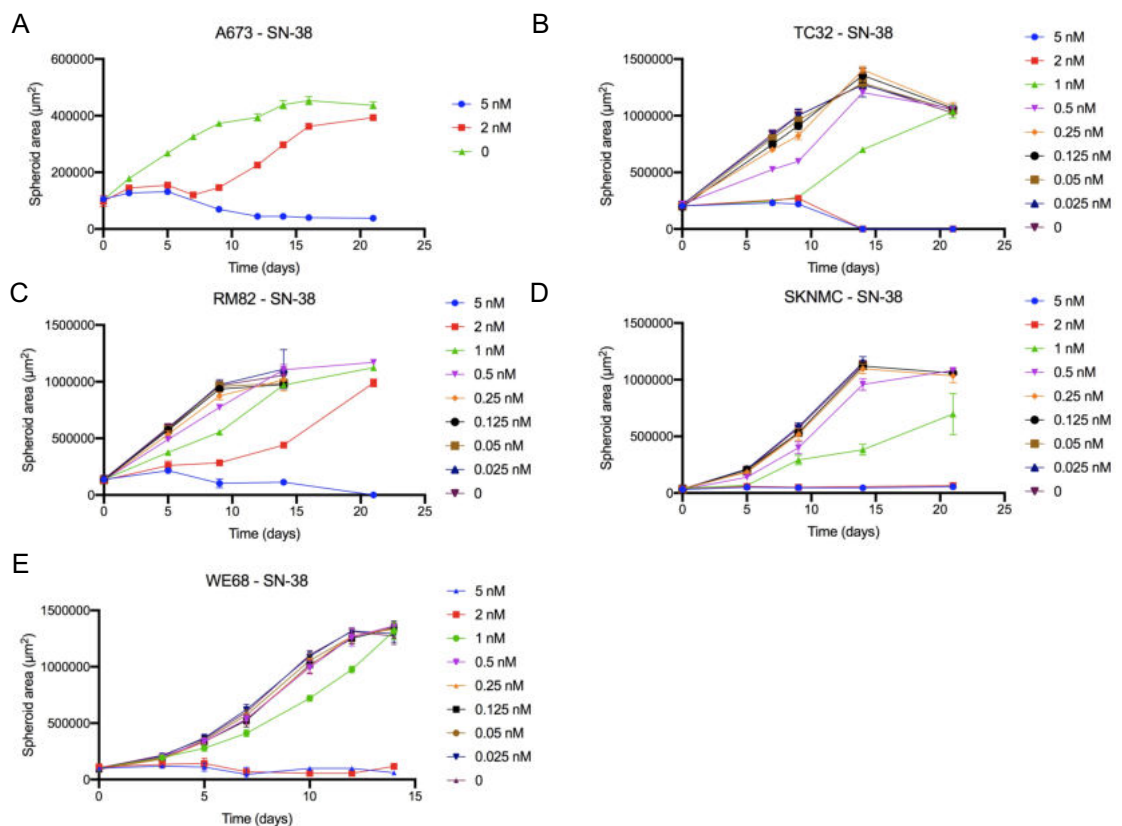
Figure 4.4 Dose-responses with SN-38 in ES spheroids.

ES spheroids from different cell lines treated with a range of SN-38 concentrations for 5 consecutive days during a 21-day cycle. Spheroid growth was assessed by measuring the cross-sectional area of spheroids throughout the indicated time points (detailed in methods 2.1.2).

Table 4.2 SN-38 pharmacokinetic data

Drug	AUC (ng h/ml)	C_{max} (ng/ml)	$t_{1/2}$ (h)
Irinotecan	2626 ±1443	726 ± 482	4.7 ± 2.3
SN-38	84 ± 67	13 ± 5.6	7.6 ± 11
Converted to nM	215 nM*h ± 170 nM*h	33 nM ± 14.27 nM	

4.2.4   Triaging combination strategies

In previous sections, the expected outcomes in the spheroid-based assay were described with the optimal result being complete cell killing (Fig. 4.3). However, the triaging of combination strategies was also contingent on an additional set of criteria, developed to select which combinations to take forward:

(A) Only combinations with concentrations deemed within the clinically achievable range based on available PK data (Table 4.1) were taken forward.

(B) In addition, evidence of a measurable biomarker in response to treatment, at a concentration satisfying point A, ensured successful target engagement. Biomarkers selected are indicated in table 4.1.

(C) Clinical drug candidates with a greater dose-response profile (based on lower GI50s, where possible) in 3D spheroids were prioritised. Dose-responses and biomarker assessment were initially carried out in A673 spheroids (Fig. 4.5).

Clinical drug candidates were tested alone and in combination with SN-38 at 2 nM combined with at 100%, 50%, and 10% of their GI50, where available. In the absence of a GI50, the concentration used was derived from points A and B in the criteria, and was therefore within a clinically achievable range and elicited a biomarker change (Fig. 4.5). Combination concentrations are indicated in table 4.3. Importantly, in the case that the selected concentrations were beyond the clinically achievable range, but 50% or 10% of that concentration were still within it, combinations with clinical drug candidates at these concentrations were still carried forward since they satisfied the criteria.
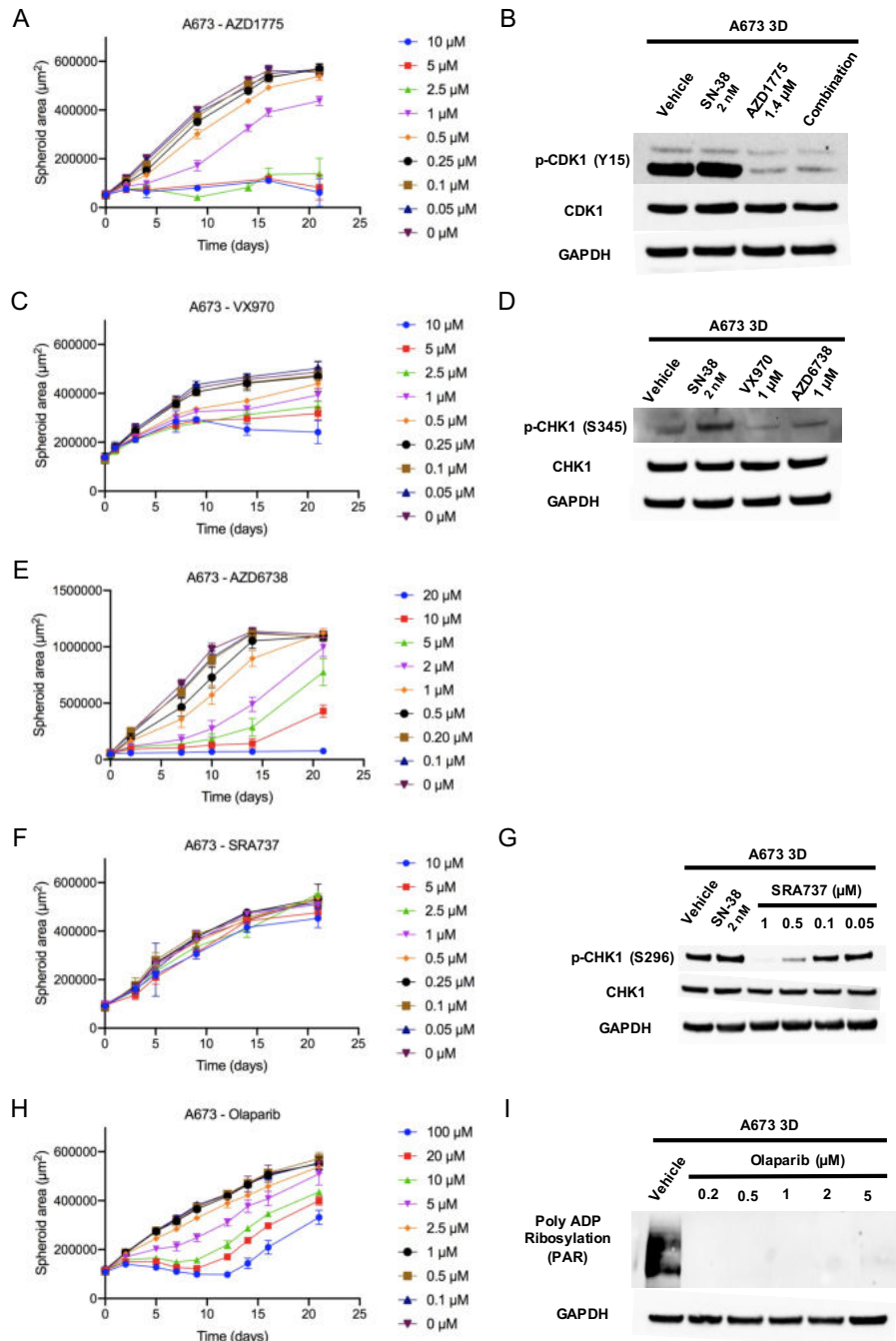
Figure 4.5 Clinical drug candidates' dose-responses and biomarker assessment.

Dose-responses with AZD1775 (A), VX-970 (C), AZD6738 (E), SRA737 (F), olaparib (H) in A673 spheroids treated for 5 days during a 21-day cycle. Corresponding biomarker assessment in A673 spheroids for each clinical drug candidate after 24 hours of treatment at the indicated concentrations. Western blot for levels of phospho-CDK1 (Y15) after AZD1775 treatment (B), phospho-CHK1 (S345) after treatment with VX-970 and AZ6738 (D), phospho-CHK1 (S296) after treatment with SRA737 (G), and polyADP-ribosylation after treatment with olaparib (I).

Table 4.3 Drug concentrations used in combination experiments

Clinical drug candidate	Concentrations (µM)		
AZD1775	1.4	0.7	0.14
AZD6738	1	0.5	0.1
VX-970	1	0.5	0.1
SRA737	1	0.5	0.1
Olaparib	1	0.5	0.1

4.2.5   Overview of combination studies results

Combination strategies exhibited a range of outcomes, as predicted (Fig 4.3). Within one treatment, growth curves had a mix of responses, for example an initial cytostatic effect followed by cell recovery, resulting in an overall growth inhibitory effect. Often these cases were dose-dependent, showing a cytotoxic effect at the highest combination concentration, but mild growth inhibition at the lowest setting. Determining the total effect of each condition took into account the initial response, its progression, and the final outcome at 21 days. This timeline of events provided hints of the mechanism behind inhibiting these drug targets and the overarching rationale of targeting the replication stress response combined with DNA damaging agents. Overall, WEE1 inhibitor AZD1775 and ATR inhibitors VX-970 and AZD6738 were identified as successful based on the criteria, causing a cytotoxic effect and/or strong growth inhibition of A673 and RM82 spheroids. The data on all clinical drug candidates in combination is presented here.

4.2.5.1   WEE1 inhibition in combination with SN-38

Single-agent treatment with selective WEE1 inhibitor AZD1775 decreased spheroid growth in a dose-dependent manner, with a GI50 at 21 days of 1.4 µM (Fig. 4.5A). At this concentration, AZD1775 successfully blocked WEE1 activity by preventing tyrosine 15 (Y15) phosphorylation on cyclin-dependent kinase 1 and 2 (CDK1/2) (Fig. 4.5B). Separate, selective detection of the phosphorylated portion of CDK1 and CDK2 on Y15 was not possible due to the phosphorylated site being located within a 13 amino acid conserved sequence on both proteins (250). Nevertheless, this indicated successful target

engagement following AZD1775 treatment. On average, the trough plasma concentration (C_{trough}) after a 225 mg BD dose was 776 nM and the maximum concentration (C_{max}) after drug was 1.38 µM (101). Using these values as a guideline, an achievable range for this clinical drug candidate meant combinations with 1.4 µM may not be clinically reachable throughout. Importantly, however, at this concentration of AZD1775, growth inhibition was too high, making it impossible to assess the impact of the combination above the single agent (Fig. 4.6A, Fig. 4.6D). However, combinations with 2 nM of SN-38 and AZD1775 at 0.7 µM (A673) and 0.1 µM (RM82) successfully delayed spheroid growth compared to single agents alone (Fig. 4.6B, Fig. 4.6F). RM82 cell line showed higher sensitivity to AZD1775 treatment. In the initial 5 days of treatment, differences in growth between conditions were difficult to discern and only during the second week of the assay, after the treatment was removed, growth changes became clearer. Overall, SN-38 in combination with WEE1 inhibition initially arrested growth compared to single agent treatment, but spheroids remained viable as shown by a visible recovery in size at the end of the assay.

Figure 4.6 WEE1 inhibition in combination with SN-38 in ES spheroids

Treatment of A673 (A-C) and RM82 (D-F) spheroids with SN-38 and AZD1775 alone and in combination at the indicated concentrations for 5-days during a 21-day cycle. Graphs represent means ± standard deviation from 6 replicates.

4.2.5.2 ATR inhibition in combination with SN-38

Two clinical drug candidates were selected to target the apical kinase of the ATR-CHK1-WEE1 axis. ATR inhibitor VX-970 showed a less pronounced dose-dependent growth inhibition compared to WEE1 inhibitor AZD1775 and did not achieve a maximal response, limiting calculation of a GI50 for this compound (Fig. 4.5C). Clinical drug candidate AZD6738 showed a growth inhibitory effect at concentrations >5 µM, but spheroid size recovery towards 21 days. As introduced before (see 1.2.3.1), one of the key downstream targets of ATR, and therefore indicative of its activity, is phosphorylation of CHK1 on serine 345 (S345) (31, 59) (Fig. 4.5D). From these experiments, a range of 1 µM, 0.5 µM, and 0.1 µM was then chosen for *in vitro* use, given sufficient inhibition of CHK1 phosphorylation on S345. Available PK studies with VX-

970 and AZD6738 were also used to corroborate whether the concentration range was clinically reachable. For VX-970, the reported maximal plasma concentration of 739.93 nM after a 1 h infusion of 60 mg/m^2, meant the selected concentration of 1 µM was potentially beyond achievable, but not 50% or 10% of it (249). Still, at this concentration there was an observable decrease in p-CHK1 (S345) by Western blot (Fig. 4.5D), making it relevant as proof-of-principle to study efficacy through ATR inhibition. Data from the PATRIOT phase I trial in solid tumours with AZD6738 was only available after the combination studies were carried out. PK data on AZD6738 provided a wider threshold for an achievable concentration with a reported C_{max} of 12.12 µM to a C_{trough} of 2.4 µM (102).

A673 spheroids responded to all concentrations of VX-970 combined with SN-38. Compared to single agent treatments, drug combinations with higher concentrations of VX-970, displayed a strong cytostatic effect followed by a decrease in spheroid size towards the end of the 21 days, indicative of cytotoxicity (Fig. 4.7A-B). At the lower setting of 0.1 µM of VX-970, combination with SN-38, only resulted in growth inhibition in cell line A673 (Fig 4.7C). Again, RM82 spheroids showed overall greater sensitivity to the targeted agent, as VX-970 concentrations of 1µM and 0.5 µM alone caused complete cell killing (Fig. 4.7D-E). However, a combined effect between agents was observed at 2 nM of SN-38 and 0.1 µM of VX-970, with severe growth stalling and a small recovery in size towards the end of the 21-day assay (Fig. 4.7F). Compared to combination treatments with VX-970, AZD6738 was overall less active at identical concentration. Only mild growth inhibition of A673 spheroids was achieved with 1 µM of AZD6738 and SN-38, but little to no effect with lower concentrations (Fig. 4.8A-C). In the more sensitive RM82 spheroids, 1 µM of AZD6738 in combination with SN-38 was necessary to cause growth inhibition (Fig. 4.8D). One caveat to these results is that the concentration range of AZD6738 could have been increased as shown by the achievable range (Table 4.1). This would have likely increased the observed effects and matched VX-970's activity.
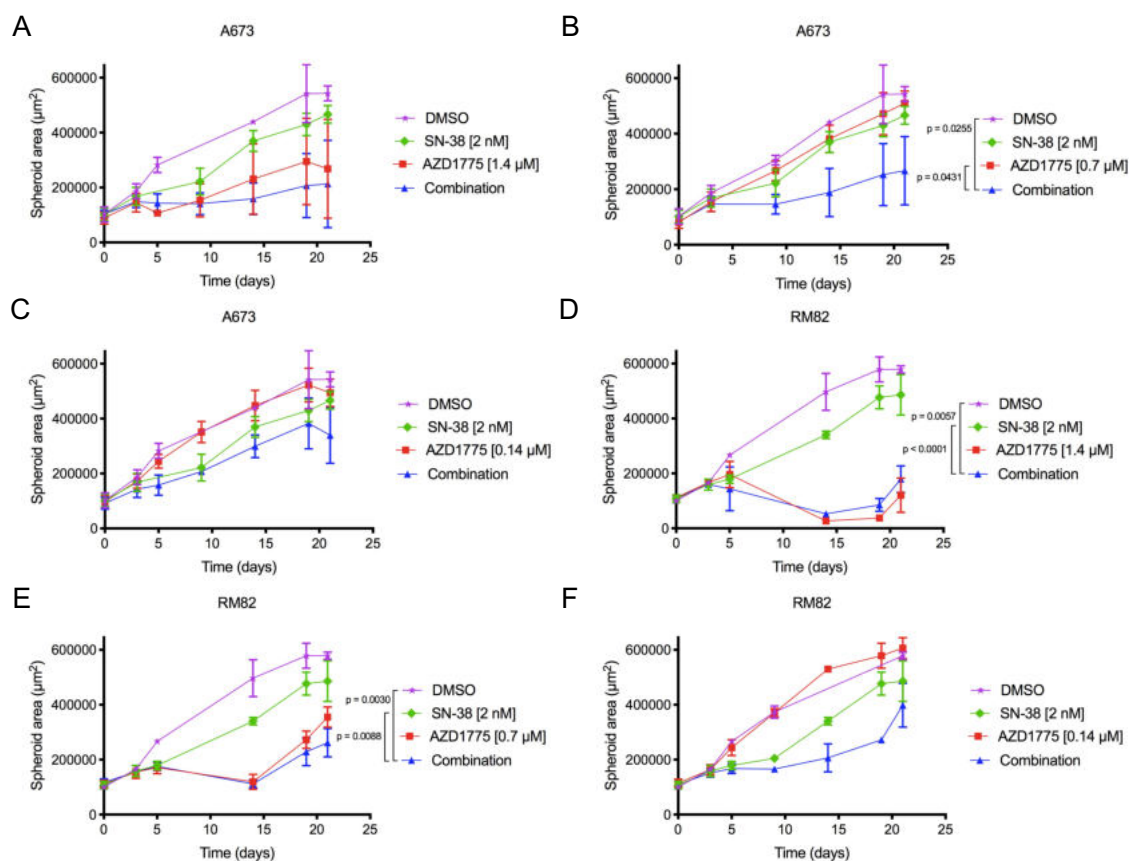
Figure 4.7 ATR inhibition with VX-970 in combination with SN-38 in ES spheroids

Treatment of A673 (A-C) and RM82 (D-F) spheroids with SN-38 and VX-970 alone and in combination at the indicated concentrations for 5-days during a 21-day cycle. Graphs represent means ± standard deviation from 6 replicates.
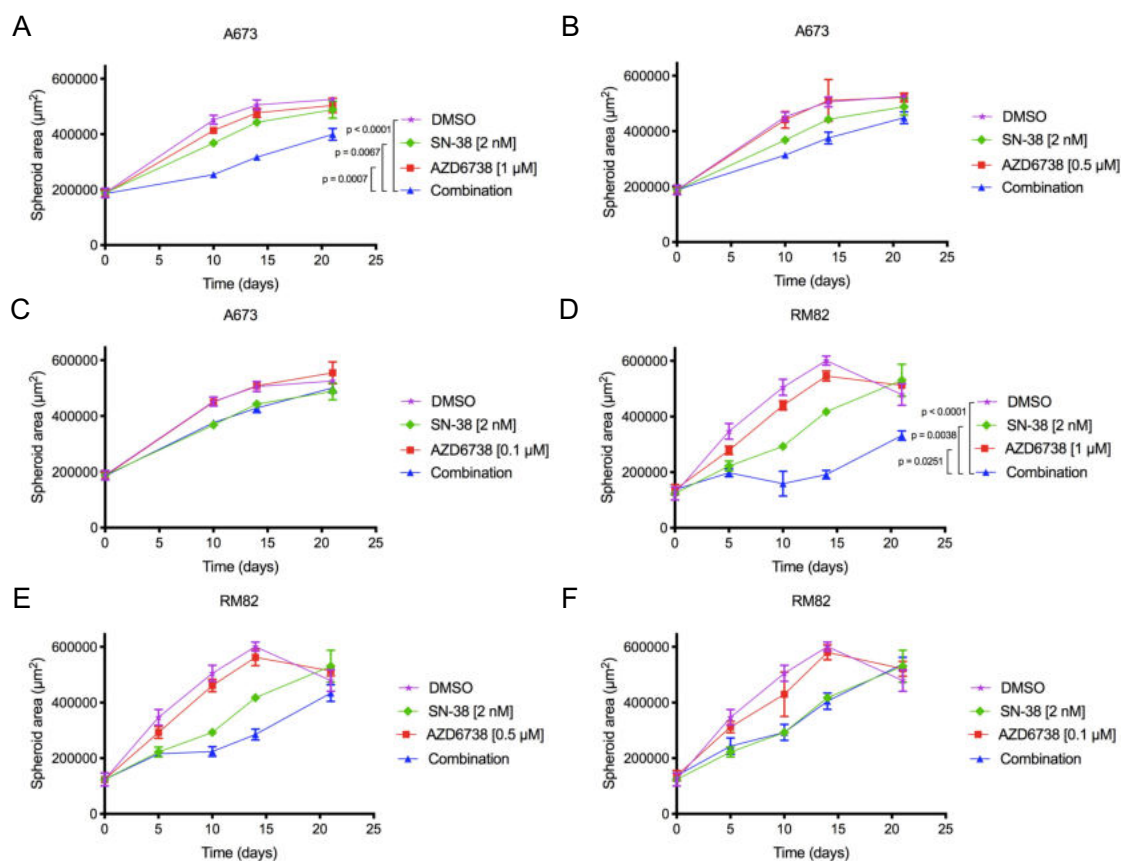
Figure 4.8 ATR inhibition with AZD6738 in combination with SN-38 in ES spheroids.

Treatment of A673 (A-C) and RM82 (D-F) spheroids with SN-38 and AZD6738 alone and in combination at the indicated concentrations for 5-days during a 21-day cycle. Graphs represent means ± standard deviation from 6 replicates.

4.2.5.3 CHK1 inhibition in combination with SN-38

Targeting the remaining kinase in the ATR-CHK1-WEE1 axis, with CHK1 inhibitor SRA737 showed no dose-response in A673 spheroids (Fig. 4.5F). To verify target engagement with SRA737, inhibition of autophosphorylation of serine 296 (S296) on CHK1 (109) was assessed by Western blot and confirmed at 1 μM, and to a lesser extent at 0.5 μM (Fig. 4.5G). A reported average C_{max} of 1.4 μM and C_{trough} of 137 nM after a 150 mg tablet per day of SRA737 meant concentrations at which target engagement was confirmed are reachable in patients. Importantly, the PK information was obtained from a dose of SRA737 designed to be used in combination, albeit with gemcitabine (100). However, CHK1 inhibition in combination with SN-38 did not impact spheroid growth in both A673 and RM82 spheroids, with only the effect of topoisomerase I inhibition visible (Fig. 4.9).
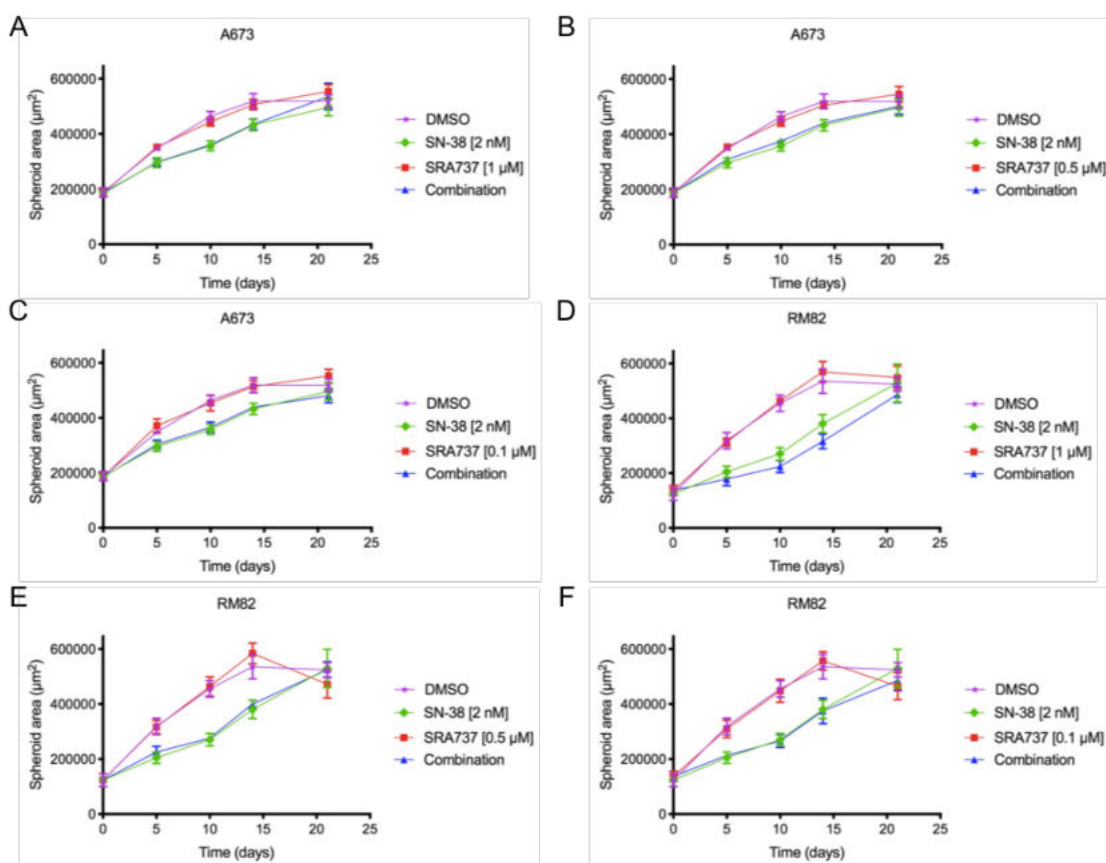
Figure 4.9 CHK1 inhibition in combination with SN-38 in ES spheroids.

Treatment of A673 (A-C) and RM82 (D-F) spheroids with SN-38 and SRA737 alone and in combination at the indicated concentrations for 5-days during a 21-day cycle. Graphs represent means ± standard deviation from 6 replicates.

4.2.5.4 PARP1 inhibition in combination with SN-38

Olaparib exists as an orally-available drug achieving high drug exposure with an average C_{max} of 13 µM when administered at clinically relevant schedules (97). Spheroid treatment with a range of olaparib concentrations showed a varied dose-response, from cytotoxicity at high concentrations to limited growth inhibition at concentrations below 5 µM (Fig. 4.5). Ultimately, all conditions showed remarkable recovery in size over time, even at concentrations beyond 10 µM (Fig. 4.5H). To confirm target engagement even when catalytic activity of PARP1 is only part of its mechanism of action (95), levels of poly ADP-ribosylation (PAR) were analysed by western blot. A range of olaparib concentrations successfully decreased the smear on the blot, indicative of PARylation (Fig. 4.5I). Concentrations of 1 µM, 0.5 µM, and 0.1 µM were then used for combination testing. Addition of SN-38 changed the response to olaparib treatment, as seen by

flattening of the curve in the first days after treatment. Whilst this was consistent with a synergistic effect in both spheroid models, the overall outcome at 21 days was the same for all treatments (Fig 4.10).
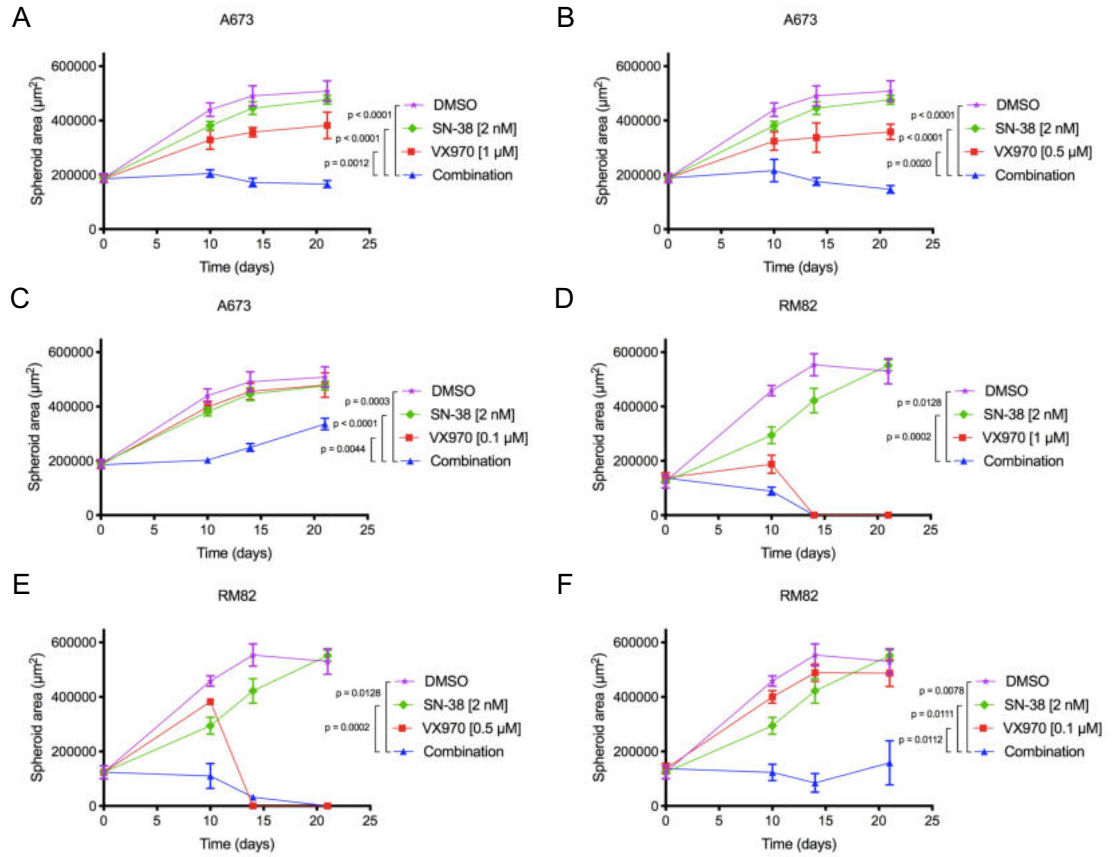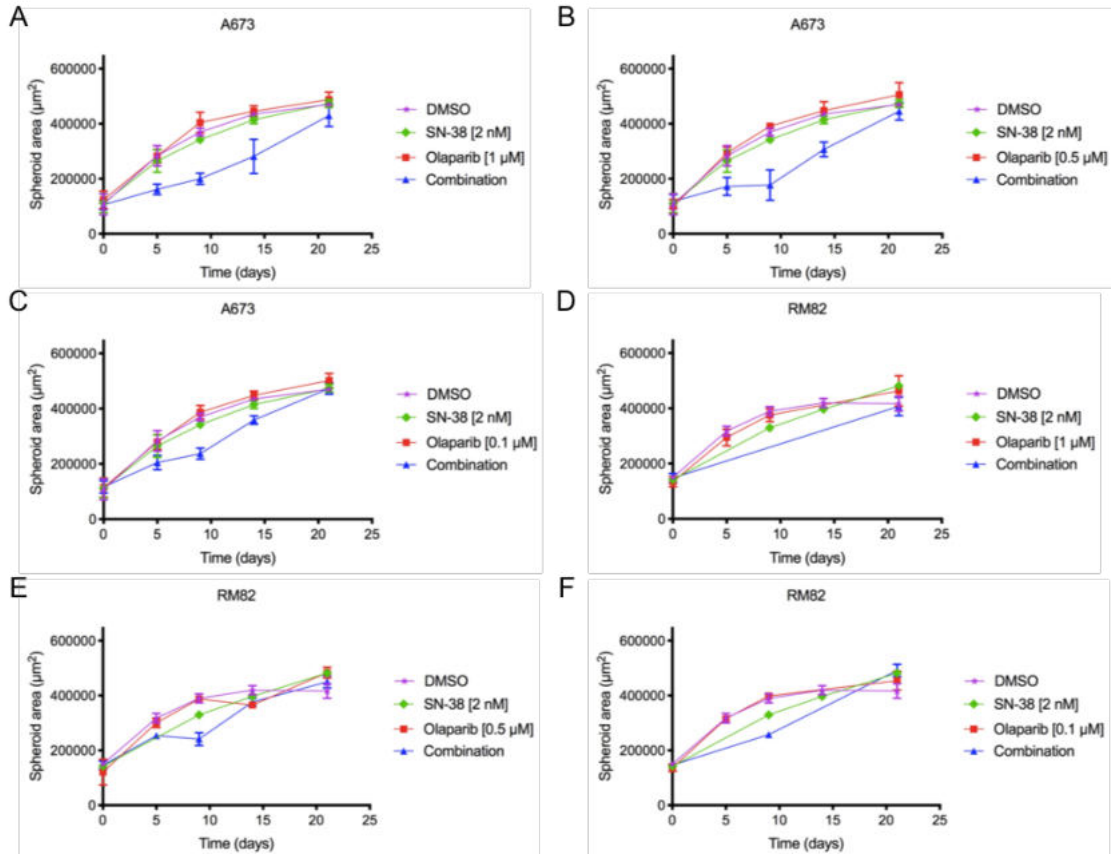

Figure 4.10 PARP1 inhibition in combination with SN-38 in ES spheroids.

Treatment of A673 (A-C) and RM82 (D-F) spheroids with SN-38 and olaparib alone and in combination at the indicated concentrations for 5-days during a 21-day cycle. Graphs represent means ± standard deviation from 6 replicates.

4.3 Discussion

4.3.1 An approach to prioritising combination strategies in ES

The approach taken to identify novel combinations yielded two successful candidates to explore and validate further. The data in this chapter showed that inhibition of the RSR in combination with irinotecan was effective as a therapeutic strategy in *in vitro* models of ES, supporting the initial hypothesis. However, it remains to be addressed whether EWS-FLI1 is the key determinant of sensitivity to therapeutic combinations exploiting this vulnerability.

The hypothesis of inhibiting a particular dependency on the RSR in ES narrowed down the potential drug targets to the three kinases in this pathway. This tailored approach enabled creating a more laborious spheroid-based assay to test their combination potential. The emphasis on clinical relevance throughout the experimental design contributed to its translational potential, but it was not without challenges and limitations. The main parameters for selecting doses were the maximal (C_{max}) and minimal ($C_{through}$) concentration in blood, along with careful consideration of the *in vivo* half-life of the drug, when available. This information, however useful, still remains only a guideline for *in vitro* use, as measurements in plasma do not capture drug distribution within the tumour. In the majority of cases direct readings from tissue are unobtainable due to the invasiveness of the procedure or are avoided to minimise potential tissue damage. This information was not available for the drugs used in this study. Despite the selected concentrations being an approximation, having a measurable biomarker corresponding to this dose, increased the confidence of successful target inhibition. Overall, extrapolating *in vivo* doses to usable concentrations *in vitro* is difficult, but it is an important consideration when carrying out pre-clinical work.

The experimental design used was influenced by the clinical setting, specifically in how patients receive chemotherapy in the form of a scheduled cycle. In this way, a 21-day assay was developed in order to mimic long-term assessment and cell recovery after damage induction and inhibition of DNA repair mechanisms. These scenarios are relevant to how drugs are administered to patients, but are often overlooked in the *in vitro* setting. Even so, adapting traditional cell-based assays to different read-outs and extended time points brought challenges. One example was establishing a standard measure of response

that enabled triaging and comparison across conditions in this type of assay. Most dose-responses resulted in spheroid recovery at 21 days, making the use of GI50s for dose-finding and rank each clinical drug candidates less useful and relevant. As a solution, determining treatment efficacy focused on changes in growth curve profiles and the overall phenotype after 21 days, prioritising cell killing effects (Fig. 4.3A). In this way, SN-38 in combination with WEE1 inhibitor AZD1775 or ATR inhibitor VX-970 were classed as true positive outcomes that had growth inhibitory and cytotoxic effects in ES spheroids. Importantly, WEE1 inhibition in combination with SN-38 was identified as a novel potential therapeutic strategy for ES. Traditionally, WEE1 is associated with its activity as checkpoint regulator of the G2/M transition, but it also has prominent roles mitigating RS and maintaining genome instability in S-phase (41, 54, 55, 77, 78). A closer examination of the effects of AZD1775 in combination with SN-38 were explored in chapter 5 in order to provide mechanistic insights into their combined effect.

4.3.2 Comparison of ATR inhibitors and their therapeutic potential for ES

The findings that ATR inhibitors worked in combination with SN-38 were not surprising, since single-agent efficacy with tool compounds targeting ATR had been seen previously in ES xenografts and was part of the rationale behind targeting the RSR (98). The discrepancy between the effects of ATR inhibitors VX-970 and AZD6738 in combination on spheroid growth could have been a dose-dependent issue. That is, the concentration range may have missed AZD6738's window of activity, since the doses used in these experiments were closer to the minimal levels measured in plasma. This means, higher concentrations of AZD6738, that are within the clinically reachable range, could have potentially improved AZD6738's efficacy in the *in vitro* assays in this study. In any case, ATR inhibition in combination with irinotecan remains an attractive therapeutic approach for ES. Both clinical drug candidates are highly specific and potent inhibitors with IC50s from isolated enzyme inhibition of <0.2 nM (VX-970) and 1 nM (AZD6738). Verification of successful target inhibition also indicated comparable decrease of phosphorylated CHK1 (S345) at 1 μM. Differences in activity and properties can be expected between compounds from different structural classes, AZD6738 being a sulfoximine morpholinopyrimidine and a more neutral molecule than the aminopyrazine VX-970, containing a basic group (251-254). These characteristics have also translated into contrasting kinome selectivity profiles, route of administration (oral v. intravenously), and PK prolife amongst others (251, 253).

The use of ATR inhibition as an anticancer treatment is being tested for tumour types with high levels of innate RS, particularly in combination with other DNA damaging and RS-inducing agents, for example cisplatin, gemcitabine, and etoposide (56). In addition, a recent study between VX-970 and topotecan found this combination to be well tolerated with partial responses and stable disease in patients with SCLC (255). Despite differences between topotecan and irinotecan (184), evidence that a similar combination is feasible, in addition to the results presented here, could be a step towards testing in this sarcoma. Other biomarkers of sensitivity include genetic backgrounds that are HR-deficient or ATM-deficient. AZD6738 is the main ATR inhibitor being tested in this context, particularly in combination with PARP1/2 inhibitor olaparib (56). VX-803 (now M4344) and BAY 1895344 are additional clinical drug candidates against ATR that were unavailable for testing at the time of the experiments in this chapter. Having caught up in their clinical development, future work exploring combinations with ATR inhibitors could incorporate them. The number of available options to target ATR and the findings in this chapter make it an attractive therapy to pursue in the future. Further evaluation of their mechanism of action, particularly in the combination setting will be crucial to develop rational schedules for their use in ES patients.

4.3.3 Challenges and experience of inhibiting CHK1 in ES

Given the reliance on the RSR, it was unexpected to see a lack of response with inhibition of CHK1, particularly when targeting the other kinases in this axis (ATR and WEE1) affected spheroid growth. However, the results with SRA737 alone and in combination with SN-38 are in agreement with other pre-clinical studies on CHK1 inhibition in this sarcoma (167). One explanation for why blocking CHK1 activity was insufficient therapeutically is due to its high levels of expression (98, 167). Nieto-Soler *et al*. (2016) had already identified CHK1 to be highly expressed in ES compared to human primary cell lines and osteosarcoma cell lines (98). Whilst this is evidence of an adaption to high levels of innate RS, it also presents a therapeutic challenge. Usually, high protein expression is a desirable feature in drug targets because it enables having a wider therapeutic window. Even so, reports using the now discontinued CHK1 inhibitor, prexasertib (LY2606368), found high abundance of CHK1 to be the limiting factor to efficacy with this therapy (167). In fact, ES cell growth was only impaired when CHK1 was depleted with siRNA or shRNA technology in addition to treatment with different CHK1 inhibitors (167). Overall, these findings demonstrated that to obtain maximal

efficacy with these agents, it is necessary to achieve complete protein inhibition. This limits the potential this treatment may have in the clinic, as ensuring sustained target inhibition in patients may not be possible.

The described experience with inhibiting this kinase could also explain results from *in vivo* studies with PDXs and cell line-derived xenografts (CDXs) of different paediatric malignancies (196). On one hand, monotherapy with prexasertib achieved tumour regression and stable disease in models of neuroblastoma, DSRCT, and RMS, but only 1 out of 14 xenograft models of ES responded to CHK1 inhibition (196). Importantly, these models also did not respond to single agent treatment with chemotherapeutic agents, cyclophosphamide or doxorubicin. In an effort to improve the effect of DNA damaging agents it was investigated whether CHK1 inhibition could sensitise non-responsive models to these forms of chemotherapy. Prexasertib in combination with irinotecan resulted in improving response in the A673 CDX model with 3 out 5 mice reporting partial regression (196). Overall, these pre-clinical studies have not resulted in CHK1 inhibition being pursued in the clinic for ES patients, in contrast to RMS and DSRCT (NCT04095221) (196, 256). Even so, SRA737 remains as the only clinically available inhibitor for this drug target, whether the focus of targeting this pathway will shift to ATR or WEE1, as evidence in ES suggests, remains to be seen.

4.3.4 PARP1 inhibition as a therapeutic strategy for ES

In the last decade, the development of PARP1 as a therapeutic target in ES has moved quickly. Initially, immunoprecipitations studies identified an interaction between PARP1 and fusion protein EWS-FLI1 (197). At a DNA level, the promoter region of *PARP1* was identified to have the canonical ETS binding motif, linking its expression to EWS-FLI1 (257). In addition, PARP1 was shown to contribute to EWS-FLI1 activity through a positive feedback loop, demonstrated by a decrease in mRNA levels of downstream targets of the fusion upon PARP1 knockdown (197). Further validation experiments have used a variety of systems to ectopically overexpress fusions bearing ETS transcription factors EWS-ERG, EWS-FLI1, and the prostate cancer fusion TMPRSS2-ERG. In this way, increased sensitivity to PARP1 inhibition in soft-agar colony formation and MTS assays was shown to be associated with the presence of these fusions (197, 198). Overall, the positive feedback loop between PARP1 and EWS-FLI1 together with high levels of

expression, important to PARP1 'trapping' as a cytotoxic mechanism (95), have made it an attractive target in ES.

In stark contrast to pre-clinical work *in vitro*, a phase II trial investigating the translational potential of PARP inhibitors in ES patients reported lack of efficacy with single-agent olaparib (199). In another phase I study with talazoparib in patients with advanced *BRCA1/2* germline mutations and other cancers, no objective response was found in ES patients (258). The findings in these clinical trials can be partially explained by the previously used ES cell lines from earlier studies not being representative of the patients recruited. Rather, these patients had received front-line chemotherapy and had evidence of tumour relapse or progression, together with potential mechanisms of resistance to this treatment (199). Even so, ES cell lines COG10 and COG6258, derived from patients who relapsed after front-line chemotherapy, had shown to be sensitive to PARP1 inhibition (197). This suggests the reasons for inefficacy with single-agent olaparib may go beyond the patient background. In results presented here, sensitivity to olaparib in 3D assays was significantly different to previous reports in 2D (198, 200). For example, spheroid assays exhibited recovery in growth after an initial response to a 5-day treatment with olaparib in a 21-day assay, overall shifting its GI50. It remains to be addressed whether there are resistance mechanisms to PARP1 inhibition that are enabled in these 3D models, but not captured in the 2D setting.

The clinical use and future of PARP1 inhibitors in this sarcoma has shifted to combination therapies. In one of the original studies by Brenner *et al.* (2012), treatment with single agent olaparib resulted in tumour growth delay, but when combined with temozolomide, tumour regression was observed in ES tumour xenografts. Similarly, several pre-clinical studies have reported improved responses in combination with a number of agents, including CDK12 inhibitors, trabectedin and radiotherapy (200, 201, 259-262). Additionally, the relapse chemotherapy agents for ES, temozolomide and irinotecan, are undergoing clinical testing as a triple combination with PARP1 inhibition (NCT02044120 and NCT01858168) (96, 189, 263). However, in the combination experiments presented in this chapter, response to olaparib was not improved significantly when administered with SN-38 in contrast to previous findings (189, 198, 200). The contrast between the effects seen here and reports in Stewart *et al*. (2014) could also be attributed to potential differences between the cell line models used and drug

response differences in 2D assays compared to 3D spheroids. Ultimately, the mechanism of sensitivity to PARP inhibition in this sarcoma remains to be fully addressed. The majority of these studies have focused on identifying DNA repair vulnerabilities in ES, particularly in the context of HR. This is not surprising due to the established synthetic lethality between BRCA1/2 deficient tumours and PARP1 inhibition (82, 97, 264). However, the literature regarding potential deficiencies is inconclusive.

Altogether, these results validated the spheroid-based assay as an approach to identify clinically relevant combination strategies. Importantly, successful combinations with WEE1 inhibition and ATR inhibition in combination with SN-38 supported targeting the RSR in combination with chemotherapy as a therapeutic strategy for ES. Further characterisation of the effects and mechanism of SN-38 in combination with WEE1 inhibition are explored in the next chapters.

Chapter 5 Characterisation of SN-38 in combination with WEE1 inhibition

5.1 Introduction

Results from the previous chapter found successful combinations which reduced ES spheroid growth and induced cytotoxicity through inhibition of ATR or WEE1 activity in combination with SN-38, the active metabolite of irinotecan. The efficacy of ATR inhibition as a single agent has already been reported in ES tumour xenografts (98). In agreement, clinical drug candidates against ATR were also identified to have an effect in combination with SN-38. It was therefore decided to prioritise and pursue the investigation of combination between SN-38 and WEE1 inhibitor AZD1775.

The aim of this chapter was to thoroughly examine the effects of these treatments in order to understand its mechanism of action and maximise its translational potential. Firstly, this treatment was validated in a range of ES cell line models as spheroids in order to identify biomarkers of sensitivity. Additionally, response to concurrent treatment of irinotecan and WEE1 inhibition was characterised by examining DNA damage induction, the effects on cell cycle progression, and the consequences of CDK1/2 dysregulation to shed more light into the mechanism of this combined treatment. Alternative regimens, such as a staggered schedule, were studied as way of investigating further the combination's potential for translation into the clinic.

5.2 Results

5.2.1 Validation of irinotecan in combination with WEE1 inhibition in ES spheroids

Response to SN-38 in combination with WEE1 inhibition was validated in additional spheroid models of ES cell lines. TC32, SKNMC, and WE68 cell lines were all treated for 5 days with SN-38, AZD1775, or concurrent treatment in a 21-day cycle, in addition to the previously tested A673 and RM82 (Fig. 5.1). The concentrations for the combination studies in this additional spheroid models were selected by performing dose-responses with the single-agents, followed by testing in combination at the sub-lethal concentrations obtained from the previous experiment. The responses to the combination treatment were classified as described in the previous chapter (Fig. 4.3). All cell lines responded to the combination treatment, with evidence of significant reduction in spheroid size, and overall growth inhibition. The extent of this effect was varied and sensitivity to each agent differed greatly. A673 cell line spheroids required the highest concentrations of the agents to elicit an effect on spheroid size (2 nM of SN-38 and 0.7 µM of AZD1775). The greatest response was observed in TC32 spheroids in which complete destruction of the spheroids was achieved, whilst spheroids treated with single agents recovered to match the untreated control (Fig. 5.1A). Cell lines RM82 and WE68 showed overall growth inhibition, with recovery in spheroid size towards the end of the assay (Fig. 5.1D-E). On the other hand, A673 and SKNMC cell lines did not recover and displayed sustained growth arrest throughout the length of the experiment (Fig. 5.1B-C).
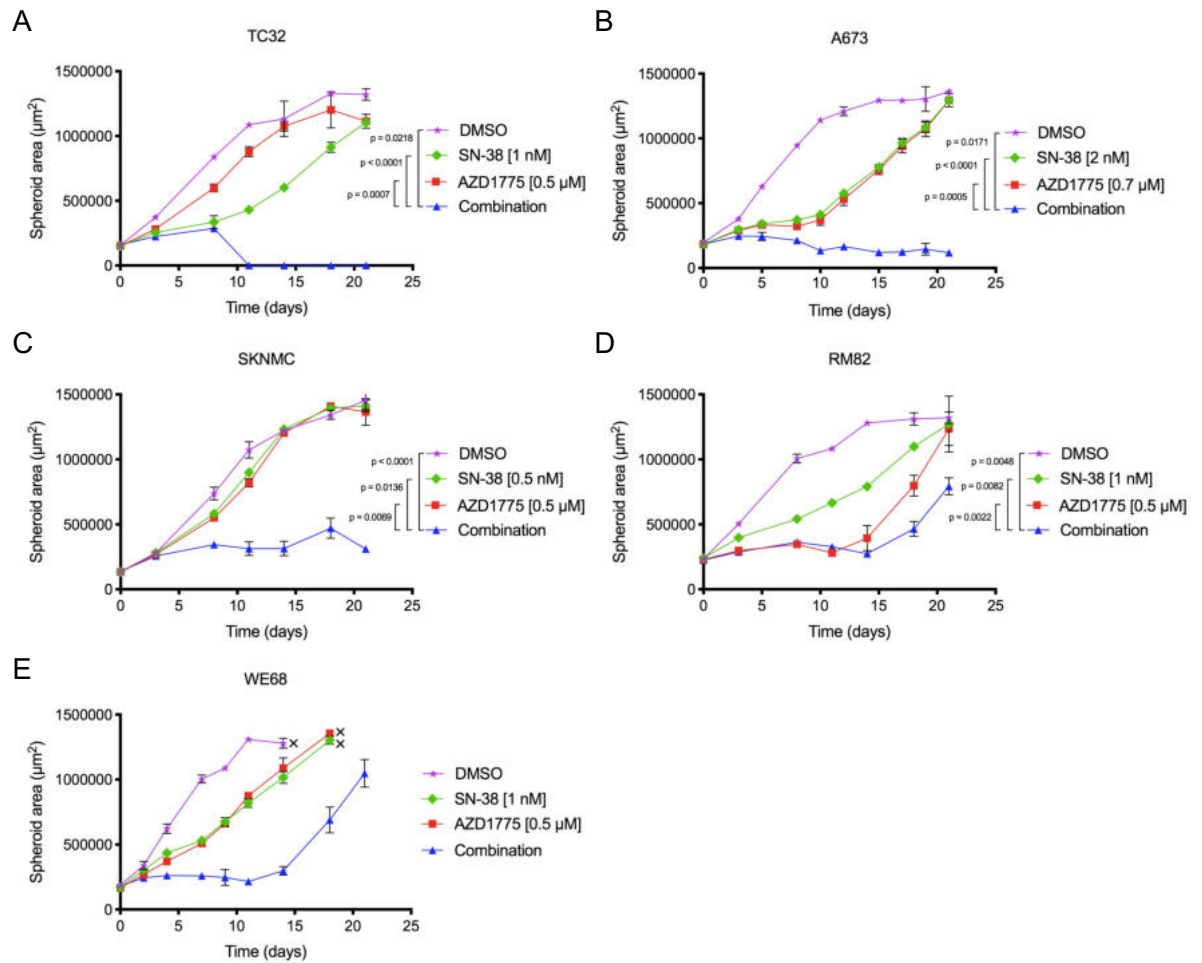
Figure 5.1 Validation of SN-38 in combination with AZD1775 in ES spheroids.

ES spheroids models TC32 (A), A673 (B), SKNMC (C), RM82 (D), and WE68 (E) were treated with SN-38, AZD1775, or concurrent treatment at the indicated concentrations. Crosses in panel E indicate that spheroid size assessment was not possible beyond the shown time points, as spheroids covered the entire area of the well. Graphs represent means ± standard deviation from 6 replicates and are representative of three independent repeats. All p-values were calculated using a repeated-measures ANOVA with Tukey's multiple comparisons test, only significant comparisons are shown.

To begin to investigate whether the mutational background of each cell line affected response, figure 5.2 was elaborated to compare their profiles. Based on these features there was no clear indication that sensitivity and differences in response could be explained by mutational status alone. Notably, the response to the combination treatment in TC32 spheroids stood out as indicative of cell death, compared to A673 and SKNMC spheroids, whose response suggested growth arrest (Fig. 5.1A). Therefore, to continue investigating these two phenotypes, the nature of the apoptotic response in these models

was investigated, particularly because TC32 cell line is p53 WT in contrast to the p53 null status in A673 cells (see 5.2.5). Thus, cell lines TC32 and A673 models were chosen for further characterisation.

	A673	SKNMC	RM82	TC32	WE68
Fusion	EWS-FLI1	EWS-FLI1	EWS-ERG	EWS-FLI1	EWS-FLI1
Fusion subtype	I	I	-	I	I
STAG2				Mutated	Mutated
CDKN2A	Complete deletion			Complete deletion	Complete deletion
TP53	Mutated	Expression loss	Mutated		
1q Status			1q gain	1q gain	1q gain
Origin	Muscle, primary tumour	Metastatic – post-chemotherapy (Vincristine, cyclophosphamide, doxorubicin, actinomycin)	Femur, primary tumour	Ileum and adjacent soft tissue, primary tumour derived at diagnosis	Fibula, primary tumour
SN-38 [nM]	2	0.5	1	1	1
AZD1775 [µM]	0.7	0.5	0.5	0.5	0.5
Response	Growth arrest	Growth arrest	Growth inhibition	Complete cell killing	Growth inhibition

Legend:
- STAG2 Mutated (dark blue)
- CDKN2A Complete deletion (blue)
- TP53 Mutated (green), Expression loss (light green)
- 1q gain (orange)

Table 5.1 Profile of ES cell lines used for spheroids models.

ES cell lines background, fusion type, and mutational profiles, including the three most common mutated genes in ES tumours *STAG2*, *CDKN2A,* and *TP53*. Concentrations of concurrent treatment of SN-38 and AZD1775 needed to produce a combined effect on spheroid growth are indicated together with the type of response.

5.2.2 Morphological characterisation

In order to characterise cell morphology after treatment, spheroids were processed, embedded in paraffin and sectioned. Samples were stained with haematoxylin and eosin (H&E). Differences in spheroid sizes were apparent between treated and untreated samples at 24 h, accentuating further after 120 h, particularly in the combination treated spheroids (Fig. 5.2 and Fig. 5.3). Spheroids sections showed a distinct region in the centre, often described as a hypoxic and/or necrotic core (4, 204). It is worth noting, these changes in particular, are not caused by the treatment. Rather, they are suggested to be due to natural gradients of nutrients and oxygen availability, which diminish towards the centre of each spheroid as its volume increases (4, 204). Therefore, the spheroid's core was excluded from the analysis of morphological changes associated with SN-38 and AZD1775 treatment. Magnification of these areas in A673 and TC32 spheroids showed

features associated with apoptosis in the form of cell swelling and nuclear condensation in the combination treated group. Additionally, there were visible nuclear abnormalities, particularly in the combination and AZD1775-treated A673 and TC32 spheroids (Fig. 5.4 and Fig. 5.5). Some of these included pyknotic nuclei, associated with an irreversible process of chromatin condensation occurring in apoptosis and necrosis (Personal communication with Dr. Anna M. Kelsey, Consultant Paediatric Histopathologist). Importantly, after 120 h (5 days) of the combination treatment, TC32 spheroids began to fragment, producing considerable cell debris in contrast to A673 spheroids (Fig. 5.4 and Fig. 5.5). Both spheroids at 120 h showed apoptotic features such as cell swelling and bursting.

Samples from both models, fixed 7 days after the beginning of the 21-day cycle, showed more pronounced differences in size. Combination-treated A673 and TC32 spheroids showed similar, but more advanced patterns of cell death. A673 spheroids in particular exhibited severe changes with nuclear abnormalities like multinucleation and pyknotic nuclei but also cytoplasmic changes. TC32 spheroids treated with SN-38 and AZD1775, appeared to break off, consistent with the effects measured in the growth curve with spheroids from this cell line model.
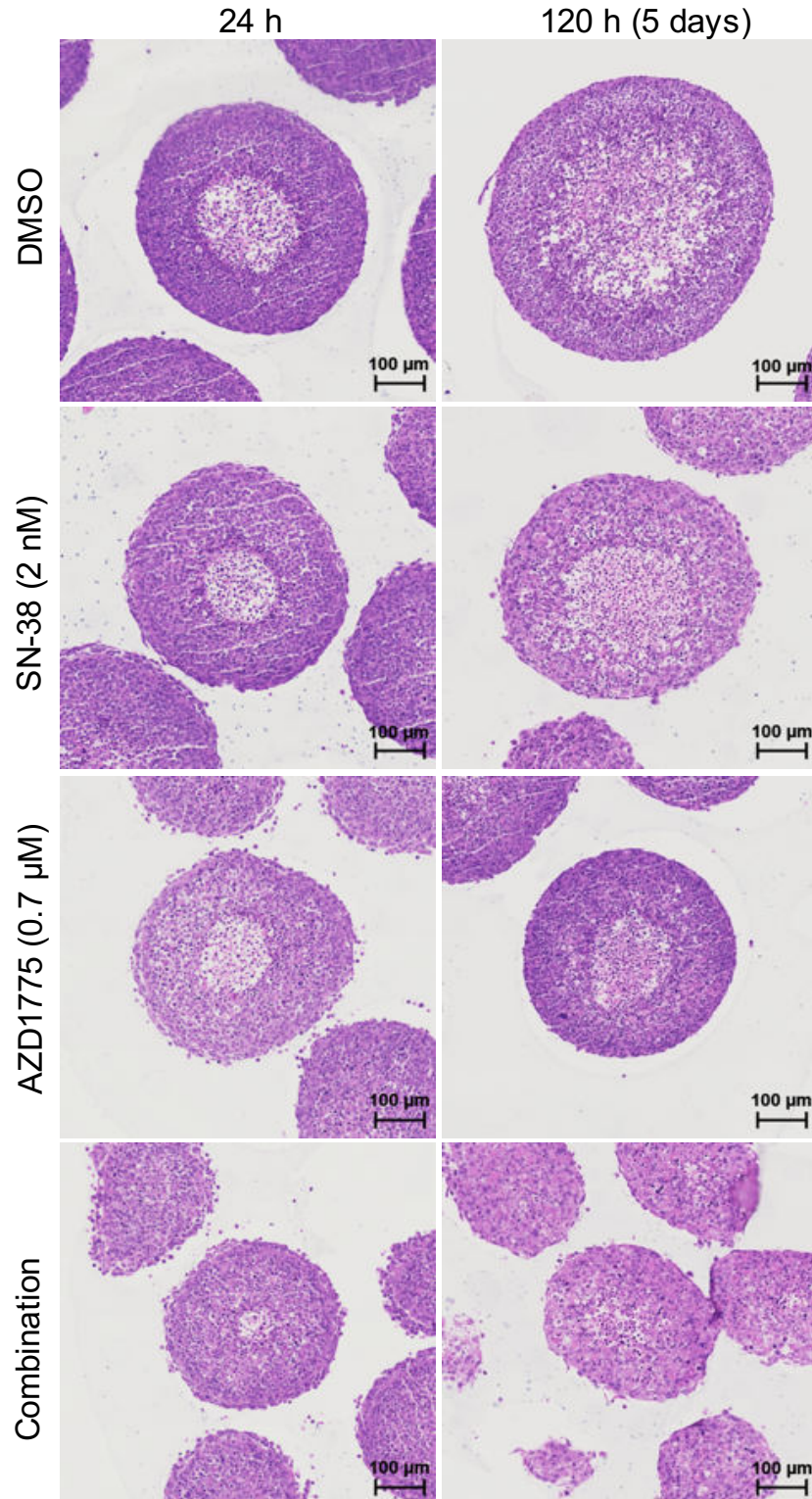
Figure 5.2 Haematoxylin and eosin staining of A673 spheroids treated with SN-38 in combination with AZD1775.

Sections of paraffin-embedded A673 spheroids stained with haematoxylin and eosin. Spheroids were treated with SN-38 (2 nM), AZD1775 (0.7 µM), or concurrent treatment for 24 h and 120 h (5 days). Images are representative of spheroids from each condition.
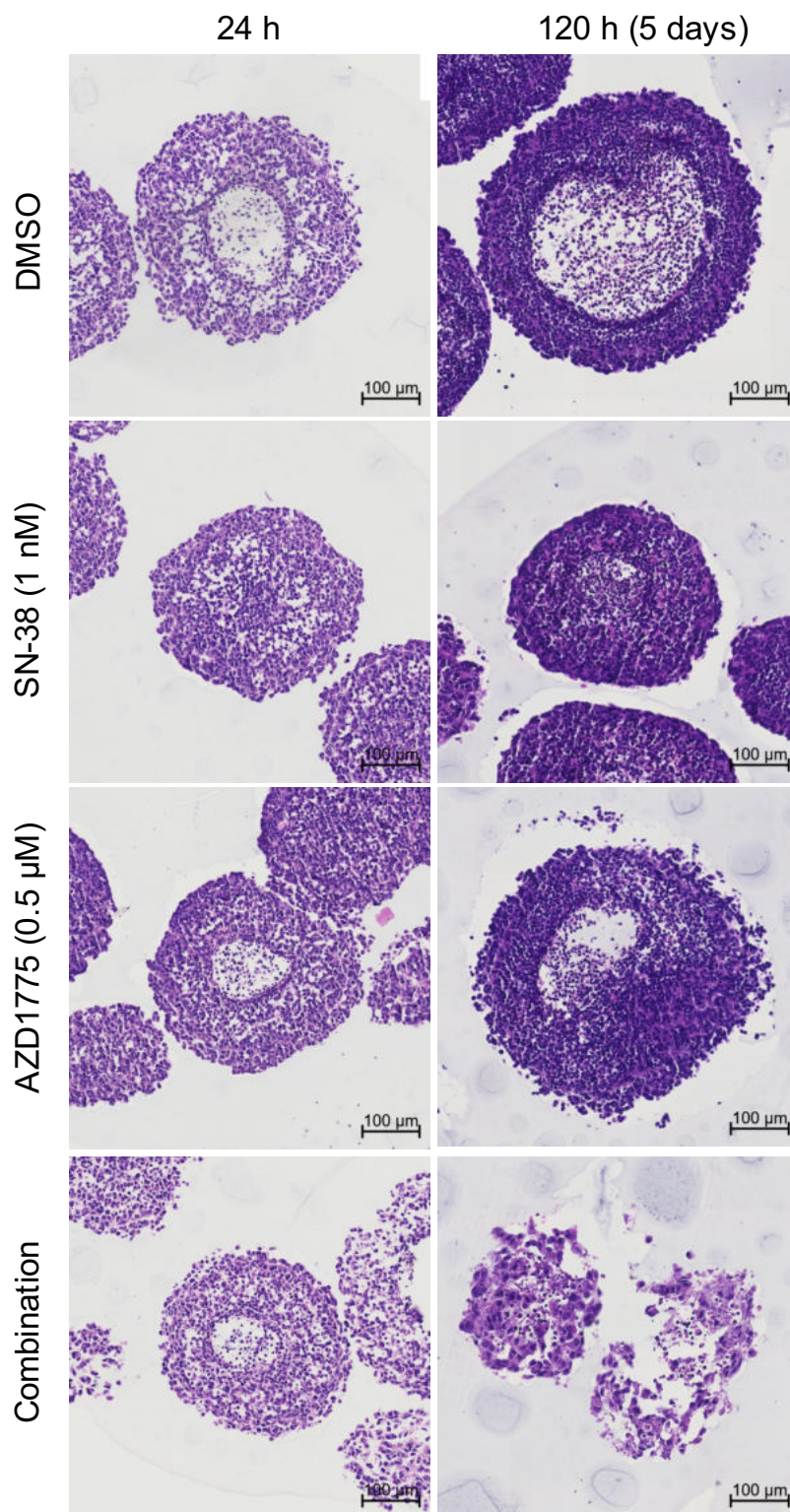
Figure 5.3 Haematoxylin and eosin staining of TC32 spheroids treated with SN-38 in combination with AZD1775.

Sections of paraffin-embedded TC32 spheroids stained with haematoxylin and eosin. Spheroids were treated with SN-38 (1 nM), AZD1775 (0.5 µM), or concurrent treatment for 24 h and 120 h (5 days). Images are representative of spheroids from each condition.
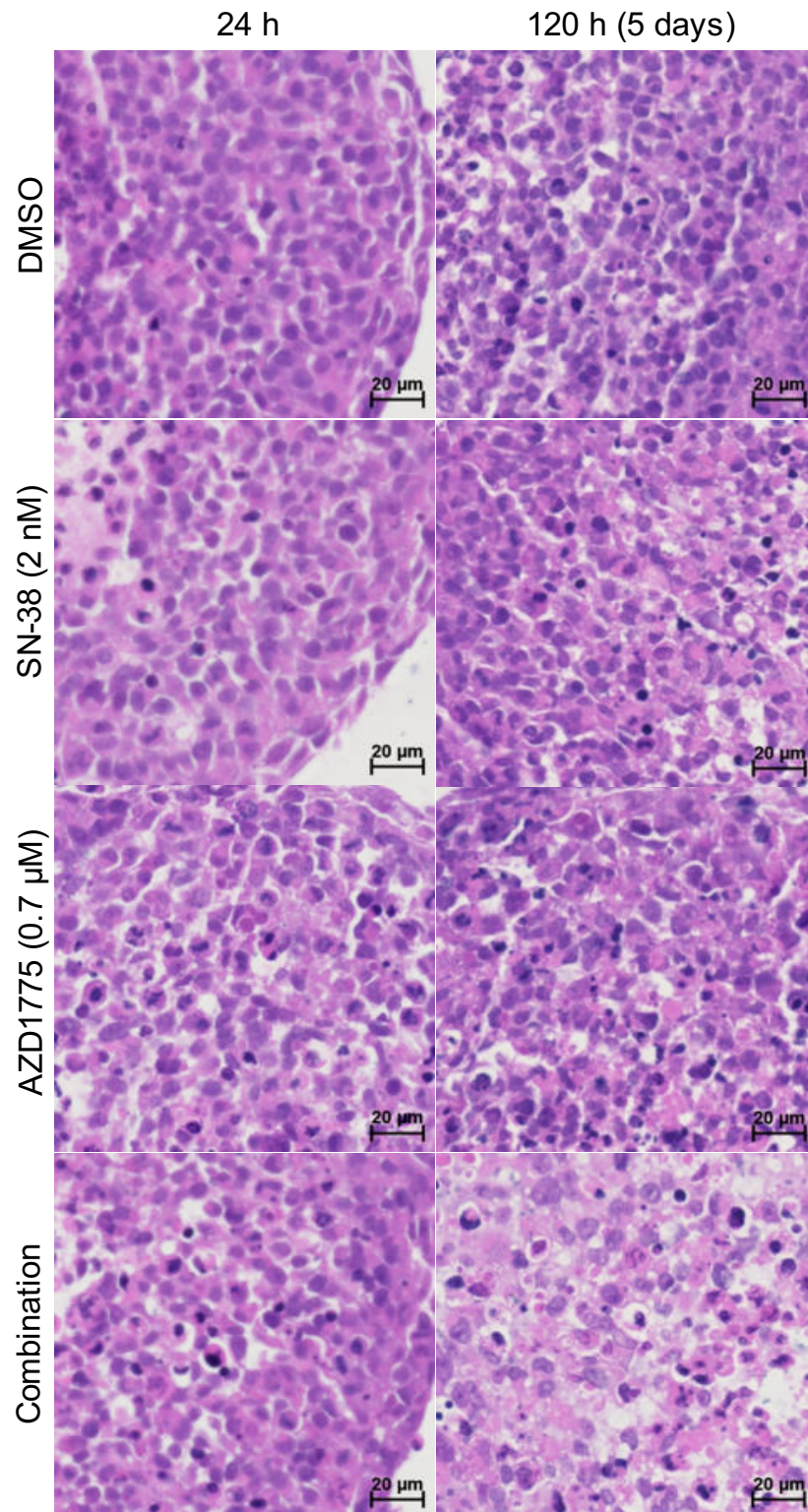
Figure 5.4 High magnification of haematoxylin and eosin staining of A673 spheroids treated with SN-38 in combination with AZD1775

High magnification sections of paraffin-embedded A673 spheroids stained with haematoxylin and eosin. Spheroids were treated with SN-38 (2 nM), AZD1775 (0.7 µM), or concurrent treatment for 24 h and 120 h.
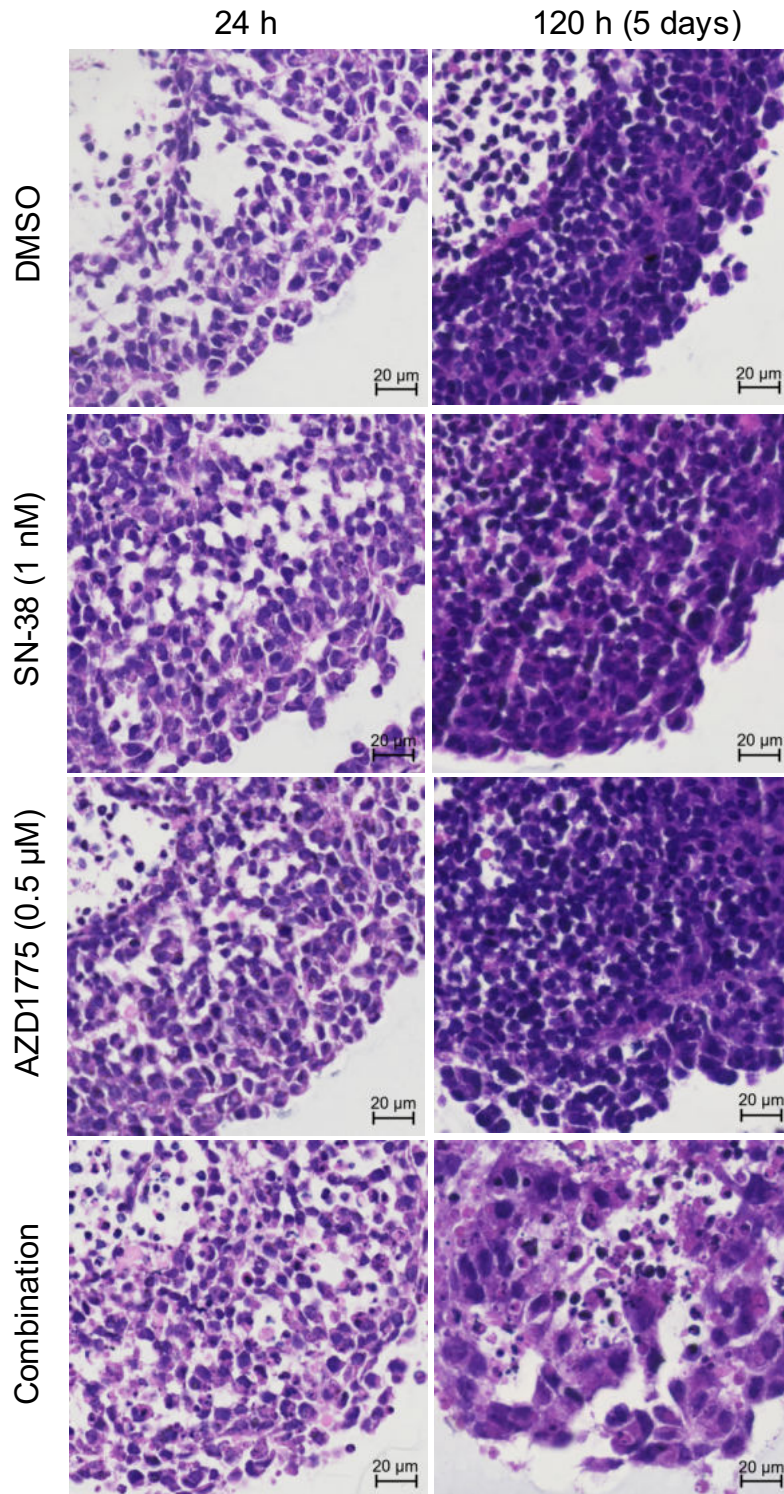
Figure 5.5 High magnification of haematoxylin and eosin staining of TC32 spheroids treated with SN-38 in combination with AZD1775.

High magnification sections of paraffin-embedded TC32 spheroids stained with haematoxylin and eosin. Spheroids were treated with SN-38 (1 nM), AZD1775 (0.5 µM), or concurrent treatment for 24 h and 120 h (5 days). Images are representative of spheroids from each condition.
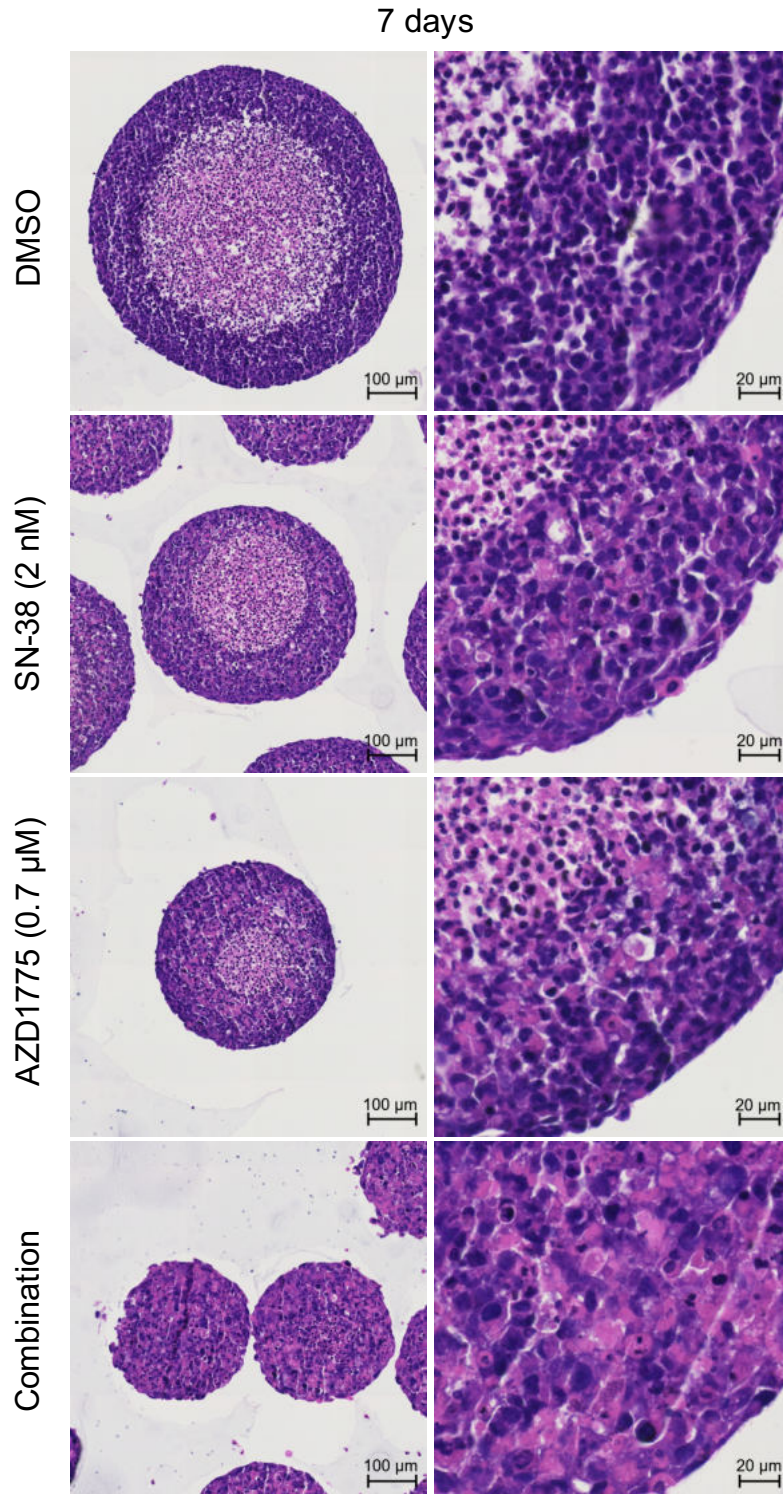
Figure 5.6 Apoptotic features following SN-38 in combination with AZD1775 treatment in A673 spheroids.

Sections of paraffin-embedded A673 spheroids stained with haematoxylin and eosin at day 7 of the 21-day cycle. Spheroids were treated with SN-38 (2 nM), AZD1775 (0.7 µM), or concurrent treatment for 5 days. Images are representative of spheroids from each condition

7 days
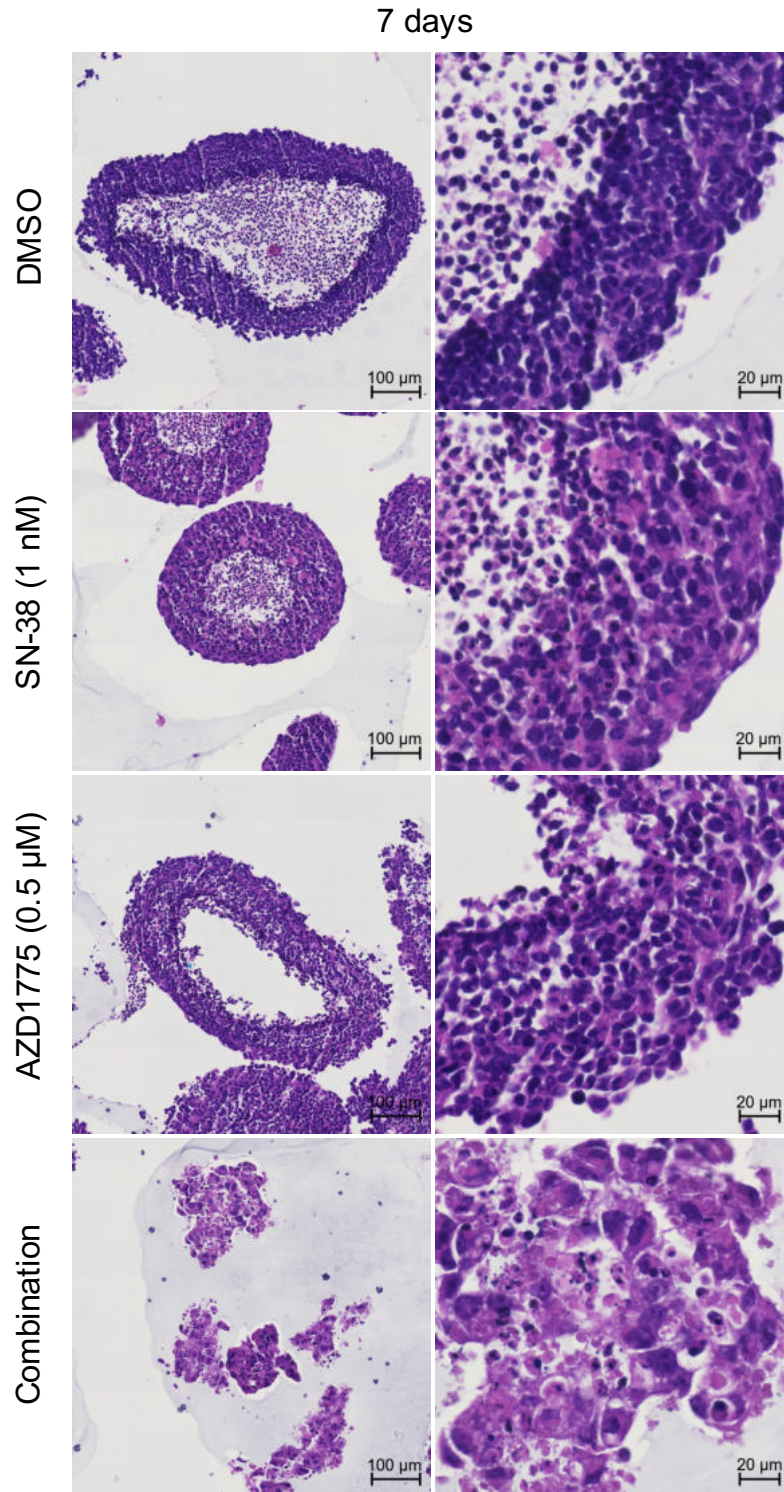
Figure 5.7 Apoptotic features following SN-38 in combination with AZD1775 treatment in TC32 spheroids.

Sections of paraffin-embedded TC32 spheroids stained with haematoxylin and eosin at day 7 of the 21-day cycle. Spheroids were treated with SN-38 (1 nM), AZD1775 (0.5 μM), or concurrent treatment for 5 days. Images are representative of spheroids from each condition

5.2.3 DNA damage markers and apoptosis assessment

Patterns of cell death and morphological changes due to concurrent treatment with SN-38 and WEE1 inhibition can be obtained from H&E staining, however these observations needed to be verified and characterised further. DNA damage in the form of DSBs was then assessed. Phosphorylation of H2AX is a central step in coordinating the response to repairing these lesions (as introduced in 1.3.1) (86, 87, 265). Thus, DNA damage after treatment was initially analysed and quantified through this measurable marker. The staining pattern of γH2AX is characterised by nuclear foci at localised sites of DNA damage, but it also appears as a pan-nuclear staining that can be associated, but is not limited to, apoptosis (265). Additionally, sections of paraffin-embedded spheroids were stained for cleaved caspase 3 (CC3), one of the main effectors of apoptosis. In its cleaved and active form, this caspase proteolytically activates additional caspases and other targets such as PARP1, also commonly used as a surrogate marker of apoptosis in its cleaved form (266).

Single agent treatment of A673 and TC32 spheroids with SN-38 and WEE1 inhibitor AZD1775 induced γH2AX foci after 6, 12 and 24 hours (Fig. 5.8, Fig. 5.9). However, the increase in this DNA damage marker, with the combined treatment in A673 spheroids, significantly exceeded single-agent treatment across all time points (Fig. 5.8B). The percentage of cells with pan-nuclear staining was far lower than localised γH2AX for all conditions (0-5%), with the combination treatment achieving the highest increase at 24 h, although not statistically significant (Fig. 5.8B). The percentage of positive cells for CC3 approximately matched the percentages of positive cells for pan-nuclear γH2AX, overall amounting to a modest apoptotic response after treatment (Fig. 5.10A). Results with TC32 spheroids showed lower percentages of γH2AX foci positive cells compared to A673 spheroids, but similar patterns of DNA damage induction after treatment (Fig 5.9B). Combination treated spheroids had the highest induction of γH2AX foci after 24 h (Fig. 5.9B). Treatment with AZD1775 alone matched the combination treatment's DNA damage induction at 6 h, but this decreased at the 24 h time point (Fig 5.9B). With regards to pan-nuclear γH2AX and CC3 positive cells, the combination treatment caused the greatest increase across all time points assessed for both of these markers (Fig. 5.9B, Fig. 5.10B). The highest percentage of cell for these markers associated with cell death were measured 24 h after treatment (Fig. 5.9B, Fig. 5.10B). Together, analysis of γH2AX foci as a DNA damage marker indicated greater accumulation caused by SN-38 in

combination with WEE1 inhibition in both A673 and TC32 spheroids. Notably, at the time points assessed, the damage generated by the combination did not lead to a large percentage of cells expressing apoptotic marker CC3 and pan-nuclear γH2AX in either of the ES models. However, TC32 spheroids did show significantly higher levels of cells positive for these markers following the combination treatment. This is supported by the phenotype of combination treatment in TC32 spheroids, which is characterised by a strong decrease in spheroid size, suggesting cell death (Fig. 5.1A). Overall, these findings demonstrated DNA damage induction after the combination treatment. Whilst a strong apoptotic response was not visible at the time points assessed, the presence of DNA damage could contribute to delaying growth, and over time, accumulate to become lethal.
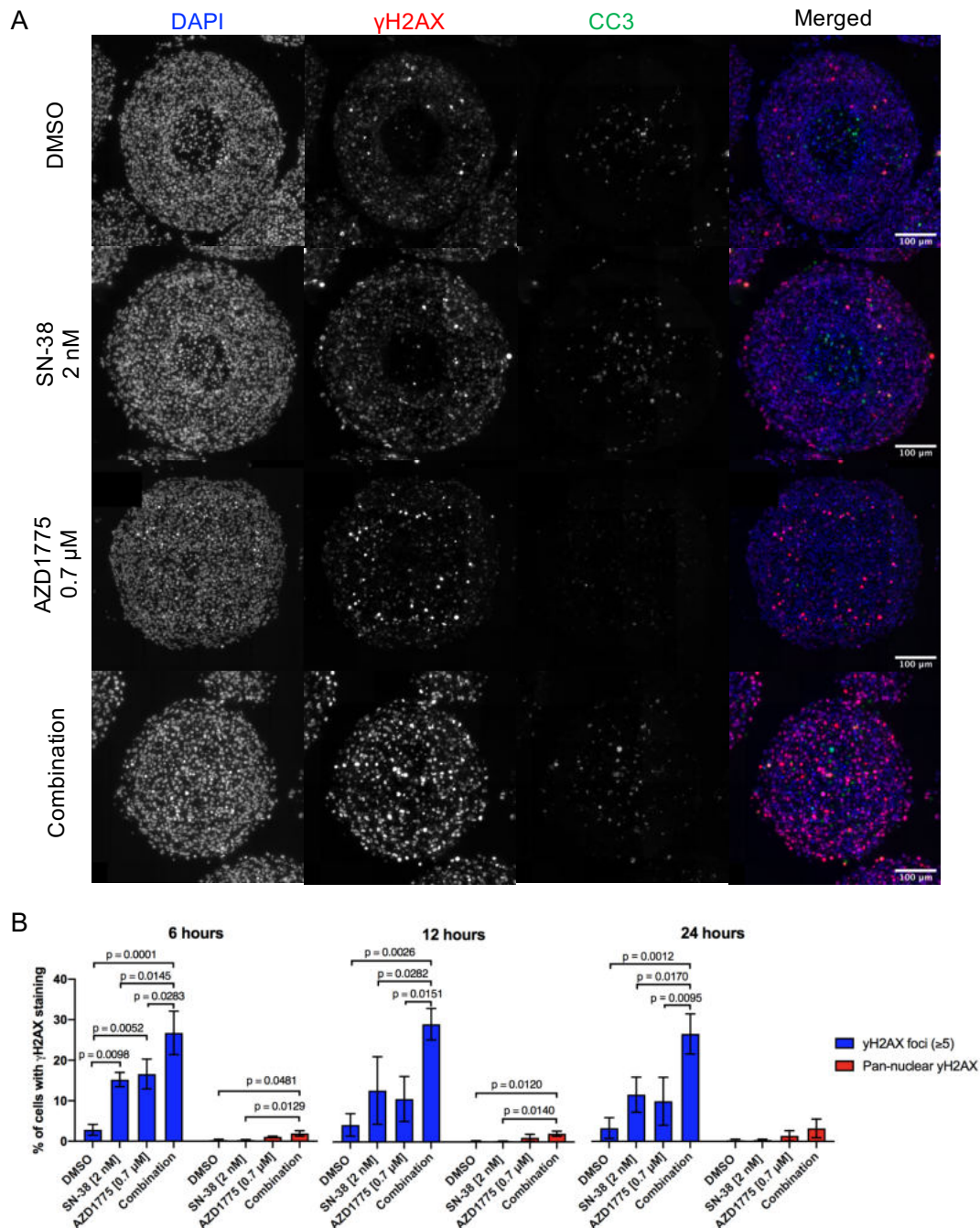
Figure 5.8 SN-38 in combination with AZD1775 causes DNA damage in A673 spheroids.

(A) Representative microscopy images showing γH2AX foci and pan-nuclear staining (red) and (green) on sections of paraffin-embedded A673 spheroids. Samples were treated with SN-38 (2 nM), AZD1775 (0.7 µM), or concurrent treatment for 6 h, 12 h, and 24 h. (B) Bar charts showing percentage of A673 cells positive for γH2AX, foci (>5) and pan-nuclear staining after treatment. >2000 nuclei were scored per condition. Graphs represent means ± standard deviation from 3-6 replicates per condition and are representative of three independent repeats. All p-values were calculated using a one-way ANOVA with Tukey's multiple comparisons test, only significant comparisons are shown.
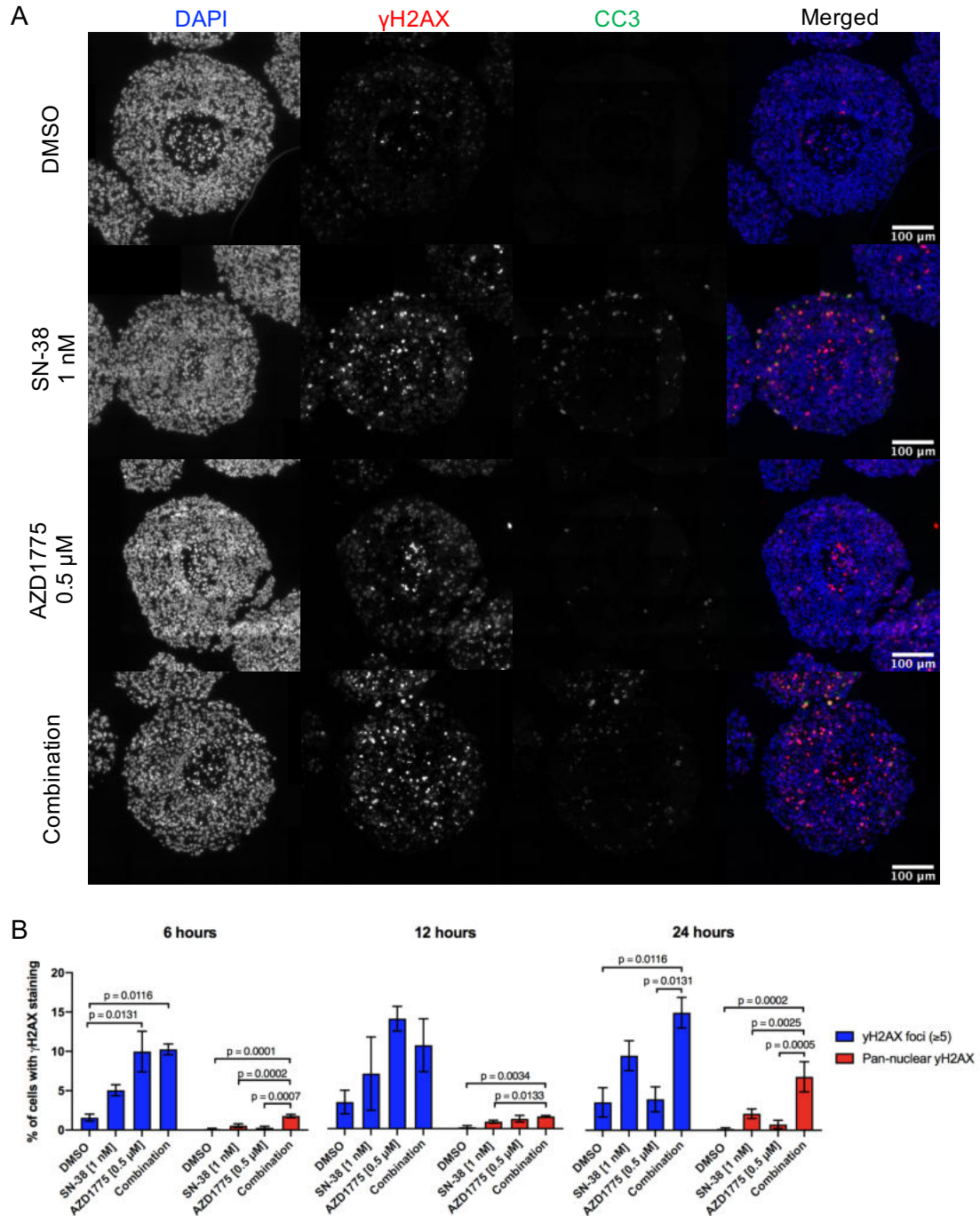
Figure 5.9 SN-38 in combination with AZD1775 causes DNA damage in TC32 spheroids.

(A) Representative microscopy images showing γH2AX foci and pan-nuclear staining (red) and CC3 (green) on sections of paraffin-embedded TC32 spheroids. Samples were treated with SN-38 (1 nM), AZD1775 (0.5 μM), or concurrent treatment for 6 h, 12 h, and 24 h. (B) Bar charts showing percentage of TC32 cells positive for γH2AX, foci (>5) and pan-nuclear staining after treatment. >2000 nuclei were scored per condition. Graphs represent means ± standard deviation from 3-6 replicates per condition and are representative of three independent repeats. All p-values were calculated using a one-way ANOVA with Tukey's multiple comparisons test, only significant comparisons are shown.

Figure 5.10 SN-38 in combination with AZD1775 causes cell death in ES spheroids.

Bar charts showing percentage of A673 (A) and TC32 (B) cells positive for CC3 staining after treatment. >2000 nuclei were scored per condition. Graphs represent means ± standard deviation from 3-6 replicates per condition and are representative of three independent repeats. All p-values were calculated using a one-way ANOVA with Tukey's multiple comparisons test, only significant comparisons are shown.

Assessment of γH2AX foci and CC3 staining was performed at a later time point (7 days from the beginning of the 21-day cycle). However, quantitative analysis of these samples was not carried out due to not being able to accurately segment nuclei in the combination-treated spheroids. This is because the DAPI staining in these samples was characterised by large areas with condensed nuclei and smaller spots with positive signal suggesting DNA fragmentation (Fig. 5.11B and 5.12B). The loss of cell membrane integrity also created a dispersed CC3 signal (Fig. 5.11B and 5.12B), affecting analysis of the levels of this marker. Nevertheless, these images showed the combination treatment, in both sets of spheroid models, led to a marked reduction in size and induction of cell death after the combination treatment as seen by positive CC3 signal, particularly in A673 spheroids. The loss of the spheroid structure and fragmentation in combination-treated TC32

spheroids suggested these were further ahead in the response and had already undergone apoptosis, which could explain the lower CC3 signal (Fig. 5.12B). Spheroids from both cell lines treated with SN-38 showed positive γH2AX staining, indicating DNA damage persisted at day 7 in the 21-day cycle, however, the growth curve results suggest this was not sufficient to cause a decrease in spheroid size.
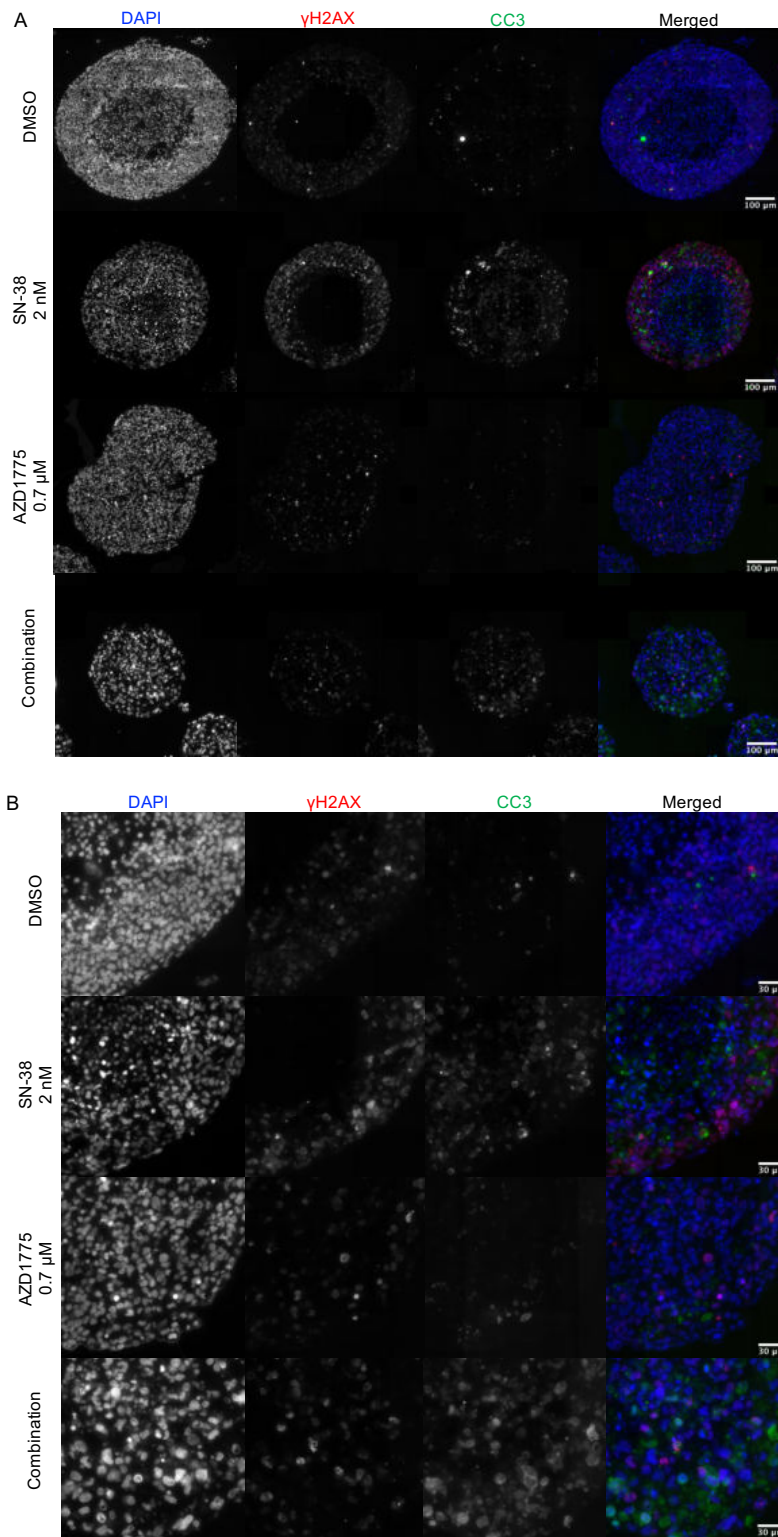
Figure 5.11 SN-38 in combination with WEE1 inhibition induces apoptosis in A673 spheroids.

(A) Representative microscopy images showing γH2AX staining (red) and CC3 (green) on sections of paraffin-embedded on whole A673 spheroids and magnified areas (B). Samples were treated with SN-38 (2 nM), AZD1775 (0.7 µM), or concurrent treatment 5 days and cultured for another 2 days prior to fixation and processing.
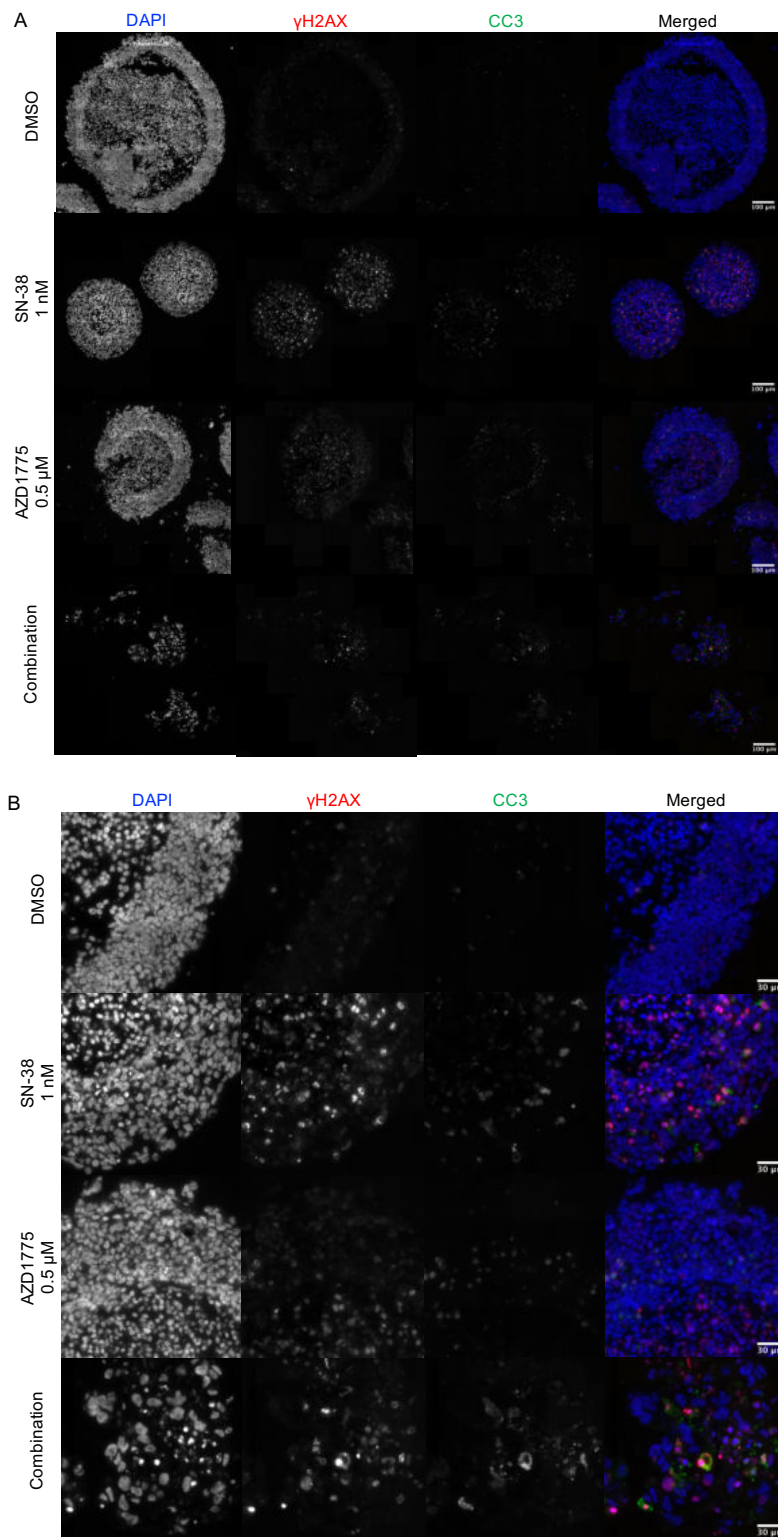
Figure 5.12 SN-38 in combination with WEE1 inhibition induces apoptosis in TC32 spheroids.

(A) Representative microscopy images showing γH2AX staining (red) and CC3 (green) on sections of paraffin-embedded on whole TC32 spheroids and magnified areas (B). Samples were treated with SN-38 (1 nM), AZD1775 (0.5 μM), or concurrent treatment 5 days and cultured for another 2 days prior to fixation and processing.

To continue to assess the nature of the DNA lesions detected, 53BP1 was measured as an additional marker of DNA damage. As introduced before, this protein can colocalise with γH2AX at DSBs and plays an important role in DNA repair signalling, contributing to determining the repair pathway of choice. Briefly, 53BP1 promotes NHEJ in G1 by antagonising resection of DNA ends, a key step for HR, which is mainly active in S and G2 phases. Immunofluorescence detection of 53BP1 showed extensive foci accumulation following single-agent SN-38 and combination treatment in A673 spheroids (Fig. 5.13A). Damage induction measured with this marker was consistent across all timepoints and comparable between these two conditions, except at 6 h, when SN-38 treatment alone had a greater percentage of 53BP1 foci positive cells (Fig. 5.13B). AZD1775 treatment did not cause significantly different 53BP1 foci formation from the untreated control (Fig. 5.13B). In contrast, assessment in TC32 spheroids showed faster induction of 53BP1 foci compared to the response in A673 spheroids. All conditions reported elevated levels after 6 h and 12 h of treatment, including AZD1775 monotherapy (Fig. 5.14B). Of note, the highest induction occurred with SN-38 alone (Fig 5.14B). The percentage of positive cells with 53BP1 foci in TC32 spheroids dropped at 24 h in all conditions in contrast to results seen in the A673 model. Overall, the two main differences, only seen in TC32 spheroids, were accumulation of this marker after WEE1 inhibition and earlier development of 53BP1 foci across all conditions. In summary, assessment of DSBs with traditional DNA damage foci suggested combination treatment resulted in greater damage induction at the time points assessed, but only when measuring DSBs decorated with γH2AX and not 53BP1. SN-38 treatment however, led to strong induction of the latter, which was also visible in the combination treatment of A673 spheroids only.

Figure 5.13 53BP1 foci analysis in A673 spheroids.

(A) Representative microscopy images showing 53BP1 foci (green) on sections of paraffin-embedded A673 spheroids. Samples were treated with SN-38 (2 nM), AZD1775 (0.7 μM), or concurrent treatment for 6 h, 12 h, and 24 h. (B) Bar charts showing percentage of A673 cells positive for 53BP1 foci (>5) after treatment. >2000 nuclei were scored per condition. Graphs represent means ± standard deviation from 3-6 replicates per condition and are representative of two independent repeats. All p-values were calculated using a one-way ANOVA with Tukey's multiple comparisons test, only significant comparisons are shown.

Figure 5.14 53BP1 foci analysis in TC32 spheroids.

(A) Representative microscopy images showing 53BP1 foci (green) on sections of paraffin-embedded TC32 spheroids. Samples were treated with SN-38 (1 nM), AZD1775 (0.5 µM), or concurrent treatment for 6 h, 12 h, and 24 h. (B) Bar charts showing percentage of TC32 cells positive for 53BP1 foci (>5) after treatment. >2000 nuclei were scored per condition. Graphs represent means ± standard deviation from 3-6 replicates per condition and are representative of two independent repeats. All p-values were calculated using a one-way ANOVA with Tukey's multiple comparisons test, only significant comparisons are shown.

During the course of assessing 53BP1 staining, areas rich in positive 53BP1 signal were observed (Fig. 5.15). These were identified to be 53BP1 nuclear bodies (NBs) (> 2 μm^2), which are DNA lesions that manifest in daughter G1 cells, but develop during mitosis from under-replicated DNA (46, 47, 267) (Fig. 5.15A). In this way, 53BP1 NBs are commonly used as a surrogate marker of RS, since under-replicated DNA can arise from pressures slowing down fork progression (54). To quantify these nuclear structures, 53BP1 foci were classified by area, with 2 μm^2 as the size threshold (Fig. 5.15C). SN-38 treatment induced the highest percentage of positive cells, primarily observed after 24 h (Fig. 5.16B). At the earlier time points of 6 h and 12 h, positive A673 cells were below 5% (Fig. 5.16B). This is consistent with 53BP1 NBs being DNA lesions that require undergoing mitosis to appear, and therefore require one full cell cycle. To verify this, additional time points at 48 h and 120 h after treatment were investigated, confirming induction of 53BP1 NBs (Fig. 5.16). The appearance of these nuclear structures was significantly higher after SN-38 treatment alone in A673 spheroids (Fig. 5.16B). Presence of 53BP1 NBs was also investigated in TC32 spheroids, where similar effects were observed with SN-38 in particular producing the strongest induction (Fig. 5.17B). Of note, 53BP1 NBs in TC32 spheroids were present as early as 6 h after treatment in contrast to the effect seen in A673 spheroids. Together, data with 53BP1 NBs confirmed SN-38's known capacity to induce RS in contrast to WEE1 inhibition, by this measure alone. However, the combination treatment did not result in greater induction of 53BP1 NBs, only matching SN-38 at 120 h after in treatment in A673 spheroids. In fact, the addition of WEE1 inhibitor AZD1775 appeared to suppress this effect.
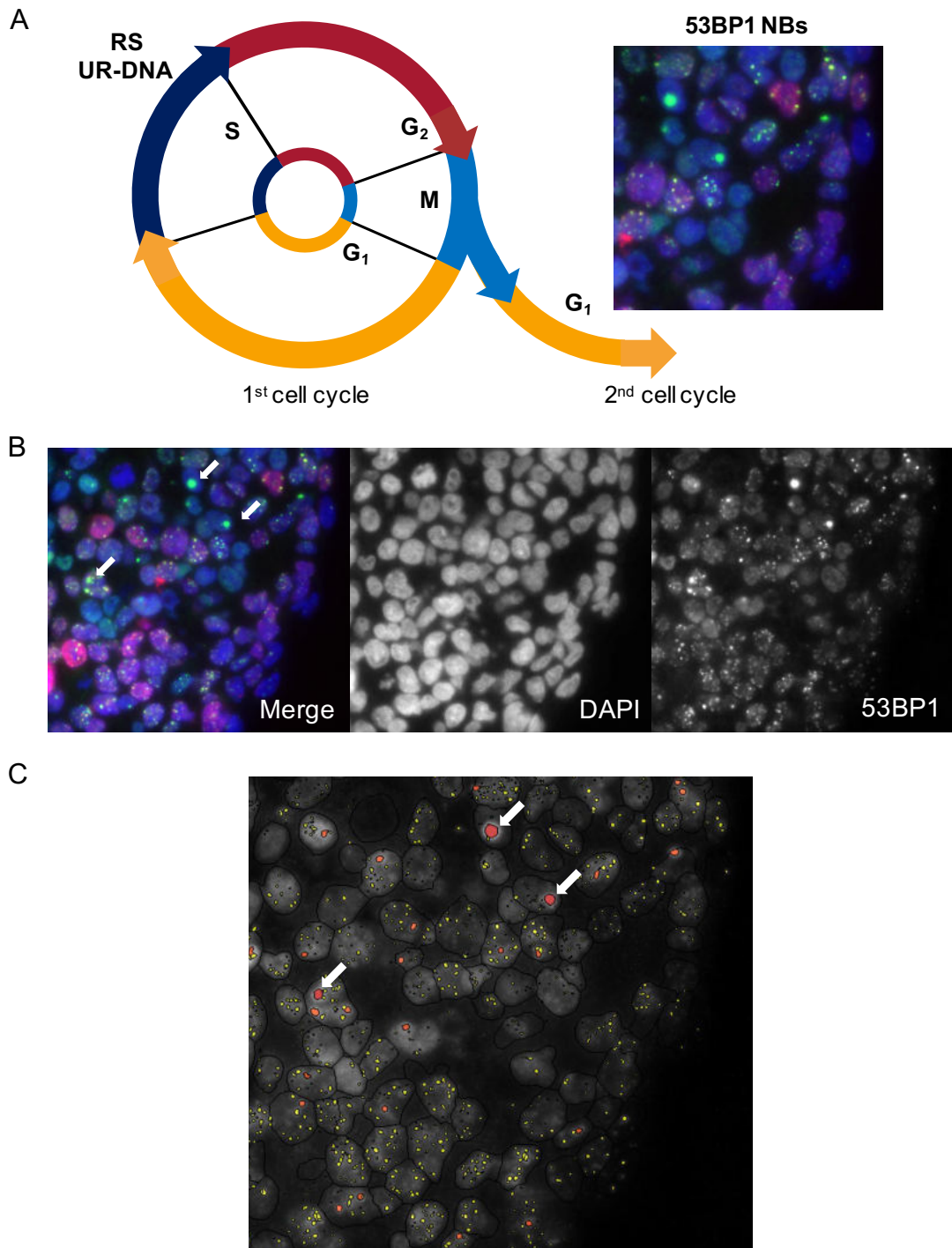
Figure 5.15 Induction of 53BP1 NBs on ES spheroids.

(A) 53BP1 NBs are DNA lesions generated in the previous cell cycle and arise from RS or under-replicated DNA. These are passed on to daughter cells, becoming visible in G1 as concentrated regions of 53BP1 (adapted from (47)). (B) Representative microscopy images showing 53BP1 NBs (green) on sections of paraffin-embedded A673 spheroids. These spots are distinct from the smaller 53BP1 foci. (C) Foci classification with Definiens Tissue Studio® using the spot detection algorithm. This was modified to count spots $>2 \ \mu m^2$ in red, filtering out 53BP1 foci smaller than this threshold in yellow and orange.
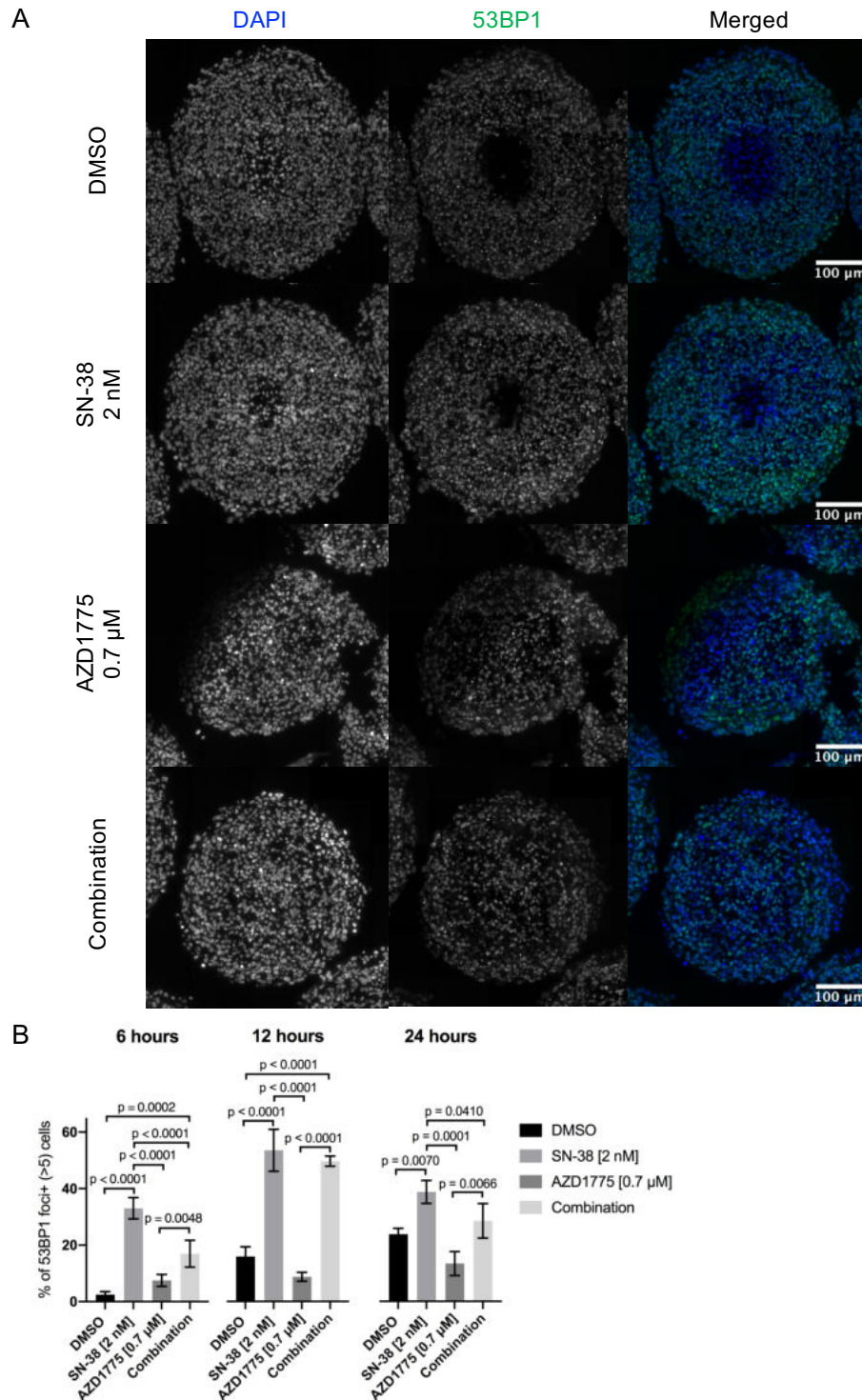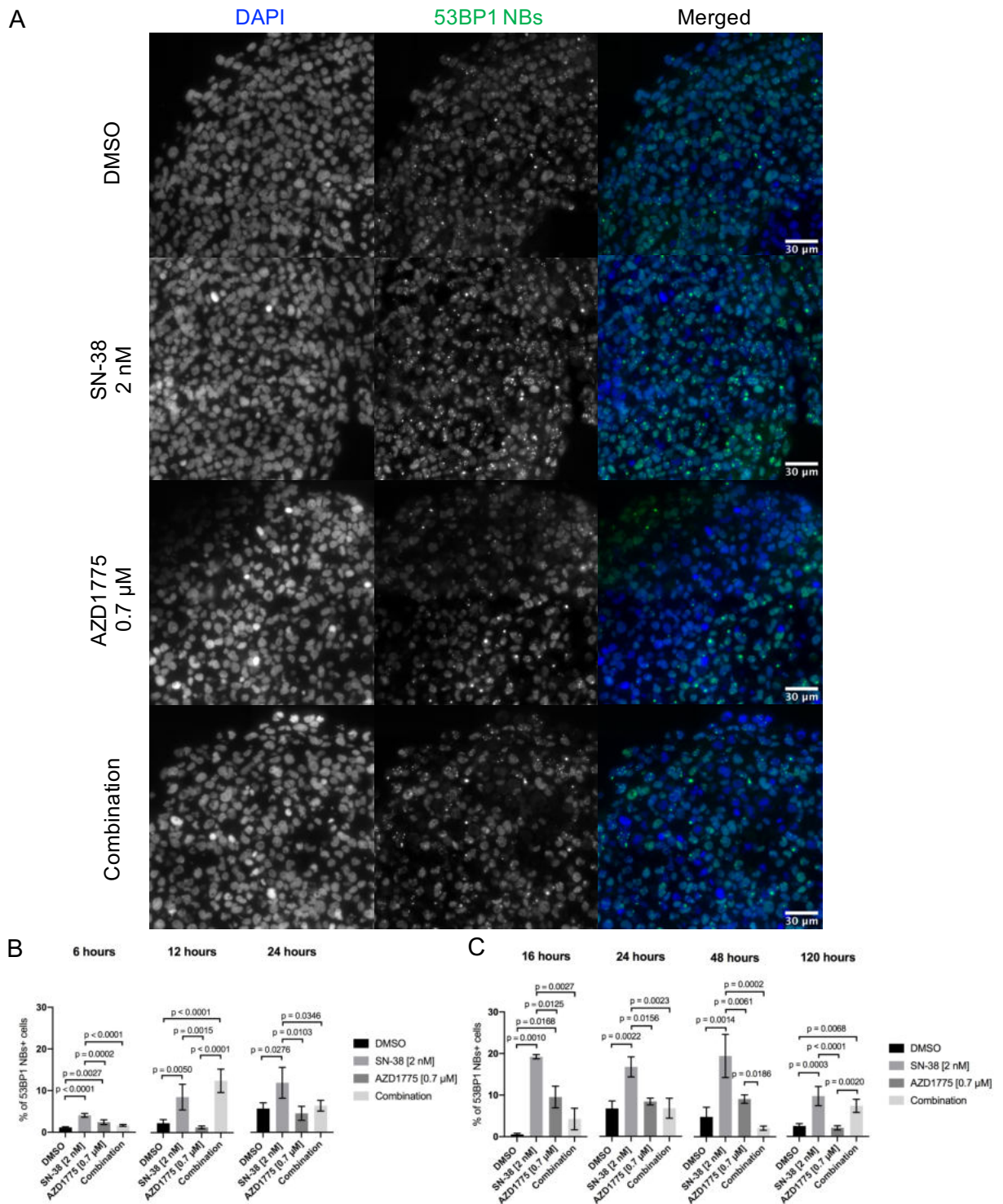
Figure 5.16 Assessment of 53BP1 NBs in A673 spheroids.

(A) Representative microscopy images showing 53BP1 nuclear bodies (green) on sections of paraffin-embedded A673 spheroids. Samples were treated with SN-38 (2 nM), AZD1775 (0.7 µM), or concurrent treatment for 6 h, 12 h, and 24 h. (B-C) Bar charts showing percentage of A673 cells positive for 53BP1 NBs (> 2 µm^2) after treatment. >2000 nuclei were scored per condition. Graphs represent means ± standard deviation from 3-6 replicates per condition and are representative of two independent repeats. All p-values were calculated using a one-way ANOVA with Tukey's multiple comparisons test, only significant comparisons are shown.
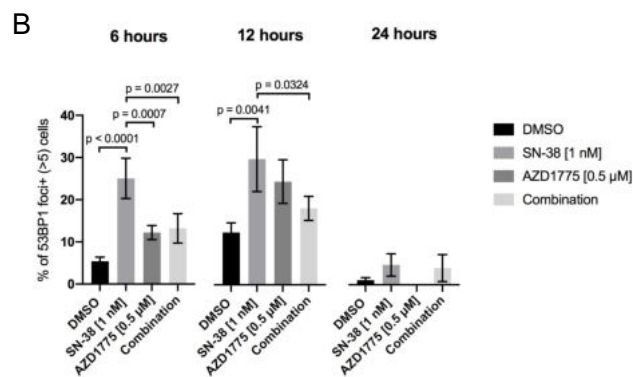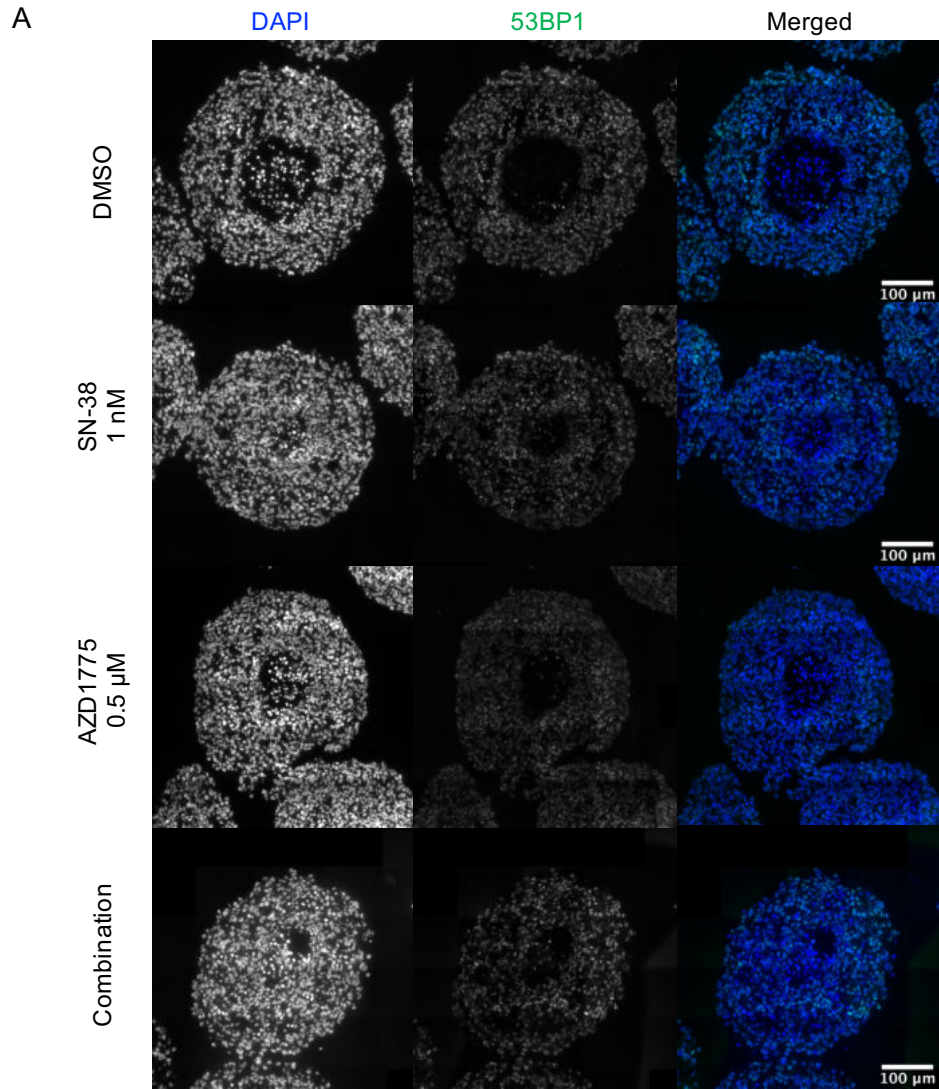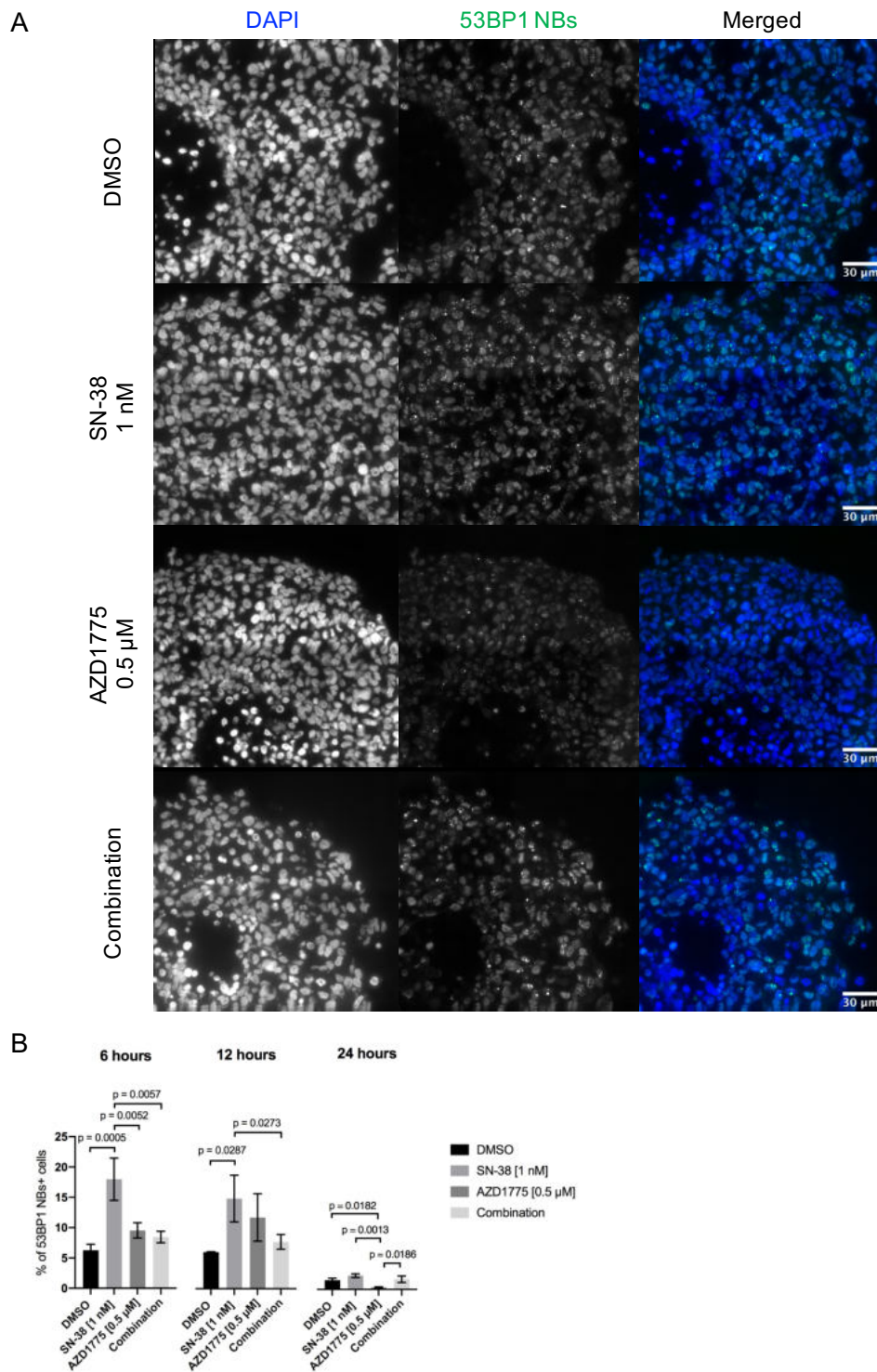
Figure 5.17 Assessment of 53BP1 NBs in TC32 spheroids.

(A) Representative microscopy images showing 53BP1 nuclear bodies (green) on sections of paraffin-embedded TC32 spheroids. Samples were treated with SN-38 (1 nM), AZD1775 (0.5 µM), or concurrent treatment for 6 h, 12 h, and 24 h. (B) Bar charts showing percentage of TC32 cells positive for 53BP1 NBs (> 2 µm^2) after treatment. >2000 nuclei were scored per condition. Graphs represent means ± standard deviation from 3-6 replicates per condition and are representative of two independent repeats. All p-values were calculated using a one-way ANOVA with Tukey's multiple comparisons test, only significant comparisons are shown.

5.2.4 Combination treatment effects on the cell cycle

To shed more light into how each treatment affected the cell cycle, the next steps were to stain for mitotic cells in sections of paraffin-embedded spheroids and perform DNA-content analysis by flow cytometry. As described before, WEE1 is the checkpoint kinase regulating the G2/M transition through phosphorylation of CDK1, which in turn prevents premature entry into mitosis. Inhibition of WEE1 was therefore expected to cause an increase in mitotic cells. As a biomarker of this, phosphorylation of histone H3 (pHH3) on serine 10 was detected through immunofluorescence staining on sections of paraffin-embedded spheroids (Fig. 5.18A and Fig. 5.19A). Percentage of pHH3 positive cells in A673 spheroids was quantified and was found to have significantly increased in both groups treated with AZD1775, compared to the untreated control and SN-38 alone (Fig. 5.18B). This effect was not as marked in TC32 spheroids, with only a modest increase in mitotic cells in single-agent AZD1775 across the three time points analysed. Interestingly, this effect was restricted to AZD1775 alone, but not combination-treated spheroids (Fig. 5.19B).
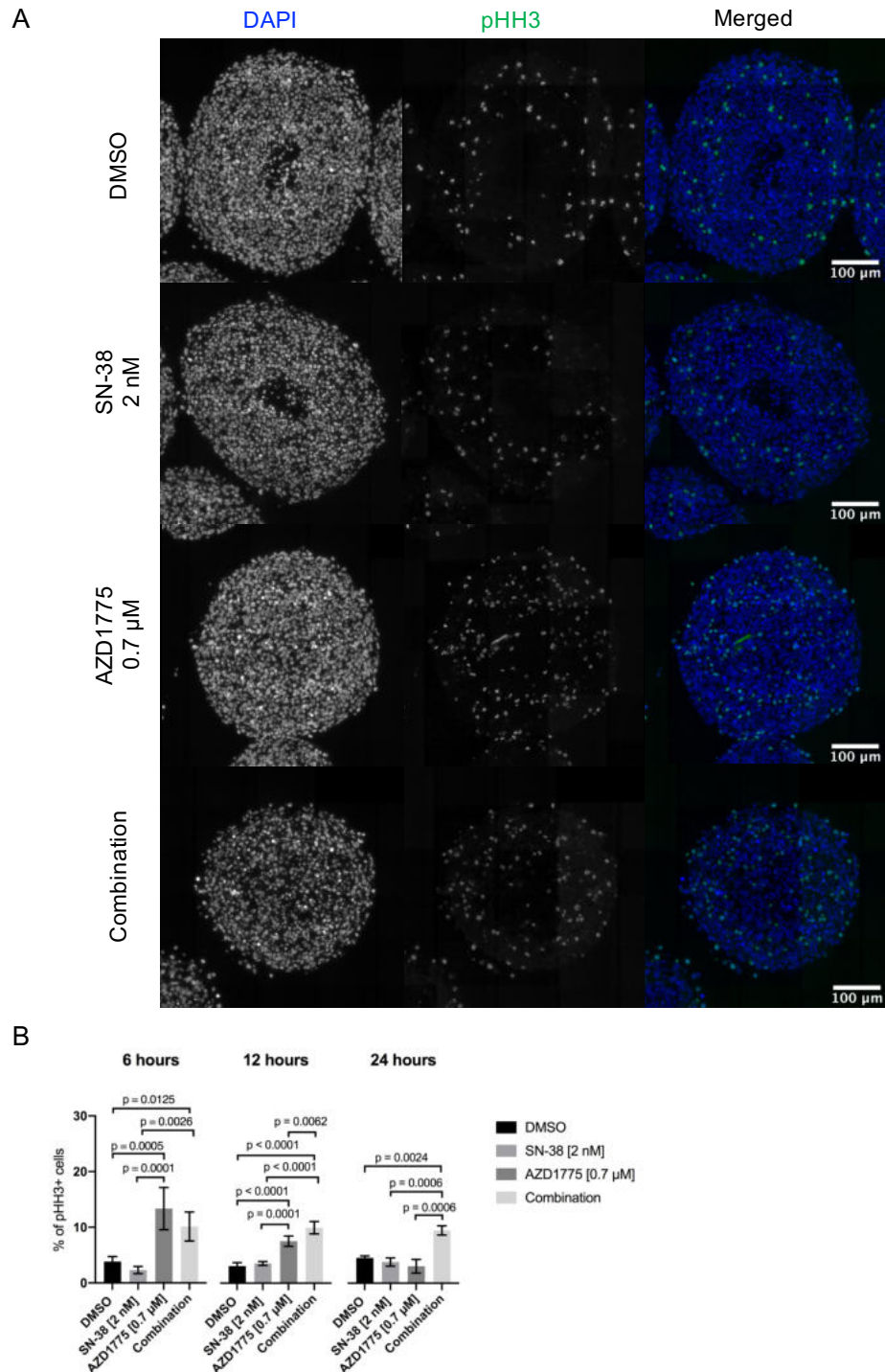
Figure 5.18 Effect of WEE1 inhibition on the number of mitotic cells in A673 spheroids.

(A) Representative microscopy images showing pHH3 staining (green) on sections of paraffin-embedded A673 spheroids. Samples were treated with SN-38 (2 nM), AZD1775 (0.7 μM), or concurrent treatment for 6 h, 12 h, and 24 h. (B) Bar charts showing percentage of A673 cells positive for pHH3 after treatment. >2000 nuclei were scored per condition. Graphs represent means ± standard deviation from 3-6 replicates per condition and are representative of two independent repeats. All p-values were calculated using a one-way ANOVA with Tukey's multiple comparisons test, only significant comparisons are shown.
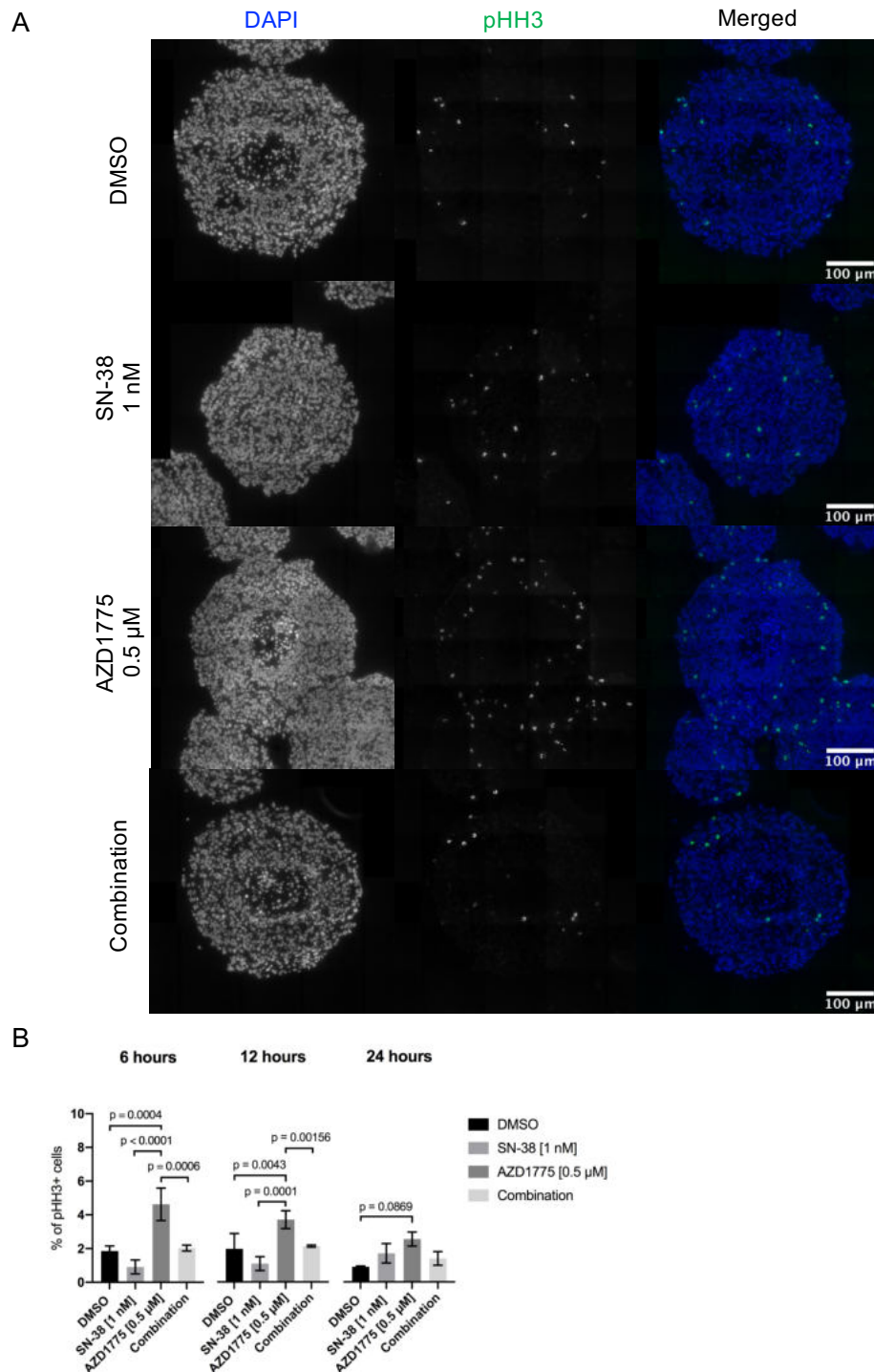
Figure 5.19 Effect of WEE1 inhibition on the number of mitotic cells in TC32 spheroids.

(A) Representative microscopy images showing pHH3 staining (green) on sections of paraffin-embedded TC32 spheroids. Samples were treated with SN-38 (1 nM), AZD1775 (0.5 μM), or concurrent treatment for 6 h, 12 h, and 24 h. (B) Bar charts showing percentage of TC32 cells positive for pHH3 after treatment. >2000 nuclei were scored per condition. Graphs represent means ± standard deviation from 3-6 replicates per condition and are representative of two independent repeats. All p-values were calculated using a one-way ANOVA with Tukey's multiple comparisons test, only significant comparisons are shown.

Investigating the treatment's impact on the cell cycle was a key step to understanding the mechanism behind the combined activity of these agents. To do so, it was important to perform this analysis on the same model system as previous experiments, since the phenotype in question was specific to how ES spheroids responded to the combined treatment. In addition, cell cycling and proliferation patterns differ between 2D and 3D cultures (268). For example, spheroids do not necessarily reflect a cell population that is dividing exponentially, unlike cells in culture dishes during the log phase. Rather, these models have been found to show distinct patterns of cell proliferation across their different regions (4, 268). To address this increased heterogeneity, DNA content analysis by flow cytometry was adapted to using spheroids as a model system, detailed in 2.15.

Cell cycle analysis revealed a strong intra-S-phase arrest in TC32 cells from dissociated spheroids, visible after 24 h and 48 h of combined SN-38 treatment and WEE1 inhibition (Fig. 5.20). This effect coincided with an increase in the sub-G1 population, denoting cell death induced by the treatment. An approximate 5% of sub-G1 cells at 24 h closely matched the percentage of CC3 positive cells at the same time point, previously assessed by immunofluorescence (Fig. 5.10B). These effects were preceded by gradual lengthening of S-phase at the earlier time points of 6 h and 10 h (Fig. 5.20). More importantly, there was an absence of cells accumulating at the G2/M checkpoint, in agreement with the effect of WEE1 inhibition. However, it is unclear whether a portion of TC32 cells were able to progress into mitosis or they largely accumulate in S-phase as suggested by the histograms (Fig. 5.20). Contrastingly, accumulation of A673 cells in S-phase was not observed after 24 h or 48 h of the combination treatment (Fig. 5.20). In fact, the cell cycle profile of these cells appeared unaffected and was more similar to that of normal progression (Fig. 5.20). Moreover, the individual effect of SN-38 on cell cycle progression was consistent in both cell lines. This was characterised by an increase of the S-phase population at 6 h, followed by G2/M accumulation between 10 h and 24 h after treatment, and lastly a return to a profile resembling normal progression, as in the untreated controls, 48 h after (Fig. 5.20, Fig. 5.21). These events matched what is known about SN-38 as an inducer of DSBs and RS, slowing down progression through S-phase followed by activation of the G2/M checkpoint to repair accumulated DNA damage. With regards to single-agent AZD1775, there was an increase in G0/G1 cells observed in TC32 cells, but not A673 (Fig. 5.20, Fig. 5.21). Removal of functional G2/M checkpoint through chemical abrogation, increases the importance of the G1-S checkpoint to

coordinate DNA repair. Importantly, TC32 cells are *TP53* WT unlike A673, enabling activation of the G1-S checkpoint, potentially responsible for the increase in the percentage of G0/G1 cells. The status of p53 may be important in the determining the response and fate following treatment of these cell lines.

In addition to how cell lines responded to treatment, cell cycle analysis highlighted further differences between cell lines, for example the overall length and proportion of phases in each cell cycle. On average, the S-phase percentage in untreated cells was higher in A673 than TC32 (31.73% and 25.18%, respectively). This also translated to a smaller G2/M population in TC32 cells compared to A673, with the opposite being true for G0/G1. This profile may be indicative of faster proliferation in A673 cells compared to TC32, consistent with the estimated doubling times for these cell lines (A673: 24 h and TC32: 36 h), albeit when cultured in 2D.
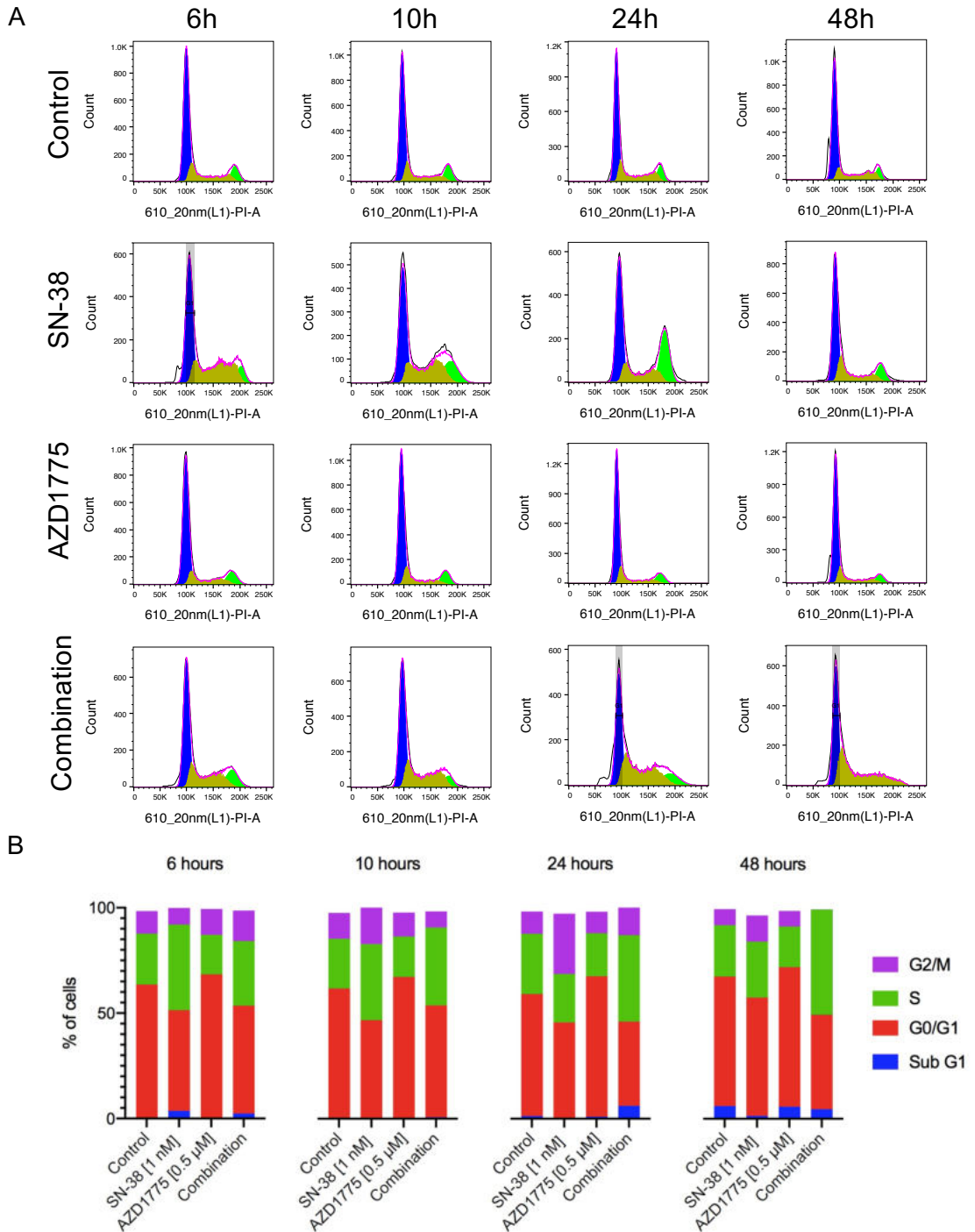
Figure 5.20 Effects of SN-38 in combination with AZD1775 on cell cycle progression of TC32 spheroids

SN-38 in combination with AZD1775 induces S-phase accumulation in TC32 spheroids. (A) Histograms of dissociated TC32 spheroids and subjected to propidium iodine (PI) labelling for DNA-content analysis by flow cytometry after treatment. TC32 spheroids were treated with SN-38 (1 nM), AZD1775 (0.5 µM), or concurrent treatment for 6 h, 12 h, and 24 h. (B) Bar charts represent means from 25,000 events per condition and are representative of two independent repeats.
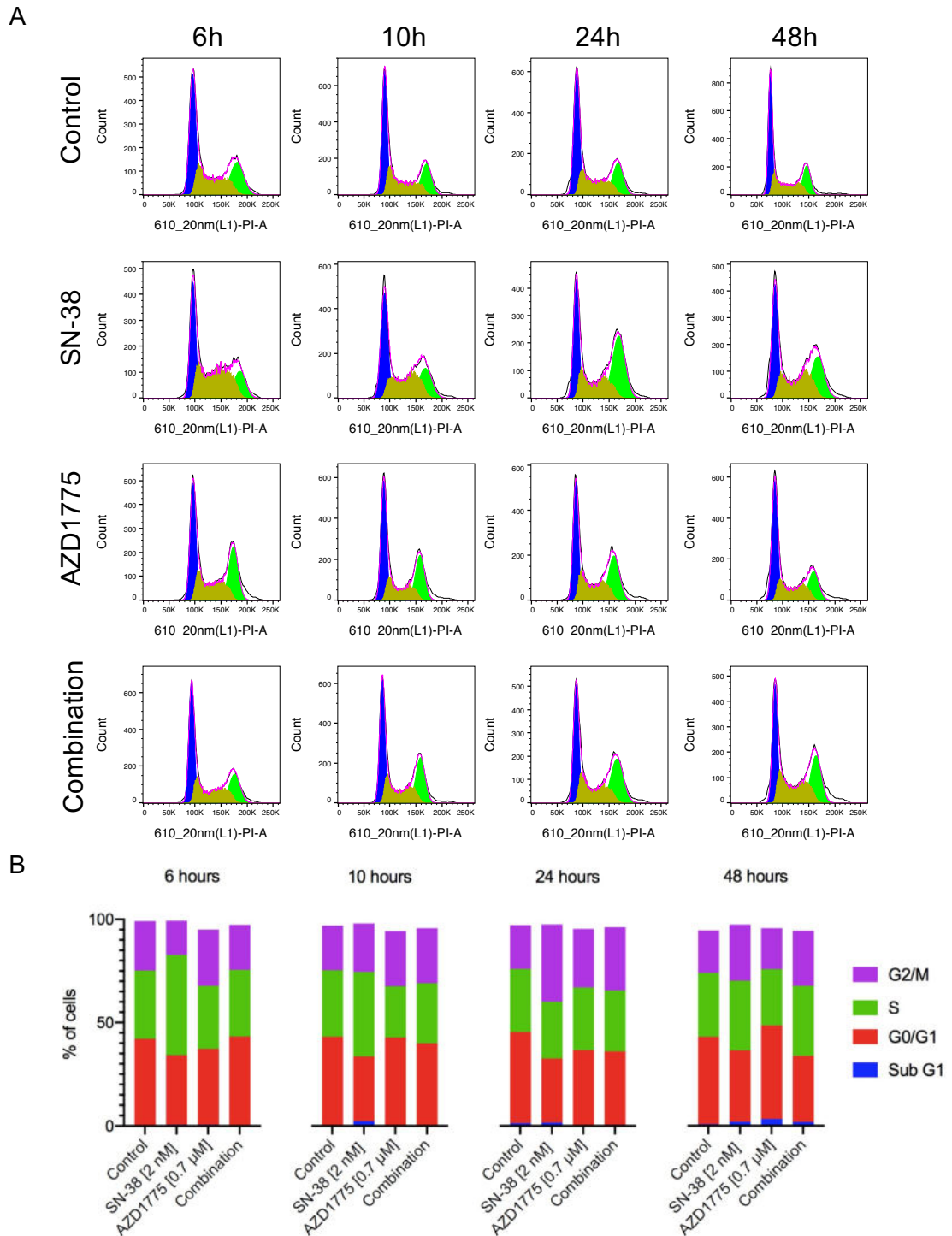
Figure 5.21 Effects of SN-38 in combination with AZD1775 on cell cycle progression of A673 spheroids.

(A) Histograms of dissociated A673 spheroids and subjected to propidium iodine (PI) labelling for DNA-content analysis by flow cytometry after treatment. A673 spheroids were treated with SN-38 (2 nM), AZD1775 (0.7 µM), or concurrent treatment for 6 h, 12 h, and 24 h. (B) Bar charts represent means from 25,000 events per condition and are representative of two independent repeats.

5.2.5 Characterising the apoptotic response following combination treatment

Previously, growth assessment following combination treatment in A673 and TC32 spheroids resulted in two different responses, one marked by growth arrest and the other by cell death, respectively (Fig. 5.1). The response following combination treatment in A673 spheroids was assessed beyond the 21-day cycle, and spheroids were shown to remain in this state without a recovery in size (Fig. 5.22). To continue investigating these two phenotypes p53 was investigated as a mediator of these responses. Notably, cell line A673 is p53-null and TC32 cell line p53 WT (Table. 5.1). Therefore, p53 activity could have been involved in the cell death response in TC32 spheroids following combination treatment was assessed. Downstream target of p53, PUMA, was investigated and detected by Western blot (Fig. 5.23A). The window to activation of these effectors of p53-mediated apoptosis was on the 5th day of the 21-day cycle. This was to be consistent with the time when spheroid size decreased in the assay. (Fig. 5.1A). Induction of PUMA expression was visible in SN-38 and combination-treated TC32 spheroids, coinciding with an increase in cleaved PARP1 (Fig. 5.23A). Densitometry analysis relative to the loading control, indicated that the levels of PUMA and cleaved PARP1 following combination treatment were higher in the combination treatment in TC32 spheroids (Fig. 5.23C). Regarding the response in A673 spheroids, these did not display activation of this downstream effector of apoptosis, as expected given its p53 status (Fig. 5.23B).
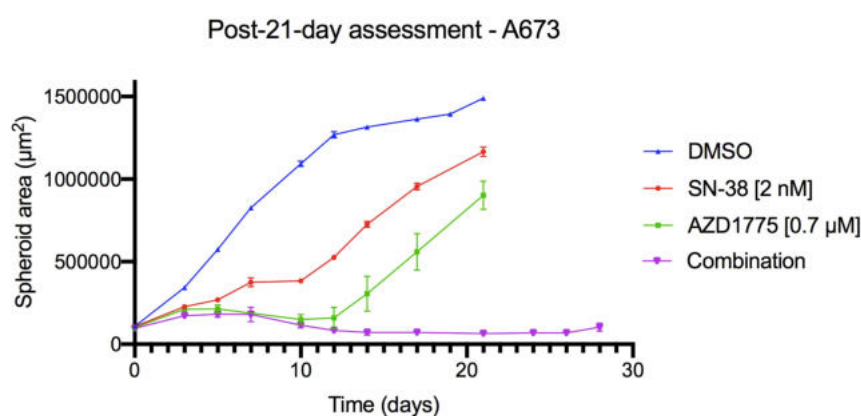
Figure 5.22 Post-21-day assessment of combination treated A673 spheroids

A673 spheroids models were treated with SN-38, AZD1775, or concurrent treatment at the indicated concentrations for 5 days in a 21-day cycle. Growth was monitored for an additional 7 days. Graphs represent means ± standard deviation from 6 replicates and are representative of two independent repeats.
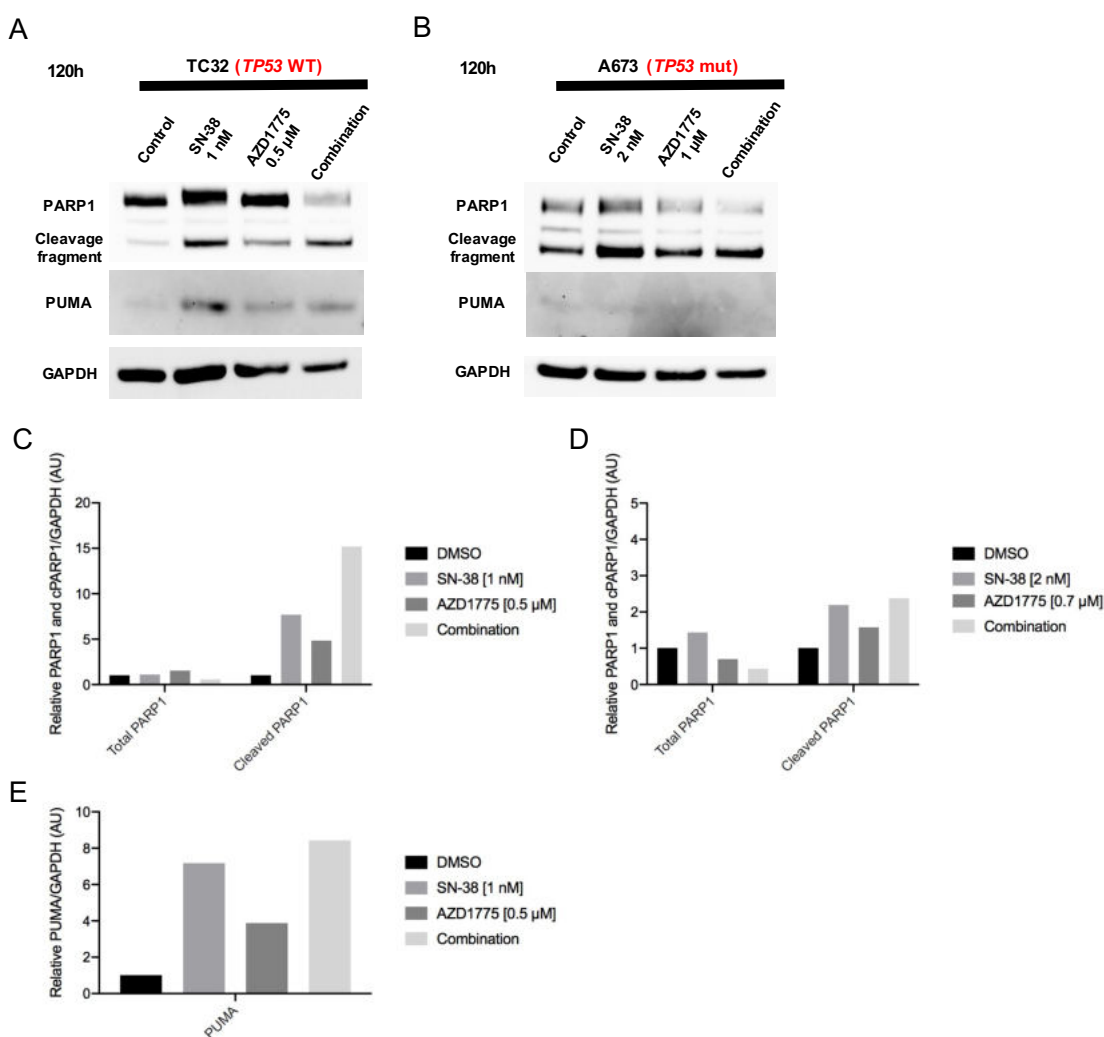
Figure 5.23 Effects of SN-38 in combination with AZD1775 on markers of apoptosis.

Protein levels of cleaved PARP1 and PUMA assessed by Western blot on TC32 spheroids (A) and A673 spheroids (B) after 120 h treatment of SN-38 (1 nM and 2 nM) and AZD1775 (0.7 μM and 1.4 μM), alone and in combination. Total PARP1 and GAPDH levels are shown as control and loading controls, respectively. Western blots are representative of at least two independent repeats. (C-E) Bar graphs with densitometry values from western blots in A and B, normalised to loading control GAPDH, and in the case of cleaved PARP1 also normalised to total PARP1 levels. Values are relative to the untreated control of each blot.

5.2.6 CDK1/2 dysregulation and degradation of RRM2

Unscheduled activation of CDK1 and CDK2 following inhibition of WEE1, results in a range of effects that affect processes in the cell cycle, particularly DNA replication in S-phase (31). Amongst these, degradation of RRM2 has been reported to occur following

AZD1775 treatment. This enzyme is the catalytic subunit of RNR, and therefore responsible for maintaining nucleotide pools. Inhibiting nucleotide metabolism limits the ability to carry out efficient DNA replication, increasing RS. (31, 41, 168). To investigate this, protein levels of RRM2 were found to decrease in both conditions treated with AZD1775 (Fig. 5.24A). Consistent with successful WEE1 inhibition, levels of phosphorylated tyrosine 15 on CDK1/2 also decreased, marking the reduction of the inactive form of these downstream targets of WEE1 (Fig. 5.24A). Decrease in RRM2 protein levels was replicated with 0.7 μM of AZD1775, which verified this effect was within the clinically achievable threshold of the WEE1 inhibitor (Fig. 5.24B). Degradation of RRM2 has been shown to be triggered by CDK2 phosphorylation of its threonine 33 residue (168). However, this enzyme's expression has also been linked to ATR activity, independently from its downstream signalling through CHK1 and WEE1, and thus CDK2 (42). To assess whether this effect was observed with ATR inhibition as well, RRM2 levels following treatment with inhibitors of this kinase were tested. Clinical drug candidates VX-970 and AZD6738 lowered RRM2 protein levels, but not to the extent that WEE1 inhibition did (Fig 5.24C). ATR inhibition decreased WEE1 activation, but only minimally, as seen by a small reduction in levels of p-CDK1/2 (Y15), suggesting limited dysregulation of CDK2 and degradation of RRM2. It remains to be addressed whether inhibiting ATR affects RRM2 expression via an alternative mechanism, independent of the ATR-CHK1-WEE1 axis (42). Of note, ATR inhibition in combination with SN-38 was also successful in decreasing spheroid growth, as reported earlier in chapter 4. However, these results suggest RRM2 status may not be relevant to the growth inhibitory effect seen with ATR inhibitors in ES spheroids. In contrast, data with AZD1775 suggests WEE1 inhibition's effect on nucleotide metabolism may act as a potential source of RS, contributing to genome instability (Fig. 5.25).
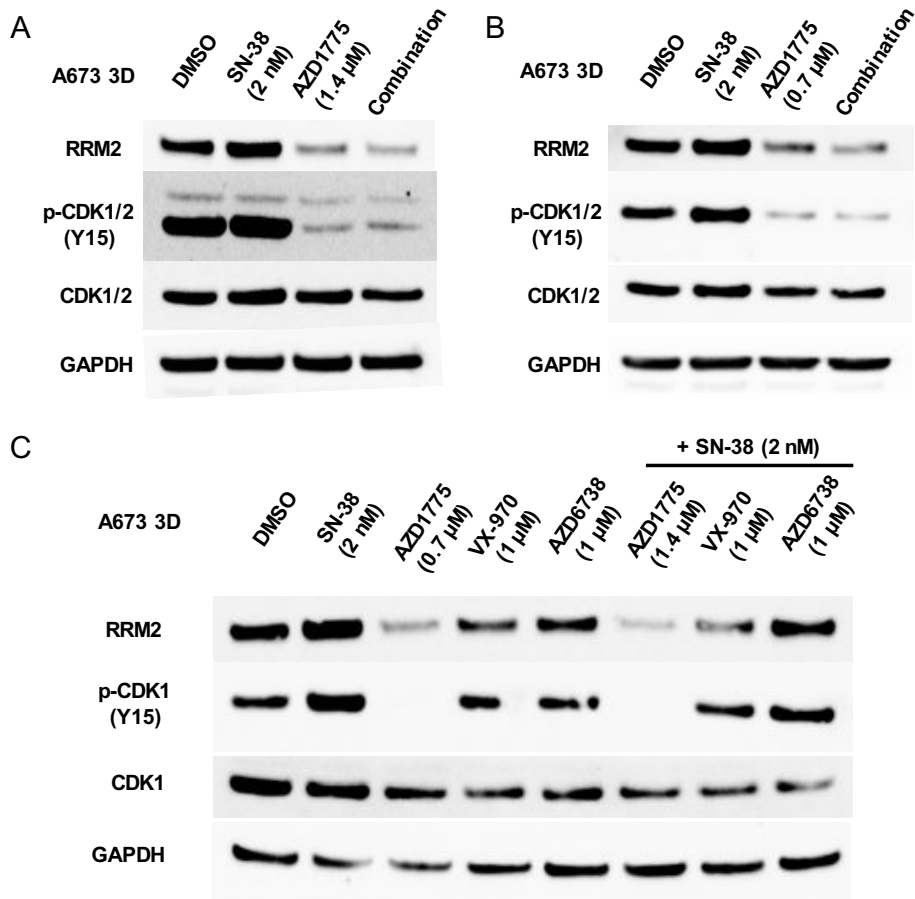
Figure 5.24 WEE1 inhibition dysregulates CDK1/2 and degrades RRM2.

Protein levels of RRM2 and phospho-CDK1/2 (Y15) assessed by Western blot on A673 spheroids after 24 h of SN-38 (2 nM) treatment in combination AZD1775 at 1.4 µM (A) and 0.7 µM (B), and ATR inhibitors VX-970 (1 µM) and AZD6738 (1 µM) (C). Total CDK1 and GAPDH levels are shown as control and loading controls, respectively. Western blots are representative of at least two independent repeats.
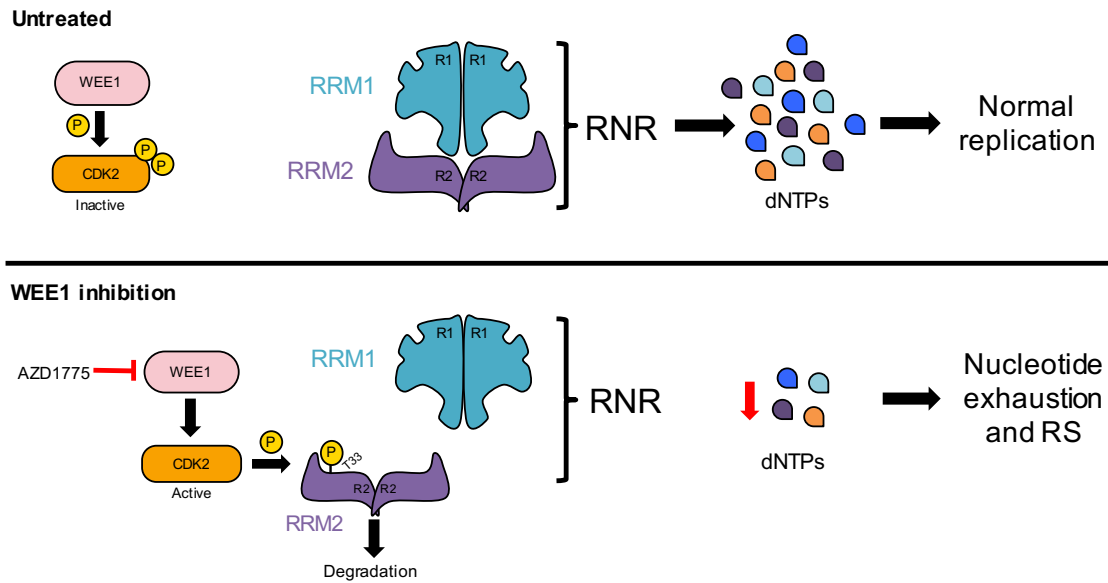
Figure 5.25 WEE1 inhibition-induced replication stress through RRM2 degradation and nucleotide depletion.

Diagram modelling WEE1 inhibition contributing through RS by disrupting nucleotide metabolism. Upon activation WEE1 phosphorylates CDK2 to regulate its activity, however inhibition with AZD1775 prevents inactivation of CDK2, maintaining it functional. In turn, dysregulated CDK2 phosphorylates RRM2 on its threonine 33 (T33) residue, triggering degradation of this homodimer subunit of RNR. Degradation of RRM2 results in inhibiting RNR and nucleotide production, contributing to RS.

For these reasons, the next step was to investigate the extent of the contribution of RRM2 degradation to the decrease in spheroid growth, obtained with SN-38 in combination with WEE1 inhibition. To begin to explore this, the dynamics and time frame of the decrease in protein levels of RRM2 were investigated with a time-course experiment. Protein assessment by Western blot revealed WEE1 activity, determined by phosphorylated CDK1/2, was sufficiently blocked after just 2 h of AZD1775 treatment, alone and in combination with SN-38 (Fig 5.26A). In terms of RRM2 protein levels, these began to decrease at 2 h (~25%), becoming significantly more apparent at 6 h (Fig. 5.26A). Degradation of RRM2 was also verified in AZD1775-treated conditions in TC32 spheroids at 24 hours, showing a smaller decrease in levels of RRM2 in spheroid lysates treated with the combination (Fig. 5.27A). Furthermore, nucleotide supplementation was tested to examine the impact of RRM2 degradation, and potential depletion of nucleotide pools, on spheroid growth. This experiment used medium supplemented with nucleosides throughout the 21-day cycle and tested the 5-day treatment of SN-38 in combination with WEE1 inhibition. Spheroid growth of A673 and TC32 spheroids was not recovered by

the addition of nucleosides, suggesting RRM2 degradation and its consequences on nucleotide metabolism do not influence the overall cytotoxic effect of the combination treatment (Fig. 5.26C and 5.27C).
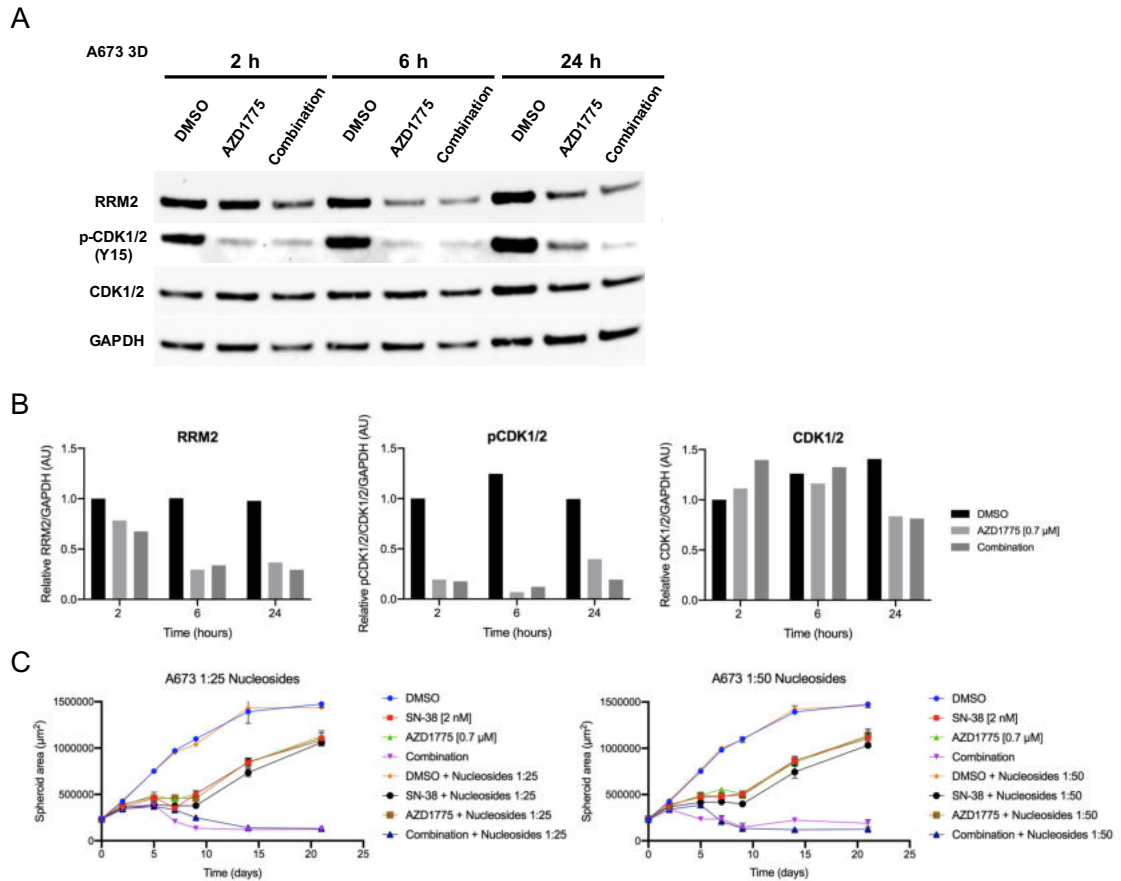
Figure 5.26 Time-course assessment of RRM2 degradation after WEE1 inhibition.

(A) Protein levels of RRM2 and phospho-CDK1/2 (Y15) assessed by Western blot on A673 spheroids after 2 h, 6 h, and 24 h of AZD1775 treatment with 0.7 µM, alone and in combination with SN-38 (2 nM). Total CDK1 and GAPDH levels are shown as control and loading controls, respectively. Western blots and graphs are representative of at least two independent repeats. (B) Bar graphs with densitometry values from western blots in A, normalised to loading control GAPDH and relative to the untreated control at 2 h for RRM2, p-CDK1/2, and CDK1/2. (C) A673 spheroids were treated with SN-38 (2 nM), AZD1775 (0.7 µM), or concurrent treatment in media supplemented with EmbryoMax Nucleosides at 1:25 and 1:50 dilutions. Growth was assessed by measuring spheroid area. Graphs represent means ± standard deviation from 6 replicates and are representative of three independent repeats.
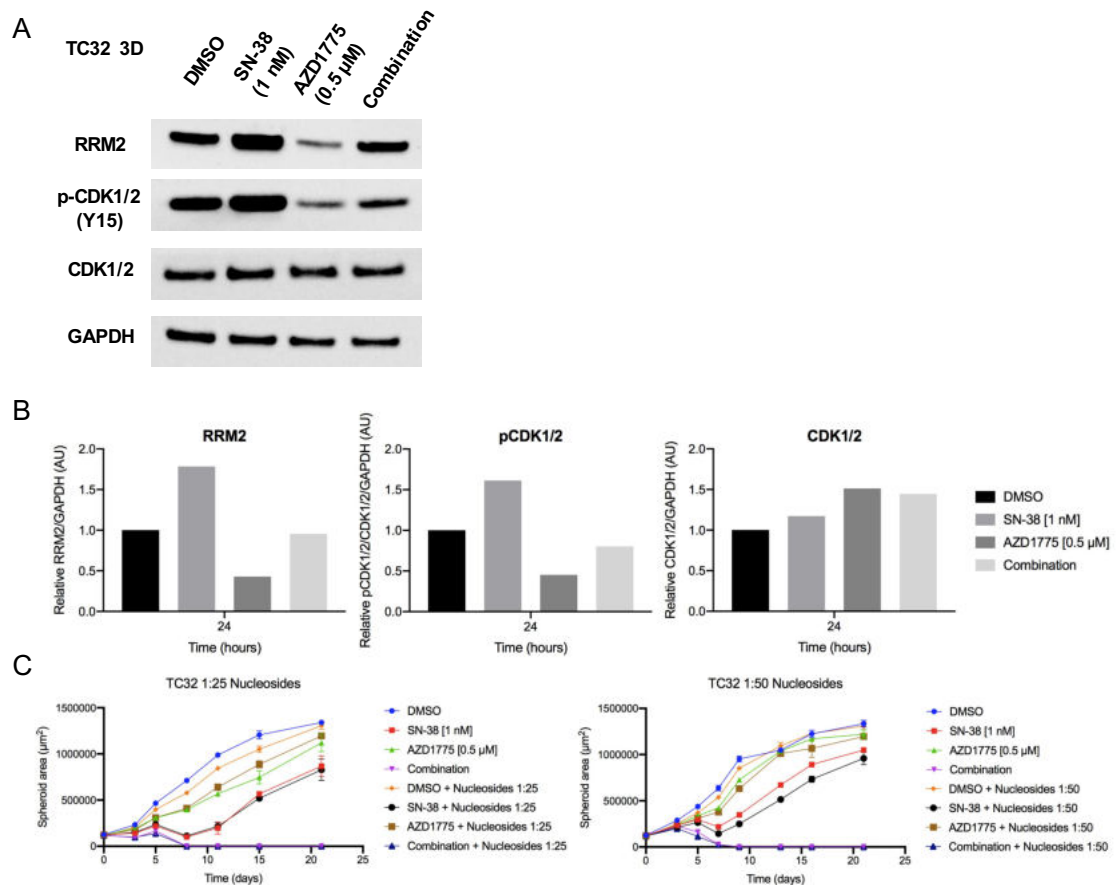
Figure 5.27 RRM2 degradation and nucleotide supplementation in TC32 spheroids

(A) Protein levels of RRM2 and phospho-CDK1/2 (Y15) assessed by Western blot on TC32 spheroids after 24 h of treatment with SN-38 (1 nM) and AZD1775 (0.7 μM), alone and in combination. Total CDK1 and GAPDH levels are shown as control and loading controls, respectively. Western blots and graphs are representative of at least two independent repeats. (B) Bar graphs with densitometry values from western blots in A, normalised to loading control GAPDH and relative to the untreated control for RRM2, p-CDK1/2, and CDK1/2. (C) TC32 spheroids were treated with SN-38 (1 nM), AZD1775 (0.5 μM), or concurrent treatment in media supplemented with EmbryoMax Nucleosides at 1:25 and 1:50 dilutions. Growth was assessed by measuring spheroid area. Graphs represent means ± standard deviation from 6 replicates and are representative of two independent repeats.

As a control experiment to verify effective supplementation with nucleosides, colon carcinoma cell line WiDr, was treated with AZD1775 with and without nucleotide supplementation (Fig 5.28). Development of AZD1775-induced DNA damage, measured by γH2AX, had been shown to be counteracted by the addition of nucleosides (39, 269). This experiment was replicated to ensure that, in our hands, the use of this supplement was working as previously shown. Indeed, increase in γH2AX intensity following WEE1

inhibition was counteracted by treating these cells in the presence of nucleosides (Fig. 5.28).
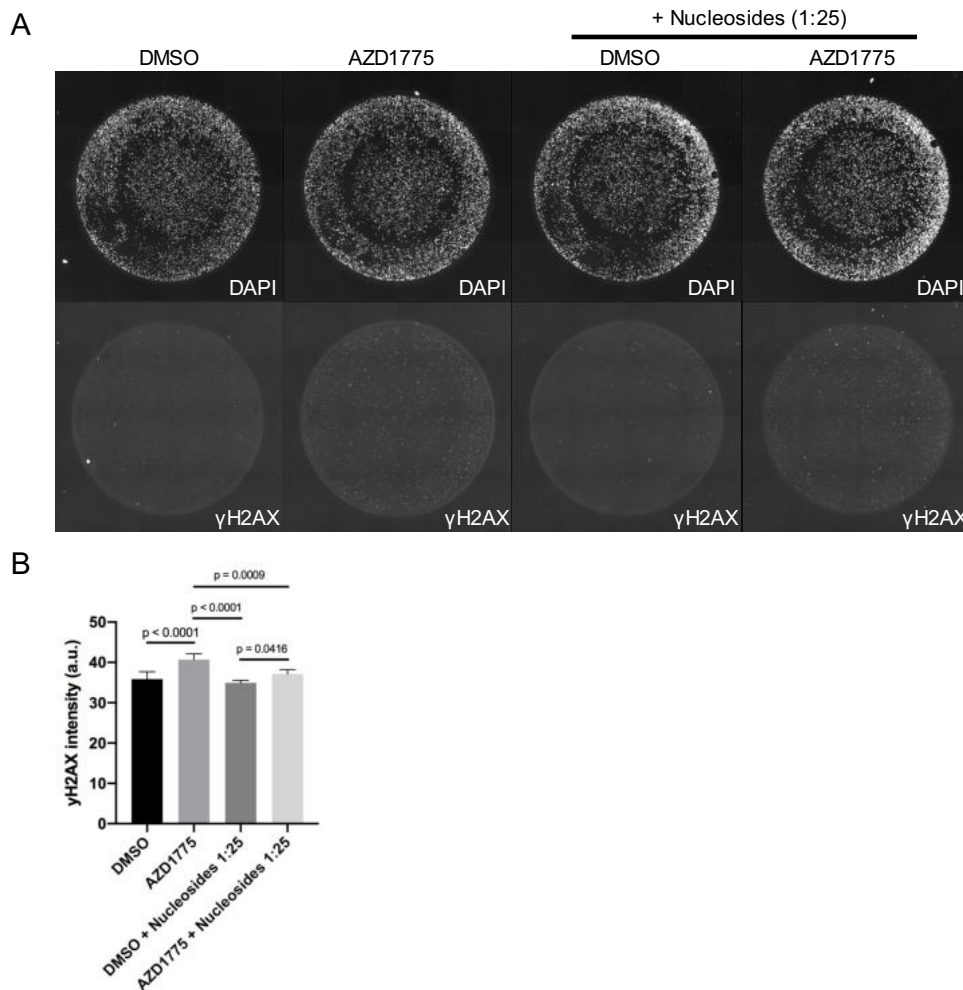
Figure 5.28 Nucleotide supplementation counteracts AZD1775-induced γH2AX.

(A) Representative images showing γH2AX staining on WiDr colorectal cell line treated with AZD1775 (250 nM) for 8 hours in the absence or presence of EmbryoMax nucleosides (1:25). (B) Bar charts showing γH2AX intensity (arbitrary unit) of WiDr cells following the indicated treatment. Graphs represent means ± standard deviation from 6 replicates per condition and are representative of one experiment.

5.2.7 Alternative schedules to investigate the translational potential of the irinotecan and WEE1 inhibition combination

The 5-day treatment with SN-38 in combination with WEE1 inhibition in a 21-day cycle was derived from a current regimen of irinotecan in paediatric patients. To examine the importance of the treatment's schedule in maintaining the outcome, alternative regimens

were explored. Mechanistically, it was hypothesised that S-phase-dependent DNA damage induction by SN-38 could prime cells for WEE1 inhibition. This was based on the idea that firstly, induction of DSBs would cause cells to arrest in G2/M, in order to enable DNA damage repair. In this way, cells accumulating at this point, would be more vulnerable to premature entry into mitosis triggered by WEE1 inhibition, particularly before the damage has been repaired. These events could result in mitotic catastrophe and cell death. Inversely, prior treatment with a WEE1 inhibitor could reduce the percentage of cells in S-phase by promoting forced entry into mitosis. This could then affect SN-38's efficacy and its mechanism of action through topoisomerase I poisoning (184). These considerations were tested as two alternative schedules, first inhibiting topoisomerase I to induce DSBs, followed by WEE1 inhibition, and vice versa (Fig. 5. 29A). However, staggering the treatments of each agent was found not to be significantly better than concurrent treatment, despite the rationale discussed above (Fig. 5.29B-C).
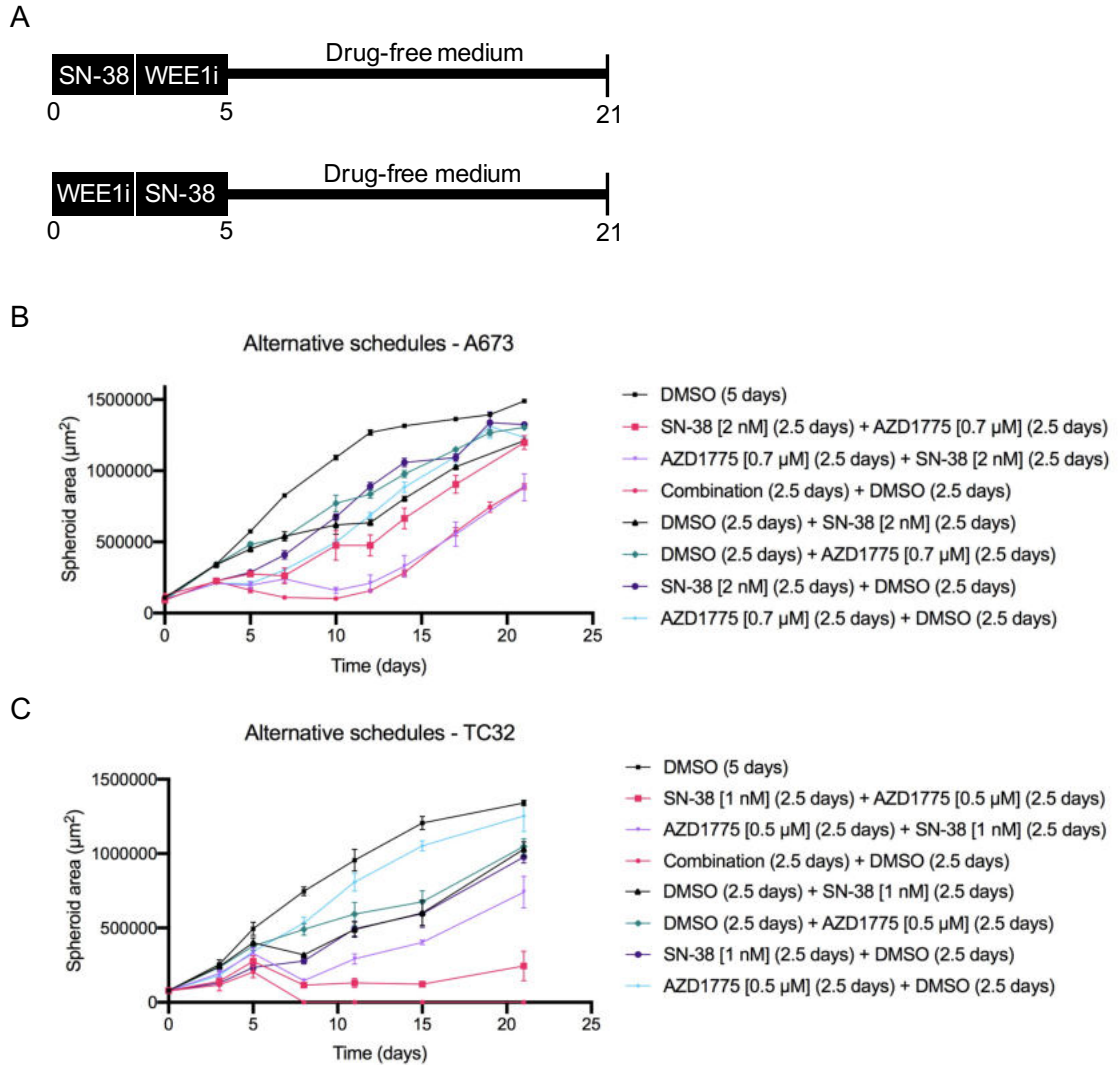
Figure 5.29 Effects of staggered SN-38 and WEE1 inhibition treatment on ES spheroids

(A) Diagram showing the schedule for staggered SN-38 and AZD1775 treatment within a 21-day cycle. A673 (B) and TC32 (C) spheroids models were treated with SN-38, AZD1775, or concurrent treatment at the indicated concentrations for the specified length of time. Graphs represent means ± standard deviation from 6 replicates and are representative of three independent repeats.

Having established that simultaneous exposure to both SN-38 and WEE1 inhibition was important to maximise response to this combination, the next step was to determine whether the duration of treatment with the WEE1 inhibitor could be reduced. This was an important consideration, in order to minimise potential toxicities associated with combination with chemotherapies. Concurrent administration of SN-38 with the WEE1 inhibitor was reduced from 5 days to 2.5 days for AZD1775 only (Fig. 5.30A). Results

with A673 spheroids showed decreasing WEE1 inhibition did not affect the overall result of the combination treatment. That is, concurrent treatment for 2.5 days only, and maintaining SN-38 for a further 2.5 days was sufficient to replicate the same growth inhibitory effect achieved by 5 days of the combination treatment (Fig. 5.30B). In contrast, shortening AZD1775's treatment in TC32 spheroids changed the treatment outcome. Initially, this model showed a strong cytotoxic effect with decreasing spheroid growth, comparable to the full 5-day combination treatment. However, there was a late recovery towards the end of the assay, which suggested viable cells remained (Fig. 5.30C). These results indicate that treatment outcome is dose-dependent and suggest the need for sustained damage induction and checkpoint inhibition. Importantly, in the clinical setting, patients would receive several rounds of this treatment cycle, potentially extending their response to irinotecan in combination with WEE1 inhibition.
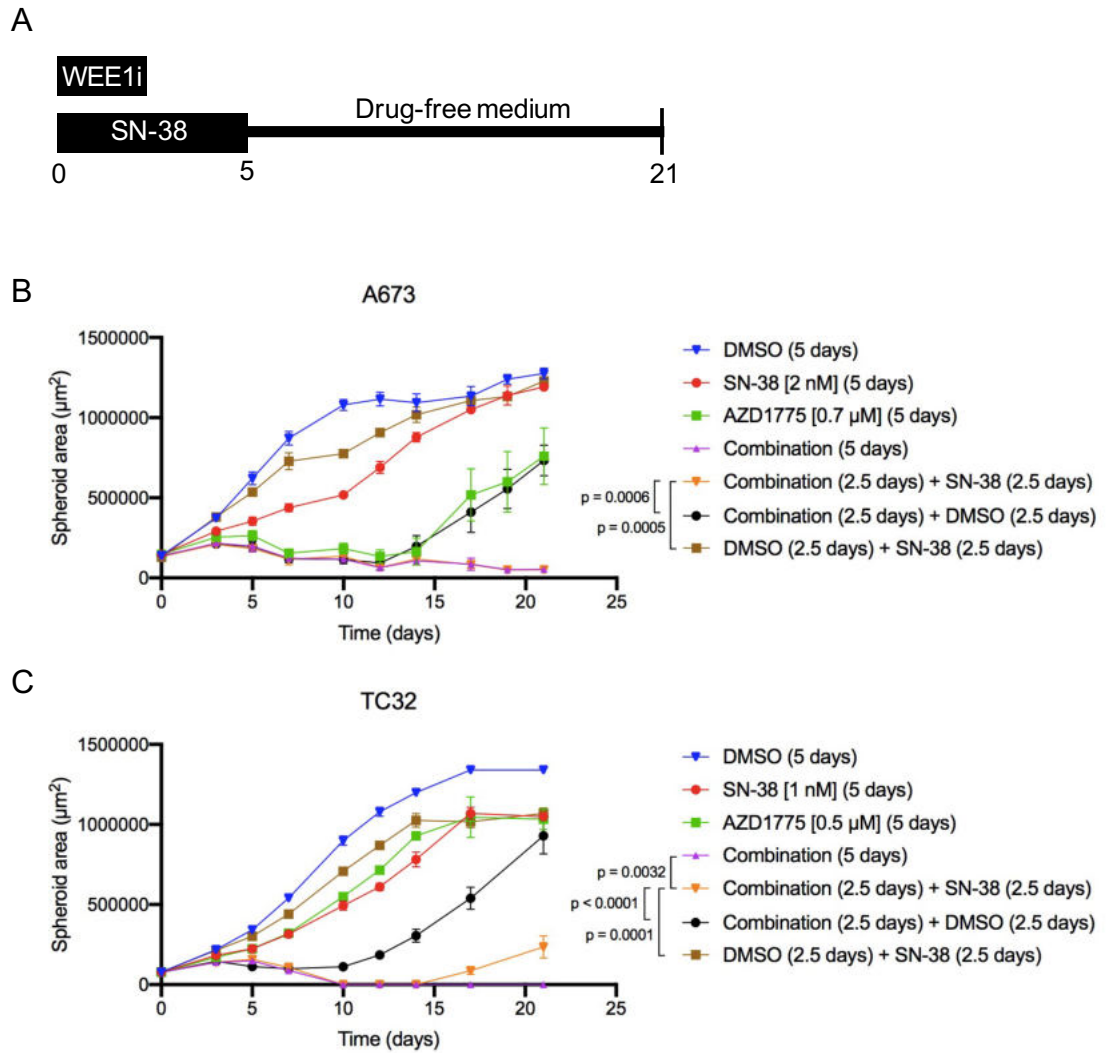
Figure 5.30 Effects of SN-38 in combination with reduced WEE1 inhibition treatment on ES spheroids

(A) Diagram showing the schedule for SN-38 in combination with reduced WEE1 inhibition treatment within a 21-day cycle. A673 (A) and TC32 (B) spheroids models were treated with SN-38, AZD1775, or concurrent treatment at the indicated concentrations for the specified length of time. Graphs represent means ± standard deviation from 6 replicates and are representative of three independent repeats. All p-values were calculated using a repeated-measures ANOVA with Tukey's multiple comparisons test, significant comparisons relevant to the question of reduced WEE1 inhibition in the combination treatment are shown.

5.3 Discussion

5.3.1 Efficacy of SN-38 in combination with WEE1 inhibition in ES

WEE1 inhibition as an anticancer therapy has been primarily used as a way to potentiate the effect of other DNA-damaging agents by inducing forced entry into mitosis, resulting in apoptosis and/or mitotic catastrophe (269). In this chemo-sensitising role, AZD1775 has been tested in combination with gemcitabine and carboplatin in solid tumours such as triple-negative breast cancer (TNBC), SCLC, and ovarian cancer (114). Aside from its synergistic effect with chemotherapy, WEE1 inhibition has also been proposed to have independent cytotoxic activity in a range of genetic backgrounds, such as *TP53*-deficient contexts (74, 99, 111, 114). This is due to p53's role as the crucial regulator of the G1-S checkpoint, whose inactivation increases the reliance on the S and G2 checkpoints to preserve genome integrity. In this way, WEE1 inhibition has been suggested to selectively kill *TP53* mutant cells (74, 111, 270). Other identified biomarkers of sensitivity to WEE1 inhibition are overexpression of cyclin E and MYC, both strongly linked to a background of oncogene-induced RS (54, 74, 271). Notably, EWS-FLI1 drives MYC expression, and directly dysregulates transcription, replication, and the cell cycle (detailed in 1.5.3) (272). Together, these reasons proposed ES as a potentially vulnerable tumour due to a dependency on the RSR in order to survive (40, 98, 168). WEE1's role in this pathway, providing cell cycle and replication control through regulation of CDK1 and CDK2 made it a promising target to investigate in this sarcoma. Additionally, combination with irinotecan would exacerbate RS and DNA damage in an already dysregulated setting, ultimately pushing ES cells towards cell death. The data presented here investigated this rationale and found this therapeutic approach to be effective against *in vitro* models of ES.

Combination of SN-38, the active metabolite of irinotecan, and WEE1 inhibitor AZD1775 was validated in a range ES spheroid models. In depth characterisation of the effects of this combination treatment uncovered two different responses in the two cell line models investigated. Broadly, treatment with SN-38 in combination with AZD1775 in A673 spheroids led to a strong inhibitory effect, arresting growth throughout the 21-day cycle. In contrast, response in TC32 spheroids was marked by complete cell death. Whilst both results are positive from a therapeutic perspective, understanding the key differences between them can contribute to maximising the efficacy of this combination

therapy. To investigate the effects of the combination treatment producing these two phenotypes, assessment of DNA damage markers, apoptosis, cell cycle effects, and the consequences of CDK1 and CDK2 dysregulation were explored. The data collected here suggests the phenotype in TC32 spheroids was primarily achieved through DNA damage accumulation causing S-phase arrest, and subsequently cell death. The evidence supporting this model is discussed here, and the key differences between the two models are highlighted.

Combination treatment in TC32 and A673 spheroids had the highest induction of γH2AX foci compared to the single agents. The presence of this marker of DSBs was also sustained in combination-treated spheroids of both models throughout the time points assessed. In TC32 spheroids, DNA damage induction by SN-38 and AZD1775 monotherapy was more time-dependent. AZD1775 in particular showed an early increase at 6 h and 12 h, and SN-38 showed elevated levels of γH2AX foci at 24 h. This was consistent with its 'poisoning' mechanism of action in which SSBs are converted to DSBs when topoisomerase I cleavage complexes collide with the replisome (184). Thus, this effect may take longer to develop due to it being restricted to cells in S-phase cells. In terms of the consequences of γH2AX foci accumulation, combination-treated TC32 spheroids had a significantly higher induction of markers associated with cell death (pan-nuclear γH2AX staining and CC3). On the other hand, A673 spheroids had a modest increase without being statistically significant. Of note, the percentage of positive cells for CC3 in both cell line models were generally low (below 7-8%). This is in agreement with the results from the growth curves, where a decrease in spheroid size or in the growth rate was not observed early, but rather towards the end of the 5-day treatment within the 21-day cycle. Together, this suggested that the DNA damage induced by the combination treatment accumulates, reaching a threshold that promotes cell death in TC32 spheroids, and to a lesser extent in A673 spheroids. Despite the use of higher concentrations of SN-38 and AZD1775 and greater induction of γH2AX foci in the A673 model, this was not sufficient to induce complete cell killing as in TC32 spheroids. Although characterisation of the combination treatment's effects in A673 spheroids provided evidence cell death, the growth curve suggested the net effect was growth arrest.

In terms of the levels 53BP1 foci, induction after treatment varied between the two spheroid models studied. A673 had a strong induction following single-agent SN-38, also

matched by the combination treatment. This, however, was not observed in TC32 spheroids, where 53BP1 foci were primarily seen in the SN-38-only group. Broadly, 53BP1 foci should colocalise with γH2AX foci. 53BP1 foci are clusters of this repair protein that contributes to determining the pathway of choice in DSB repair through antagonising BRCA1 activity, and preventing resection of DNA ends (92, 273). Overall, their activity promotes NHEJ, which is mainly active in G1, in contrast to HR occurring in S and G2 phases (92). In the context of the data collected, the presence of 53BP1 foci in treated spheroids served as indicator of DNA damage, but more specifically as early evidence that NHEJ/HR repair activity has started. This marker, however, is not definitive indication that NHEJ activity has been favoured, as 53BP1 can still be displaced and excluded from damage sites (274). It remains to be addressed why the DSBs induced by the combination treatment in TC32 spheroids did not result in persistent 53BP1 foci accumulation, like in A673 spheroids. One possibility answering this question could be WEE1 inhibition's impact on DSB repair and recruitment of this particular DNA damage repair protein. Reports in the literature have found WEE1 inhibition to suppress 53BP1 foci formation through CDK1 activity (275). More importantly, aberrant activation of CDK1 through WEE1 inhibition has been shown to inactivate HR (275). Future work could investigate how SN-38 in combination with AZD1775 affect the repair pathway of choice in these two models. This is particularly relevant in light of ES tumours being suggested to phenocopy a BRCA1-deficient context due to BRCA1 being chromatin-bound (37). It may be the case that the efficacy of this treatment is linked to unscheduled CDK1 activity, mediating DSB repair pathway of choice.

Quantification of 53BP1 NBs was differentiated from traditional 53BP1 foci by size, however this could lead to possible misinterpretation. As cells accumulate more of either of these markers, their size becomes smaller due to the limiting pool of 53BP1 and/or its recruitment factors, such as RNF168. Therefore, in order to specifically identify these NBs, which are restricted to G1, one possible improvement would be to stain for cyclin A, expressed in S and G2. In this way, G1 cells, negative for this marker and positive for 53BP1 NBs could be accurately quantified improving the analysis of this DNA damage factor. Considering this caveat, using 53BP1 NBs as a surrogate marker of RS (46) did not indicate accumulation of this form of damage following the combination treatment in either of the models tested. In contrast, single-agent SN-38 resulted in high levels of 53BP1 staining, particularly in A673 spheroids. 53BP1 NBs are known to form on DNA

lesions associated with RS, particularly arising from under-replicated DNA (46). Regarding the combination treatment, whilst RS levels could have increased as a result of the activity of the two agents, cells may not have been able to divide, passing on these lesions to daughter cells and entering G1, where 53BP1 NBs become apparent (46, 47, 267). Future work assessing 53BP1 NBs in G1 cells could explore this possibility and clarify the nature of this signal. When assessing the effects of the combination treatment on the cell cycle in TC32 spheroids, profiles indicated accumulation in S-phase after 24 and 48 hours of treatment. This, together with the lack of increase in mitotic cells (pHH3 positive) after the combination treatment, suggested TC32 spheroids undergo S-phase arrest, potentially stopping them from entering mitosis. Therefore, the model explaining the combined effects of SN-38 and AZD1775 in TC32 spheroids suggests DNA damage induction triggers S-phase arrest followed by an apoptotic response (Fig. 5.32). It would be interesting to verify whether the majority of DNA damage is specific to S-phase to confirm if concurrent SN-38 and AZD1775 treatment combine to trigger replication catastrophe in ES cells. These future studies could test RPA exhaustion as an explanation to cell death in S-phase (65, 276).

One key difference between TC32 and A673 spheroids was that cells were able to progress through the cell cycle without accumulating in S-phase, following concurrent treatment of SN-38 and AZD1775. Whilst the induced DNA damage contributed to growth inhibition in A673 spheroids, over time this effect was maintained becoming growth arrest. It is possible that cell cycle analysis or assessing proliferation of A673 spheroids at a later time point could give more definitive evidence to support this hypothesis. Whilst both models showed DNA damage accumulation after concurrent treatment of SN-38 and WEE1 inhibition, the difference was in the consequences this had. The ability for DNA damage induction to activate cell death, rather than growth arrest appeared to be a key factor in the response of these spheroid models (Fig. 5.31).
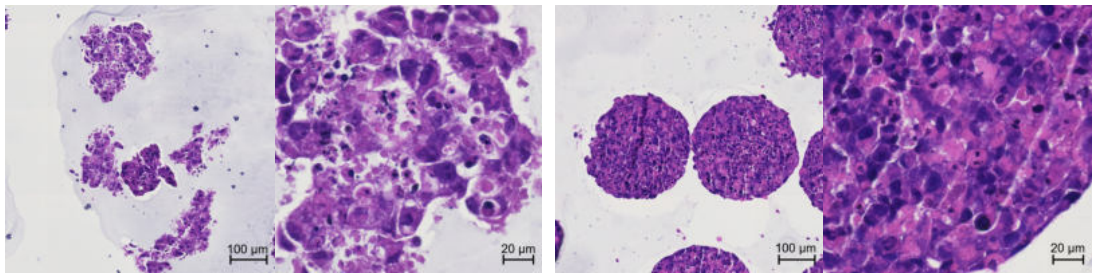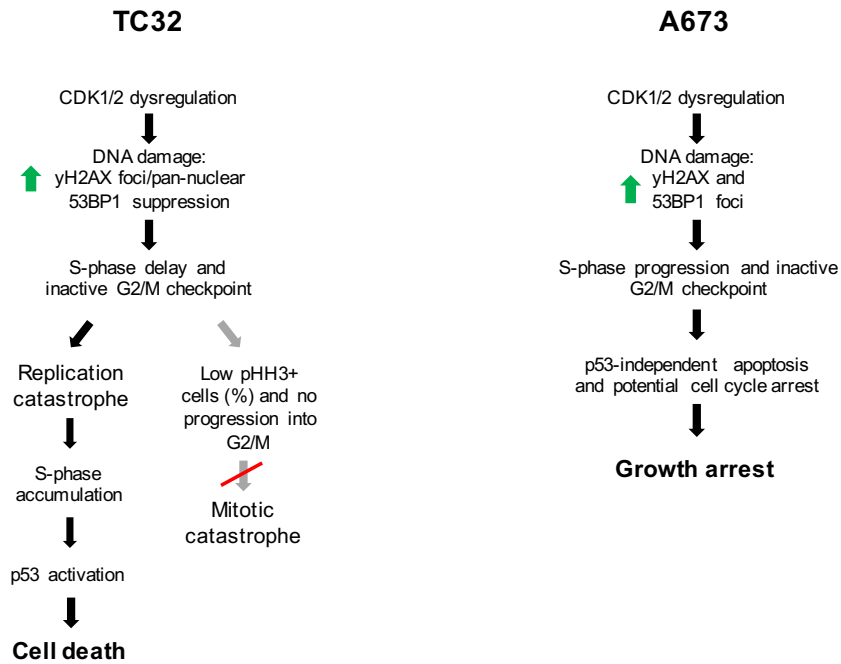
Figure 5.31 Proposed model of mechanism of activity of irinotecan in combination with WEE1 inhibition.

5.3.2 Towards identifying biomarkers of response to SN-38 in combination with WEE1 inhibition

Although the focus of this therapeutic approach was aimed at the vulnerability created by EWS-FLI1, this fusion protein exists in a context of few, but important genetic mutations affecting cell behaviour (130-132). These mutations can contribute to disease progression and patient prognosis, for example, tumours with *TP53* and *STAG2* mutations are known to lead to worse outcomes (130). In this study, the response to SN-38 in combination with WEE1 inhibition was also shaped by genetic alterations found in A673 and TC32 cell lines. A673 cells are *TP53* mutated and contain a *CDKN2A* deletion, also affecting p53

stability and the G1-S checkpoint. TC32 cells, on the other hand, are *TP53* WT, but also have mutations in *CDK2NA* and *STAG2*. As hinted at in the previous model describing the effects of the combination treatment (Fig. 5.31), A673 cells' inability to elicit a strong apoptotic response could have been a decisive factor in its response. This could be attributed to lack of p53 activity in this cell line, previously confirmed in the literature (277, 278). In contrast, *TP53* WT TC32 spheroids showed induction of pro-apoptotic proteins downstream of p53, overall supporting the view that SN-38 in combination with AZD1775 triggered DNA damage-induced apoptosis in this cell line. This model also suggests the *CDKN2A* deletion present in TC32 cells was not sufficient to disrupt p53 activity, as evidenced by upregulation of protein expression of PUMA. Overall, the presence of functional p53 may be beneficial to an enhanced apoptotic response following DNA damage. There are examples in the literature in p53 WT cancer cell lines where this is the case (279). This, however, was not observed in the growth curve of combination-treated spheroids of WE68, the other *TP53* WT ES cell line in the panel validated. Future work could investigate a wider range of *TP53* WT ES cell lines, which in fact are more representative of the majority of ES tumours, as only 5-7% of cases display these mutations (130-132). This, together with a functional experiment testing the role of p53 in driving this apoptotic response, could pave the way to establish p53 status as a biomarker of sensitivity to this combination treatment. One example of an experiment would be assessing the response to the combination treatment in TC32 spheroids where p53 has also been inactivated, with the caveat that p53-independent mechanisms may also play a role. In addition, the inverse experiment could also be tested in A673 spheroids through reactivation of p53 as a means to promote a greater apoptotic response.

With regards to the results with A673 cell line, it is likely alternative mediators of apoptosis contributed to the increase in CC3 measured by immunofluorescence, the histological changes observed, and PARP1 cleavage. Additionally, the growth arrest observed could not have been triggered through canonical activation of p21 inducing G1-S arrest due to the p53-deficient context in A673 spheroids. To investigate alternative mechanisms coordinating this response, future work could look at other activators of apoptosis such as p53 analogues, p63 and p73, together with E2F1, which regulates *TP73* transcription (280) (Fig. 5.32). Importantly, E2F1 is upregulated by EWS-FLI1 and therefore its roles in p73 activity could be explored (281).

SN-38 + WEE1i

↓

DNA damage

EWS-FLI1   CHK1/CHK2

E2F1
*stabilisation –
transcription*

p73   Activation of other
p53 analogues
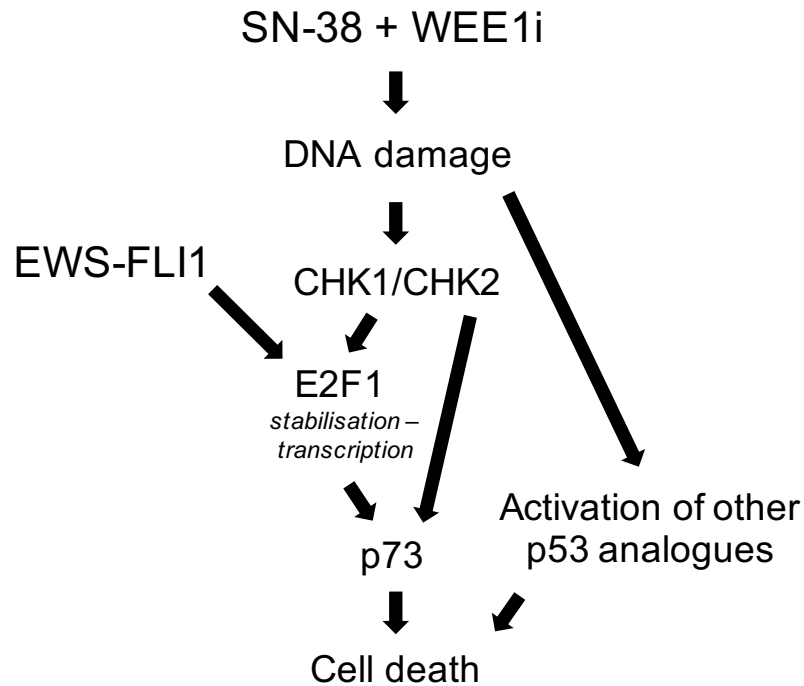
Cell death

Figure 5.32 p53-independent mechanisms of apoptosis in response to SN-38 in combination with WEE1 inhibition.

Diagram showing a model for additional mechanisms contributing to a cell death response in A673 spheroids upon treatment with SN-38 in combination with WEE1 inhibition. These mechanisms could involve p53 analogues, for example, p73 activated via CHK1 and CHK2 and through stabilisation and transcription activity of EWS-FLI1 target E2F1(280, 281).

Beyond characterising the response in A673 spheroids, a key question left to answer is why the combination treatment not sufficient to result in complete cell killing, even after the 21-day cycle assessed (Fig. 5.22). One possibility is that there are additional mechanisms contributing to mediate DNA damage and RS accumulation, prior the triggering of an apoptotic response in a p53-independent manner. Sustained E2F-dependent transcription has been identified to play such role, and could therefore help to deal with RS-induced DNA damage (282). Notably, EWS-FLI1 is known to coordinate E2F signalling, by favouring a switch from transcriptional repressor E2F4 towards activator E2F3, and by upregulating E2F1 (281, 283). Therefore, exploring whether this model (Fig. 5.33) applies to A673 cells, and more widely to the ES context, would be an interesting area to pursue in the future. Another possibility that could be explored is whether the remaining cell population in A673 spheroids is resistant to the treatment, and

if so, whether this was acquired or innate. Innate resistance could suggest the presence of a cancer stem cell population, able to avoid DNA damage induction by being in a quiescent state, but yet capable of re-establishing the parental tumour. Cells of these characteristics have been previously found in ES (284). More recently, modulation of EWS-FLI1 expression has been found to be a determinant of different cell states in ES cells, including proliferation (159). In this way, levels of the fusion protein could be a mechanism to lower proliferation, and so, minimising the damage induced by drugs that require cell cycling, like SN-38/irinotecan.
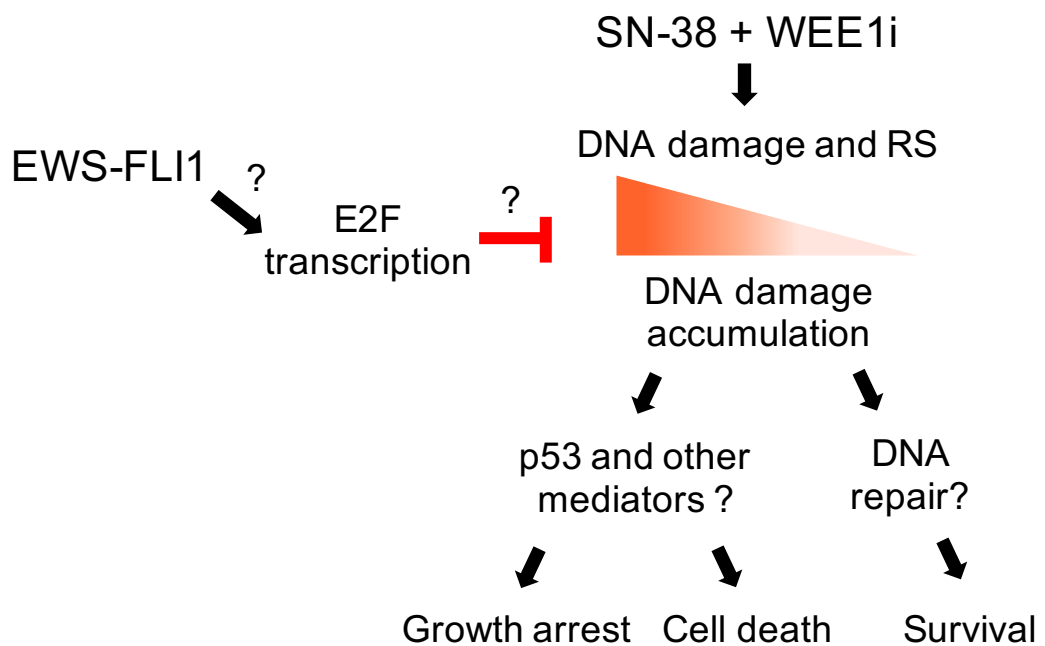
Figure 5.33 Sustained E2F transcription as a potential mechanism mediating RS-induced DNA damage.

Diagram showing a model in which EWS-FLI1-driven E2F transcription could be preventing RS-induced DNA damage accumulation, which in turn affects the response to SN-38 in combination with WEE1 inhibition. This mechanism could potentially influence the outcome between DNA repair, growth arrest, and cell death. Presently, it is unknown whether EWS-FLI1 driven E2F transcription contributes to dealing with endogenous or exogenous RS and the resulting DNA damage.

Aside from p53 activity, the status of *STAG2* has been found to be important in replication fork progression, as this regulates the interaction between the cohesin ring and the replication machinery (133). Its absence was identified to stall DNA synthesis and hinder fork stability leading to replication fork collapse (133). In this way, TC32 cells possessing

a mutation on *STAG2* maybe be more vulnerable to RS and DNA-damage induction in S-phase, thus resulting in the stronger response to the combination treatment. Whilst patients with *STAG2* mutations are found in only approximately 15-21%, these are also associated with poorer outcome, and therefore validation of this as a biomarker of sensitivity for this therapy would be important (132). Interestingly, in non-cancer cells *TP53* mutations overcome the intra-S phase block induced by the presence of *STAG2* mutations (133). It has been suggested that in ES tumours exhibiting both *STAG2* and *TP53* loss, the genomic instability created by STAG2 deficiency results in further genetic alterations. Importantly, STAG2-deficient cancers were found to have a dependency on DSB repair factors in HR and NHEJ, together with sensitivity to DSB-inducing agents (133). These reports are in agreement with the overarching hypothesis of ES being vulnerable to inhibition of the RSR, either through to EWS-FLI1-driven RS and/or *STAG2* mutations.

5.3.3   WEE1 inhibition and dysregulation of S-phase specific processes

The hypothesis and the effects of the combination treatment were centred around a dysregulated S-phase and replication. For these reasons, additional effects of unscheduled activity of CDK1 and CDK2, induced by WEE1 inhibition, were investigated further. As introduced before, WEE1 plays an important role in regulating nucleotide metabolism; its pharmacological inhibition is known to promote degradation of RRM2, the key catalytic subunit in the RNR complex supplying nucleotides for cellular processes (41, 55). It has been hypothesised that in an environment of high levels of RS, as in ES, disrupting nucleotide metabolism can have detrimental consequences to cell survival as the demand for these substrates is higher (55). An example of this is sensitivity to hydroxyurea and gemcitabine (inhibitors of RNR) in contexts of RS (108, 168, 206). WEE1 inhibition has been shown to mimic these effects through unscheduled activity of CDK2, which in turn phosphorylates RRM2 on threonine 33 triggering its degradation (41, 42, 168). The cytotoxic activity of single-agent AZD1775 in ES cells was recently linked to its effect on RRM2 expression, which is also overexpressed in this sarcoma (168, 285). Through a rescue experiment ectopically expressing RRM2 with T33A mutation, which renders it irresponsive to ubiquitin-mediated-proteolysis, sensitivity to WEE1 inhibition was successfully diminished (41, 168).

Given the established role of WEE1 in nucleotide metabolism, the involvement of this effect in the phenotype of the combination treatment was investigated. Unscheduled activation of CDK1/2 and degradation of RRM2 were successfully validated in both cell lines. However, nucleotide supplementation failed to recover the growth inhibition and cytotoxic effect of SN-38 in combination with AZD1775 in either of the spheroid models. Of note, these results were also not able to shift the sensitivity to single-agent AZD1775 in spheroids in contrast to the reported findings in the literature (168). One possible explanation for this could be a compensatory mechanism by p53R2. RNR is traditionally composed of two subunits, RRM1 and RRM2, which catalyse the reduction of ribonucleotide diphosphates to deoxyribonucleotide diphosphates (286). Expression of the smaller catalytic subunit RRM2 is usually higher and regulated throughout the cell cycle with a peak in S-phase and degradation in G1 (42, 286). Nucleotide supply in G1 is provided by an alternative form of RNR, in which homolog p53R2 encoded by *RRM2b* substitutes RRM2, when expression of this subunit is low (287). Despite p53R2 activation being p53-dependent, its expression is not exclusive to this mechanism. Independent activation has also been shown to occur through p73, FOXO3, and E2F1 (288, 289). In this way, p53R2 activation could have contributed as a back-up for RRM2 degraded by WEE1 inhibition, alleviating the disruption on nucleotide metabolism.

5.3.4 Evaluating the translational potential of irinotecan in combination with WEE1 inhibition

A recent clinical study investigating the combination of AZD1775 with irinotecan in children and adolescents established the maximum tolerated dose and recommended phase II dose (RP2D) for this combination in daily treatments for five days every 21 days (113). Importantly, assessment of anti-tumour activity found partial response in one ES patient out of four, suggesting activity in this heavily pre-treated relapsed cohort (113). However, further investigation of this combination for relapsed ES patients may be affected by a recent randomised comparison of relapse regimens in ES (183). This study found combination between topotecan and cyclophosphamide, and high-dose ifosfamide monotherapy, to be superior to irinotecan/temozolomide (183). As the randomisation continues, topotecan still remains as a viable combination partner, albeit with a different pharmacological profile (182, 184). Although the results presented here focused on irinotecan, these findings serve as proof-of-principle and could be applicable to other topoisomerase I inhibitors, including topotecan.

The introduction of novel targeted therapies to chemotherapeutic regimens involves careful consideration of toxicities, PK and PD parameters, whilst trying to maximise response. In these regimens, there is often room for incorporating mechanistic-based decisions to establish a schedule to obtain maximal efficacy with this therapy. One example of this is staggering combination therapies consisting of DNA-damaging agents and inhibitors of DNA repair proteins. This is because pre-treating cells with DNA repair inhibitors can sensitise them to the DNA damage induced by chemotherapy and/or radiotherapy. Based on this rationale, a recent clinical study of CHK1 inhibition in combination with cyclophosphamide, an ES front-line chemotherapy agent, investigated different schedules (196). However, results indicated concurrent treatment provided the best response over sequential treatments (196). Nevertheless, there are other cases, such as combination between CHK1 inhibition and gemcitabine, where response is improved with a staggered treatment in which cells are pre-treated with a CHK1 inhibitor (110, 290). Regarding results with SN-38 in combination with WEE1 inhibition, a staggered schedule was less effective than concurrent treatment. In this way, the hypothesis that unscheduled entry into mitosis induced by WEE1 inhibition, would carry forward previously accumulated damage, and then cause mitotic catastrophe and apoptosis, was not favoured by the evidence presented. Rather, combined exposure appeared to work best to induce greater DNA damage and push cells towards cell death. In fact, concurrent treatment could be reduced to only 2.5 days, keeping SN-38 for the entire 5 days, while maintaining the same response in A673 spheroids. On the other hand, reducing AZD1775 treatment to 2.5 days in combination-treated TC32 spheroids resulted in recovery in size towards the end of the assay. Although this suggests viable cells remained after treatment, at this point in a 21-day cycle, patients would receive another round of the same cycle. However, it remains to be addressed whether this population is resistant to the combination treatment and continues to have tumorigenic capacity. Altogether, the evidence presented in this chapter provides a strong rationale for the use of topoisomerase I inhibitors in combination with WEE1 inhibition as a therapeutic approach in ES.

Chapter 6 EWS-FLI1 mediates sensitivity to irinotecan and WEE1 inhibition combination

6.1 Introduction

Having characterised the response to SN-38 in combination with WEE1 inhibition in *in vitro* 3D models of ES, the final step in this project was to investigate the role of EWS-FLI1 in mediating sensitivity to this treatment. The activity of the treatment's dependence on expression of the fusion protein would suggest a fusion-specific response, supporting the use of this therapy for this sarcoma by linking it to its main oncogenic driver. As recently shown, the presence of the fusion protein in ES dysregulates transcription resulting in conflicts with the replication machinery (37). This results in an acquired dependency on DNA repair pathways resolving RS by protecting fork progression and promoting fork restart (40, 98, 168). Based on this knowledge, this thesis hypothesised ES cells could be vulnerable to inhibition of WEE1 activity, a key player in the RSR, and further induction of RS by SN-38.

To test this hypothesis, ectopic expression of EWS-FLI1 was chosen as a model system amongst other alternatives discussed (6.3). Here, the process of establishing an inducible model to express EWS-FLI1 is presented and proof-of-concept of the fusion protein as an inducer of sensitivity to SN-38 and AZD1775 treatment was obtained through assays carried out in 2D.

6.2 Results

6.2.1 Developing an inducible model of ectopic expression of EWS-FLI1

U-2 OS cells were selected to stably express the TetR protein through transfection with plasmid pCAGTetRnls (detailed in 2.17.1) (Fig. 6.1), also containing a puromycin resistance gene to enable selection of successfully transfected clones. Next, monoclonal expansion of transfected cells kept under selection was performed to ensure homogenous expression of TetR (Fig. 6.1A, detailed in 2.17.3). These U-2 OS clones were screened for expression of TetR (Fig. 6.1B-C) and clones A1, B3 and B4, containing the highest protein expression were then carried forward. Immunofluorescence detection of TetR was also performed to verify protein expression was indeed homogeneous across these clone populations (Fig 6.D). Stably transfected clones A1, B3 and B4 were then transfected with pcDNA ™5/TO-*EWS-FLI1*, which had the fusion gene placed under the control of a tetracycline-responsive promoter. In this way, upon addition of doxycycline (synthetic analogue of tetracycline), protein expression of EWS-FLI1 was successfully induced and detected in U-2 OS clones containing the vector with the fusion gene (Fig. 6.2). This demonstrated effective transfection and induction of the fusion protein.
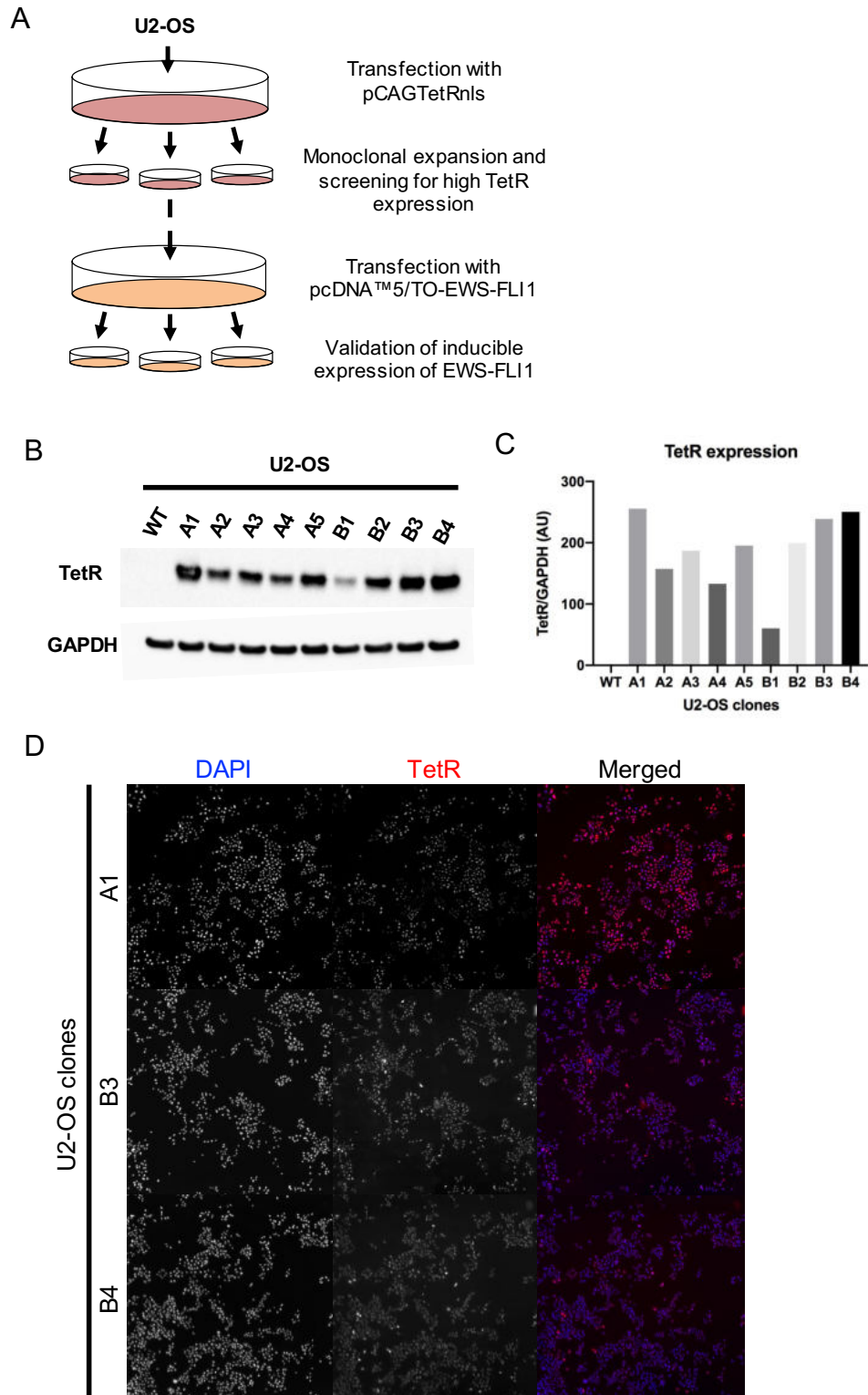
Figure 6.1 Developing an inducible model of EWS-FLI1 expression

(A) Diagram showing the workflow to create the doxycycline-inducible model of EWS-FLI1 expression in U-2 OS cells. (B) Protein levels of TetR assessed by Western blot on transfected U-2 OS clones. GAPDH levels are shown as a loading control. (C) Bar graphs with densitometry values for TetR normalised to loading control GAPDH. (D) Representative images of immunofluorescence detection of TetR (red) in U-2 OS A1, B3 and B4 clones.

A
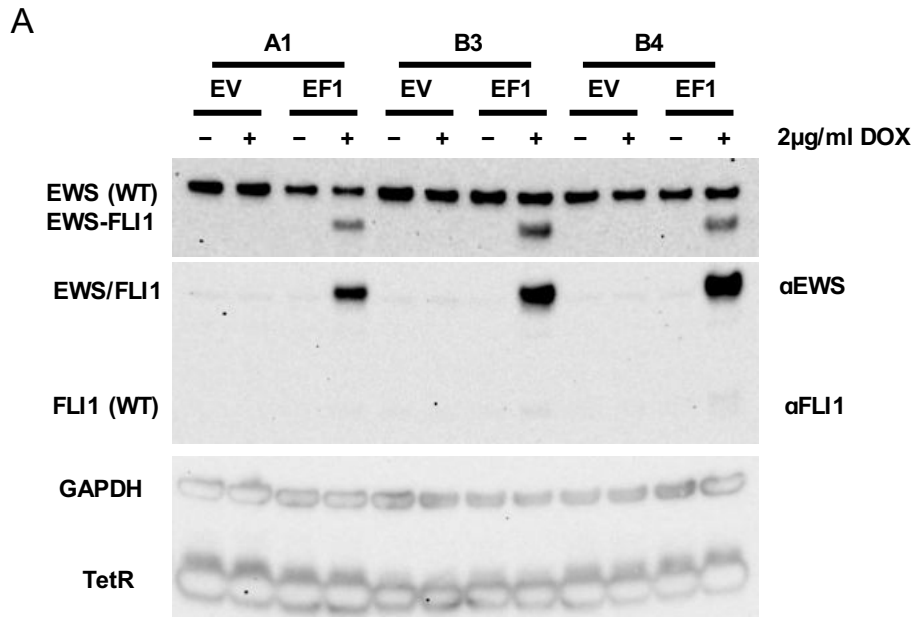
Figure 6.2 Inducible EWS-FLI1 expression in U-2 OS cells

(A) Protein levels of EWS-FLI1 assessed by Western blot on the transfected U-2 OS clones A1, B3, and B4 with pcDNA ™5/TO-*EWS-FLI1* and an empty vector (EV), as a control. Clones were treated with doxycycline (DOX) (2 µg/ml). Fusion protein was detected with antibodies directed against EWS and FLI1. GAPDH levels are shown as a loading control.

6.2.2   Establishing drug combination doses for SN-38 and AZD1775

In order to investigate the effect of EWS-FLI1 expression on sensitivity to the combination treatment, it was important to determine the doses at which a combined effect between SN-38 and AZD1775 could be studied. Unfortunately, it was not possible to culture U-2 OS clones A1, B3, B4 transfected with pcDNA ™5/TO-*EWS-FLI1* as spheroids, in contrast to the parental line U-2 OS, and despite testing different growing conditions (291). For these reasons, the following experiments were carried out in 2D in order to provide proof-of-principle that presence of the fusion protein sensitises cells to SN-38 in combination with WEE1 inhibition. U-2 OS B3 clone was then selected to carry out dose-responses for these two agents, with and without induction of EWS-FLI1 expression. The timing for the drug treatment was 72 h after the addition of doxycycline (Fig. 6.3A). At this point, the level of EWS-FLI1 protein was verified by Western blot prior to drug treatment (Fig. 6.3B). SN-38 did not produce an observable dose-response at a dose range of 10 nM to 0.05 nM, previously used to calculate dose-responses in ES

spheroid models. At 10 nM there was a marginal decrease to approximately 80%-75% of cell viability (Fig. 6.3C). Notably, induction of EWS-FLI1 expression did not sensitise these cells to SN-38. In contrast, AZD1775 treatment resulted in a strong dose-response in B3 EF1 U-2 OS clones, and importantly, this was shifted by expression of EWS-FLI1, seen as a change in GI50 from 1.40 µM to 0.24 µM. To continue investigating the response to SN-38 in this system, an increased dose-range of up to 40 nM was tested (Fig. 6.3D). These higher concentrations of SN-38 increased the response by reducing cell viability further, with 40 nM obtaining a decrease in cell viability just beyond 50% in cell expressing EWS-FLI1. However, the variable slope model used to calculate GI50s from dose-response curves was unable to determine one from this data. Nevertheless, the changes in cell viability suggested a degree of sensitisation to SN-38 following EWS-FLI1 expression (Fig. 6.3E). To move forward with testing whether expression of the fusion protein sensitised cells to the combination treatment, 40 nM of SN-38 was chosen to be tested concurrently with the GI50 obtained with AZD1775 in EWS-FLI1 expressing cells (0.24 µM).
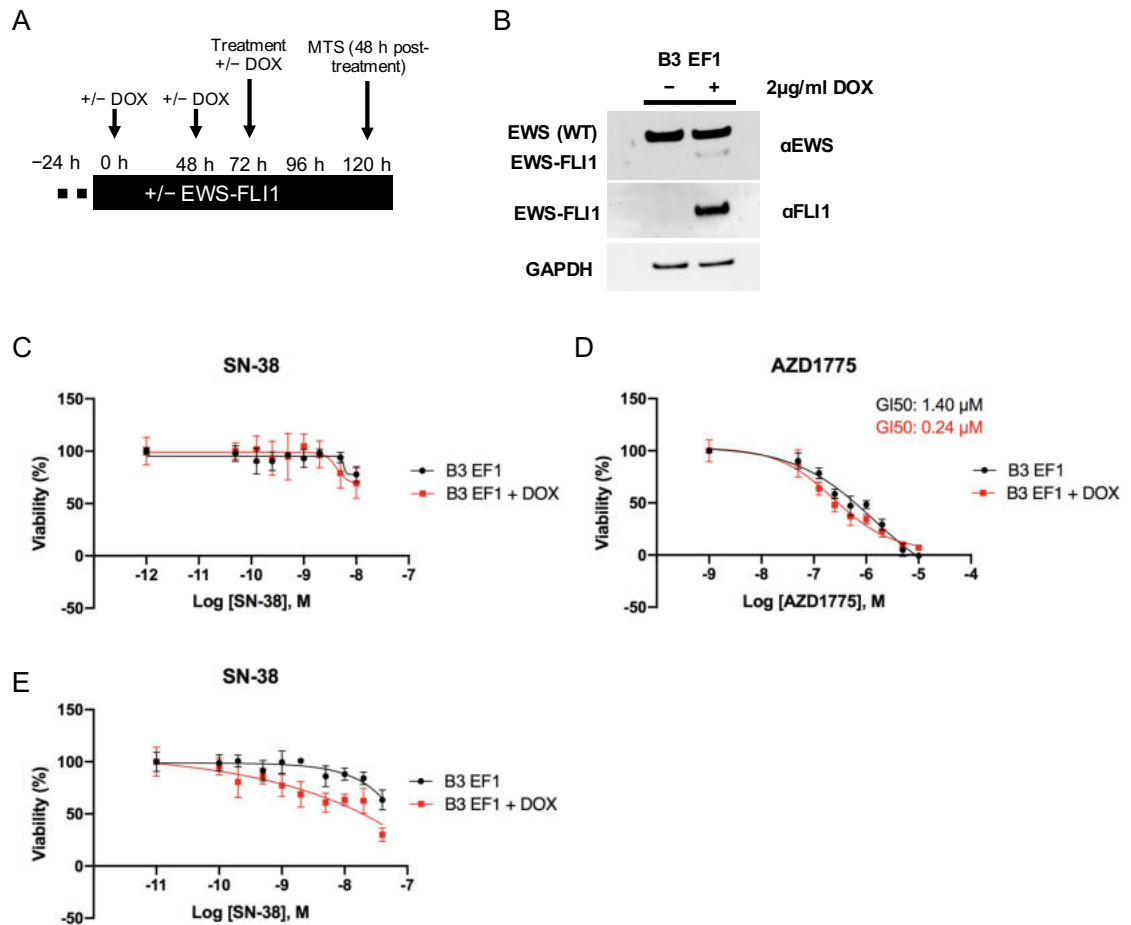
Figure 6.3 Sensitivity to single agent SN-38 and AZD1775 upon induction of EWS-FLI1.

(A) Diagram showing the schedule for EWS-FLI1 induction and drug treatment in cells with and without doxycycline (DOX). (B) Protein levels of EWS and FLI1 assessed by Western blot on U-2 OS B3 EF1 clones +/– doxycycline (DOX) (2 μg/ml) for 72 h. GAPDH levels are shown as a loading control. Dose-responses to SN-38 (C and E) and AZD1775 in B3 EF1 U-2 OS clones (D). Cell viability was assessed by MTS assay, 48 h after drug treatment and normalised to the untreated control. Means ± SD of 6 replicates, graphs are representative of two independent repeats.

6.2.3   Investigating the effect of EWS-FLI1 expression on sensitivity to SN-38 in combination with WEE1 inhibition.

Using the same schedule for EWS-FLI1 induction and drug treatments as before, combination of SN-38 (40 nM) and AZD1775 (0.24 μM) was tested on U-2 OS B3 clones with and without expression of EWS-FLI1. Single agents were also again tested as controls and B3 clone cells stably transfected with an empty vector (EV), with and without doxycycline. Levels of EWS-FLI1 protein were checked in B3 EF1 cells at 72 h

post-induction to confirm presence of the fusion protein at the time of drugging (Fig. 6.4A). Cell viability measured after 48 h of treatment showed a decrease in all combination-treated groups, importantly, this was significantly greater when expression of EWS-FLI1 was induced (EF1+DOX) (Fig. 6.4B). Single-agent treatment with SN-38, but not AZD1775, resulted in greater reduction in cell viability in EWS-FLI1-expressing cells as well (Fig. 6.4B). In addition, induction of EWS-FLI1 with doxycycline in B3 EF1 cells did not affect cell viability, 72 h after doxycycline induction (Fig. 6.4C). Altogether, these findings support the hypothesis that the presence of the fusion protein is linked to sensitivity to this combination treatment.
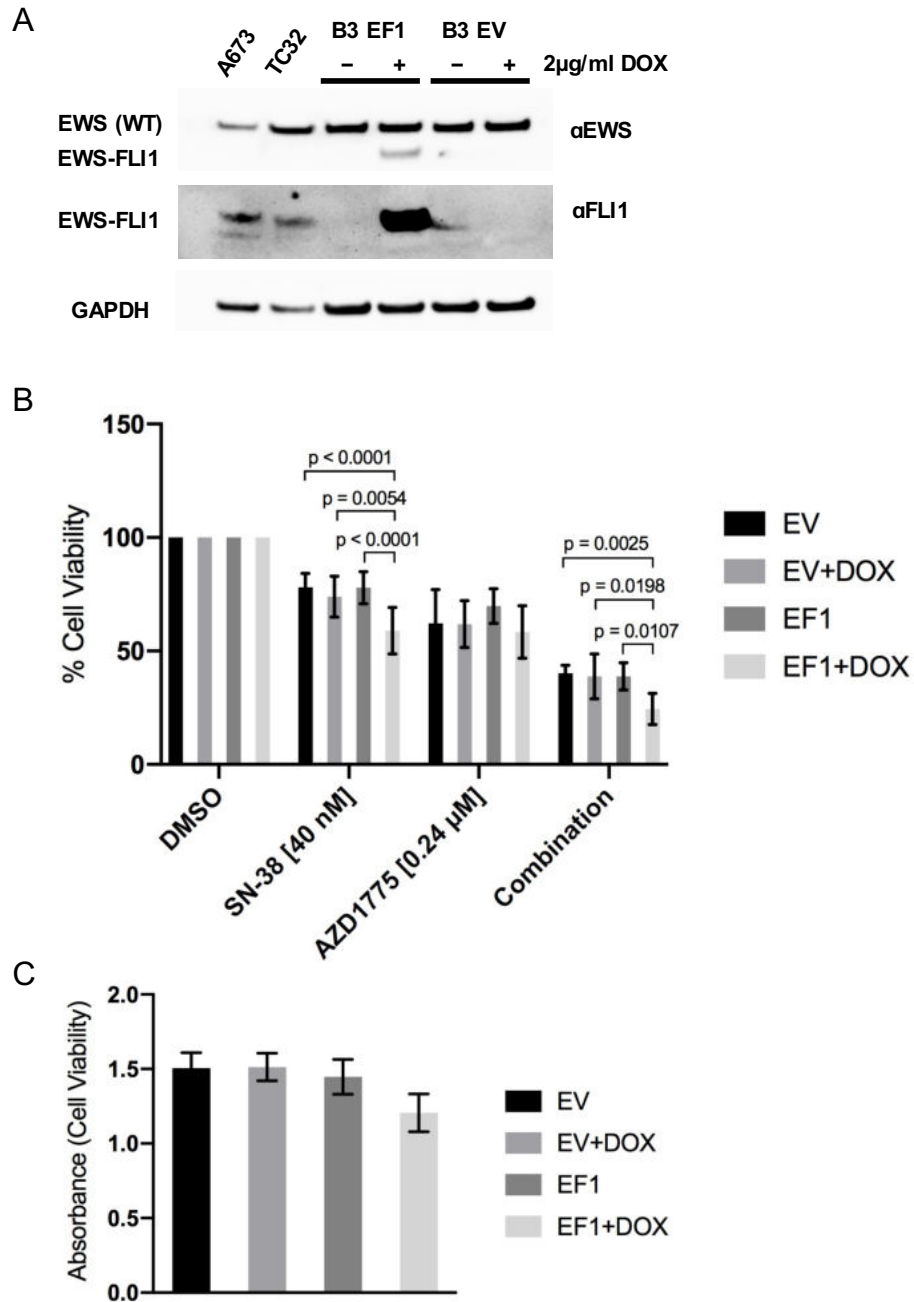
Figure 6.4 Sensitivity to SN-38 in combination with WEE1 inhibtion upon induction of EWS-FLI1.

(A) Protein levels of EWS and FLI1 assessed by Western blot on A673, TC32, and U-2 OS B3 EF1 and EV clones +/– doxycycline (DOX) for 72 h. GAPDH levels are shown as a loading control. U-2 OS B3 EF1 and EV clones +/– doxycycline (DOX) (2 μg/ml) treated with SN-38 (40 nM) and AZD1775 (0.24 μM), alone and in combination. (B) Cell viability was assessed by MTS assay, 48 h after drug treatment and normalised to the respective untreated control. (C) Cell viability was assessed by MTS assay 72 h post-induction with DOX; absorbance measurements are shown. Means ± SD of 6 replicates, graphs are representative of two independent repeats. All p-values were calculated using a two-way ANOVA with Tukey's multiple comparisons test, only significant comparisons are shown.

6.3 Discussion

6.3.1 *In vitro* models of EWS-FLI1 fusion protein activity

Research in ES has primarily employed two strategies to investigate the role of EWS-FLI1 in the oncogenic transformation of this sarcoma: knockdown of EWS-FLI1 or ectopic expression of the fusion. These two methods have distinct benefits and limitations, serving different purposes as models of the fusion gene's activity. Regarding knockdown of EWS-FLI1, siRNAs directed against the FLI1 portion of the fusion gene have been used *in vitro* and *in vivo* (292-295). These are specific to the fusion protein owing to the absence of WT FLI1 expression, and have been demonstrated to reduce the ES oncogenic phenotype (158, 293). Importantly, a key obstacle to this approach is that the majority of ES cell lines do not survive depletion of the fusion protein, and upon knockdown, these undergo cell cycle alterations and apoptosis (281). One system that has managed to overcome this problem, is a doxycycline-inducible knockdown model of EWS-FLI1 in A673 cells (155, 296). In this system, expression of the fusion can be successfully modulated and reduced to a point where apoptosis is not induced and viability remains, albeit with a marked reduction in proliferation levels (155, 158). In recent reports, further characterisation of this model has led to the suggestion of a spectrum of EWS-FLI1 expression, able to mediate cell-to-cell heterogeneity in ES tumours (158, 159). These changes in phenotype, underpinned by EWS-FLI1 protein levels, consisted in differences in proliferation and invasion, affecting their tumourigenic potential (158, 159). It remains to be addressed whether ES cells *in vivo* can fluctuate between these states through modulation of EWS-FLI1 expression, beyond existing as independent heterogeneous cells. Microenvironmental factors known to affect EWS-FLI1 expression such as hypoxia, have been proposed as potential modulators and may hold further clues about their ability to adapt through changes in the fusion protein (159, 160). Overall, these findings have added a new layer of complexity to EWS-FLI1-mediated tumorigenicity.

In the context of this project, depleting the fusion protein to investigate the link between EWS-FLI1 expression and sensitivity to irinotecan in combination with WEE1 inhibition was not a suitable method. This is because reducing EWS-FLI1 protein levels decreases proliferation, limiting the effect SN-38 can have on DNA replication in S-phase. In the same way, the extent of the combined effect of AZD1775, which exacerbates RS and

DNA damage accumulation in S-phase, would have been affected. Therefore, to evaluate how EWS-FLI1 expression affected this treatment, it was necessary to have a system where proliferation was not affected to enable the mechanism of action of SN-38 and WEE1 inhibition. This requirement highlighted a potential limitation to this combination treatment, as this will primarily target cycling cells. The existence of intra-tumoural heterogeneity with cells expressing lower levels of EWS-FLI1 could be a potential mechanism of resistance to this therapy. This is similar to chemotherapy that relies on inducing DNA damage in fast-cycling cancer cells and has the disadvantage of not targeting quiescent populations. In the context of ES, tumour cells with reduced levels of the fusion protein could represent a similar population. Whilst the abundance of these cells in ES tumours is not clear, it is possible to hypothesise that this population would be less responsive to this proposed treatment.

To functionally demonstrate that the presence of EWS-FLI1 mediates sensitivity to the combination treatment, ectopic expression of this oncoprotein in an alternative system was necessary. This approach is also not without its own difficulties and caveats. Given that the cell of origin of ES remains unknown, different permissible environments have been tested for ectopic expression of EWS-FLI1. Recently, some of the demands for EWS-FLI1 permissibility were found to involve high expression of factors resolving replication fork stalling and collapse to deal with fusion-driven endogenous levels of RS (40). Lack of this adaptation could be part of the reason why expression of the fusion protein in mouse embryonic fibroblasts and primary fibroblasts results in cell death (297, 298). It is likely that without mechanisms to protect cells from the accumulation of RS and DNA damage, these two contribute to an unsustainable state of genomic instability upon expression of EWS-FLI1. Human MSCs have been regarded as the putative cell of origin of this sarcoma, where expression of the fusion protein induces gene expression changes characteristic of ES (146, 155). However, these cells are not capable of stable expression of the ES oncoprotein in contrast to iPSCs, hESCs, and neural crest stem cells (40, 299, 300). Whilst there is not a perfect system to study ectopic expression of EWS-FLI1, the experience of trying to model this oncogene has served to understand its behaviour and molecular requirements. Some heterologous models where EWS-FLI1 has been successfully expressed include osteosarcoma cell line U-2 OS (37), epithelial cell line HeLa (301, 302), rhabdomyosarcoma cell line RD (303), and human embryonic kidney (HEK) 293 cells (297). These cell lines all possess different backgrounds with

different mutations, expression patterns, and behaviour, and therefore can give nuances to EWS-FLI1 expression. To test sensitivity to SN-38 and AZD1775, U-2 OS cells were selected for stable expression of the fusion protein, as reported in Gorthi *et al*. (2018) (37). Additionally, expression of EWS-FLI1 in this system had been shown to mimic part of the phenotype of fusion-driven dysregulated transcription and the resulting activation and dependency on the RSR (37).

6.3.2   EWS-FLI1-mediated sensitivity to SN-38 in combination with WEE inhibition

The results obtained showed increased sensitivity to SN-38 and AZD1775, alone and in combination, when EWS-FLI1 expression was induced. These findings supported the hypothesis that EWS-FLI, as source of oncogene-induced RS, renders ES tumours sensitive to inhibition of proteins involved in the RSR and to RS-inducing agents enhancing replicative damage. Importantly, induction of EWS-FLI1 did not significantly affect viability in untreated cells at the time point assessed. This suggests that the change in sensitivity to the combination treatment, upon expression of the fusion protein, was not likely to have occurred due to changes in proliferation of cells expressing EWS-FLI1. Rather the observed effect could be through the proposed oncogenic properties of the fusion protein rendering cells reliant on the RSR. However, one important caveat to these findings is the extent to which the oncogenic phenotype of this sarcoma is mimicked by ectopically expressing EWS-FLI1. Even if induction of the fusion protein is achieved in this system, evidence of an acquired dependency on the RSR due to the pressures imposed on replication by EWS-FLI1 dysregulation is needed (37, 98). Examples of some of the phenotypic changes caused by EWS-FLI1, which could be further validated in this model can be taken from reports characterising the existing RS in this tumour. For example, ES cell lines have been identified to have high levels of CHK1 expression as a mechanism to counteract oncogene-induced RS (98). Additionally, cell lines from this tumour type have been shown to have a decreased replication fork rate compared to other malignant and non-malignant cell lines (98). Fork progression following induction of EWS-FLI1 expression has not been measured, but other forms of dysregulation of replication have been reported, such as the induction of R-loop formation through EWS-FLI1 expression in U-2 OS cells (37). The presence of R-loops was proposed to be caused by transcriptional dysregulation due to a dominant-negative effect on protein EWS (37, 169). Specifically, EWS-FLI1 lacks the ability of full-length EWS to inhibit phosphorylation of the CTD on RNAPII to regulate transcription. This results in a permanently

hyperphosphorylated form of this polymerase and thus in aberrant transcription, leading to conflicts with the replication machinery (32, 37, 38). Of note, detection of R-loops with the S9.6 antibody recognising these RNA:DNA hybrids may not be specific enough to reliably use this as a biomarker (304). Future work could prioritise exploring increased activation of the RSR as further validation of this model.

Another biomarker known to mediate sensitivity to topoisomerase I inhibitors and combinations between PARP1 inhibition and temozolomide in ES is SLFN11, which is positively regulated by EWS-FLI1 (305). Tumours with higher expression have been associated with increased response to the treatments mentioned and overall present better tumour-free survival rates (305). For these reasons, increased SLFN11 expression could be investigated in the inducible model of EWS-FLI1 due to its role mediating response to irinotecan and given that it is a target of the fusion protein. In the experiments in this chapter, sensitivity to SN-38 was lower in U-2 OS clones, requiring 40 nM to approximate a GI50 after 48 h of treatment in 2D. Notably, in spheroid models of ES, 1 nM or 2 nM (depending on the cell line), was sufficient to inhibit growth and promote cell death alone and in combination with WEE1 inhibition. The fold change in concentration to obtain a response in U-2 OS B3 clone suggests other differences beyond ES cell lines being more sensitive to SN-38. It likely that these could be due to drug response being different in 2D compared to 3D models. This highlights the importance for future work to investigate inducible expression of EWS-FLI1 in 3D. Unfortunately, U-2 OS clones A1, B3 and B4 transfected with pcDNA ™5/TO-*EWS-FLI1* did not grow as spheroids, despite the parental line U-2 OS being able to do so (291). Alternative heterologous systems for inducible expression of EWS-FLI1 that are amenable to spheroid culture could be used in the future.

Further characterisation of a model of ectopic expression of EWS-FLI1 could also determine whether expressing the fusion protein for 72 h in this non-ES system is sufficient to develop the ES oncogenic phenotype. It could be the case that this is a model resembling the initial stage of ES tumourigenesis instead of a fully accustomed system, able to deal with the genomic instability caused by high endogenous levels of RS and EWS-FLI1 activity. It is possible to speculate that the latter would be more sensitive to the combination treatment, given a stronger reliance on the RSR. One potential experiment to address this question could be to induce EWS-FLI1 expression over a

longer period of time, monitoring changes in the RSR regarding upregulated expression and activation. The aim here would be to test if it is possible to develop greater reliance on factors resolving RS and DSB signalling by sustained EWS-FLI1 expression. One important point to consider is that long-term expression of the fusion protein in U-2 OS cells, or another permissible cell line, may cause further changes than desired in an effort to adapt to the activity of this oncoprotein. As identified recently, there are gene expression patterns in the ES cell-of-origin that, upon the chromosomal translocation creating the fusion of *EWSR1* and *FLI1*, help to deal with the dysregulation of transcription and replication (40). These reported mechanisms, such as expression of FANCI, FANCD2, FANCA, and FEN1 may not necessarily be developed over time in a heterologous system expressing EWS-FLI1, due to differences in the background and disease subtype. For example, in the case of U-2 OS cells, despite a partially shared bone lineage with ES, this cell line possesses a distinct mutational background. An example of this is a mutation in the *ATRX* gene associated with the alternative-lengthening of telomeres (ALT) pathway (306). This telomerase-independent mechanism for telomere maintenance is specific to cancer cells and has been associated with a defective G2/M checkpoint and dysregulated DSB repair. In this way, the existing genomic instability in U-2 OS cells may confound a potential increase in RS, presence of R-loops, and an activated RSR upon expression of EWS-FLI1. The genomically complex background of this cell line could provide a narrow window to observing additional fusion-driven stress, limiting the potential of this model.

Altogether, short-term induction of EWS-FLI1 in this system was sufficient to enhance sensitivity to SN-38 in combination with AZD1775, providing proof-of-concept that this treatment can selectively target ES. Further validation of the U-2 OS model for ectopic expression of this fusion protein is still required.

Chapter 7 Discussion

The primary objective of this project was to investigate novel therapies targeting vulnerabilities associated with EWS fusion proteins in ES, the most common of these oncoproteins being EWS-FLI1. As the main driver of this sarcoma, EWS-FLI1 is at the heart of the mechanisms promoting malignant transformation, causing ES cells to become accustomed to aberrantly activated signalling for tumour development and survival. Direct inhibition of this fusion protein is currently not possible. Therefore, as an alternative, this project sought to develop targeted therapies exploiting dependencies that arise from the presence of the fusion. These therapies focused on two key processes hijacked by EWS-FLI, known to contribute to establishing the transcriptional signature of this sarcoma: (i) epigenetic rewiring through histone modifying enzymes (143, 144, 149, 150) and (ii) transcriptional dysregulation (37, 98).

The first part of this project (Chapter 3) was dedicated to assess the effects of catalytic inhibition of KDM1A. This demethylase, as part of a chromatin remodelling complex, is able to mediate transcriptional activation and downregulation of EWS-FLI1 target genes (149, 150). However, inhibition of its demethylase function as a strategy to reverse this signature and induce cell death proved to be insufficient (307). Whilst KDM1A remains a potential target in this sarcoma (237, 238), the lack of effects through disruption of its catalytic activity suggested a role beyond its canonical function.

The second therapeutic strategy explored in this project did not take the traditional approach of limiting or reverting EWS-FLI1-mediated oncogenic signalling. Rather, the rationale was to take advantage of the dysregulated transcriptional context brought about by the fusion protein, and specifically target the dependencies counteracting the resulting RS and genomic instability (37, 98). In particular, combination between irinotecan and WEE inhibition was found to be effective against spheroid models of ES. Lastly, an inducible model of ectopic expression of EWS-FLI1 supported the hypothesis of the fusion being the source of this targetable vulnerability. Together, these findings identified a potential combination therapy for this highly aggressive sarcoma.

7.1 Future prospects for targeting KDM1A as a therapeutic strategy

Increasingly, ES has come to be recognised predominantly as an epigenetic disease owing to the vast rewiring of the transcriptome initiated by a fusion protein (143, 144, 308). Importantly, these epigenetic changes occur in a context of a few other genetic mutations (130-132), highlighting the ability of a single oncogenic event in the form of a fusion protein to cause widespread chromatin changes promoting malignant transformation. Other examples of this have been seen in fusion-driven sarcomas, such as rhabdomyosarcoma (RMS) and synovial sarcoma (SS) (309, 310). Here, some of the challenges of novel therapies exploiting dysregulated epigenetic states in cancer are discussed in the context of ES.

KDM1A, in conjunction with the NuRD complex, had been shown to be recruited by EWS-FLI1 to establish the transcriptional programme in this sarcoma (149, 150). This functional role and its overexpression in this tumour, made therapeutically inhibiting this demethylase an attractive approach. Previously, targeting of this demethylase with a tool compound had been shown to reverse the ES transcriptional signature and induce cell death in ES cell lines (149, 150). However, evidence in this project found inhibition of KDM1A's demethylase activity to be insufficient to induce cytotoxicity and to modify expression of EWS-FLI1 target genes in *in vitro* models of ES (307). These results highlighted a discrepancy in our understanding of KDM1A-regulated gene expression, suggesting unexplored demethylase-independent functions contributing to the potential mechanism in ES. Supporting this view, non-canonical functions have been recently found to be responsible for gene expression regulation instead of histone demethylation in other malignant and non-malignant contexts (229, 231, 240). The use of an enzymatic-deficient KDM1A mutant (K661A) has been key to demonstrate its scaffolding roles, enabling transcriptional changes through protein-protein interactions with other substrates (228, 231). Interestingly, catalytic inhibitors of KDM1A in AML, previously thought to act by suppressing its demethylase activity, have now been found to disrupt an interaction with transcription factor GFI1 (228, 231). These results support the observed lack of activity in ES, as GFI1 plays a specific and critical role in AML through repression of myeloid differentiation (311). This also highlights the context-dependent specificity of epigenetic inhibitors. Intriguingly, drug-resistant mutants to GSK-LSD1, one of the catalytic inhibitors of KDM1A, were found to have mutations in the catalytic site, which

inactivates KDM1A's demethylase function, but did not affect AML survival (231). This further indicated that the cytotoxic effects of KDM1A inhibitors in AML operate by disrupting another function of the catalytic site, that is separate from the overall enzymatic activity, but relevant for binding GFI1 (231). It is possible to suggest that the activity of tool compound SP-2509 in ES must occur through a disruption of key interactions between KDM1A, the NuRD complex, and EWS-FLI1 important for gene regulation.

This experience demonstrated one of the challenges faced by epigenetic-based therapies, in which the intricate mechanisms of gene expression regulation have not been fully elucidated, limiting the extent to which they can be used therapeutically. However, it is only through disentangling the ambiguous roles of the enzymatic and non-enzymatic functions of epigenetic regulators, like KDM1A, that the exact contribution of these proteins can be teased out. Another example is EZH2, which is overexpressed in various solid tumours, including lung cancer, prostate cancer, ES, and RMS, amongst others (153, 239, 312, 313). Its function has been associated with repression of gene expression through its catalytic function in PRC2, but also with its non-canonical role as a transcriptional co-activator (153, 239, 312).Therefore, therapeutic targeting of EZH2 needs to incorporate these alternative roles, inhibiting them accordingly and when necessary. The process of designing and validating compounds against epigenetic targets has been shaped by our traditional understanding of them. However, the mounting evidence for roles beyond their catalytic function could pave the way for novel compounds aimed at blocking further protein-protein interactions. In this way, future epigenetic therapies could become more directed with tailored drug design for specific biological contexts (314).

In the case of ES, interaction of the EWS portion of the fusion with chromatin remodelling complexes, such as BAF complexes and the NuRD complex, is key to the capacity of EWS-FLI1 to epigenetically rewire expression patterns (143, 144, 149, 153). Interaction with BAF complexes in particular, is shared with the other FET family protein members TAF15 and FUS, which possess an intrinsically-disordered peptide sequence found to be essential for EWS-FL11 transcriptional activation of target genes (144). The FET proteins are able to perform interchangeable roles and are present in fusions in other sarcomas as well (122, 169, 315). The intrinsically-disordered prion-like domain in the FET proteins has also been suggested to confer further abilities to form transcriptional "hubs" with

greater output than transcription factors bound to a single site in the promoter region (315, 316). This complex form of epigenetically-controlled transcription in ES, and potentially other FET fusion protein-driven sarcomas, affects chromatin organisation creating specific demands for epigenetic marks and nucleosome distribution (315). This has the potential of opening novel vulnerabilities related to the epigenetic regulators that make rewiring possible. Within this area, possible targets include the so-called "movers", enabling nucleosome shifts to allow for chromatin accessibility, such as BAF complexes, which have already been linked to EWS-FLI1 reprogramming (144, 317, 318). However, the limited number of selective inhibitors for the ATPase subunits of these ATP-dependent chromatin remodellers presents a challenge (319, 320). Importantly, the targeting of core subunits like BRG1 may result in high toxicity due to the essential nature of their activity, thus limiting the therapeutic window of this inhibitors (320). Similarly, acetyltransferase p300 responsible for the acetylation of H3K27, characteristic of super enhancer activity and an open chromatin state in ES could be a potential target (143, 308). Already, there is ongoing work to develop selective inhibitors of this target for prostate cancer (321).

Overall, a deeper understanding of how specific epigenetic regulators work in ES is needed, despite the progress made in the overarching processes used. It will be important to study the consequences of normalising the epigenetic changes mediated by EWS-FLI1, and whether this form of oncogene withdrawal is sufficient as a therapy. This is because compensatory mechanisms and redundancy in the activity of epigenetic regulators could add to the unpredictability of therapies aimed at reverting malignant epigenetic signatures (314, 317). By integrating the lessons from current epigenetic therapies, ES may yet benefit from developments from this field.

7.2 Replication stress as a targetable vulnerability in ES

As with epigenetic-based therapies, research into the disease mechanisms of ES has improved the understanding of potential vulnerabilities in this sarcoma and how these can be clinically targeted. The work in this thesis contributed to these efforts, focusing on RS-inducing therapies that exploit an acquired dependency on the RSR in this tumour. This response is necessary to mitigate EWS-FLI1-driven genomic instability, and therefore, it makes these therapies specific in the context of ES.

For years it had been suggested that EWS' roles in preserving genome stability, transcriptional regulation, and mRNA processing differed from EWS-FLI1's functions in this sarcoma (37, 118, 164, 165, 169, 322). More recently, this has been confirmed by showing that EWS-FLI1 is actively in contention with EWS in a dominant-negative manner. In particular, this results in constitutive activation of RNAPII and aberrant transcription, amongst other novel oncogenic properties used by EWS-FLI1 to reprogram ES cells (detailed in 1.5) (37, 308). This, however, is not without consequences for this tumour, as this dysregulated form of transcription disrupts other cellular processes such as DNA replication, causing genotoxic damage (37). The resulting genomic instability has been associated with presence of R-loops and RS, slowing down fork progression (33, 37, 38, 98). To counteract the consequential endogenous RS driven by EWS-FLI1, ES cells have developed a hyperactivated RSR, becoming profoundly sensitive to its inhibition, as demonstrated here and in other reports (37, 40, 98, 167, 168).

From a clinical perspective, defining the vulnerability in ES and context of these tumours is an important step to develop therapies that can succeed, as not every attempt to inhibiting the RSR has been successful in this sarcoma. For example, high levels of CHK1 expression demonstrated the importance of the RSR in this cancer (98), but the abundance of this protein also limited efficacy with CHK1 inhibitors (167, 196). In accordance with the results in this project, WEE1 and ATR inhibition remain as more suitable targets in ES. Despite their concerted activity, these proteins possess unique roles and mechanisms that could make a difference therapeutically. In a study of diffuse large B-cell lymphoma (DLBCL), WEE1 inhibitor AZD1775 and ATR inhibitor AZD6738 were found to have distinct roles in DNA damage induction in phases of the cell cycle (54). Investigating whether there is a differential response in ES could guide the clinical development of this

strategies to maximise response, particularly in combination therapies with topoisomerase inhibitors exacerbating RS. Alongside, other DNA repair defects that could potentially contribute to this vulnerability have been investigated in ES, but results have not been conclusive (189, 200, 201). The main piece of evidence is perhaps the finding that BRCA1 is sequestered to chromatin, incapacitating this important HR factor, even when ES cell lines present robust BRCA1 expression (37, 200). However, better understanding of this proposed deficiency is needed, since PARP1 inhibition as a single-agent did not produce significant responses in patients (199), despite high expression in this tumour through direct upregulation by EWS-FLI1 and this suggested *BRCA1*-deficient-like state (37, 197). Therefore, rather than a conventional DNA repair defect, the findings in this study supported the view that ES has an increased reliance on the RSR as a way to mitigate DNA damage arising from EWS-FLI1-driven processes. Nevertheless, it is still possible that a requirement for proficient DSB repair in this sarcoma is also necessary to work in concert with the RSR.

The results in this work proposed a combination strategy between irinotecan and WEE1 inhibition, but it is likely that other RS stress inducing therapies could be effective, as it has been previously shown with ATR (98). Given that dysregulation of transcription arises from a dominant-negative effect on the WT function of EWS (37), which is also fused in other sarcomas, it is possible to hypothesise that these other EWS fusion-driven tumours may share this defect. As such, the combination treatment proposed here, could have wider therapeutic implications for these malignancies. In our experience, an *in vitro* model of DSRCT bearing the EWS-WT1 fusion, shows sensitivity to SN-38 and WEE1 inhibition in combination, and also when inhibiting CHK1 (Data not shown). Whilst less is known about the disease mechanisms in this paediatric tumour, it appears there are several similarities with ES (323). One example of this is high expression of SLFN11, which has also been linked to its sensitivity to irinotecan and PARP1 inhibition (324). In ES, however, *SLFN11* has been shown to be a target gene of EWS-FLI1 via the ETS canonical motif, whereas the mechanism of upregulation in DSRCT remains unknown. Importantly, the clinical presentation of this disease is widely different, and alternative splicing events in WT1 create different isoforms of this fusion protein, where alterations of the DNA-binding domain result in activation of different target genes (123, 323, 325). Still, the shared sensitivities, potentially stemming from loss of EWS WT function, are an interesting prospect and offer additional targets for this highly aggressive tumour with

poor prognosis and no targeted therapy available (323, 326). Further work could seek to validate some of the dysregulated mechanisms in ES in this other tumour, and search for signs of endogenous RS.

Various models of cancer propose that transformed cells are dependent on expression of oncogenes, promoting aberrant proliferation and survival signalling (5, 10, 327). When confronted with oncogene inactivation *in vitro*, cancer cells usually undergo growth arrest or cell death (48, 280, 328). Paradoxically, overexpression of a potent oncogene, or even two together, can also result in apoptosis in cancer cells (3). This suggests that oncogenic activity has to be carefully managed to maintain tumour growth and survival without an "oncogene overdose" (329, 330). Anti-cancer therapies usually aim to disrupt oncogenic signalling by either suppressing or promoting it in order to induce cell death. For these reasons understanding how EWS-FLI1 activity is coordinated will be a challenge for future therapies. Recent work, using single-cell transcriptomic analysis as an indirect measure of the fusion protein's activity, revealed that proliferating ES cells were limited to a range of intermediate EWS-FLI1 activity (159). In contrast, less common populations at the boundaries of EWS-FLI1 activity (high and low) were not proliferative. It is tempting to suggest that this could be a potential system restraining excessive oncogenic signalling by EWS-FLI1, in addition to mechanisms preserving genomic integrity, such as the RSR (40, 98).

Other important implications of this recent report relate to the efficacy of irinotecan in combination with WEE1 inhibition. As results in this thesis suggested, the presence and activity of EWS-FLI1 is responsible for the vulnerability targeted in this project. Specifically, the response to RS-inducing therapies is mechanistically linked to the proliferation and cell cycle patterns dictated by the fusion protein. Inversely, it can be hypothesised that the low EWS-FLI1 activity in these rare ES cell populations could decrease sensitivity to such treatments. For these reasons, an important research area in the next years will be understanding the mechanisms behind these heterogenous EWS-FLI1 states. Already, microenvironmental factors have been proposed to contribute to this form of intratumoural heterogeneity (159, 160, 193). Future studies on their involvement will need models such as spheroids that can mimic tumour proliferation patterns and oxygen gradients (4, 247). Lastly, understanding how these mechanisms operate could lead to combination therapies aimed at sensitising cells with low fusion

protein activity in order to prevent EWS-FLI1-driven heterogeneity as a source of drug-resistance.

References

1. Nowell PC. The clonal evolution of tumor cell populations. Science. 1976;194(4260):23-8.
2. Sanchez-Vega F, Mina M, Armenia J, Chatila WK, Luna A, La KC, et al. Oncogenic Signaling Pathways in The Cancer Genome Atlas. Cell. 2018;173(2):321-37 e10.
3. Ambrogio C, Barbacid M, Santamaria D. In vivo oncogenic conflict triggered by co-existing KRAS and EGFR activating mutations in lung adenocarcinoma. Oncogene. 2017;36(16):2309-18.
4. Riffle S, Pandey RN, Albert M, Hegde RS. Linking hypoxia, DNA damage and proliferation in multicellular tumor spheroids. BMC Cancer. 2017;17(1):338.
5. Hanahan D, Weinberg RA. Hallmarks of cancer: the next generation. Cell. 2011;144(5):646-74.
6. Dagogo-Jack I, Shaw AT. Tumour heterogeneity and resistance to cancer therapies. Nat Rev Clin Oncol. 2018;15(2):81-94.
7. Pompili L, Porru M, Caruso C, Biroccio A, Leonetti C. Patient-derived xenografts: a relevant preclinical model for drug development. J Exp Clin Cancer Res. 2016;35(1):189.
8. Langley RR, Fidler IJ. The seed and soil hypothesis revisited--the role of tumor-stroma interactions in metastasis to different organs. Int J Cancer. 2011;128(11):2527-35.
9. Schneider G, Schmidt-Supprian M, Rad R, Saur D. Tissue-specific tumorigenesis: context matters. Nat Rev Cancer. 2017;17(4):239-53.
10. Hanahan D, Weinberg RA. The hallmarks of cancer. Cell. 2000;100(1):57-70.
11. Jackson SP, Bartek J. The DNA-damage response in human biology and disease. Nature. 2009;461(7267):1071-8.
12. Gaillard H, Garcia-Muse T, Aguilera A. Replication stress and cancer. Nat Rev Cancer. 2015;15(5):276-89.
13. Goding CR. Commentary. A picture of Mitf in melanoma immortality. Oncogene. 2011;30(20):2304-6.
14. Croce CM. Oncogenes and cancer. N Engl J Med. 2008;358(5):502-11.
15. Pylayeva-Gupta Y, Grabocka E, Bar-Sagi D. RAS oncogenes: weaving a tumorigenic web. Nat Rev Cancer. 2011;11(11):761-74.
16. Sizemore GM, Pitarresi JR, Balakrishnan S, Ostrowski MC. The ETS family of oncogenic transcription factors in solid tumours. Nat Rev Cancer. 2017;17(6):337-51.
17. Tanaka H, Watanabe T. Mechanisms Underlying Recurrent Genomic Amplification in Human Cancers. Trends Cancer. 2020;6(6):462-77.
18. Carr MI, Jones SN. Regulation of the Mdm2-p53 signaling axis in the DNA damage response and tumorigenesis. Transl Cancer Res. 2016;5(6):707-24.
19. Gao Q, Liang WW, Foltz SM, Mutharasu G, Jayasinghe RG, Cao S, et al. Driver Fusions and Their Implications in the Development and Treatment of Human Cancers. Cell Rep. 2018;23(1):227-38 e3.
20. Quintas-Cardama A, Cortes J. Molecular biology of bcr-abl1-positive chronic myeloid leukemia. Blood. 2009;113(8):1619-30.
21. Finger LR, Harvey RC, Moore RC, Showe LC, Croce CM. A common mechanism of chromosomal translocation in T- and B-cell neoplasia. Science. 1986;234(4779):982-5.
22. Laugesen A, Helin K. Chromatin repressive complexes in stem cells, development, and cancer. Cell Stem Cell. 2014;14(6):735-51.

23.   Kumar R, Li DQ, Muller S, Knapp S. Epigenomic regulation of oncogenesis by chromatin remodeling. Oncogene. 2016;35(34):4423-36.

24.   Ehrlich M. DNA hypomethylation in cancer cells. Epigenomics. 2009;1(2):239-59.

25.   Knudson AG, Jr. Mutation and cancer: statistical study of retinoblastoma. Proc Natl Acad Sci U S A. 1971;68(4):820-3.

26.   Payne SR, Kemp CJ. Tumor suppressor genetics. Carcinogenesis. 2005;26(12):2031-45.

27.   Morrill SA, Amon A. Why haploinsufficiency persists. Proc Natl Acad Sci U S A. 2019;116(24):11866-71.

28.   de Vries A, Flores ER, Miranda B, Hsieh HM, van Oostrom CT, Sage J, et al. Targeted point mutations of p53 lead to dominant-negative inhibition of wild-type p53 function. Proc Natl Acad Sci U S A. 2002;99(5):2948-53.

29.   Macheret M, Halazonetis TD. DNA replication stress as a hallmark of cancer. Annu Rev Pathol. 2015;10:425-48.

30.   Zeman MK, Cimprich KA. Causes and consequences of replication stress. Nat Cell Biol. 2014;16(1):2-9.

31.   Kotsantis P, Petermann E, Boulton SJ. Mechanisms of Oncogene-Induced Replication Stress: Jigsaw Falling into Place. Cancer Discov. 2018;8(5):537-55.

32.   Santos-Pereira JM, Aguilera A. R loops: new modulators of genome dynamics and function. Nat Rev Genet. 2015;16(10):583-97.

33.   Sollier J, Cimprich KA. Breaking bad: R-loops and genome integrity. Trends Cell Biol. 2015;25(9):514-22.

34.   Petropoulos M, Champeris Tsaniras S, Taraviras S, Lygerou Z. Replication Licensing Aberrations, Replication Stress, and Genomic Instability. Trends Biochem Sci. 2019;44(9):752-64.

35.   Keszthelyi A, Minchell NE, Baxter J. The Causes and Consequences of Topological Stress during DNA Replication. Genes (Basel). 2016;7(12).

36.   Dominguez-Sola D, Gautier J. MYC and the control of DNA replication. Cold Spring Harb Perspect Med. 2014;4(6).

37.   Gorthi A, Romero JC, Loranc E, Cao L, Lawrence LA, Goodale E, et al. EWS-FLI1 increases transcription to cause R-loops and block BRCA1 repair in Ewing sarcoma. Nature. 2018;555(7696):387-91.

38.   Hamperl S, Cimprich KA. The contribution of co-transcriptional RNA:DNA hybrid structures to DNA damage and genome instability. DNA Repair (Amst). 2014;19:84-94.

39.   Aarts M, Bajrami I, Herrera-Abreu MT, Elliott R, Brough R, Ashworth A, et al. Functional Genetic Screen Identifies Increased Sensitivity to WEE1 Inhibition in Cells with Defects in Fanconi Anemia and HR Pathways. Mol Cancer Ther. 2015;14(4):865-76.

40.   Miller HE, Gorthi A, Bassani N, Lawrence LA, Iskra BS, Bishop AJR. Reconstruction of Ewing Sarcoma Developmental Context from Mass-Scale Transcriptomics Reveals Characteristics of EWSR1-FLI1 Permissibility. Cancers (Basel). 2020;12(4).

41.   Pfister SX, Markkanen E, Jiang Y, Sarkar S, Woodcock M, Orlando G, et al. Inhibiting WEE1 Selectively Kills Histone H3K36me3-Deficient Cancers by dNTP Starvation. Cancer Cell. 2015;28(5):557-68.

42.   D'Angiolella V, Donato V, Forrester FM, Jeong YT, Pellacani C, Kudo Y, et al. Cyclin F-mediated degradation of ribonucleotide reductase M2 controls genome integrity and DNA repair. Cell. 2012;149(5):1023-34.

43.   Bashir T, Pagano M. Cdk1: the dominant sibling of Cdk2. Nat Cell Biol. 2005;7(8):779-81.

44.   Aleem E, Kiyokawa H, Kaldis P. Cdc2-cyclin E complexes regulate the G1/S phase transition. Nat Cell Biol. 2005;7(8):831-6.

45.   Zhong Y, Nellimoottil T, Peace JM, Knott SR, Villwock SK, Yee JM, et al. The level of origin firing inversely affects the rate of replication fork progression. J Cell Biol. 2013;201(3):373-83.

46.   Lukas C, Savic V, Bekker-Jensen S, Doil C, Neumann B, Pedersen RS, et al. 53BP1 nuclear bodies form around DNA lesions generated by mitotic transmission of chromosomes under replication stress. Nat Cell Biol. 2011;13(3):243-53.

47.   Spies J, Lukas C, Somyajit K, Rask MB, Lukas J, Neelsen KJ. 53BP1 nuclear bodies enforce replication timing at under-replicated DNA to limit heritable DNA damage. Nat Cell Biol. 2019;21(4):487-97.

48.   Di Micco R, Fumagalli M, Cicalese A, Piccinin S, Gasparini P, Luise C, et al. Oncogene-induced senescence is a DNA damage response triggered by DNA hyper-replication. Nature. 2006;444(7119):638-42.

49.   Bester AC, Roniger M, Oren YS, Im MM, Sarni D, Chaoat M, et al. Nucleotide deficiency promotes genomic instability in early stages of cancer development. Cell. 2011;145(3):435-46.

50.   Nevis KR, Cordeiro-Stone M, Cook JG. Origin licensing and p53 status regulate Cdk2 activity during G(1). Cell Cycle. 2009;8(12):1952-63.

51.   Bretones G, Delgado MD, Leon J. Myc and cell cycle control. Biochim Biophys Acta. 2015;1849(5):506-16.

52.   Eilers M, Schirm S, Bishop JM. The MYC protein activates transcription of the alpha-prothymosin gene. EMBO J. 1991;10(1):133-41.

53.   Schuhmacher M, Staege MS, Pajic A, Polack A, Weidle UH, Bornkamm GW, et al. Control of cell growth by c-Myc in the absence of cell division. Curr Biol. 1999;9(21):1255-8.

54.   Young LA, O'Connor LO, de Renty C, Veldman-Jones MH, Dorval T, Wilson Z, et al. Differential Activity of ATR and WEE1 Inhibitors in a Highly Sensitive Subpopulation of DLBCL Linked to Replication Stress. Cancer Res. 2019;79(14):3762-75.

55.   Beck H, Nahse-Kumpf V, Larsen MS, O'Hanlon KA, Patzke S, Holmberg C, et al. Cyclin-dependent kinase suppression by WEE1 kinase protects the genome through control of replication initiation and nucleotide consumption. Mol Cell Biol. 2012;32(20):4226-36.

56.   Lecona E, Fernandez-Capetillo O. Targeting ATR in cancer. Nat Rev Cancer. 2018;18(9):586-95.

57.   Blackford AN, Jackson SP. ATM, ATR, and DNA-PK: The Trinity at the Heart of the DNA Damage Response. Mol Cell. 2017;66(6):801-17.

58.   Marechal A, Zou L. RPA-coated single-stranded DNA as a platform for post-translational modifications in the DNA damage response. Cell Res. 2015;25(1):9-23.

59.   O'Connor MJ. Targeting the DNA Damage Response in Cancer. Mol Cell. 2015;60(4):547-60.

60.   O'Connor MJ, Martin NM, Smith GC. Targeted cancer therapies based on the inhibition of DNA strand break repair. Oncogene. 2007;26(56):7816-24.

61.   Buisson R, Boisvert JL, Benes CH, Zou L. Distinct but Concerted Roles of ATR, DNA-PK, and Chk1 in Countering Replication Stress during S Phase. Mol Cell. 2015;59(6):1011-24.

62.   Katayama K, Fujita N, Tsuruo T. Akt/protein kinase B-dependent phosphorylation and inactivation of WEE1Hu promote cell cycle progression at G2/M transition. Mol Cell Biol. 2005;25(13):5725-37.

63.   Liu H, Takeda S, Kumar R, Westergard TD, Brown EJ, Pandita TK, et al. Phosphorylation of MLL by ATR is required for execution of mammalian S-phase checkpoint. Nature. 2010;467(7313):343-6.

64.   Guo C, Kumagai A, Schlacher K, Shevchenko A, Shevchenko A, Dunphy WG. Interaction of Chk1 with Treslin negatively regulates the initiation of chromosomal DNA replication. Mol Cell. 2015;57(3):492-505.

65.   Toledo L, Neelsen KJ, Lukas J. Replication Catastrophe: When a Checkpoint Fails because of Exhaustion. Mol Cell. 2017;66(6):735-49.

66.   Neelsen KJ, Lopes M. Replication fork reversal in eukaryotes: from dead end to dynamic response. Nat Rev Mol Cell Biol. 2015;16(4):207-20.

67.   Quinet A, Lemacon D, Vindigni A. Replication Fork Reversal: Players and Guardians. Mol Cell. 2017;68(5):830-3.

68.   Mijic S, Zellweger R, Chappidi N, Berti M, Jacobs K, Mutreja K, et al. Replication fork reversal triggers fork degradation in BRCA2-defective cells. Nat Commun. 2017;8(1):859.

69.   Gari K, Decaillet C, Stasiak AZ, Stasiak A, Constantinou A. The Fanconi anemia protein FANCM can promote branch migration of Holliday junctions and replication forks. Mol Cell. 2008;29(1):141-8.

70.   Rossi ML, Ghosh AK, Bohr VA. Roles of Werner syndrome protein in protection of genome integrity. DNA Repair (Amst). 2010;9(3):331-44.

71.   Nurse P. Universal control mechanism regulating onset of M-phase. Nature. 1990;344(6266):503-8.

72.   Solomon MJ, Glotzer M, Lee TH, Philippe M, Kirschner MW. Cyclin activation of p34cdc2. Cell. 1990;63(5):1013-24.

73.   Wood DJ, Endicott JA. Structural insights into the functional diversity of the CDK-cyclin family. Open Biol. 2018;8(9).

74.   Geenen JJJ, Schellens JHM. Molecular Pathways: Targeting the Protein Kinase Wee1 in Cancer. Clin Cancer Res. 2017;23(16):4540-4.

75.   The Broad Institute. DepMap 20Q2 Public. . 2020 ed2020.

76.   Meyers RM, Bryan JG, McFarland JM, Weir BA, Sizemore AE, Xu H, et al. Computational correction of copy number effect improves specificity of CRISPR-Cas9 essentiality screens in cancer cells. Nat Genet. 2017;49(12):1779-84.

77.   Dominguez-Kelly R, Martin Y, Koundrioukoff S, Tanenbaum ME, Smits VA, Medema RH, et al. Wee1 controls genomic stability during replication by regulating the Mus81-Eme1 endonuclease. J Cell Biol. 2011;194(4):567-79.

78.   Duda H, Arter M, Gloggnitzer J, Teloni F, Wild P, Blanco MG, et al. A Mechanism for Controlled Breakage of Under-replicated Chromosomes during Mitosis. Dev Cell. 2016;39(6):740-55.

79.   Lieber MR. The mechanism of double-strand DNA break repair by the nonhomologous DNA end-joining pathway. Annu Rev Biochem. 2010;79:181-211.

80.   Betermier M, Bertrand P, Lopez BS. Is non-homologous end-joining really an inherently error-prone process? PLoS Genet. 2014;10(1):e1004086.

81.   Cannan WJ, Pederson DS. Mechanisms and Consequences of Double-Strand DNA Break Formation in Chromatin. J Cell Physiol. 2016;231(1):3-14.

82.   Farmer H, McCabe N, Lord CJ, Tutt AN, Johnson DA, Richardson TB, et al. Targeting the DNA repair defect in BRCA mutant cells as a therapeutic strategy. Nature. 2005;434(7035):917-21.

83.   Lord CJ, Ashworth A. PARP inhibitors: Synthetic lethality in the clinic. Science. 2017;355(6330):1152-8.
84.   Sung P, Klein H. Mechanism of homologous recombination: mediators and helicases take on regulatory functions. Nat Rev Mol Cell Biol. 2006;7(10):739-50.
85.   Krejci L, Altmannova V, Spirek M, Zhao X. Homologous recombination and its regulation. Nucleic Acids Res. 2012;40(13):5795-818.
86.   Scully R, Xie A. Double strand break repair functions of histone H2AX. Mutat Res. 2013;750(1-2):5-14.
87.   Rogakou EP, Pilch DR, Orr AH, Ivanova VS, Bonner WM. DNA double-stranded breaks induce histone H2AX phosphorylation on serine 139. J Biol Chem. 1998;273(10):5858-68.
88.   Liu J, Luo S, Zhao H, Liao J, Li J, Yang C, et al. Structural mechanism of the phosphorylation-dependent dimerization of the MDC1 forkhead-associated domain. Nucleic Acids Res. 2012;40(9):3898-912.
89.   Spycher C, Miller ES, Townsend K, Pavic L, Morrice NA, Janscak P, et al. Constitutive phosphorylation of MDC1 physically links the MRE11-RAD50-NBS1 complex to damaged chromatin. J Cell Biol. 2008;181(2):227-40.
90.   Sartori AA, Lukas C, Coates J, Mistrik M, Fu S, Bartek J, et al. Human CtIP promotes DNA end resection. Nature. 2007;450(7169):509-14.
91.   Moynahan ME, Chiu JW, Koller BH, Jasin M. Brca1 controls homology-directed DNA repair. Mol Cell. 1999;4(4):511-8.
92.   Daley JM, Sung P. 53BP1, BRCA1, and the choice between recombination and end joining at DNA double-strand breaks. Mol Cell Biol. 2014;34(8):1380-8.
93.   Heyer WD, Ehmsen KT, Liu J. Regulation of homologous recombination in eukaryotes. Annu Rev Genet. 2010;44:113-39.
94.   Bryant HE, Schultz N, Thomas HD, Parker KM, Flower D, Lopez E, et al. Specific killing of BRCA2-deficient tumours with inhibitors of poly(ADP-ribose) polymerase. Nature. 2005;434(7035):913-7.
95.   Murai J, Huang SY, Das BB, Renaud A, Zhang Y, Doroshow JH, et al. Trapping of PARP1 and PARP2 by Clinical PARP Inhibitors. Cancer Res. 2012;72(21):5588-99.
96.   ESP1/SARC025 Global Collaboration: A Phase I Study of a Combination of the PARP Inhibitor, Niraparib and Temozolomide and/or Irinotecan Patients With Previously Treated, Incurable Ewing Sarcoma.
97.   Fong PC, Boss DS, Yap TA, Tutt A, Wu P, Mergui-Roelvink M, et al. Inhibition of poly(ADP-ribose) polymerase in tumors from BRCA mutation carriers. N Engl J Med. 2009;361(2):123-34.
98.   Nieto-Soler M, Morgado-Palacin I, Lafarga V, Lecona E, Murga M, Callen E, et al. Efficacy of ATR inhibitors as single agents in Ewing sarcoma. Oncotarget. 2016;7(37):58759-67.
99.   Leijen S, van Geel RM, Sonke GS, de Jong D, Rosenberg EH, Marchetti S, et al. Phase II Study of WEE1 Inhibitor AZD1775 Plus Carboplatin in Patients With TP53-Mutated Ovarian Cancer Refractory or Resistant to First-Line Therapy Within 3 Months. J Clin Oncol. 2016;34(36):4354-61.
100.   Banerji U, Plummer ER, Moreno V, Ang JE, Quinton A, Drew Y, et al. A phase I/II first-in-human trial of oral SRA737 (a Chk1 inhibitor) given in combination with low-dose gemcitabine in subjects with advanced cancer. Journal of Clinical Oncology. 2019;37(15_suppl):3095-.
101.   Do K, Wilsker D, Ji J, Zlott J, Freshwater T, Kinders RJ, et al. Phase I Study of Single-Agent AZD1775 (MK-1775), a Wee1 Kinase Inhibitor, in Patients With Refractory Solid Tumors. J Clin Oncol. 2015;33(30):3409-15.

102.   Dillon MT, Boylan Z, Smith D, Guevara J, Mohammed K, Peckitt C, et al. PATRIOT: A phase I study to assess the tolerability, safety and biological effects of a specific ataxia telangiectasia and Rad3-related (ATR) inhibitor (AZD6738) as a single agent and in combination with palliative radiation therapy in patients with solid tumours. Clin Transl Radiat Oncol. 2018;12:16-20.

103.   Etemadmoghadam D, Weir BA, Au-Yeung G, Alsop K, Mitchell G, George J, et al. Synthetic lethality between CCNE1 amplification and loss of BRCA1. Proc Natl Acad Sci U S A. 2013;110(48):19489-94.

104.   Josse R, Martin SE, Guha R, Ormanoglu P, Pfister TD, Reaper PM, et al. ATR inhibitors VE-821 and VX-970 sensitize cancer cells to topoisomerase i inhibitors by disabling DNA replication initiation and fork elongation responses. Cancer Res. 2014;74(23):6968-79.

105.   Ray Chaudhuri A, Nussenzweig A. The multifaceted roles of PARP1 in DNA repair and chromatin remodelling. Nat Rev Mol Cell Biol. 2017;18(10):610-21.

106.   Sangster-Guity N, Conrad BH, Papadopoulos N, Bunz F. ATR mediates cisplatin resistance in a p53 genotype-specific manner. Oncogene. 2011;30(22):2526-33.

107.   Huntoon CJ, Flatten KS, Wahner Hendrickson AE, Huehls AM, Sutor SL, Kaufmann SH, et al. ATR inhibition broadly sensitizes ovarian cancer cells to chemotherapy independent of BRCA status. Cancer Res. 2013;73(12):3683-91.

108.   Goss KL, Koppenhafer SL, Harmoney KM, Terry WW, Gordon DJ. Inhibition of CHK1 sensitizes Ewing sarcoma cells to the ribonucleotide reductase inhibitor gemcitabine. Oncotarget. 2017;8(50):87016-32.

109.   Walton MI, Eve PD, Hayes A, Henley AT, Valenti MR, De Haven Brandon AK, et al. The clinical development candidate CCT245737 is an orally active CHK1 inhibitor with preclinical activity in RAS mutant NSCLC and Emicro-MYC driven B-cell lymphoma. Oncotarget. 2016;7(3):2329-42.

110.   Montano R, Thompson R, Chung I, Hou H, Khan N, Eastman A. Sensitization of human cancer cells to gemcitabine by the Chk1 inhibitor MK-8776: cell cycle perturbation and impact of administration schedule in vitro and in vivo. BMC Cancer. 2013;13:604.

111.   Ku BM, Bae YH, Koh J, Sun JM, Lee SH, Ahn JS, et al. Mutational status of TP53 defines the efficacy of Wee1 inhibitor AZD1775 in KRAS-mutant non-small cell lung cancer. Oncotarget. 2017;8(40):67526-37.

112.   Kolb EA, Houghton PJ, Kurmasheva RT, Mosse YP, Maris JM, Erickson SW, et al. Preclinical evaluation of the combination of AZD1775 and irinotecan against selected pediatric solid tumors: A Pediatric Preclinical Testing Consortium report. Pediatr Blood Cancer. 2020;67(5):e28098.

113.   Cole KA, Pal S, Kudgus RA, Ijaz H, Liu X, Minard CG, et al. Phase I Clinical Trial of the Wee1 Inhibitor Adavosertib (AZD1775) with Irinotecan in Children with Relapsed Solid Tumors: A COG Phase I Consortium Report (ADVL1312). Clin Cancer Res. 2020;26(6):1213-9.

114.   Leijen S, van Geel RM, Pavlick AC, Tibes R, Rosen L, Razak AR, et al. Phase I Study Evaluating WEE1 Inhibitor AZD1775 As Monotherapy and in Combination With Gemcitabine, Cisplatin, or Carboplatin in Patients With Advanced Solid Tumors. J Clin Oncol. 2016;34(36):4371-80.

115.   Children with Cancer UK. Ewing sarcoma 2017 [updated 2017. Available from: https://www.childrenwithcancer.org.uk/childhood-cancer-info/cancer-types/ewing-sarcoma/.

116.   Group CsCL. Ewing sarcoma in children [On line]. Macmillan2016 [updated August 2016. Available from:

http://www.macmillan.org.uk/cancerinformation/cancertypes/childrenscancers/typesofchildrenscancers/ewingssarcoma.aspx.

117.   Delattre O, Zucman J, Plougastel B, Desmaze C, Melot T, Peter M, et al. Gene fusion with an ETS DNA-binding domain caused by chromosome translocation in human tumours. Nature. 1992;359(6391):162-5.

118.   Arvand A, Denny CT. Biology of EWS/ETS fusions in Ewing's family tumors. Oncogene. 2001;20(40):5747-54.

119.   van Doorninck JA, Ji L, Schaub B, Shimada H, Wing MR, Krailo MD, et al. Current treatment protocols have eliminated the prognostic advantage of type 1 fusions in Ewing sarcoma: a report from the Children's Oncology Group. J Clin Oncol. 2010;28(12):1989-94.

120.   Le Deley MC, Delattre O, Schaefer KL, Burchill SA, Koehler G, Hogendoorn PC, et al. Impact of EWS-ETS fusion type on disease progression in Ewing's sarcoma/peripheral primitive neuroectodermal tumor: prospective results from the cooperative Euro-E.W.I.N.G. 99 trial. J Clin Oncol. 2010;28(12):1982-8.

121.   Gangwal K, Sankar S, Hollenhorst PC, Kinsey M, Haroldsen SC, Shah AA, et al. Microsatellites as EWS/FLI response elements in Ewing's sarcoma. Proc Natl Acad Sci U S A. 2008;105(29):10149-54.

122.   Schwartz JC, Cech TR, Parker RR. Biochemical Properties and Biological Functions of FET Proteins. Annu Rev Biochem. 2015;84:355-79.

123.   Gerald WL, Haber DA. The EWS-WT1 gene fusion in desmoplastic small round cell tumor. Semin Cancer Biol. 2005;15(3):197-205.

124.   Brody RI, Ueda T, Hamelin A, Jhanwar SC, Bridge JA, Healey JH, et al. Molecular analysis of the fusion of EWS to an orphan nuclear receptor gene in extraskeletal myxoid chondrosarcoma. Am J Pathol. 1997;150(3):1049-58.

125.   Crozat A, Aman P, Mandahl N, Ron D. Fusion of CHOP to a novel RNA-binding protein in human myxoid liposarcoma. Nature. 1993;363(6430):640-4.

126.   Sorensen PH, Lessnick SL, Lopez-Terrada D, Liu XF, Triche TJ, Denny CT. A second Ewing's sarcoma translocation, t(21;22), fuses the EWS gene to another ETS-family transcription factor, ERG. Nat Genet. 1994;6(2):146-51.

127.   Jeon IS, Davis JN, Braun BS, Sublett JE, Roussel MF, Denny CT, et al. A variant Ewing's sarcoma translocation (7;22) fuses the EWS gene to the ETS gene ETV1. Oncogene. 1995;10(6):1229-34.

128.   Urano F, Umezawa A, Hong W, Kikuchi H, Hata J. A novel chimera gene between EWS and E1A-F, encoding the adenovirus E1A enhancer-binding protein, in extraosseous Ewing's sarcoma. Biochem Biophys Res Commun. 1996;219(2):608-12.

129.   Peter M, Couturier J, Pacquement H, Michon J, Thomas G, Magdelenat H, et al. A new member of the ETS family fused to EWS in Ewing tumors. Oncogene. 1997;14(10):1159-64.

130.   Tirode F, Surdez D, Ma X, Parker M, Le Deley MC, Bahrami A, et al. Genomic landscape of Ewing sarcoma defines an aggressive subtype with co-association of STAG2 and TP53 mutations. Cancer Discov. 2014;4(11):1342-53.

131.   Crompton BD, Stewart C, Taylor-Weiner A, Alexe G, Kurek KC, Calicchio ML, et al. The genomic landscape of pediatric Ewing sarcoma. Cancer Discov. 2014;4(11):1326-41.

132.   Brohl AS, Solomon DA, Chang W, Wang J, Song Y, Sindiri S, et al. The genomic landscape of the Ewing Sarcoma family of tumors reveals recurrent STAG2 mutation. PLoS Genet. 2014;10(7):e1004475.

133.   Mondal G, Stevers M, Goode B, Ashworth A, Solomon DA. A requirement for STAG2 in replication fork progression creates a targetable synthetic lethality in cohesin-mutant cancers. Nat Commun. 2019;10(1):1686.

134.   Solomon DA, Kim T, Diaz-Martinez LA, Fair J, Elkahloun AG, Harris BT, et al. Mutational inactivation of STAG2 causes aneuploidy in human cancer. Science. 2011;333(6045):1039-43.

135.   van der Lelij P, Lieb S, Jude J, Wutz G, Santos CP, Falkenberg K, et al. Synthetic lethality between the cohesin subunits STAG1 and STAG2 in diverse cancer contexts. Elife. 2017;6.

136.   Bailey ML, O'Neil NJ, van Pel DM, Solomon DA, Waldman T, Hieter P. Glioblastoma cells containing mutations in the cohesin component STAG2 are sensitive to PARP inhibition. Mol Cancer Ther. 2014;13(3):724-32.

137.   Kim WY, Sharpless NE. The regulation of INK4/ARF in cancer and aging. Cell. 2006;127(2):265-75.

138.   Mackintosh C, Ordonez JL, Garcia-Dominguez DJ, Sevillano V, Llombart-Bosch A, Szuhai K, et al. 1q gain and CDT2 overexpression underlie an aggressive and highly proliferative form of Ewing sarcoma. Oncogene. 2012;31(10):1287-98.

139.   Allis CD, Jenuwein T. The molecular hallmarks of epigenetic control. Nat Rev Genet. 2016;17(8):487-500.

140.   Creyghton MP, Cheng AW, Welstead GG, Kooistra T, Carey BW, Steine EJ, et al. Histone H3K27ac separates active from poised enhancers and predicts developmental state. Proc Natl Acad Sci U S A. 2010;107(50):21931-6.

141.   Plass C, Pfister SM, Lindroth AM, Bogatyrova O, Claus R, Lichter P. Mutations in regulators of the epigenome and their connections to global chromatin patterns in cancer. Nat Rev Genet. 2013;14(11):765-80.

142.   Gangwal K, Close D, Enriquez CA, Hill CP, Lessnick SL. Emergent Properties of EWS/FLI Regulation via GGAA Microsatellites in Ewing's Sarcoma. Genes Cancer. 2010;1(2):177-87.

143.   Riggi N, Knoechel B, Gillespie SM, Rheinbay E, Boulay G, Suva ML, et al. EWS-FLI1 utilizes divergent chromatin remodeling mechanisms to directly activate or repress enhancer elements in Ewing sarcoma. Cancer Cell. 2014;26(5):668-81.

144.   Boulay G, Sandoval GJ, Riggi N, Iyer S, Buisson R, Naigles B, et al. Cancer-Specific Retargeting of BAF Complexes by a Prion-like Domain. Cell. 2017.

145.   Lewis MW, Li S, Franco HL. Transcriptional control by enhancers and enhancer RNAs. Transcription. 2019;10(4-5):171-86.

146.   Riggi N, Suva ML, Suva D, Cironi L, Provero P, Tercier S, et al. EWS-FLI-1 expression triggers a Ewing's sarcoma initiation program in primary human mesenchymal stem cells. Cancer Res. 2008;68(7):2176-85.

147.   Grunewald TGP, Cidre-Aranaz F, Surdez D, Tomazou EM, de Alava E, Kovar H, et al. Ewing sarcoma. Nat Rev Dis Primers. 2018;4(1):5.

148.   Kadoch C, Crabtree GR. Mammalian SWI/SNF chromatin remodeling complexes and cancer: Mechanistic insights gained from human genomics. Sci Adv. 2015;1(5):e1500447.

149.   Sankar S, Bell R, Stephens B, Zhuo R, Sharma S, Bearss DJ, et al. Mechanism and relevance of EWS/FLI-mediated transcriptional repression in Ewing sarcoma. Oncogene. 2013;32(42):5089-100.

150.   Sankar S, Theisen ER, Bearss J, Mulvihill T, Hoffman LM, Sorna V, et al. Reversible LSD1 inhibition interferes with global EWS/ETS transcriptional activity and impedes Ewing sarcoma tumor growth. Clin Cancer Res. 2014;20(17):4584-97.

151.   Lai AY, Wade PA. Cancer biology and NuRD: a multifaceted chromatin remodelling complex. Nat Rev Cancer. 2011;11(8):588-96.

152.   Smits AH, Jansen PW, Poser I, Hyman AA, Vermeulen M. Stoichiometry of chromatin-associated protein complexes revealed by label-free quantitative mass spectrometry-based proteomics. Nucleic Acids Res. 2013;41(1):e28.

153.   Richter GH, Plehm S, Fasan A, Rossler S, Unland R, Bennani-Baiti IM, et al. EZH2 is a mediator of EWS/FLI1 driven tumor growth and metastasis blocking endothelial and neuro-ectodermal differentiation. Proc Natl Acad Sci U S A. 2009;106(13):5324-9.

154.   Riggi N, Suva ML, Stamenkovic I. Ewing's sarcoma origin: from duel to duality. Expert Rev Anticancer Ther. 2009;9(8):1025-30.

155.   Tirode F, Laud-Duval K, Prieur A, Delorme B, Charbord P, Delattre O. Mesenchymal stem cell features of Ewing tumors. Cancer Cell. 2007;11(5):421-9.

156.   Anderson ND, de Borja R, Young MD, Fuligni F, Rosic A, Roberts ND, et al. Rearrangement bursts generate canonical gene fusions in bone and soft tissue tumors. Science. 2018;361(6405).

157.   Sheffield NC, Pierron G, Klughammer J, Datlinger P, Schonegger A, Schuster M, et al. DNA methylation heterogeneity defines a disease spectrum in Ewing sarcoma. Nat Med. 2017;23(3):386-95.

158.   Franzetti GA, Laud-Duval K, van der Ent W, Brisac A, Irondelle M, Aubert S, et al. Cell-to-cell heterogeneity of EWSR1-FLI1 activity determines proliferation/migration choices in Ewing sarcoma cells. Oncogene. 2017;36(25):3505-14.

159.   Aynaud MM, Mirabeau O, Gruel N, Grossetete S, Boeva V, Durand S, et al. Transcriptional Programs Define Intratumoral Heterogeneity of Ewing Sarcoma at Single-Cell Resolution. Cell Rep. 2020;30(6):1767-79 e6.

160.   Aryee DN, Niedan S, Kauer M, Schwentner R, Bennani-Baiti IM, Ban J, et al. Hypoxia modulates EWS-FLI1 transcriptional signature and enhances the malignant properties of Ewing's sarcoma cells in vitro. Cancer Res. 2010;70(10):4015-23.

161.   Musa J, Grunewald TGP. Interaction between somatic mutations and germline variants contributes to clinical heterogeneity in cancer. Mol Cell Oncol. 2020;7(1):1682924.

162.   Musa J, Cidre-Aranaz F, Aynaud MM, Orth MF, Knott MML, Mirabeau O, et al. Cooperation of cancer drivers with regulatory germline variants shapes clinical outcomes. Nat Commun. 2019;10(1):4128.

163.   Grunewald TG, Bernard V, Gilardi-Hebenstreit P, Raynal V, Surdez D, Aynaud MM, et al. Chimeric EWSR1-FLI1 regulates the Ewing sarcoma susceptibility gene EGR2 via a GGAA microsatellite. Nat Genet. 2015;47(9):1073-8.

164.   Paronetto MP, Minana B, Valcarcel J. The Ewing sarcoma protein regulates DNA damage-induced alternative splicing. Mol Cell. 2011;43(3):353-68.

165.   Bertolotti A, Melot T, Acker J, Vigneron M, Delattre O, Tora L. EWS, but not EWS-FLI-1, is associated with both TFIID and RNA polymerase II: interactions between two members of the TET family, EWS and hTAFII68, and subunits of TFIID and RNA polymerase II complexes. Mol Cell Biol. 1998;18(3):1489-97.

166.   Sanchez G, Delattre O, Auboeuf D, Dutertre M. Coupled alteration of transcription and splicing by a single oncogene: boosting the effect on cyclin D1 activity. Cell Cycle. 2008;7(15):2299-305.

167.   Koppenhafer SL, Goss KL, Terry WW, Gordon DJ. mTORC1/2 and Protein Translation Regulate Levels of CHK1 and the Sensitivity to CHK1 Inhibitors in Ewing Sarcoma Cells. Mol Cancer Ther. 2018;17(12):2676-88.

168.   Koppenhafer SL, Goss KL, Terry WW, Gordon DJ. Inhibition of the ATR-CHK1 Pathway in Ewing Sarcoma Cells Causes DNA Damage and Apoptosis via the CDK2-Mediated Degradation of RRM2. Mol Cancer Res. 2020;18(1):91-104.

169.   Kovar H. Dr. Jekyll and Mr. Hyde: The Two Faces of the FUS/EWS/TAF15 Protein Family. Sarcoma. 2011;2011:837474.

170.   Chansky HA, Hu M, Hickstein DD, Yang L. Oncogenic TLS/ERG and EWS/Fli-1 fusion proteins inhibit RNA splicing mediated by YB-1 protein. Cancer Res. 2001;61(9):3586-90.

171.   Sanchez G, Bittencourt D, Laud K, Barbier J, Delattre O, Auboeuf D, et al. Alteration of cyclin D1 transcript elongation by a mutated transcription factor up-regulates the oncogenic D1b splice isoform in cancer. Proc Natl Acad Sci U S A. 2008;105(16):6004-9.

172.   Batsche E, Yaniv M, Muchardt C. The human SWI/SNF subunit Brm is a regulator of alternative splicing. Nat Struct Mol Biol. 2006;13(1):22-9.

173.   Solomon DA, Wang Y, Fox SR, Lambeck TC, Giesting S, Lan Z, et al. Cyclin D1 splice variants. Differential effects on localization, RB phosphorylation, and cellular transformation. J Biol Chem. 2003;278(32):30339-47.

174.   Lu F, Gladden AB, Diehl JA. An alternatively spliced cyclin D1 isoform, cyclin D1b, is a nuclear oncogene. Cancer Res. 2003;63(21):7056-61.

175.   Mascarenhas L, Lyden ER, Breitfeld PP, Walterhouse DO, Donaldson SS, Paidas CN, et al. Randomized phase II window trial of two schedules of irinotecan with vincristine in patients with first relapse or progression of rhabdomyosarcoma: a report from the Children's Oncology Group. J Clin Oncol. 2010;28(30):4658-63.

176.   Le Deley MC, Paulussen M, Lewis I, Brennan B, Ranft A, Whelan J, et al. Cyclophosphamide compared with ifosfamide in consolidation treatment of standard-risk Ewing sarcoma: results of the randomized noninferiority Euro-EWING99-R1 trial. J Clin Oncol. 2014;32(23):2440-8.

177.   Womer RB, West DC, Krailo MD, Dickman PS, Pawel BR, Grier HE, et al. Randomized controlled trial of interval-compressed chemotherapy for the treatment of localized Ewing sarcoma: a report from the Children's Oncology Group. J Clin Oncol. 2012;30(33):4148-54.

178.   Kovar H. Ewing's sarcoma and peripheral primitive neuroectodermal tumors after their genetic union. Curr Opin Oncol. 1998;10(4):334-42.

179.   Ferrari S, Bertoni F, Mercuri M, Sottili S, Versari M, Bacci G. Ewing's sarcoma of bone: relation between clinical characteristics and staging. Oncol Rep. 2001;8(3):553-6.

180.   Bomgaars LR, Bernstein M, Krailo M, Kadota R, Das S, Chen Z, et al. Phase II trial of irinotecan in children with refractory solid tumors: a Children's Oncology Group Study. J Clin Oncol. 2007;25(29):4622-7.

181.   Casey DA, Wexler LH, Merchant MS, Chou AJ, Merola PR, Price AP, et al. Irinotecan and temozolomide for Ewing sarcoma: the Memorial Sloan-Kettering experience. Pediatr Blood Cancer. 2009;53(6):1029-34.

182.   Wagner L. Camptothecin-based regimens for treatment of ewing sarcoma: past studies and future directions. Sarcoma. 2011;2011:957957.

183.   McCabe MG, Kirton L, Khan M, Fenwick N, Dirksen U, Gaspar N, et al. Results of the second interim assessment of rEECur, an international randomized controlled trial of chemotherapy for the treatment of recurrent and primary refractory Ewing sarcoma (RR-ES). Journal of Clinical Oncology. 2020;38(15_suppl):11502-.

184.   Pommier Y. Topoisomerase I inhibitors: camptothecins and beyond. Nat Rev Cancer. 2006;6(10):789-802.

185.   Houghton PJ, Stewart CF, Cheshire PJ, Richmond LB, Kirstein MN, Poquette CA, et al. Antitumor activity of temozolomide combined with irinotecan is partly independent of O6-methylguanine-DNA methyltransferase and mismatch repair phenotypes in xenograft models. Clin Cancer Res. 2000;6(10):4110-8.

186.   Gilbert DC, Chalmers AJ, El-Khamisy SF. Topoisomerase I inhibition in colorectal cancer: biomarkers and therapeutic targets. Br J Cancer. 2012;106(1):18-24.

187.   Wagner LM, Perentesis JP, Reid JM, Ames MM, Safgren SL, Nelson MD, Jr., et al. Phase I trial of two schedules of vincristine, oral irinotecan, and temozolomide (VOIT) for children with relapsed or refractory solid tumors: a Children's Oncology Group phase I consortium study. Pediatr Blood Cancer. 2010;54(4):538-45.

188.   Ramchandani RP, Wang Y, Booth BP, Ibrahim A, Johnson JR, Rahman A, et al. The role of SN-38 exposure, UGT1A1*28 polymorphism, and baseline bilirubin level in predicting severe irinotecan toxicity. J Clin Pharmacol. 2007;47(1):78-86.

189.   Stewart E, Goshorn R, Bradley C, Griffiths LM, Benavente C, Twarog NR, et al. Targeting the DNA repair pathway in Ewing sarcoma. Cell Rep. 2014;9(3):829-41.

190.   Gatz SA, Rubino J, Rossoni C, Andre N, Aerts I, Thebaud E, et al. AcSé-ESMART: European Proof of Concept Therapeutic Stratification Trial of Molecular Anomalies in Relapsed or Refractory Tumors in Children and Adolescents–Arm D: Olaparib and irinotecan. Journal of Clinical Oncology. 2019;37(15_suppl):10047-.

191.   Federico SM, Stewart E, Coleman JL, Bishop MW, Santana VM, Lam C, et al. Phase I study of talazoparib and irinotecan in children and young adults with recurrent/refractory solid tumors. Journal of Clinical Oncology. 2017;35(15_suppl):10542-.

192.   Fiskus W, Sharma S, Shah B, Portier BP, Devaraj SG, Liu K, et al. Highly effective combination of LSD1 (KDM1A) antagonist and pan-histone deacetylase inhibitor against human AML cells. Leukemia. 2014;28(11):2155-64.

193.   El-Naggar AM, Somasekharan SP, Wang Y, Cheng H, Negri GL, Pan M, et al. Class I HDAC inhibitors enhance YB-1 acetylation and oxidative stress to block sarcoma metastasis. EMBO Rep. 2019;20(12):e48375.

194.   A Phase I/II Clinical Trial of Vidaza With Abraxane in Patients With Advanced/Metastatic Solid Tumors and Breast Cancer. https://ClinicalTrials.gov/show/NCT00748553.

195.   Theisen ER, Pishas KI, Saund RS, Lessnick SL. Therapeutic opportunities in Ewing sarcoma: EWS-FLI inhibition via LSD1 targeting. Oncotarget. 2016;7(14):17616-30.

196.   Lowery CD, Dowless M, Renschler M, Blosser W, VanWye AB, Stephens JR, et al. Broad Spectrum Activity of the Checkpoint Kinase 1 Inhibitor Prexasertib as a Single Agent or Chemopotentiator Across a Range of Preclinical Pediatric Tumor Models. Clin Cancer Res. 2019;25(7):2278-89.

197.   Brenner JC, Feng FY, Han S, Patel S, Goyal SV, Bou-Maroun LM, et al. PARP-1 inhibition as a targeted strategy to treat Ewing's sarcoma. Cancer Res. 2012;72(7):1608-13.

198.   Garnett MJ, Edelman EJ, Heidorn SJ, Greenman CD, Dastur A, Lau KW, et al. Systematic identification of genomic markers of drug sensitivity in cancer cells. Nature. 2012;483(7391):570-5.

199.   Choy E, Butrynski JE, Harmon DC, Morgan JA, George S, Wagner AJ, et al. Phase II study of olaparib in patients with refractory Ewing sarcoma following failure of standard chemotherapy. BMC Cancer. 2014;14:813.

200.   Gill SJ, Travers J, Pshenichnaya I, Kogera FA, Barthorpe S, Mironenko T, et al. Combinations of PARP Inhibitors with Temozolomide Drive PARP1 Trapping and Apoptosis in Ewing's Sarcoma. PLoS One. 2015;10(10):e0140988.

201.   Iniguez AB, Stolte B, Wang EJ, Conway AS, Alexe G, Dharia NV, et al. EWS/FLI Confers Tumor Cell Synthetic Lethality to CDK12 Inhibition in Ewing Sarcoma. Cancer Cell. 2018;33(2):202-16 e6.

202.   Moffat JG, Rudolph J, Bailey D. Phenotypic screening in cancer drug discovery - past, present and future. Nat Rev Drug Discov. 2014;13(8):588-602.

203.   Wilding JL, Bodmer WF. Cancer cell lines for drug discovery and development. Cancer Res. 2014;74(9):2377-84.

204.   Langhans SA. Three-Dimensional in Vitro Cell Culture Models in Drug Discovery and Drug Repositioning. Front Pharmacol. 2018;9:6.

205.   Evans DMT, B. A. 3D Cell Culture Models. In: Hoffman RM, editor. Patient-Derived Mouse Models of Cancer. Molecular and Translational Medicine. 1 ed: Humana Press; 2017.

206.   Eastman A. Improving anticancer drug development begins with cell culture: misinformation perpetrated by the misuse of cytotoxicity assays. Oncotarget. 2017;8(5):8854-66.

207.   Komlodi-Pasztor E, Sackett DL, Fojo AT. Inhibitors targeting mitosis: tales of how great drugs against a promising target were brought down by a flawed rationale. Clin Cancer Res. 2012;18(1):51-63.

208.   Ghandi M, Huang FW, Jane-Valbuena J, Kryukov GV, Lo CC, McDonald ER, 3rd, et al. Next-generation characterization of the Cancer Cell Line Encyclopedia. Nature. 2019;569(7757):503-8.

209.   Smith PK, Krohn RI, Hermanson GT, Mallia AK, Gartner FH, Provenzano MD, et al. Measurement of protein using bicinchoninic acid. Anal Biochem. 1985;150(1):76-85.

210.   M. WJ. The Bicinchoninic Acid (BCA) Assay for Protein Quantitation. In: M. WJ, editor. The Protein Protocols Handbook: Humana Press; 2002. p. 11-4.

211.   Watson JV, Chambers SH, Smith PJ. A pragmatic approach to the analysis of DNA histograms with a definable G1 peak. Cytometry. 1987;8(1):1-8.

212.   Loganathan SN, Tang N, Fleming JT, Ma Y, Guo Y, Borinstein SC, et al. BET bromodomain inhibitors suppress EWS-FLI1-dependent transcription and the IGF1 autocrine mechanism in Ewing sarcoma. Oncotarget. 2016;7(28):43504-17.

213.   Chou DM, Adamson B, Dephoure NE, Tan X, Nottke AC, Hurov KE, et al. A chromatin localization screen reveals poly (ADP ribose)-regulated recruitment of the repressive polycomb and NuRD complexes to sites of DNA damage. Proc Natl Acad Sci U S A. 2010;107(43):18475-80.

214.   Hosseini A, Minucci S. A comprehensive review of lysine-specific demethylase 1 and its roles in cancer. Epigenomics. 2017;9(8):1123-42.

215.   Wang Y, Zhang H, Chen Y, Sun Y, Yang F, Yu W, et al. LSD1 is a subunit of the NuRD complex and targets the metastasis programs in breast cancer. Cell. 2009;138(4):660-72.

216.   Chen Y, Yang Y, Wang F, Wan K, Yamane K, Zhang Y, et al. Crystal structure of human histone lysine-specific demethylase 1 (LSD1). Proc Natl Acad Sci U S A. 2006;103(38):13956-61.

217.   Forneris F, Binda C, Vanoni MA, Battaglioli E, Mattevi A. Human histone demethylase LSD1 reads the histone code. J Biol Chem. 2005;280(50):41360-5.

218.   Zhu D, Holz S, Metzger E, Pavlovic M, Jandausch A, Jilg C, et al. Lysine-specific demethylase 1 regulates differentiation onset and migration of trophoblast stem cells. Nat Commun. 2014;5:3174.

219.   Bennani-Baiti IM, Machado I, Llombart-Bosch A, Kovar H. Lysine-specific demethylase 1 (LSD1/KDM1A/AOF2/BHC110) is expressed and is an epigenetic drug target in chondrosarcoma, Ewing's sarcoma, osteosarcoma, and rhabdomyosarcoma. Hum Pathol. 2012;43(8):1300-7.

220.   Maes T, Mascaro C, Tirapu I, Estiarte A, Ciceri F, Lunardi S, et al. ORY-1001, a Potent and Selective Covalent KDM1A Inhibitor, for the Treatment of Acute Leukemia. Cancer Cell. 2018;33(3):495-511 e12.

221.   Mohammad HP, Smitheman KN, Kamat CD, Soong D, Federowicz KE, Van Aller GS, et al. A DNA Hypomethylation Signature Predicts Antitumor Activity of LSD1 Inhibitors in SCLC. Cancer Cell. 2015;28(1):57-69.

222.   Hitchin JR, Blagg J, Burke R, Burns S, Cockerill MJ, Fairweather EE, et al. Development and evaluation of selective, reversible LSD1 inhibitors derived from fragments. Medchemcomm. 2013;4(11):1513-22.

223.   The Structural Genomics Consortium. GSK-LSD1 A chemical probe for LSD1 2014 [Available from: https://www.thesgc.org/chemical-probes/GSK-LSD1.

224.   Pishas KI, Drenberg CD, Taslim C, Theisen ER, Johnson KM, Saund RS, et al. Therapeutic targeting of KDM1A/LSD1 in Ewing sarcoma with SP-2509 engages the endoplasmic reticulum stress response. Mol Cancer Ther. 2018.

225.   McCabe MT, Ott HM, Ganji G, Korenchuk S, Thompson C, Van Aller GS, et al. EZH2 inhibition as a therapeutic strategy for lymphoma with EZH2-activating mutations. Nature. 2012;492(7427):108-12.

226.   Mosammaparast N, Kim H, Laurent B, Zhao Y, Lim HJ, Majid MC, et al. The histone demethylase LSD1/KDM1A promotes the DNA damage response. J Cell Biol. 2013;203(3):457-70.

227.   Pishas KI, Lessnick SL. Recent advances in targeted therapy for Ewing sarcoma. F1000Res. 2016;5.

228.   Maiques-Diaz A, Spencer GJ, Lynch JT, Ciceri F, Williams EL, Amaral FMR, et al. Enhancer Activation by Pharmacologic Displacement of LSD1 from GFI1 Induces Differentiation in Acute Myeloid Leukemia. Cell Rep. 2018;22(13):3641-59.

229.   Sehrawat A, Gao L, Wang Y, Bankhead A, 3rd, McWeeney SK, King CJ, et al. LSD1 activates a lethal prostate cancer gene network independently of its demethylase function. Proc Natl Acad Sci U S A. 2018.

230.   Harris WJ, Huang X, Lynch JT, Spencer GJ, Hitchin JR, Li Y, et al. The histone demethylase KDM1A sustains the oncogenic potential of MLL-AF9 leukemia stem cells. Cancer Cell. 2012;21(4):473-87.

231.   Vinyard ME, Su C, Siegenfeld AP, Waterbury AL, Freedy AM, Gosavi PM, et al. CRISPR-suppressor scanning reveals a nonenzymatic role of LSD1 in AML. Nat Chem Biol. 2019;15(5):529-39.

232.   Adamo A, Sese B, Boue S, Castano J, Paramonov I, Barrero MJ, et al. LSD1 regulates the balance between self-renewal and differentiation in human embryonic stem cells. Nat Cell Biol. 2011;13(6):652-9.

233.   Kovar H, Alonso J, Aman P, Aryee DN, Ban J, Burchill SA, et al. The first European interdisciplinary ewing sarcoma research summit. Front Oncol. 2012;2:54.

234.   Sonnemann J, Zimmermann M, Marx C, Ebert F, Becker S, Lauterjung ML, et al. LSD1 (KDM1A)-independent effects of the LSD1 inhibitor SP2509 in cancer cells. Br J Haematol. 2017.

235. Baell JB, Holloway GA. New substructure filters for removal of pan assay interference compounds (PAINS) from screening libraries and for their exclusion in bioassays. J Med Chem. 2010;53(7):2719-40.

236. Mould DP, McGonagle AE, Wiseman DH, Williams EL, Jordan AM. Reversible inhibitors of LSD1 as therapeutic agents in acute myeloid leukemia: clinical significance and progress to date. Med Res Rev. 2015;35(3):586-618.

237. Clinical Trial of SP-2577 (Seclidemstat) in Patients With Relapsed or Refractory Ewing Sarcoma.

238. Phase 1 Trial of the LSD1 Inhibitor SP-2577 (Seclidemstat) in Patients With Advanced Solid Tumors.

239. Kim J, Lee Y, Lu X, Song B, Fong KW, Cao Q, et al. Polycomb- and Methylation-Independent Roles of EZH2 as a Transcription Activator. Cell Rep. 2018;25(10):2808-20 e4.

240. Tamaoki J, Takeuchi M, Abe R, Kaneko H, Wada T, Hino S, et al. Splicing- and demethylase-independent functions of LSD1 in zebrafish primitive hematopoiesis. Sci Rep. 2020;10(1):8521.

241. A Study of INCB059872 in Relapsed or Refractory Ewing Sarcoma [Available from: https://ClinicalTrials.gov/show/NCT03514407.

242. Bauer TM, Besse B, Martinez-Marti A, Trigo JM, Moreno V, Garrido P, et al. Phase I, Open-Label, Dose-Escalation Study of the Safety, Pharmacokinetics, Pharmacodynamics, and Efficacy of GSK2879552 in Relapsed/Refractory SCLC. J Thorac Oncol. 2019;14(10):1828-38.

243. Safety, Clinical Activity, Pharmacokinetics (PK) and Pharmacodynamics Study of GSK2879552, Alone or With Azacitidine, in Subjects With High Risk Myelodysplastic Syndromes (MDS).

244. Investigation of GSK2879552 in Subjects With Relapsed/Refractory Small Cell Lung Carcinoma.

245. A Phase I Dose Escalation Study of GSK2879552 in Subjects With Acute Myeloid Leukemia (AML).

246. St. Jude Children's Research H, BioMarin P, Alliance P, Pfizer. Talazoparib Plus Irinotecan With or Without Temozolomide in Children With Refractory or Recurrent Solid Malignancies. 2020.

247. Lawlor ER, Scheel C, Irving J, Sorensen PH. Anchorage-independent multi-cellular spheroids as an in vitro model of growth signaling in Ewing tumors. Oncogene. 2002;21(2):307-18.

248. Palmerini E, Jones RL, Setola E, Picci P, Marchesi E, Luksch R, et al. Irinotecan and temozolomide in recurrent Ewing sarcoma: an analysis in 51 adult and pediatric patients. Acta Oncol. 2018;57(7):958-64.

249. Kiesel BF, Scemama J, Parise RA, Villaruz L, Iffland A, Doyle A, et al. LC-MS/MS assay for the quantitation of the ATR kinase inhibitor VX-970 in human plasma. J Pharm Biomed Anal. 2017;146:244-50.

250. Sakurikar N, Eastman A. Critical reanalysis of the methods that discriminate the activity of CDK2 from CDK1. Cell Cycle. 2016;15(9):1184-8.

251. Charrier JD, Durrant SJ, Golec JM, Kay DP, Knegtel RM, MacCormick S, et al. Discovery of potent and selective inhibitors of ataxia telangiectasia mutated and Rad3 related (ATR) protein kinase as potential anticancer agents. J Med Chem. 2011;54(7):2320-30.

252. Vendetti FP, Lau A, Schamus S, Conrads TP, O'Connor MJ, Bakkenist CJ. The orally active and bioavailable ATR kinase inhibitor AZD6738 potentiates the anti-tumor

effects of cisplatin to resolve ATM-deficient non-small cell lung cancer in vivo. Oncotarget. 2015;6(42):44289-305.

253. Foote KM, Nissink JWM, McGuire T, Turner P, Guichard S, Yates JWT, et al. Discovery and Characterization of AZD6738, a Potent Inhibitor of Ataxia Telangiectasia Mutated and Rad3 Related (ATR) Kinase with Application as an Anticancer Agent. J Med Chem. 2018;61(22):9889-907.

254. Foote KM, Lau A, Nissink JW. Drugging ATR: progress in the development of specific inhibitors for the treatment of cancer. Future Med Chem. 2015;7(7):873-91.

255. Thomas A, Redon CE, Sciuto L, Padiernos E, Ji J, Lee MJ, et al. Phase I Study of ATR Inhibitor M6620 in Combination With Topotecan in Patients With Advanced Solid Tumors. J Clin Oncol. 2018;36(16):1594-602.

256. Memorial Sloan Kettering Cancer C. A Study of the Drugs Prexasertib, Irinotecan, and Temozolomide in People With Desmoplastic Small Round Cell Tumor and Rhabdomyosarcoma. 2022.

257. Soldatenkov VA, Albor A, Patel BK, Dreszer R, Dritschilo A, Notario V. Regulation of the human poly(ADP-ribose) polymerase promoter by the ETS transcription factor. Oncogene. 1999;18(27):3954-62.

258. de Bono J, Ramanathan RK, Mina L, Chugh R, Glaspy J, Rafii S, et al. Phase I, Dose-Escalation, Two-Part Trial of the PARP Inhibitor Talazoparib in Patients with Advanced Germline BRCA1/2 Mutations and Selected Sporadic Cancers. Cancer Discov. 2017;7(6):620-9.

259. Ordonez JL, Amaral AT, Carcaboso AM, Herrero-Martin D, del Carmen Garcia-Macias M, Sevillano V, et al. The PARP inhibitor olaparib enhances the sensitivity of Ewing sarcoma to trabectedin. Oncotarget. 2015;6(22):18875-90.

260. Smith MA, Reynolds CP, Kang MH, Kolb EA, Gorlick R, Carol H, et al. Synergistic activity of PARP inhibition by talazoparib (BMN 673) with temozolomide in pediatric cancer models in the pediatric preclinical testing program. Clin Cancer Res. 2015;21(4):819-32.

261. Investigation of GSK2879552 in Subjects With Relapsed/Refractory Small Cell Lung Carcinoma: https://ClinicalTrials.gov/show/NCT02034123; [

262. Lee HJ, Yoon C, Schmidt B, Park DJ, Zhang AY, Erkizan HV, et al. Combining PARP-1 inhibition and radiation in Ewing sarcoma results in lethal DNA damage. Mol Cancer Ther. 2013;12(11):2591-600.

263. Phase I Study of Olaparib and Temozolomide for Ewings Sarcoma or Rhabdoomyosarcoma.

264. Scott CL, Swisher EM, Kaufmann SH. Poly (ADP-ribose) polymerase inhibitors: recent advances and future development. J Clin Oncol. 2015;33(12):1397-406.

265. Meyer B, Voss KO, Tobias F, Jakob B, Durante M, Taucher-Scholz G. Clustered DNA damage induces pan-nuclear H2AX phosphorylation mediated by ATM and DNA-PK. Nucleic Acids Res. 2013;41(12):6109-18.

266. Porter AG, Janicke RU. Emerging roles of caspase-3 in apoptosis. Cell Death Differ. 1999;6(2):99-104.

267. Harrigan JA, Belotserkovskaya R, Coates J, Dimitrova DS, Polo SE, Bradshaw CR, et al. Replication stress induces 53BP1-containing OPT domains in G1 cells. J Cell Biol. 2011;193(1):97-108.

268. Beaumont KA, Anfosso A, Ahmed F, Weninger W, Haass NK. Imaging- and Flow Cytometry-based Analysis of Cell Position and the Cell Cycle in 3D Melanoma Spheroids. J Vis Exp. 2015(106):e53486.

269.   Aarts M, Sharpe R, Garcia-Murillas I, Gevensleben H, Hurd MS, Shumway SD, et al. Forced mitotic entry of S-phase cells as a therapeutic strategy induced by inhibition of WEE1. Cancer Discov. 2012;2(6):524-39.

270.   Moser R, Xu C, Kao M, Annis J, Lerma LA, Schaupp CM, et al. Functional kinomics identifies candidate therapeutic targets in head and neck cancer. Clin Cancer Res. 2014;20(16):4274-88.

271.   Russell MR, Levin K, Rader J, Belcastro L, Li Y, Martinez D, et al. Combination therapy targeting the Chk1 and Wee1 kinases shows therapeutic efficacy in neuroblastoma. Cancer Res. 2013;73(2):776-84.

272.   Dauphinot L, De Oliveira C, Melot T, Sevenet N, Thomas V, Weissman BE, et al. Analysis of the expression of cell cycle regulators in Ewing cell lines: EWS-FLI-1 modulates p57KIP2and c-Myc expression. Oncogene. 2001;20(25):3258-65.

273.   Panier S, Boulton SJ. Double-strand break repair: 53BP1 comes into focus. Nat Rev Mol Cell Biol. 2014;15(1):7-18.

274.   Chapman JR, Sossick AJ, Boulton SJ, Jackson SP. BRCA1-associated exclusion of 53BP1 from DNA damage sites underlies temporal control of DNA repair. J Cell Sci. 2012;125(Pt 15):3529-34.

275.   Krajewska M, Heijink AM, Bisselink YJ, Seinstra RI, Sillje HH, de Vries EG, et al. Forced activation of Cdk1 via wee1 inhibition impairs homologous recombination. Oncogene. 2013;32(24):3001-8.

276.   Toledo LI, Altmeyer M, Rask MB, Lukas C, Larsen DH, Povlsen LK, et al. ATR prohibits replication catastrophe by preventing global exhaustion of RPA. Cell. 2013;155(5):1088-103.

277.   May WA, Grigoryan RS, Keshelava N, Cabral DJ, Christensen LL, Jenabi J, et al. Characterization and drug resistance patterns of Ewing's sarcoma family tumor cell lines. PLoS One. 2013;8(12):e80060.

278.   Aryee DN, Niedan S, Ban J, Schwentner R, Muehlbacher K, Kauer M, et al. Variability in functional p53 reactivation by PRIMA-1(Met)/APR-246 in Ewing sarcoma. Br J Cancer. 2013;109(10):2696-704.

279.   Roos WP, Batista LF, Naumann SC, Wick W, Weller M, Menck CF, et al. Apoptosis in malignant glioma cells triggered by the temozolomide-induced DNA lesion O6-methylguanine. Oncogene. 2007;26(2):186-97.

280.   Roos WP, Kaina B. DNA damage-induced cell death by apoptosis. Trends Mol Med. 2006;12(9):440-50.

281.   Stoll G, Surdez D, Tirode F, Laud K, Barillot E, Zinovyev A, et al. Systems biology of Ewing sarcoma: a network model of EWS-FLI1 effect on proliferation and apoptosis. Nucleic Acids Res. 2013;41(19):8853-71.

282.   Bertoli C, Herlihy AE, Pennycook BR, Kriston-Vizi J, de Bruin RAM. Sustained E2F-Dependent Transcription Is a Key Mechanism to Prevent Replication-Stress-Induced DNA Damage. Cell Rep. 2016;15(7):1412-22.

283.   Schwentner R, Papamarkou T, Kauer MO, Stathopoulos V, Yang F, Bilke S, et al. EWS-FLI1 employs an E2F switch to drive target gene expression. Nucleic Acids Res. 2015;43(5):2780-9.

284.   Suva ML, Riggi N, Stehle JC, Baumer K, Tercier S, Joseph JM, et al. Identification of cancer stem cells in Ewing's sarcoma. Cancer Res. 2009;69(5):1776-81.

285.   Goss KL, Gordon DJ. Gene expression signature based screening identifies ribonucleotide reductase as a candidate therapeutic target in Ewing sarcoma. Oncotarget. 2016;7(39):63003-19.

286.   Chabes A, Thelander L. Controlled protein degradation regulates ribonucleotide reductase activity in proliferating mammalian cells during the normal cell cycle and in response to DNA damage and replication blocks. J Biol Chem. 2000;275(23):17747-53.

287.   Pontarin G, Ferraro P, Hakansson P, Thelander L, Reichard P, Bianchi V. p53R2-dependent ribonucleotide reduction provides deoxyribonucleotides in quiescent human fibroblasts in the absence of induced DNA damage. J Biol Chem. 2007;282(23):16820-8.

288.   Cho EC, Kuo ML, Liu X, Yang L, Hsieh YC, Wang J, et al. Tumor suppressor FOXO3 regulates ribonucleotide reductase subunit RRM2B and impacts on survival of cancer patients. Oncotarget. 2014;5(13):4834-44.

289.   Nakano K, Balint E, Ashcroft M, Vousden KH. A ribonucleotide reductase gene is a transcriptional target of p53 and p73. Oncogene. 2000;19(37):4283-9.

290.   Warren NJH, Eastman A. Comparison of the different mechanisms of cytotoxicity induced by checkpoint kinase I inhibitors when used as single agents or in combination with DNA damage. Oncogene. 2020;39(7):1389-401.

291.   Baek N, Seo OW, Kim M, Hulme J, An SS. Monitoring the effects of doxorubicin on 3D-spheroid tumor cells in real-time. Onco Targets Ther. 2016;9:7207-18.

292.   Dohjima T, Lee NS, Li H, Ohno T, Rossi JJ. Small interfering RNAs expressed from a Pol III promoter suppress the EWS/Fli-1 transcript in an Ewing sarcoma cell line. Mol Ther. 2003;7(6):811-6.

293.   Chansky HA, Barahmand-Pour F, Mei Q, Kahn-Farooqi W, Zielinska-Kwiatkowska A, Blackburn M, et al. Targeting of EWS/FLI-1 by RNA interference attenuates the tumor phenotype of Ewing's sarcoma cells in vitro. J Orthop Res. 2004;22(4):910-7.

294.   Kovar H, Ban J, Pospisilova S. Potentials for RNAi in sarcoma research and therapy: Ewing's sarcoma as a model. Semin Cancer Biol. 2003;13(4):275-81.

295.   Hu-Lieskovan S, Heidel JD, Bartlett DW, Davis ME, Triche TJ. Sequence-specific knockdown of EWS-FLI1 by targeted, nonviral delivery of small interfering RNA inhibits tumor growth in a murine model of metastatic Ewing's sarcoma. Cancer Res. 2005;65(19):8984-92.

296.   Carrillo J, Garcia-Aragoncillo E, Azorin D, Agra N, Sastre A, Gonzalez-Mediero I, et al. Cholecystokinin down-regulation by RNA interference impairs Ewing tumor growth. Clin Cancer Res. 2007;13(8):2429-40.

297.   Lessnick SL, Dacwag CS, Golub TR. The Ewing's sarcoma oncoprotein EWS/FLI induces a p53-dependent growth arrest in primary human fibroblasts. Cancer Cell. 2002;1(4):393-401.

298.   Deneen B, Denny CT. Loss of p16 pathways stabilizes EWS/FLI1 expression and complements EWS/FLI1 mediated transformation. Oncogene. 2001;20(46):6731-41.

299.   Gordon DJ, Motwani M, Pellman D. Modeling the initiation of Ewing sarcoma tumorigenesis in differentiating human embryonic stem cells. Oncogene. 2016;35(24):3092-102.

300.   von Levetzow C, Jiang X, Gwye Y, von Levetzow G, Hung L, Cooper A, et al. Modeling initiation of Ewing sarcoma in human neural crest cells. PLoS One. 2011;6(4):e19305.

301.   Garcia-Dominguez DJ, Hontecillas-Prieto L, Leon EA, Sanchez-Molina S, Rodriguez-Nunez P, Moron FJ, et al. An inducible ectopic expression system of EWSR1-FLI1 as a tool for understanding Ewing sarcoma oncogenesis. PLoS One. 2020;15(6):e0234243.

302.   Mendiola M, Carrillo J, Garcia E, Lalli E, Hernandez T, de Alava E, et al. The orphan nuclear receptor DAX1 is up-regulated by the EWS/FLI1 oncoprotein and is highly expressed in Ewing tumors. Int J Cancer. 2006;118(6):1381-9.

303.   Hu-Lieskovan S, Zhang J, Wu L, Shimada H, Schofield DE, Triche TJ. EWS-FLI1 fusion protein up-regulates critical genes in neural crest development and is responsible for the observed phenotype of Ewing's family of tumors. Cancer Res. 2005;65(11):4633-44.

304.   Hartono SR, Malapert A, Legros P, Bernard P, Chedin F, Vanoosthuyse V. The Affinity of the S9.6 Antibody for Double-Stranded RNAs Impacts the Accurate Mapping of R-Loops in Fission Yeast. J Mol Biol. 2018;430(3):272-84.

305.   Tang SW, Bilke S, Cao L, Murai J, Sousa FG, Yamade M, et al. SLFN11 Is a Transcriptional Target of EWS-FLI1 and a Determinant of Drug Response in Ewing Sarcoma. Clin Cancer Res. 2015;21(18):4184-93.

306.   Lovejoy CA, Li W, Reisenweber S, Thongthip S, Bruno J, de Lange T, et al. Loss of ATRX, genome instability, and an altered DNA damage response are hallmarks of the alternative lengthening of telomeres pathway. PLoS Genet. 2012;8(7):e1002772.

307.   Romo-Morales A, Aladowicz E, Blagg J, Gatz SA, Shipley JM. Catalytic inhibition of KDM1A in Ewing sarcoma is insufficient as a therapeutic strategy. Pediatr Blood Cancer. 2019;66(9):e27888.

308.   Tomazou EM, Sheffield NC, Schmidl C, Schuster M, Schonegger A, Datlinger P, et al. Epigenome mapping reveals distinct modes of gene regulation and widespread enhancer reprogramming by the oncogenic fusion protein EWS-FLI1. Cell Rep. 2015;10(7):1082-95.

309.   McBride MJ, Pulice JL, Beird HC, Ingram DR, D'Avino AR, Shern JF, et al. The SS18-SSX Fusion Oncoprotein Hijacks BAF Complex Targeting and Function to Drive Synovial Sarcoma. Cancer Cell. 2018;33(6):1128-41 e7.

310.   Gryder BE, Yohe ME, Chou HC, Zhang X, Marques J, Wachtel M, et al. PAX3-FOXO1 Establishes Myogenic Super Enhancers and Confers BET Bromodomain Vulnerability. Cancer Discov. 2017;7(8):884-99.

311.   Hones JM, Botezatu L, Helness A, Vadnais C, Vassen L, Robert F, et al. GFI1 as a novel prognostic and therapeutic factor for AML/MDS. Leukemia. 2016;30(6):1237-45.

312.   Comet I, Riising EM, Leblanc B, Helin K. Maintaining cell identity: PRC2-mediated regulation of transcription and cancer. Nat Rev Cancer. 2016.

313.   Simon JA, Lange CA. Roles of the EZH2 histone methyltransferase in cancer epigenetics. Mutat Res. 2008;647(1-2):21-9.

314.   Pfister SX, Ashworth A. Marked for death: targeting epigenetic changes in cancer. Nat Rev Drug Discov. 2017;16(4):241-63.

315.   Nacev BA, Jones KB, Intlekofer AM, Yu JSE, Allis CD, Tap WD, et al. The epigenomics of sarcoma. Nat Rev Cancer. 2020.

316.   Chong S, Dugast-Darzacq C, Liu Z, Dong P, Dailey GM, Cattoglio C, et al. Imaging dynamic and selective low-complexity domain interactions that control gene transcription. Science. 2018;361(6400).

317.   Bates SE. Epigenetic Therapies for Cancer. N Engl J Med. 2020;383(7):650-63.

318.   Selvanathan SP, Graham GT, Grego AR, Baker TM, Hogg JR, Simpson M, et al. EWS-FLI1 modulated alternative splicing of ARID1A reveals novel oncogenic function through the BAF complex. Nucleic Acids Res. 2019;47(18):9619-36.

319.   Chory EJ, Kirkland JG, Chang CY, D'Andrea VD, Gourisankar S, Dykhuizen EC, et al. Chemical Inhibitors of a Selective SWI/SNF Function Synergize with ATR Inhibition in Cancer Cell Killing. ACS Chem Biol. 2020;15(6):1685-96.

320.   Papillon JPN, Nakajima K, Adair CD, Hempel J, Jouk AO, Karki RG, et al. Discovery of Orally Active Inhibitors of Brahma Homolog (BRM)/SMARCA2 ATPase Activity for the Treatment of Brahma Related Gene 1 (BRG1)/SMARCA4-Mutant Cancers. J Med Chem. 2018;61(22):10155-72.

321.   Lasko LM, Jakob CG, Edalji RP, Qiu W, Montgomery D, Digiammarino EL, et al. Discovery of a selective catalytic p300/CBP inhibitor that targets lineage-specific tumours. Nature. 2017;550(7674):128-32.

322.   Kai M. Roles of RNA-Binding Proteins in DNA Damage Response. Int J Mol Sci. 2016;17(3):310.

323.   Loktev A, Shipley JM. Desmoplastic small round cell tumor (DSRCT): emerging therapeutic targets and future directions for potential therapies. Expert Opin Ther Targets. 2020;24(4):281-5.

324.   Mellado-Lagarde M, Federico SM, Tinkle C, Shelat A, Stewart E. PARP inhibitor combination therapy in desmoplastic small round cell tumors. Journal of Clinical Oncology. 2017;35(15_suppl):e23212-e.

325.   Bulbul A, Fahy BN, Xiu J, Rashad S, Mustafa A, Husain H, et al. Desmoplastic Small Round Blue Cell Tumor: A Review of Treatment and Potential Therapeutic Genomic Alterations. Sarcoma. 2017;2017:1278268.

326.   Stuart-Buttle CE, Smart CJ, Pritchard S, Martin D, Welch IM. Desmoplastic small round cell tumour: a review of literature and treatment options. Surg Oncol. 2008;17(2):107-12.

327.   Weinstein IB. Cancer. Addiction to oncogenes--the Achilles heal of cancer. Science. 2002;297(5578):63-4.

328.   Jain M, Arvanitis C, Chu K, Dewey W, Leonhardt E, Trinh M, et al. Sustained loss of a neoplastic phenotype by brief inactivation of MYC. Science. 2002;297(5578):102-4.

329.   Keller RR, Gunther EJ. Evolution of Relapse-Proficient Subclones Constrained by Collateral Sensitivity to Oncogene Overdose in Wnt-Driven Mammary Cancer. Cell Rep. 2019;26(4):893-905 e4.

330.   Amin AD, Rajan SS, Groysman MJ, Pongtornpipat P, Schatz JH. Oncogene Overdose: Too Much of a Bad Thing for Oncogene-Addicted Cancer Cells. Biomark Cancer. 2015;7(Suppl 2):25-32.

Appendices

Attached copy of publication from the work in this thesis: Romo-Morales A, Aladowicz E, Blagg J, Gatz SA, Shipley JM. Catalytic inhibition of KDM1A in Ewing sarcoma is insufficient as a therapeutic strategy. Pediatr Blood Cancer. 2019;66(9):e27888.

RESEARCH ARTICLE

Pediatric Blood & Cancer

aspho
The American Society of
Pediatric Hematology/Oncology

WILEY

Check for updates

Catalytic inhibition of KDM1A in Ewing sarcoma is insufficient as a therapeutic strategy

Antonio Romo-Morales[1] (iD) | Ewa Aladowicz[1] | Julian Blagg[2] | Susanne A. Gatz[1,3] | Janet M. Shipley[1]

[1]Sarcoma Molecular Pathology Team, Divisions of Molecular Pathology and Cancer Therapeutics, The Institute of Cancer Research, London, UK

[2]Cancer Research UK Cancer Therapeutics Unit, Division of Cancer Therapeutics, The Institute of Cancer Research, London, UK

[3]Cancer Research UK Clinical Trials Unit, Institute of Cancer and Genomic Sciences, University of Birmingham, Edgbaston, Birmingham, UK

Correspondence
Janet Shipley, Sarcoma Molecular Pathology Team, Divisions of Molecular Pathology and Cancer Therapeutics, 15 Cotswold Road, Sutton, Surrey SM2 5NG, UK.
Email: janet.shipley@icr.ac.uk

Abstract

Background: Ewing sarcoma and desmoplastic small round cell tumors (DSRCT) are rare and clinically aggressive sarcomas usually characterized by oncogenic fusion proteins involving EWS. Emerging studies of Ewing sarcoma have demonstrated EWS-FLI1-driven chromatin remodeling as a key aspect of tumorigenicity. In particular, the lysine-specific demethylase KDM1A/LSD1 is linked to transcriptional regulation of target genes orchestrated by the EWS portion of the fusion protein interacting with repressive chromatin-remodeling complexes. Consistent with this model, depletion of KDM1A supports it is a molecular therapeutic target in Ewing sarcoma cells, but effective drugs need to be identified.

Procedure: A comprehensive phenotypic analysis of the effects of catalytic KDM1A inhibitors ORY-1001 and GSK2879552, including clinically relevant doses, was carried out in 2D and 3D spheroid models of Ewing sarcoma and DSRCT.

Results: Catalytic inhibition of KDM1A did not affect cell viability in 2D and 3D assays and had no impact on invasion in a 3D assay.

Conclusions: Overall, evidence presented here does not support inhibition of KDM1A catalytic demethylase activity as an effective therapeutic strategy for Ewing sarcoma or DSRCT. However, roles of KDM1A beyond its demethylase activity should be considered for these sarcomas.

KEYWORDS

3D models, Ewing sarcoma, GSK2879552, histone demethylase, KDM1A/LSD1, ORY-1001

1 | INTRODUCTION

Ewing sarcoma is a rare and highly aggressive sarcoma affecting children and young adults. Recent developments in our understanding of the molecular mechanisms underlying this disease have not yet translated into significant improvements in patients' outcomes, and treatment has remained unchanged.[1]

Ewing sarcoma is characterized by chromosomal rearrangements between the gene *EWSR1* and gene members of the ETS-domain family of transcription factors; approximately 85% to 90% of Ewing sarcoma tumors exhibit *FLI1* as the *EWSR1* fusion partner.[2] Additional *EWSR1* chromosomal translocations exist, such as fusion with *WT1*, found in 95% of cases of desmoplastic small round cell tumor (DSRCT).[3,4]
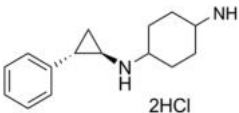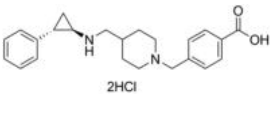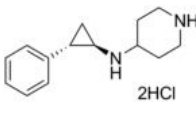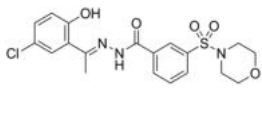
EWS-FLI1 has been identified as the main driver of Ewing sarcoma tumorigenicity through unique pioneer properties that increase genome-wide chromatin accessibility at GGAA microsatellite repeats.[5–7] This is achieved through histone-modifying enzymes and chromatin-remodeling complexes changing the epigenetic status

---

TABLE 1 KDM1A inhibitors

Compound	ORY-1001	GSK2879552	GSK-LSD1	SP2509
Structure				
	IC_{50}: 18 nM	K_{iapp} of 1.7 μM	IC_{50}: 16 nM	IC_{50}: 13 nM
Mechanism of action	Irreversible inhibitor covalently modifying the FAD cofactor (22)	Irreversible inhibitor covalently modifying the FAD cofactor (23)	Irreversible inhibitor covalently modifying the FAD cofactor (23)	Reversible noncompetitive inhibitor (43)
Clinical status	Phase I/IIa study in AML (EudraCT Number: 2013-002447-29) and SCLC (NCT02913443)	Phase I studies in SCLC (NCT02034123) and AML (NCT02177812) have been terminated because the risk benefit does not favor continuation. Phase I/II study in MDS (NCT02929498)	NA	NA

of genomic regions and creating de novo enhancer elements that establish the Ewing sarcoma transcriptional signature.[8–10] In particular, the nucleosome remodeling deacetylase complex (NuRD; also known as Mi-2), a multi-subunit chromatin-remodeling complex commonly associated with repression of transcriptional activity, was identified to be relevant in the silencing of EWS-FLI1 target genes.[10,11] Essentially, the catalytic activity in the NuRD complex involves deacetylation by histone deacetylase 2 (HDAC2) and 3 (HDAC3), coupled with demethylation by lysine-specific demethylase 1 (KDM1A; also referred to as LSD1, AOF2, and BHC110).[9,10]

The working model proposed by Sankar et al consists of EWS-FLI1 binding to promoters of repressed target genes, followed by the recruitment of the NuRD complex through interaction between its subunits chromodomain 4 (CHD4) and metastasis-associated protein 1 (MTA1) and the EWS portion of the fusion protein. Following treatment with SP2509, a tool compound targeting KDM1A, the EWS-FLI1-driven transcriptional signature of both upregulated and downregulated genes was reversed.[10] Inhibition of KDM1A with SP2509 also resulted in apoptosis and disruption of the oncogenic phenotype.[10]

KDM1A is a well-characterized histone lysine demethylase belonging to the family of flavin-dependent amine oxidases that has an important role in stem cell maintenance through transcriptional repression.[12-14] This demethylase is also overexpressed in Ewing sarcoma and other sarcomas including DSRCT and rhabdomyosarcoma.[15-17] Moreover, the key role of the EWS portion of the fusion protein in the interaction with repressive chromatin-remodeling complexes makes inclusion of DSRCT, possessing the EWS-WT1 fusion, relevant to study alongside EWS-FLI1 in Ewing sarcoma.[8,9]

Currently, the KDM1A inhibitor ORY-1001 is being investigated in the clinic in adult patients with acute myeloid leukemia (AML) and small cell lung cancer (SCLC). In addition, a trial with GSK2879552 has recently been stopped citing that the benefits do not outweigh the risk in relapsed refractory SCLC[18–21] (Table 1). These compounds are potent irreversible inhibitors of KDM1A, which covalently modify the FAD cofactor of this demethylase to inhibit catalytic activity.[22,23]

However, their use as a therapeutic strategy for Ewing sarcoma has not been comprehensively assessed. Given the rationale for targeting KDM1A in Ewing sarcoma, in this work, we sought to test the potential for repurposing these clinical candidates against KDM1A as a novel treatment for these sarcomas.

The current report investigates the effect of catalytic inhibitors of KDM1A on cell viability in 2D and 3D models, and invasion using a 3D spheroid assay. Importantly, we show that clinically available inhibitors of KDM1A catalytic demethylase activity, despite having an effect on viability at a low nanomolar range against leukemia cell lines, do not have an effect in preclinical models of Ewing sarcoma and DSRCT. Therefore, catalytic inhibition of KDM1A should not be considered as a therapeutic strategy for Ewing sarcoma.

2 | METHODS

2.1 | Cell lines

Ewing sarcoma cell lines A673 and TC71 were kindly provided by Dr. Enrique de Álava (IBiS, Spain). The desmoplastic small round cell tumor cell line JN-DSRCT-1[24] was obtained from Sean B. Lee, and leukemia cell lines MV(4;11) and MOLT-4 were obtained from DSMZ, Germany. Cell lines used were cultured in the appropriate media supplemented with 10% fetal bovine serum (Gibco, Thermo Fisher Scientific, UK), 1% penicillin–streptomycin (Gibco), and 1% GlutaMAX (Gibco) in a humidified incubator at 37°C and 5% CO_2. Standard procedures were utilized for maintenance, freezing, and thawing. Cells were Mycoplasma-free tested with the PlasmoTest Mycoplasma Detection Kit (InvivoGen, UK) according to instructions. Cell lines were authenticated with short tandem repeat testing using the GenePrint 10 system (Promega, UK).

2.2 | Reagents and drug treatments

The following KDM1A inhibitors were used: ORY-1001, GSK2879552, GSK-LSD1, and SP2509 (Table 1; SelleckChem, UK). Stocks (10 mM)

were prepared in H_2O for ORY-1001 and GSK2879552, and in DMSO for GSK-LSD1 and SP2509 and stored at −80°C.

2.3 | Cell viability assays

A673 cells were seeded at 2000 cells/well, TC71 cells at 4000 cells/well, and JN-DSRCT-1 at 4000 cells/well in 96-well plates for viability assays (six replicates for each condition). Viability was assessed by an MTS (3-(4,5-dimethyl-2-yl)-5-(3-carboxymethoxyphenyl)-2-(4-sulfophenyl)-2H-tetrazolium, inner salt) assay using the CellTiter 96 Aqueous One Solution Cell Proliferation Assay (Promega). Media were replaced with 100 μL of Opti-MEM and 20 μL of CellTiter 96 Aqueous One Solution Cell Proliferation Assay. Plates were incubated for two hours in normal culturing conditions prior to measuring the absorbance of each well at 492 nm.

For MV(4;11) and MOLT-4 viability assays, cells were seeded at 100 000/well (6-well plate) and cultured for the indicated time. Viable cell counts were determined by Trypan blue assay (Sigma-Aldrich, UK).

2.4 | 3D spheroid culture

Three-dimensional spheroids were generated and cultured using the GravityTRAP ULA Plate 96-well (PerkinElmer, UK) unless otherwise indicated. Prior to seeding, wells were pre-wet with 40 μL of medium. One thousand cells in 70 μL were seeded into each well. Plates were spun for two minutes at 250 RCF to remove trapped air bubbles. Routine medium changes were performed every 48 hours by carefully aspirating the medium from the ledge at the inside wall of the well and replenishing it with fresh medium.

2.5 | Image analysis of 3D spheroids

Digital images of spheroids were captured throughout the duration of the experiments using an IN Cell Analyzer 2200 imaging system (GE Healthcare Life Sciences, UK), and the surface area was assessed at the focal plane with maximum diameter with IN Cell Investigator IN Developer Toolbox (GE Healthcare Life Sciences).

2.6 | Western blot analysis

2.6.1 | H3K4me2 immunoblot

Following treatment, 2.5×10^5 cells were lysed with 50 μL of 3× Laemmli buffer made up with 2 mL of 1 M Tris Base pH 6.8, 3 mL of 100% Glycerol, 8 mL of 10% SDS, 300 μL of 1% bromophenol blue, and 400 μL of β-mercaptoethanol (freshly added at the time of whole-cell lysate preparation).

Standard protein extraction with cell lysis buffer (Cell Signaling Technology, UK) and Western blot analysis techniques were used for remaining Western blots. Five to 30 micrograms of protein extract or 5 μL of whole-cell lysate in 3X Laemmli buffer was loaded into wells of a NuPAGE 4% to 12% Bis-Tris protein gels (Invitrogen, Thermo Fisher Scientific, UK). Protein gels were transferred onto PVDF membranes with iBlot2 transfer stacks on the iBlot2 transfer system (Invitrogen)

following the manufacturer's instructions. The iBlot2 transfer system was run at 20 V for seven minutes.

Densitometry values for each band were normalized to total protein or housekeeping control of the control sample band and relative to the indicated control. Western blots are representative of at least two independent repeats.

2.7 | 3D invasion assay

A673 and TC71 cells were seeded at a density of 500 cells per well in ultra-low attachment (ULA) round-bottom 96-well plates (Corning, UK). After three days of culturing, spheroids were treated with KDM1A inhibitors at the indicated concentration for 10 days. Fifty microliters of medium was removed from each well and replaced with 50 μL of fresh medium with drug every 48 hours. Following treatment, 50 μL of medium was removed and carefully replaced with 50 μL of Matrigel (Corning) containing drug, achieving a final concentration of Matrigel of 4.5 mg/mL. Plates were then incubated at 37°C and 5% CO_2 in an IncuCyte Zoom (Sartorius, UK) for 48 hours where images were taken every hour to monitor invasion.

2.8 | qRT-PCR

RNA was extracted with TRIzol according to the manufacturer's protocol.[25] A673 cell line cDNA was synthesized using the High Capacity cDNA Reverse Transcriptase kit (Applied Biosystems, CA, USA) following the manufacturer's instructions. Multiplex PCR reactions were set up in triplicate in 384-well optical-reaction PRC plates (Applied Biosystems) and run on a ViiA 7 Real-Time PCR System (Applied Biosystems, CA, USA). The following TaqMan probes were used: LOX Hs00942480_m1, TGFBR2 Hs00234253_m1, HMOX1 Hs01110250_m1, *E2F1* Hs00153451_m1, and *CAV1* Hs00971716_m1. Human RPLPO endogenous control (Applied Biosystems, CA, USA) was used to normalize gene expression.

2.9 | Statistical analysis

GraphPad PRISM 7 and R studio 3.3.2 were used to carry out the statistical analyses. Error bars represent means ± standard deviation from various independent experiments as indicated in figure legends. Statistical significance was measured by one-way ANOVA with post hoc Sidak test for multiple comparisons and two-way ANOVA with post hoc Dunnett test and Sidak test where applicable. $P < 0.05$ was considered significant and indicated by *, $P < 0.01$ is indicated by **, $P < 0.001$ is indicated by ***, and $P < 0.0001$ is indicated by ****.

3 | RESULTS

Presently, there is no evidence demonstrating whether the clinical drug candidates for KDM1A have activity in preclinical models of Ewing sarcoma. To begin to address this question, Ewing sarcoma cell lines A673 and TC71 were treated with compounds for 96 hours to investigate the effect of KDM1A inhibition on cell viability. The cell lines tested

showed no sensitivity to treatment with the irreversible inhibitors of KDM1A demethylase function: ORY-1001 and GSK2879552 (Figure 1). Conversely, treatment with tool compound SP2509 revealed a rapid decrease in viability with GI50s in the submicromolar range (A673: 123 nM and TC71: 355 nM). Morphological assessment of cells following treatment with clinical drug candidates showed no differences between treated and untreated. Cell morphology in the SP2509-treated cells was consistent with apoptosis (Figure S1A).[9,10] These effects were replicated in the DSRCT cell line, only showing sensitivity to SP2509 and not to the clinical drug candidates (Figure S1B). To address the discrepancy between the KDM1A inhibitors, a chemical probe validated as a potent and selective inhibitor of KDM1A catalytic demethylase activity (GSK-LSD1) was also tested in these sarcoma cell lines (http://www.thesgc.org/chemical-probes/LSD1).[23,26] Again, treatment had no meaningful effect on cell viability, with only a 50% reduction at 10 μM in one cell line (TC71; Figure 1; Supporting Information Figure S1C). KDM1A protein levels were unaffected following treatment with clinical drug candidates ORY-1001 and GSK2879552 after 48, 72, 96, and 168 hours (Supporting Information Figure S1D–S1E).

Importantly, consistent with their in vitro inhibition of KDM1A demethylase activity, all four compounds were able to modulate KDM1A-mediated demethylation of the H3K4 methyl mark, a well-characterized KDM1A substrate.[15] Following 72 hours of treatment with 2 μM for all drugs, including the tool compound GSK-LSD1, there was an increase in the global levels of H3K4me2 in both Ewing sarcoma cell lines (Figure 1 and 1D). Furthermore, to investigate the impact on EWS-FLI1-driven transcription, we selected downstream target genes of the fusion protein and assessed by qRT-PCR following treatment with ORY-1001 and GSK2879552. Extended exposure of up to two weeks (336 hours) was conducted to ensure prolonged catalytic inhibition. We did not observe a biologically relevant change in expression of five target genes at a range of time points following treatment with ORY-1001 and GSK2879552 at 2 and 10 μM, despite statistical significance (Figure 1F). As a positive control, treatment with tool compound SP2509 (250 nM) reversed expression of *LOX* and *HMOX1* in agreement with previous reports, but not *TGFBR2* or EWS-FLI1 activated genes *E2F1* and *CAV1* (Supporting Information Figure S1F–S1H),[9,10] possibly due to the lower concentration used in our experiments.

To further demonstrate compound activity, we assessed the response of leukemia cells, previously shown to be sensitive to inhibition of KDM1A catalytic function by ORY-1001 in the nanomolar range.[22] In agreement with published findings, the clinical candidate ORY-1001, as well as chemical probe GSK-LSD1, showed a reduction in cell viability upon treatment with compound at 10 nM concentrations in two leukemia cell lines (Supporting Information Figure S2A and S2B). The clinical candidate GSK2879552 also decreased cell viability at 2 μM (Supporting Information Figure S2C).

To perform a more comprehensive evaluation of the effect of KDM1A inhibition, assessment of cell viability experiments was expanded to 3D models of Ewing sarcoma. Three-dimensional cell culture systems have become more prominent in preclinical studies due to

their ability to more closely represent tissue compartments and enable longer experimental time frames.[27] Tumor spheroids, for example, can recapitulate aspects of the tumor microenvironment that ultimately influence drug response.[28] A673 spheroid cultures were treated with ORY-1001 and SP2509 for 10 days with a dose range between 0.3 and 10 μM (Figure 2 and 2B). Again, no effect on growth was observed with the irreversible inhibitor of KDM1A catalytic function ORY-1001, whereas SP2509 was active, albeit at higher concentrations compared with 2D cultures (Figure 2 and 2B). Drugs targeting epigenetic modifying enzymes often require prolonged inhibition for maximal drug potency and response to treatment.[22,23,29] We therefore additionally treated spheroids for up to 21 days with a maximum concentration of 100 μM of both clinical candidates (ORY-1001 and GSK2879552). Both clinical candidates had no effect upon spheroid growth (Figure 2 and 2E), even in the extended assay.

Finally, KDM1A has been reported to have a role in migration and invasion.[30] To complete the phenotypic assessment of KDM1A inhibition, we evaluated if Ewing sarcoma cells showed a change in their invasive phenotype upon inhibition of KDM1A catalytic demethylase activity. A673 and TC71 spheroids were pretreated for 10 days with the KDM1A inhibitors, and subsequently cultured in a Matrigel matrix, in which invasion was monitored for a further 48 hours. A comparison of the total spheroid area indicated that KDM1A inhibition had no impact on the invaded area (Figure 3 and 3B; Supporting Information Figure S3). Consistent with our previous results, the measured spheroid area was not affected in the 10-day pretreatment with either 2 μM or 10 μM concentrations of compound (Figure 3; Supporting Information Figure S3). Again, we included the chemical probe GSK-LSD1 in the assay; it also had no effect on invasion (Figure 3 and 3B; Supporting Information Figure S3).

4 | DISCUSSION

The Ewing sarcoma gene-expression profile heavily relies on EWS-FLI1 coordinating vast epigenetic rewiring through the recruitment and activity of chromatin-remodeling complexes.[7,8,31] In this context, KDM1A, an active subunit of the NuRD complex, has been reported to have an important role in repressing and activating target genes of the fusion protein EWS-FLI1.[9,10] The functional role of KDM1A in Ewing sarcoma oncogenesis, alongside high expression in this and other sarcomas such as DSRCT, has made it a promising therapeutic target.[32,33] In light of this, our aim was to assess the therapeutic potential of KDM1A inhibitors (ORY-1001 and GSK2879552) in Ewing sarcoma models.

Global or promoter-specific accumulation of methylation of H3K4 is not always seen following KDM1A inhibition regardless of decreased KDM1A activity.[23,34] However, in our findings, the global change in H3K4me2 upon treatment with all KDM1A inhibitors demonstrated capacity to effectively inhibit KDM1A catalytic activity. Importantly, this did not translate into reversal of expression of EWS-FLI1 downstream target genes by ORY-1001 and GSK2879552 analyzed by qRT-PCR.
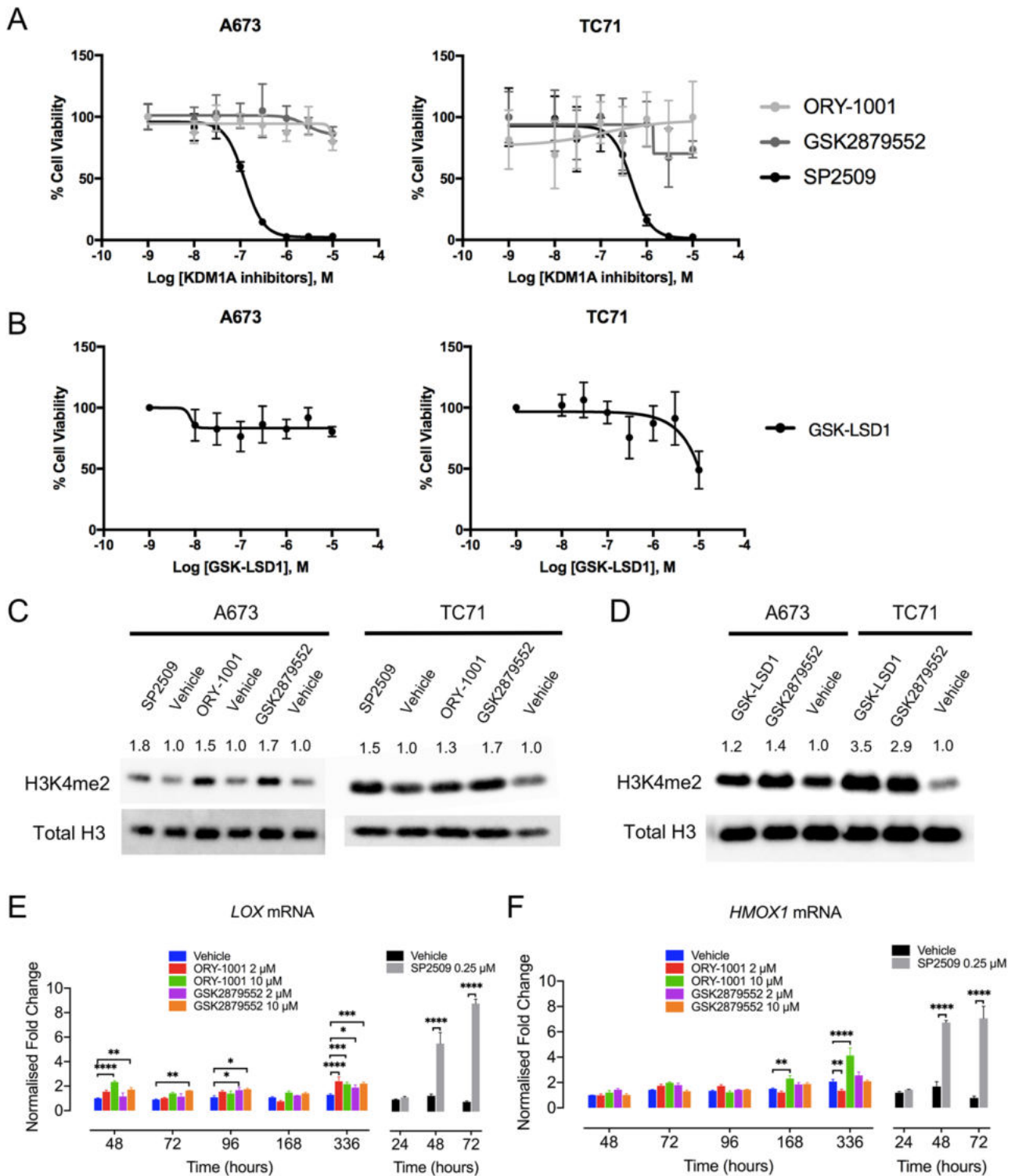
FIGURE 1 Effects of KDM1A inhibition on Ewing sarcoma cell lines. (A–B) Ewing sarcoma cell lines A673 and TC71 were exposed to a range of concentrations of KDM1A inhibitors for 96 hours. Cell viability was assessed by MTS assay. Means ± SD of 6 replicates; graphs are representative of three independent repeats. (C–D) Western blot of H3K4me2 of A673 and TC71 cell lines treated with KDM1A inhibitors (SP2509, ORY-1001, GSK2879552, and GSK-LSD1) (2 μM) and their respective vehicle controls. Densitometry values shown above each blot were normalized to total H3 and relative to each vehicle control. Western blots are representative of at least two independent repeats. (E–F) Effect of KDM1A inhibitors on EWS-FLI1 target genes expression. qRT-PCR analysis of *LOX* and *HMOX1* in A673 cells treated with vehicle or KDM1A inhibitors ORY-1001 (2 μM, 10 μM), GSK2879552 (2 μM, 10 μM), and SP2509 (250 nM). Normalized fold change was adjusted to human *RPLPO* endogenous control. Means ± SD of three replicates. Data are representative of two independent repeats. Statistical analysis: two-way ANOVA with Dunnett and Sidak multiple comparisons test, not significant comparisons are not shown; * $P < 0.05$; ** $P < 0.01$; *** $P < 0.001$; **** $P < 0.0001$
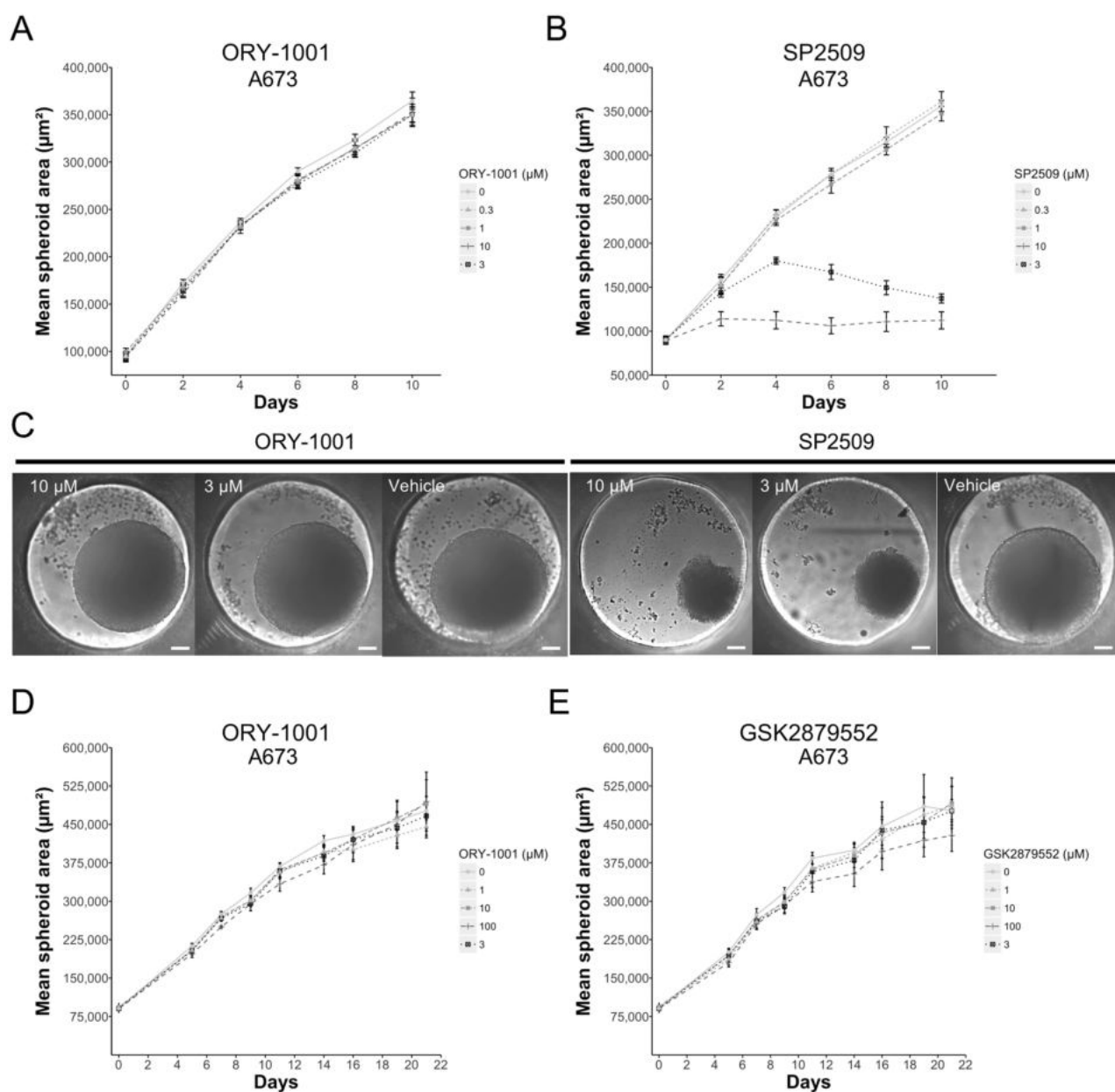
FIGURE 2 Effect of KDM1A inhibitors on the cell proliferation of Ewing sarcoma spheroids. Growth curve of A673 spheroids treated with a range of concentrations of KDM1A inhibitors ORY-1001 (A) and SP2509 (B) for 10 days. (C) Wells containing representative spheroids at day 10 of treatment with ORY-1001 and SP2509 at 10 μM, 3 μM, and vehicle, respectively. Scale bars: 100 μm. Long-term treatment of A673 spheroids with clinical candidates ORY-1001 (D) and GSK2879552 (E) for 21 days. Maximum area at greater width of a sphere was measured in images taken over the different time courses. Means ± SD of 6–10 replicates

Catalytic inhibition of KDM1A with the clinical drug candidates ORY-1001 and GSK2879552 reproduced the reported decrease in cell viability in leukemia cell lines.[22] On the other hand, repurposing of these clinical compounds for Ewing sarcoma did not exhibit anticancer activity in 2D and 3D viability assays even at concentrations up to 100 μM. A validated potent and selective chemical probe for inhibition of KDM1A catalytic function (http://www.thesgc.org/chemical-probes/LSD1),[23,26] which shares the same chemical scaffold with the clinical candidate compounds and has the same mechanism of action through irreversible covalent modification of the FAD cofactor, also had no effect on the cell viability of Ewing sarcoma cells in 2D

and 3D. Prolonged inhibition, as a means to achieve maximal efficacy, as in reports with inhibitors of Enhancer of Zeste Homolg 2 (EZH2) in lymphoma, did not alter the response to these inhibitors of KDM1A catalytic function.[22,23,29]

KDM1A's reported role in modulating self-renewal and differentiation in embryonic stem cells also encompasses regulation of migration during normal mammalian development.[14,35] Importantly, in solid tumors, high levels of KDM1A have been associated with metastasis, and inhibition of this demethylase has been shown to attenuate migration and invasion in breast cancer cell lines.[30] Metastasis is a key problem in Ewing sarcoma with patients with disseminated
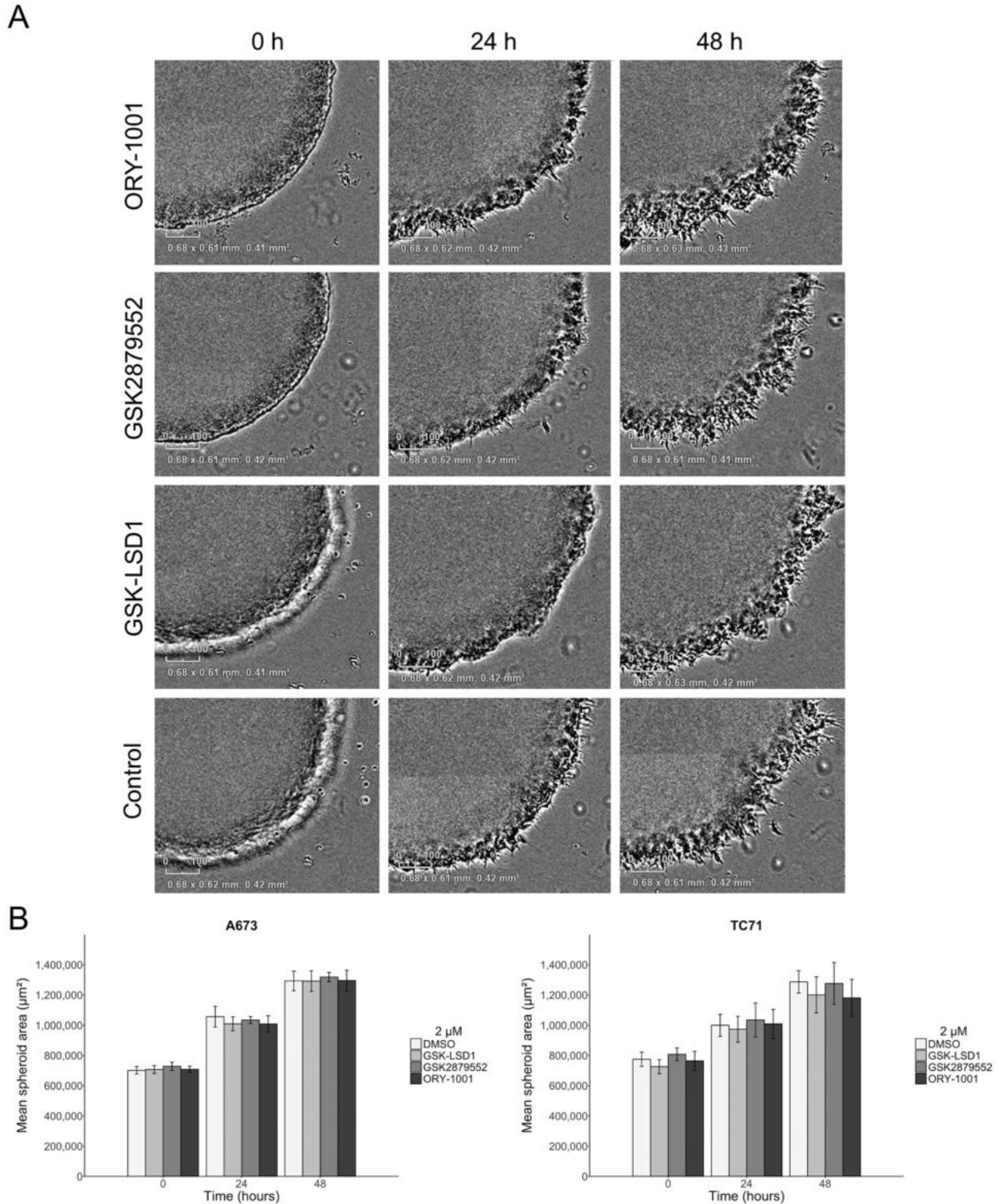
FIGURE 3 Effects of KDM1A inhibitors on the invasion of Ewing sarcoma spheroids. (A) Three-dimensional spheroid invasion assay with Ewing sarcoma cell lines A673 spheroids pretreated with KDM1A clinical drug candidates: ORY-1001 and GSK2879552 and tool compound GSK-LSD1 for 10 days (2 μM). (B) A673 and TC71 total spheroid area measured with IncuCyte ZOOM software for 48 hours (10-day pretreatment with 2 μM). Means ± SD of 3–5 replicates; graphs are representative of two independent repeats. Statistical analysis: two-way ANOVA and Dunnett multiple comparison test, $P < 0.05$ between drugs tested within the same time point

disease showing dismal survival below 30%.[36] Therefore, investigating invasion as part of the phenotypic assessment of KDM1A inhibition was highly relevant. However, in our 3D invasion assay, KDM1A inhibition did not alter the invasive phenotype, and it particularly failed to suppress invasion in Ewing sarcoma spheroids.

The disease context and the nature of the role that KDM1A plays in various malignancies are key determinants of KDM1A inhibition as a therapeutic strategy. In leukemia, KDM1A demethylase activity acts as a key silencer of regulators of hematopoiesis, essential in maintaining leukemia stem cells.[37] This transcriptional repression and differentiation arrest can be relieved through inhibition of KDM1A catalytic function or protein knockdown.[22,37] However, in the context of Ewing sarcoma, despite the observed change in the methylation levels of H3K4, inhibition of KDM1A catalytic function was insufficient to modulate a selection of known target genes of EWS-FLI and impair Ewing sarcoma cells survival. This suggests catalytic activity of KDM1A may not contribute to establishing EWS-FLI1's transcriptional program. Recent findings showed that shRNA-mediated depletion of KDM1A in Ewing sarcoma cells resulted in severe growth impairment and cell death, confirming their dependency on this demethylase.[38] The discrepancy between our results through inhibition of KDM1A catalytic function and knockdown of the multidomain protein strongly suggests a non-canonical role for KDM1A, independent from its demethylase function. These characteristics coincide with other epigenetic regulators such as EZH2. Its emerging methyltransferase- and polycomb-independent roles provide novel therapeutic potential for inhibitors disrupting its docking capacity.[39]

In line with this model, recent reports in prostate cancer cell lines described a scaffolding role for KDM1A, whereby catalytically inactive KDM1A was still able to establish the prostate cancer gene network and ensure survival of castration-resistant prostate cancer cell lines.[40] This was further confirmed with the tool compound SP2509, proposed as an allosteric inhibitor binding to the H3 pocket region of KDM1A, capable of inducing cell death in prostate cancer cell lines. Similarly, this could also explain the previously observed reversal of the EWS-FL1 signature effects with SP2509 in Ewing sarcoma cells.[10] However, it is noteworthy that SP2509 has been shown to effectively cause cell death regardless of KDM1A expression in a leukemia KDM1A knockout cell line and its isogenic control.[41] In addition to disrupting KDM1A's complex formation capabilities, SP2509 may have additional cytotoxic effects independent from KDM1A binding. Consistent with this, 2-hydroxyphenyl-hydrazone structural motif within SP2509 has previously been identified as a pan-assay interference flag and has the potential to elicit promiscuous biological activity.[42–44] KDM1A's role as a docking element for additional proteins may play a more prominent part in Ewing sarcoma cells survival than previously considered.[15]

Our work is particularly timely and pertinent as a drug of the same mechanistic class of KDM1A inhibitors as the irreversible KDM1A demethylase inhibitors tested here has entered phase I trials in Ewing sarcoma patients (NCT03514407). In summary, we demonstrate that the clinical candidates ORY-1001 and GSK2879552, which act predominantly as inhibitors of KDM1A catalytic function, are not effective against in vitro models of Ewing sarcoma. The data presented here do not support clinical trials exploring inhibition of KDM1A demethylase function as a therapeutic strategy for the treatment of Ewing sarcoma and DSRCT.

CONFLICTS OF INTEREST

The authors declare no conflicts of interest.

AUTHORS' CONTRIBUTIONS

AR conducted the experiments and analyzed data. AR, EA, SAG, JS designed the project. SAG and JS supervised the project. AR drafted the manuscript and all authors participated in writing the manuscript and approved the final version.

DATA AVAILABILITY STATEMENT

The data that support the findings of this study are available from the corresponding author upon reasonable request.

ORCID

Antonio Romo-Morales https://orcid.org/0000-0003-1779-7178

REFERENCES

1. Grunewald TGP, Cidre-Aranaz F, Surdez D, et al. Ewing sarcoma. *Nat Rev Dis Primers*. 2018;4(1):5.
2. Delattre O, Zucman J, Plougastel B, et al. Gene fusion with an ETS DNA-binding domain caused by chromosome translocation in human tumours. *Nature*. 1992;359(6391):162-165.
3. Gerald WL, Haber DA. The EWS-WT1 gene fusion in desmoplastic small round cell tumor. *Semin Cancer Biol*. 2005;15(3):197-205.
4. Kovar H, Dr. Jekyll and Mr. Hyde: the two faces of the FUS/EWS/TAF15 protein family. *Sarcoma*. 2011;2011:837474.
5. Gangwal K, Close D, Enriquez CA, Hill CP, Lessnick SL. Emergent properties of EWS/FLI regulation via GGAA microsatellites in Ewing's sarcoma. *Genes Cancer*. 2010;1(2):177-187.
6. Gangwal K, Sankar S, Hollenhorst PC, et al. Microsatellites as EWS/FLI response elements in Ewing's sarcoma. *Proc Natl Acad Sci U S A*. 2008;105(29):10149-10154.
7. Riggi N, Knoechel B, Gillespie SM, et al. EWS-FLI1 utilizes divergent chromatin remodeling mechanisms to directly activate or repress enhancer elements in Ewing sarcoma. *Cancer Cell*. 2014;26(5):668-681.
8. Boulay G, Sandoval GJ, Riggi N, et al. Cancer-specific retargeting of BAF complexes by a prion-like domain. *Cell*. 2017;171(1):163-178.e19.
9. Sankar S, Bell R, Stephens B, et al. Mechanism and relevance of EWS/FLI-mediated transcriptional repression in Ewing sarcoma. *Oncogene*. 2013;32(42):5089-5100.
10. Sankar S, Theisen ER, Bearss J, et al. Reversible LSD1 inhibition interferes with global EWS/ETS transcriptional activity and impedes Ewing sarcoma tumor growth. *Clin Cancer Res*. 2014;20(17):4584-4597.

11. Lai AY, Wade PA. Cancer biology and NuRD: a multifaceted chromatin remodelling complex. *Nat Rev Cancer*. 2011;11(8):588-596.

12. Maiques-Diaz A, Somervaille TC. LSD1: biologic roles and therapeutic targeting. *Epigenomics*. 2016;8(8):1103-1116.

13. Shi Y, Lan F, Matson C, et al. Histone demethylation mediated by the nuclear amine oxidase homolog LSD1. *Cell*. 2004;119(7):941-953.

14. Adamo A, Sese B, Boue S, et al. LSD1 regulates the balance between self-renewal and differentiation in human embryonic stem cells. *Nat Cell Biol*. 2011;13(6):652-659.

15. Forneris F, Binda C, Vanoni MA, Battaglioli E, Mattevi A. Human histone demethylase LSD1 reads the histone code. *J Biol Chem*. 2005;280(50):41360-41365.

16. Bennani-Baiti IM, Machado I, Llombart-Bosch A, Kovar H. Lysine-specific demethylase 1 (LSD1/KDM1A/AOF2/BHC110) is expressed and is an epigenetic drug target in chondrosarcoma, Ewing's sarcoma, osteosarcoma, and rhabdomyosarcoma. *Hum Pathol*. 2012;43(8):1300-1307.

17. Schildhaus HU, Riegel R, Hartmann W, et al. Lysine-specific demethylase 1 is highly expressed in solitary fibrous tumors, synovial sarcomas, rhabdomyosarcomas, desmoplastic small round cell tumors, and malignant peripheral nerve sheath tumors. *Hum Pathol*. 2011;42(11):1667-1675.

18. Safety, clinical activity, pharmacokinetics (PK) and pharmacodynamics study of GSK2879552, alone or with azacitidine, in subjects with high risk myelodysplastic syndromes (MDS). Available from: https://clinicaltrials.gov/ct2/show/NCT02929498?term=GSK2879552&. NLM identifier: NCT02929498.

19. Investigation of GSK2879552 in subjects with relapsed/refractory small cell lung carcinoma. Available from: https://clinicaltrials.gov/ct2/show/NCT02034123?term=GSK2879552&rank=2. NLM identifier: NCT02034123.

20. A phase I dose escalation study of GSK2879552 in subjects with acute myeloid leukemia (AML). Available from: https://clinicaltrials.gov/ct2/show/NCT02177812?term=KDM1A+inhibitors. NLM identifier: NCT02177812.

21. A dose finding and expansion study of RO7051790 administered orally in participants with relapsed, extensive-stage disease small cell lung cancer (ED SCLC). Available from: https://clinicaltrials.gov/ct2/show/NCT02913443?term=RO7051790&rank=1. NLM identifier: NCT02913443.

22. Maes T, Mascaro C, Tirapu I, et al. ORY-1001, a potent and selective covalent KDM1A inhibitor, for the treatment of acute leukemia. *Cancer Cell*. 2018;33(3):495-511. e412.

23. Mohammad HP, Smitheman KN, Kamat CD, et al. A DNA hypomethylation signature predicts antitumor activity of LSD1 inhibitors in SCLC. *Cancer Cell*. 2015;28(1):57-69.

24. Nishio J, Iwasaki H, Ishiguro M, et al. Establishment and characterization of a novel human desmoplastic small round cell tumor cell line, JN-DSRCT-1. *Lab Invest*. 2002;82(9):1175-1182.

25. Rio DC, Ares M, Hannon GJ, Nilsen TW. Purification of RNA using TRIzol (TRI reagent). *Cold Spring Harbor Protocols*. 2010;2010(6). pdb.prot5439.

26. The Structural Genomics Consortium. GSK-LSD1. A chemical probe for LSD1. *Chemical Probes* 2014; https://www.thesgc.org/chemical-probes/GSK-LSD1. Accessed 12 July, 2018.

27. Langhans SA. Three-dimensional in vitro cell culture models in drug discovery and drug repositioning. *Front Pharmacol*. 2018;9:6.

28. Riffle S, Pandey RN, Albert M, Hegde RS. Linking hypoxia, DNA damage and proliferation in multicellular tumor spheroids. *BMC Cancer*. 2017;17(1):338.

29. McCabe MT, Ott HM, Ganji G, et al. EZH2 inhibition as a therapeutic strategy for lymphoma with EZH2-activating mutations. *Nature*. 2012;492(7427):108-112.

30. Wang Y, Zhang H, Chen Y, et al. LSD1 is a subunit of the NuRD complex and targets the metastasis programs in breast cancer. *Cell*. 2009;138(4):660-672.

31. Riggi N, Suva ML, Suva D, et al. EWS-FLI-1 expression triggers a Ewing's sarcoma initiation program in primary human mesenchymal stem cells. *Cancer Res*. 2008;68(7):2176-2185.

32. Pishas KI, Lessnick SL. Recent advances in targeted therapy for Ewing sarcoma. *F1000Res*. 2016;5. pii: F1000 Faculty Rev-2077.

33. Theisen ER, Pishas KI, Saund RS, Lessnick SL. Therapeutic opportunities in Ewing sarcoma: EWS-FLI inhibition via LSD1 targeting. *Oncotarget*. 2016;7(14):17616-17630.

34. Maiques-Diaz A, Spencer GJ, Lynch JT, et al. Enhancer activation by pharmacologic displacement of LSD1 from GFI1 induces differentiation in acute myeloid leukemia. *Cell Rep*. 2018;22(13):3641-3659.

35. Zhu D, Holz S, Metzger E, et al. Lysine-specific demethylase 1 regulates differentiation onset and migration of trophoblast stem cells. *Nat Commun*. 2014;5:3174.

36. Kovar H, Alonso J, Aman P, et al. The first European interdisciplinary Ewing sarcoma research summit. *Front Oncol*. 2012; 2:54.

37. Harris WJ, Huang X, Lynch JT, et al. The histone demethylase KDM1A sustains the oncogenic potential of MLL-AF9 leukemia stem cells. *Cancer Cell*. 2012;21(4):473-487.

38. Pishas KI, Drenberg CD, Taslim C, et al. Therapeutic targeting of KDM1A/LSD1 in Ewing sarcoma with SP-2509 engages the endoplasmic reticulum stress response. *Mol Cancer Ther*. 2018.

39. Kim J, Lee Y, Lu X, et al. Polycomb- and methylation-independent roles of EZH2 as a transcription activator. *Cell Rep*. 2018;25(10):2808-2820. e2804.

40. Sehrawat A, Gao L, Wang Y, et al. LSD1 activates a lethal prostate cancer gene network independently of its demethylase function. *Proc Natl Acad Sci U S A*. 2018;115(18):E4179-E4188.

41. Sonnemann J, Zimmermann M, Marx C, et al. LSD1 (KDM1A)-independent effects of the LSD1 inhibitor SP2509 in cancer cells. *Br J Haematol*. 2018;183(3):494-497.

42. Baell JB, Holloway GA. New substructure filters for removal of pan assay interference compounds (PAINS) from screening libraries and for their exclusion in bioassays. *J Med Chem*. 2010;53(7):2719-2740.

43. Hitchin JR, Blagg J, Burke R, et al. Development and evaluation of selective, reversible LSD1 inhibitors derived from fragments. *Medchemcomm*. 2013;4(11):1513-1522.

44. Mould DP, McGonagle AE, Wiseman DH, Williams EL, Jordan AM. Reversible inhibitors of LSD1 as therapeutic agents in acute myeloid leukemia: clinical significance and progress to date. *Med Res Rev*. 2015;35(3):586-618.

SUPPORTING INFORMATION

Additional supporting information may be found online in the Supporting Information section at the end of the article.